RESEARCH IN ADVANCED PHOTOELECTRIC INFORMATION STORAGE

TECHNICAL DOCUMENTARY REPORT NO. RTD-TDR-63-4134

November 1963

Air Force Avionics Laboratory
Research and Technology Division
Air Force Systems Command
Wright-Patterson Air Force Base, Ohio

Project No. 6263, Task No. 626302

(Prepared under Contract No. AF33(657)8715 by W.G. Reininger, A.S. Jensen, and W.G. Beran of the Westinghouse Electric Corporation, Baltimore, Maryland.

AD UNCLASSIFIED

Westinghouse Electric Corp., Baltimore, Md.
RESEARCH IN ADVANCED PHOTOELECTRIC INFORMATION STORAGE
Final rept. on Photoelectric Storage,
by W.G. Reininger, A.S. Jensen, and W.G. Beran. 26 Nov 63, [156]p. incl.illus. tables, 9 refs. (Rept. no. 437D)
(Contract AF33(657)8715, Proj. 6263, Task 626302)
(RTD-TDR-63-4134) Unclassified report

DESCRIPTORS: (Storage tubes, Photocathodes, Electrostatic Accelerators, Aperture response, Bar pattern.)

Improvements of the tape storage camera tube increased the resolution from 40 to 75 line pairs per millimeter for small rasters at 5-percent response. Response curves showing 60 line pairs per millimeter at 10-percent response were measured. No grating disturbance or any effect of grating orientation was observed. The hard copy film photo of the display kinescope showed 23 line pairs per millimeter (retina dimension) resolution, 8 shades of gray resolvable by the eye, and a contrast of 80 percent. When the stored picture was underscanned by 18X to show only the AF test pattern,

(over)

64 line pairs per millimeter were resolved. Photodiodes were made to test the image section operation. Aperture response curves had a 5-percent response of 98 line pairs per millimeter, which when corrected for the aperture response of the lens became 220 line pairs per millimeter. A technique was developed for measuring the aperture response curves of lenses and image displays. Studies indicated that a mechanical means (harmonic drive) may be best for smooth tape drive.

FOREWORD

This report was prepared by the Westinghouse Electric Corporation, Baltimore, Maryland on Air Force Contract AF33-(657)8715, "Research in Advanced Photoelectric Information Storage." The work was administered under the direction of the Reconnaissance Laboratory, Aeronautical Systems Division, Mr. J. Fulton was project engineer for the Laboratory.

The studies of this contract, which started in June 1962 and concluded in July 1963, were a continuation of the contract AF33(616)6666, Task 62766 which began in July 1959 and ended in May 1962. Both contracts represent an effort of the Special Electron Devices Section of Westinghouse Electric Corporation, Applied Research Department, Baltimore, Maryland.

This is the final report and it concludes the work on contract AF33(657)8715. The contractor's report number is 437D.

ABSTRACT

On this contract, Westinghouse Electric Corporation has conducted for the U. S. Air Force Aeronautical Systems Division an applied research program aimed at developing a sensor suitable for reconnaissance under adverse illumination conditions and having both high resolution and large total information storage capacity. Under a prior contract, AF33(616)-6666, a preliminary concept of an electro-optical tape storage camera was evolved. This utilizes a tape camera storage tube with a photoemissive retina sensitive in the visible spectrum which can store a large amount of information on electrostatic tape reeled within the vacuum tube and read this information electronically. The objective of this present program was to perform a comprehensive series of experiments upon each component required in this tape storage camera tube in order to determine the state of the art achieved to date and to perform additional applied research in areas in which improvement could be made.

During this past year, improvements have been made to increase resolution from 40 to the present 75 line pairs per millimeter for small rasters at 5-percent response. Using an 0.8-inch by 0.6-inch raster, with a 100-percent contrast bar pattern, response curves have been measured showing 60 line pairs per millimeter at 10-percent response. Response curves measured immediately after writing and again on the same stored picture after 51 hours of storage are identical when normalized to account for a decay of amplitude to 60 percent of the original. No grating disturbance signal has yet been observed nor has any effect of grating orientation.

When a scene with a maximum of 50-percent contrast is stored on a 0.7-inch square raster with an average exposure of 0.8 meter-candle-second on a 50-microampere per lumen S-20 photocathode and read off with a 0.1 microampere beam, with a 10-mc amplifier and a 5-second frame time, the hard copy film photo of the display kinescope shows 23 line pairs per millimeter (retina dimension) resolution, 8 shades of gray resolvable by the eye, and a contrast of 80 percent. This is short of the theoretical predications by a factor of 6 in exposure and a factor of 6 in resolution. When the stored picture is underscanned by 18X to show only the AF test pattern, 64 line pairs per millimeter are resolved.

Photodiodes were made to test the image section operation. Aperture response curves had a 5-percent response of 98 line pairs per millimeter, which when corrected for the aperture response of the lens became 220 line pairs per millimeter. This should be close to the theoretical chromatic aberration limit for a 10 Kev photodiode. A technique has been developed for measuring the aperture response curves of lenses and image displays.

An electronic shutter has been developed which operates in the image section. A 1000-volt pulse operated this shutter for exposures as short as 100 microseconds.

Reading times as long as 10 minutes with signal amplitude loss of less than 50 percent were common. Some study of methods for smooth tape drive through the vacuum wall indicates that a mechanical means, known as a harmonic drive, may be the best.

This technical documentary report has been reviewed and is approved.

TABLE OF CONTENTS

LIST OF ILLUSTRATIONS

LIST OF TABLES

BIBLIOGRAPHY

1. INTRODUCTION*

Westinghouse has been conducting an applied research program for the Aerial Reconnaissance Laboratory of the Aeronautical Systems Division of the U.S. Air Force under contract number AF33(657)8715 on an electro-optical tape storage camera tube, frequently referred to as the Television Information Storage Tube or TVIST project. It is essentially a continuation of the work done previously on contract number AF33-(616)6666. During the first 8 months, the object of the program was the building and operation of an experimental sealed-off tape storage camera in accord with the preliminary concept evolved on the prior contract. For the last 4 months the program was redirected to perform a comprehensive series of experiments on each component of the tape storage camera tube to determine the performance status of each and to perform additional applied research in areas where improvement could be made.

Briefly, in the tape storage camera tube (figure 1-1) image information is written by photoelectrons magnetically focused as an electron charge pattern on the storage tape. An auxiliary electron gun can also be used to write information from other sources with a finely focused electron beam. The storage tape is reeled on spools inside the vacuum in a manner similar to motion picture film. It is comprised of a thin metal base which is an electroformed replica of a diffraction grating, upon the broad slopes of which a good dielectric such as magnesium fluoride is shadow evaporated, leaving the narrow and more vertical surface as an exposed metal grille.

For the writing, reading, erasing, and priming operations the storage tape is moved beneath the respective electron sources. The reading is done with a specially developed finely focused electron beam, the stored charge pattern acting as a control grid to modulate the return beam to an electron multiplier output. Thus, the reading is nondestructive, permitting greater percentage of reading beam modulation, large dynamic range, variable reading scan speed, and multicopy output. The metal grille of the storage target acts as an electrostatic shield to prevent adjacent stored signals from microdeflecting the beam, thus providing better resolution and more reliable

* Manuscript released by the author August 1963 for publication as an ASD Technical Documentary Report.

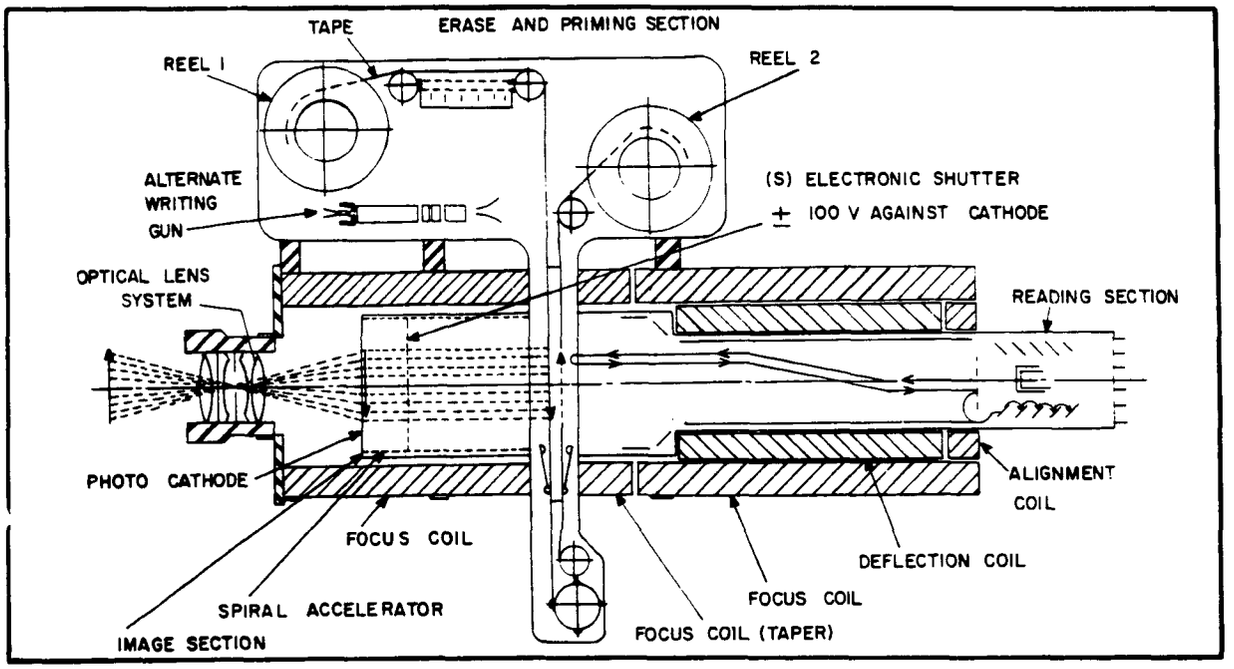

Figure 1-1. Prototype Functional Diagram

scanning linearity. The grille structure is much smaller than the reading beam spot size so that it does not contribute a disturbance signal nor does it limit resolution.

For a more detailed description of the construction, operation, and theory of the tape storage camera tube, the reader is referred to the final report on contract number AF33(616)6666, Aeronautical Systems Division Technical Documentary Report ASD-TDR-62-990, dated 30 November 1962.

In pursuit of this past year's program, three important classes of sealed-off experimental tubes were used in addition to demountable vacuum system arrangements. Some of these are shown in figure 1-2. A photodiode comprising a photocathode, accelerator electrodes, and a phosphor screen simulated the image section. An experimental reading section with an electron gun and either a slit target or a monoscope target was used to measure reading aperture response, electron beam spot size, current density distribution, control grid transfer characteristic, and electron energy distribution. A grating target storage camera tube referred to in the prior contract final report as a "flip-over" target was widely used to determine the resolution, storage, and sensitivity characteristics. It comprises an image section: photocathode and accelerator electrodes; coaxial with a reading section; electron gun and wall electrode in the deflection region; and between these a grating storage target which is a piece of the storage tape plated thick to be rigid and mounted in such a manner tha

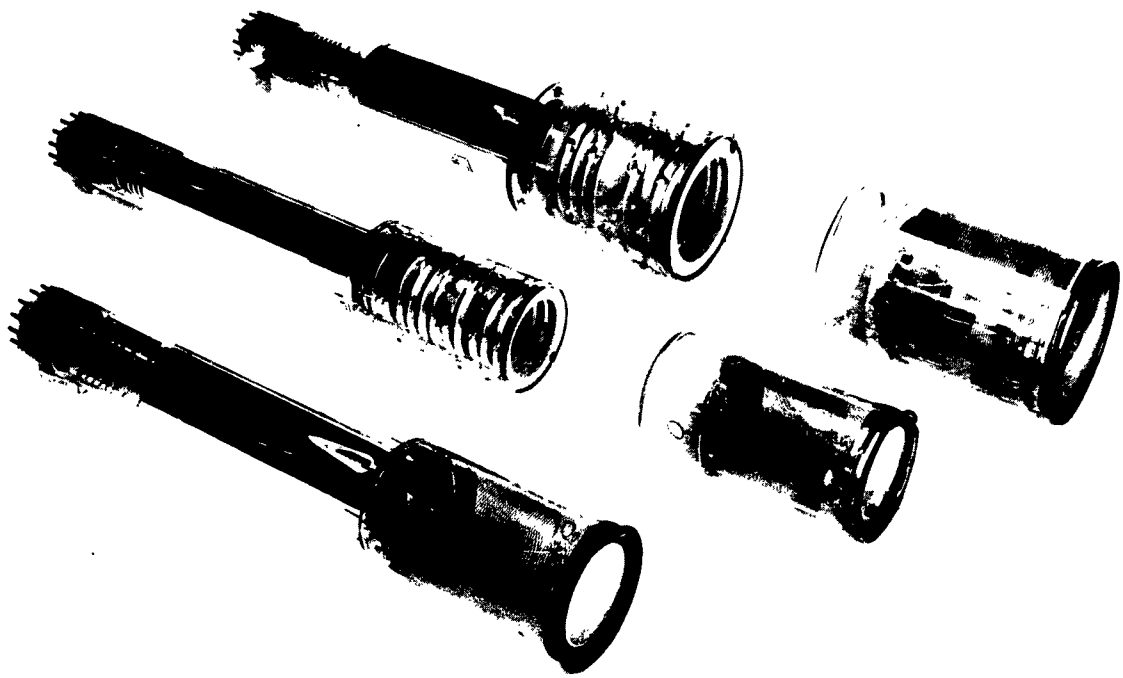

Figure 1-2. Experimental Tubes

2. PHOTOELECTRIC SURFACE

An image section somewhat similar to that used on an image orthicon is used to form a photoelectron image on the storage target of the electrostatic tape storage camera tube. The image is formed by an axial magnetic focusing field; an axial uniform electric field accelerates the photoelectrons. The resolution of such photoelectron writing surpasses by far any scanning electron beam writing.

An optical lens system produces a real picture in the plane of the photocathode. From regions of high light level more photoelectrons are emitted and they are accelerated through an adequate electromagnetic focusing system onto the dielectric of the storage means. This acceleration can be done to about 500 ev (between the first and second cross overs of the secondary emission curve) which for high sensitivity should be chosen at the voltage of the maximum secondary emission. In another mode the photoelectrons are accelerated to about 10 Kev; in this case the EBIC (electron bombardment induced conductivity) is used for writing on the storage dielectric.

2.1 PHOTOCATHODE

Three different types of photocathodes were investigated for their yield in microamperes per lumen, compatibility of the materials used with the accelerator elements, and the different target materials. Furthermore the geometry of the evaporators was important for the uniformity of the response of the surface elements of the photocathode.

The yield measurements were referred to a standard lamp which had been calibrated by the Bureau of Standards. The calibration chart shows the candle power produced versus filament current and corresponding color temperature. The yield measurements were made at a color temperature of 2870°K.

2.1.1 The Bialkali Photocathode

In the beginning of the work on TVIST, photocathodes without cesium were used in order to keep the cesium vapor from degrading the storage dielectric. For this reason bialkali photocathodes were chosen. As it is known, these bialkali photocathodes are lower in yield than the trialkali or S-20 ones, being only in the order of 10 to 60 microamperes per lumen rather than 120 to 190 microamperes per lumen.

It has been noticed that the electron multiplier for the return beam had much lower gain than those which were used with photocathodes containing cesium. It is suspected that the presence of cesium vapor enhanced the gain per multiplier stage by producing a thin surface alloy with the magnesium oxide (on silver) used there. At bialkali photocathodes, six dynodes instead of the usual five were incorporated and gains of 200 were achieved for the return beam signal in this way.

2.1.2 S-11 Photocathodes

These photocathodes which consist of an antimony-cesium deposit on the entrance window have a relatively low yield of about 10 to 65 microamperes per lumen. They were used to give a guidance for evaporator channel, geometry, and process schedules for uniform and reproducible photocathodes.

In one mode the antimony and the cesium were alternately released by evaporating from the antimony beads and from the cesium channels with monitoring of the photocurrent until optimum was reached.

In the other mode the antimony was first evaporated from a source which was not part of the tube structure. After the proper opacity of the antimony on the window was reached, the unit was let down to air and the image section cup was sealed to the tube. A cesium channel and a palladium tubing for the introduction of H_2 were included in the tube structure. Hydrogen was admitted by heating the palladium tube. The antimony was heated, and the hydrogen reduced the oxgen on the antimony. Later the cesium was released. This complicated activation scheme was used with spiral accelerators to make electric field obstruction by activating channels as small as possible.

2.1.3 S-20 Photocathodes

During early work with sealed-off storage camera tubes, it was found that most of the time the storage targets lost their storage quality after the admission of the cesium vapor and it was feared that only bialkali photocathodes with their lower yield could be used. However, it was soon found that tubes with leaky storage targets could be repaired by heating the storage surface by directed infrared radiation and/or by a careful sparking of the storage base while all the other electrodes were on ground.

Bombardment of the storage surface with uniform 10 kilovolts writing electrons did a good cleaning job also. Storage plates treated in this way showed improvements over the first 20 storages until they had such low loss of the stored signal strength that the reading signal amplitude after 41 hours storage was 60 percent of that immediately after writing.

This compatibility of cesium with the storage medium opened the possibility of the use of the highly sensitive trialkali S-20 photocathodes.

Yields of about 120 microamperes per lumen and more were reached in the "flip-over" grating target storage camera tubes and the overall sensitivity of these tubes was about that of regular Kodak Plus-X film developed under normal conditions. These photosurfaces were stable over a 6-month use of these tubes. No new cleaning process of the storage surface was necessary after the previously mentioned one. In figure 2-1 the spectral response of these photocathodes as measured with a monochromater are shown.

2.1.4 Gold Photocathodes

For demountable systems none of these alkali photocathodes could be used. Gold is stable in air, but with its relatively high work function of about 4.7 ev it can be used only with UV light of a corresponding short wavelength, less than 0.25 micron.

These photocathodes were used in the demountable vacuum system. They showed a relatively low but highly constant yield. Often the photocathodes were used with one or several fine aluminium island areas superimposed by shadow evaporation through fine metal meshes (100, 250, 500, and 750 mesh). This permitted early crude resolution measurements to be made.

2.2 UNIFORMITY

The photocurrent yield of several cathodes was measured as a function of position in the following way. The photocathode in a photodiode was installed on a carriage which had a movement perpendicular to the incoming light beam. Figure 2-2 shows this carriage setup used for resolution measurements. The light from a lamp fed by a constant current supply was set up about 15 feet from a black metal screen which had a hole, 0.1250-inch in diameter, in the center. The photocathode on the carriage had its center behind the hole in the screen and it could be moved on the carriage to both sides so that the light beam through the hole could strike the photocathode at points along a diameter. All stray light was kept from the photocathode. In this way a light beam of constant intensity could strike all points of the photocathode. Approximately 190 volts were used to collect the photoelectrons after experiments had shown that this potential was far above a level which would have built up space charges.

Measurements were made on nine tubes; the results are shown in table 2-1 and figure 2-3. There are two curves in the figure, one for each of two perpendicular

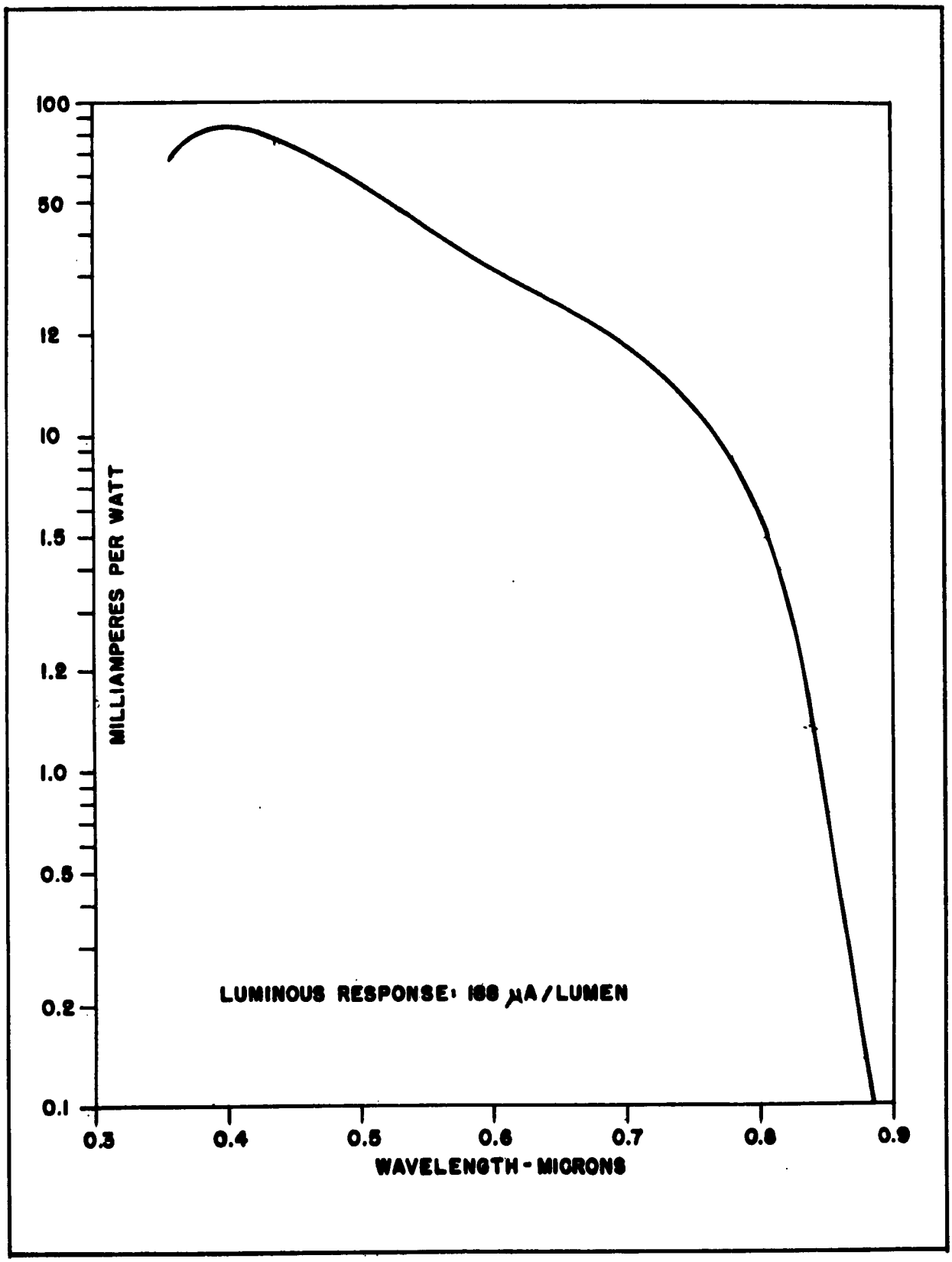

Figure 2-1. S-20 Photocathode Spectral Response

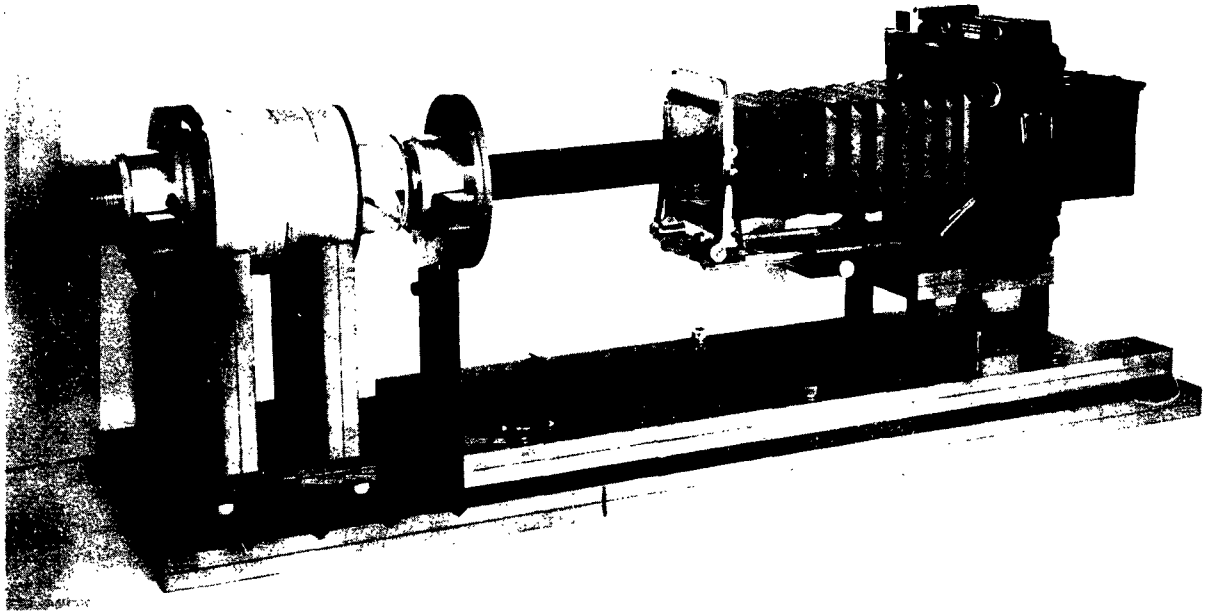

Figure 2-2. Test Carriage for Photodiode Uniformity and Resolution Measurements

diameters. It can be seen that the photocurrent yield for some photocathodes varies by as much as 27 percent over the whole surface, but that later ones vary by only 11 percent.

On some photocathodes the measurements were made at both high and low intensity beam. Both showed a similar deviation from uniformity of about ±6 percent. No influence of photocathode surface resistance could be detected.

The illumination of the photocathode at the 0.125-inch aperture was measured and the mean value of photocurrent was integrated over the active surface. The measured total yields matched the integrated values within ±10 percent.

TABLE 2-1

PHOTOCATHODE UNIFORMITY

Tube Number	Tube Diameter (inch)	Yield (microamperes) per lumen)	Microamperes at							
			-1.25 Inches	-0.75 Inch	-0.5 Inch	-0.25 Inch	+0.25 Inch	+0.5 Inch	+0.75 Inch	+1.25 Inches
PD-6	4.5	10.0	0.33	0.30	0.29	0.29	0.29	0.27	0.27	0.29
PD-3	4.5	2.2	0.073	0.063	0.062	0.062	0.073	0.080	0.090	0.11
E-7042	4.5	54.0	1.7	1.6	1.5	1.3	1.2	1.4	1.6	1.8
3009	4.5	26.0	1.75	1.1	1.1	1.1	0.81	0.60	0.60	0.95
3035	4.5	31.0	0.42	0.68	0.82	0.76	0.73	0.83	0.95	1.3
6022	3	3.4	-	0.029	0.042	0.062	0.12	0.20	0.19	-
13	3	8.5	-	0.22	0.02	0.15	0.22	0.28	0.36	-
12	3	45.0	-	1.6	1.2	0.73	0.54	0.68	0.58	-

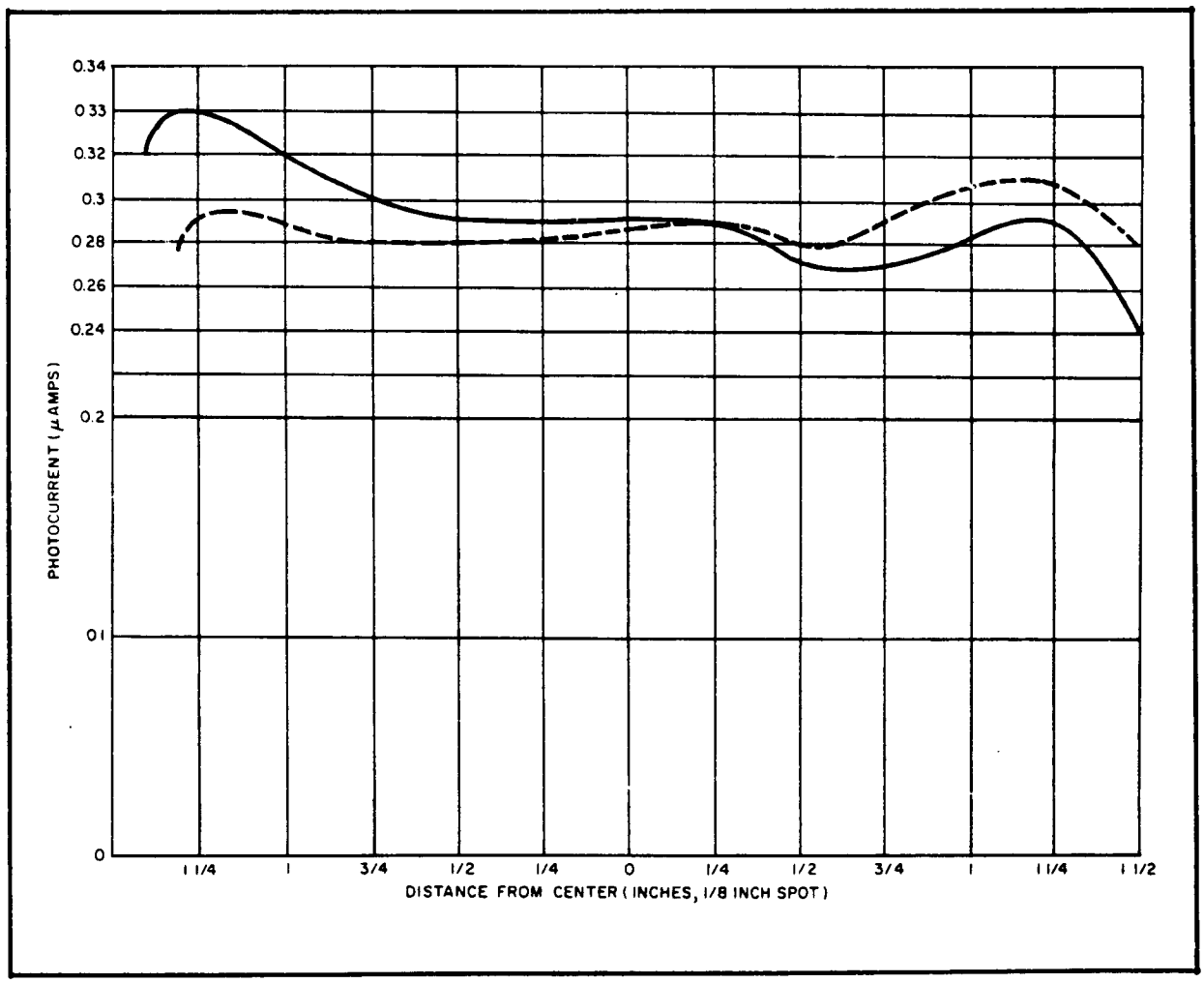

Figure 2-3. Photocathode Uniformity Tube Number, PD-6

3. ELECTRON OPTICS OF THE IMAGE SECTION

One goal of this study was to improve resolution of the photoelectric picture on the storage surface for the writing process. A second goal was to increase the usable area of the photocathode and of the storage target, to avoid pin cushion or barrel distortions and loss of resolution from the center, and to maintain uniformity of writing speed and sensitivity.

3.1 PHOTODIODE CONSTRUCTION

For the electron optical studies, photodiode tubes consisting of a photocathode, accelerating means, and an output phosphor were made. The first tubes had nine accelerating cylinders which were connected to appropriate voltages from a bleeder circuit with one potentiometer for each accelerator cylinder. These tubes were built with a 3-inch and later with a 4.5-inch outside diameter. The normal settled phosphor was soon found to limit resolution because of its grain size. Phosphors vacuum evaporated and baked into the glass surface were not sensitive enough. Finally, cataphoretically deposited phosphors combined a useful sensitivity with the high resolutions of better than 150 line pairs per millimeter. These are made by electrostatically settling the very fine charged particles from an emulsion suspension.

Some of the latest photodiodes were made with a re-entrant exit window. This was done to provide for the use of microscopes with short focal length objectives without any intermediate optical systems. Later, additional optics had to be used for the resolution measurements. Figure 1-2 shows 3- and 4.5-inch photodiodes and grating target storage camera tubes with cylinder and with spiral accelerators.

3.2 ELECTROSTATIC ACCELERATORS

Cylinder accelerators had the disadvantage that the cylinders reduced the distortion free cross section of the accelerating field. Further, the nine cylinders were supported by 27 supports in the glass envelope and each cylinder had to be connected to a fairly high voltage on the bleeder circuit since 10 kv accelerating voltage was used. With the nine cylinder accelerators it had been found that a nearly linear increasing accelerator voltage gave the highest resolution and lowest distortion.

Experiments were conducted to produce a uniform resistance spiral of about 50 megohms on the inside of the glass tubing of the image section. At 10 kv there are only 2 watts to be dissipated over the relative large area. The thickness of the spiral deposit had to be very small for the relatively high resistance. The spiral material had to be compatible with the materials used in the photocathodes. Chromium vacuum evaporation deposited onto the specially cleaned inside of the glass cylinder resulted in spirals of the required resistance value which could not be scratched off the glass substrate with steel and which was not changed by the presence of the photocathode materials. Both the spirals and the photocathode showed no change over periods lasting more than 6 months.

These spirals were measured turn by turn and they show a constant resistance value for each turn. The spiral acts as a bleeder and a field electrode at the same time. The voltage of about 10 kv drops gradually in equal increments per length or turn. The accelerating electric field so formed is uniform and the electric force is a constant.

3.3 MAGNETIC FIELD

In the final TVIST tube writing and reading focusing is done by a magnetic field as described in Report ASD-TDR-62-990; contract AF33(616)6666. Both fields have the same direction, strength, and distribution. They support each other. The same principle was used in the "flip-over" grating target storage camera tubes where one field is just the extension of the other.

For the evaluation of the photodiodes, special magnet coils were designed for the 3- and 4.5-inch models. Extension coils for the 3- and 4.5-inch image orthicon coils were computed for 10 kv acceleration.

The magnet coils are laid out in such a way that all electrons emanating from one point of the photocathode are focused to a point on the phosphor or the storage target after running through one or two Larmor spirals.

In paragraph 3.5.2 it is shown that the excellent center resolution falls off toward the periphery. This was ascribed to irregularities in the electromagnetic focusing field. Therefore the magnetic field was measured with a gauss meter for points throughout its volume as shown in figure 3-1. The values of magnetic field in gauss at each of these points are shown in table 3-1.

The difference of the field strength in the x-plane and the y-plane was so small that only the x-plane field strengths are plotted in the figures. Figure 3-2 shows the variation of the magnetic field as a function of position along a path parallel to the

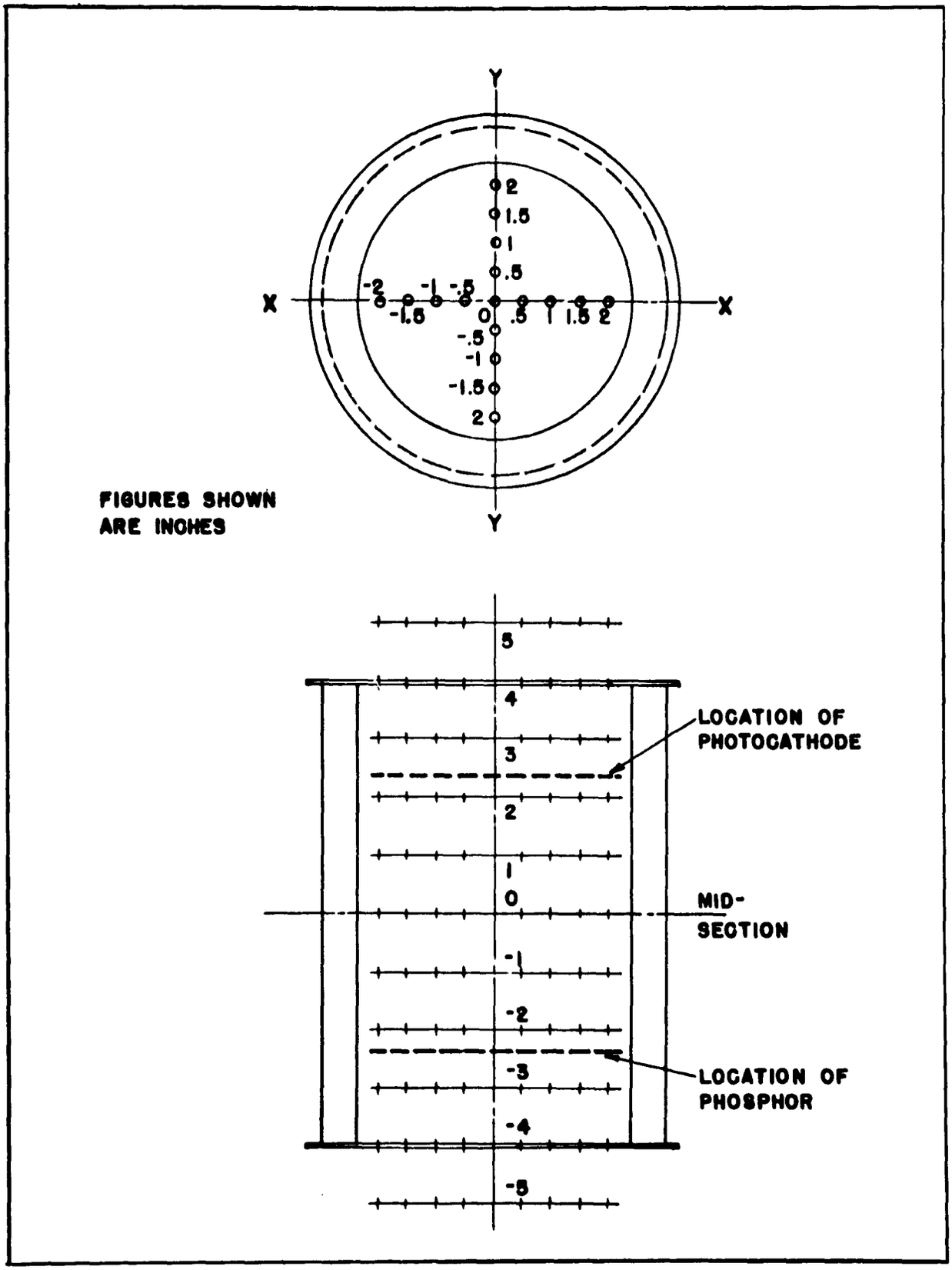

Figure 3-1. Magnetic Field Measurements on 4.5-Inch Focus Coil

TABLE 3-1

MAGNETIC FIELD IN 4.5-INCH FOCUS COIL IN GAUSS

Displacement From Axis in inches	Section (inches)										
	+5	+4	+3	+2	+1	0	-1	-2	-3	-4	-5
X-direction											
+2	21.0	34.5	50.0	58.0	62.0	63.0	62.0	58.0	50.0	35.5	22.0
+1.5	25.5	35.5	48.5	56.0	60.5	62.0	61.0	56.5	48.5	36.0	23.5
+1	24.5	36.0	47.5	55.0	60.0	61.0	60.0	55.0	47.0	35.5	24.5
+0.5	25.5	36.5	47.5	54.0	59.5	61.0	59.5	54.5	46.5	35.5	24.5
0	26.2	37.0	47.7	55.0	59.5	61.0	59.0	54.0	46.0	35.5	24.5
-0.5	26.0	37.0	47.7	55.0	60.0	61.0	59.5	54.0	46.2	35.2	24.5
-1	24.5	36.2	47.5	55.5	60.0	61.5	60.0	56.0	47.5	34.0	24.5
-1.5	24.5	36.7	49.2	57.0	61.5	63.0	61.5	57.0	48.7	36.2	23.5
-2	21.7	35.0	49.5	57.5	61.5	63.0	61.5	57.5	49.5	35.2	21.5
Y-direction											
+2	22.0	35.5	50.0	58.0	62.0	63.0	62.0	58.0	49.5	35.2	21.5
+1.5	23.7	35.5	48.0	56.0	60.5	61.5	60.5	56.0	47.5	35.5	23.3
+1	24.5	35.5	47.0	55.0	59.5	61.0	59.5	55.0	46.5	35.7	24.5
+0.5	25.0	35.8	46.5	54.0	59.0	60.0	59.0	54.0	46.5	35.7	25.0
0	25.3	36.0	46.5	54.0	59.0	60.0	58.5	54.0	45.5	35.5	24.5
-0.5	25.0	35.8	46.7	54.0	59.0	60.5	59.0	54.5	46.5	35.8	24.8
-1	24.0	35.3	48.8	55.0	59.5	61.0	60.0	55.5	47.6	36.5	25.0
-1.5	23.0	35.3	48.2	56.0	61.0	62.0	61.0	57.0	48.5	36.2	23.7
-2	21.0	35.0	50.0	58.0	62.0	63.5	62.5	59.0	51.0	36.5	22.0

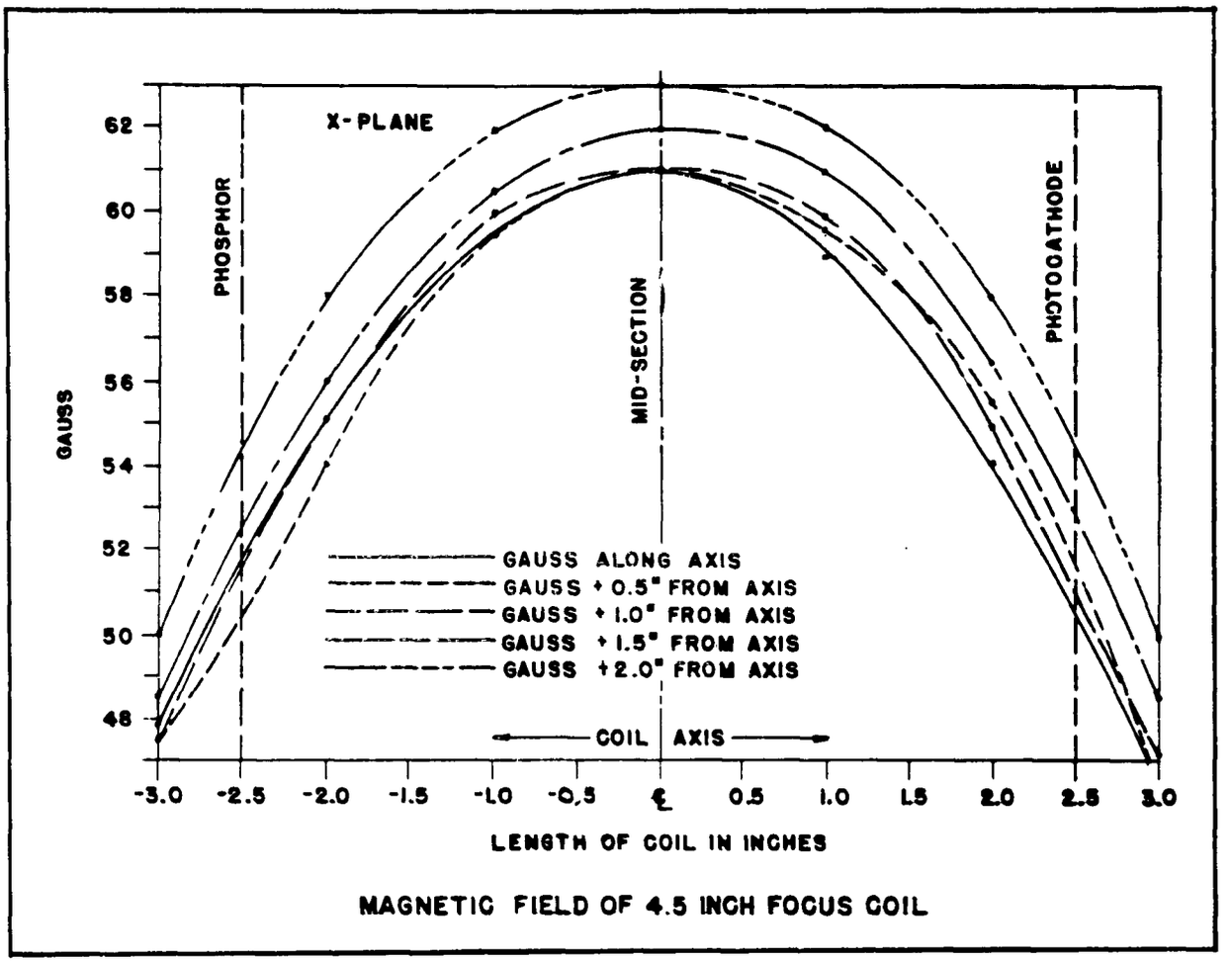

Figure 3-2. Longitudinal Variation of Magnetic Field

coil axis. Each curve is for a path at a different radial distance from the axis. Figure 3-3 shows the variation of the magnetic field as a function of radius on the photocathode side of the coil midsection. Figure 3-4 is the same on the phosphor side of the coil midsection. Note that the magnetic field scale starts at 47 gauss, and that small differences in the field strength are exaggerated.

It can be seen that the difference between the magnetic field strength at the photocathode and the phosphor was less than 3 percent. There is, therefore, no appreciable reduction or magnification between optical and stored pictures.

In the longitudinal plot of figure 3-2, it can be seen that the field density increases from the photocathode and phosphor considerably towards the middle section of the coil. This means that the lines of force are convex toward the axis. Also there is a difference of about 8 percent in field strength between points along the axis and points

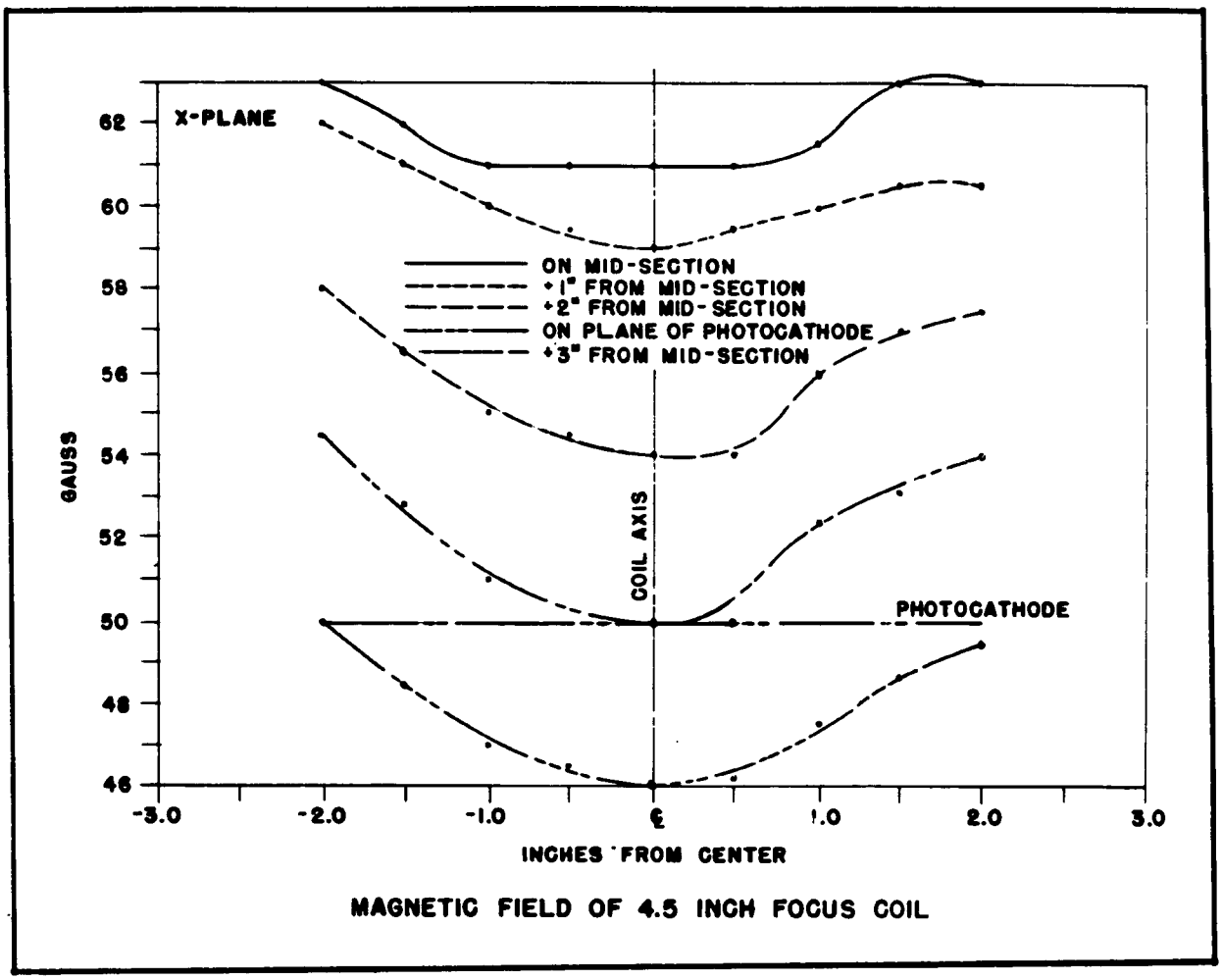

Figure 3-3. Radial Variation of Magnetic Field

as much as 2 inches from the axis (only the region within 1.5 inches from the center will be used for frames of 2 by 2 inches).

3.4 ELECTRONIC SHUTTER

An electronic shutter was designed, built, and operated on the demountable system. Figure 3-5a shows a schematic representation of the shutter envelope assembly. The spiral is discontinued in the area of the mesh, and a continuous ring of conductive material is deposited on the inside of the envelope in this region. This ensures that the mesh is at the same potential as the accelerator at that point. It was determined that only a few volts negative (with respect to the photocathode) were necessary to cut off completely the photoelectrons from the photocathode. Since the mesh is at 9 kv negative potential with the shutter open, the total voltage swing for the photoelectron cutoff is only 1000 volts. No evidence of the shutter could be seen

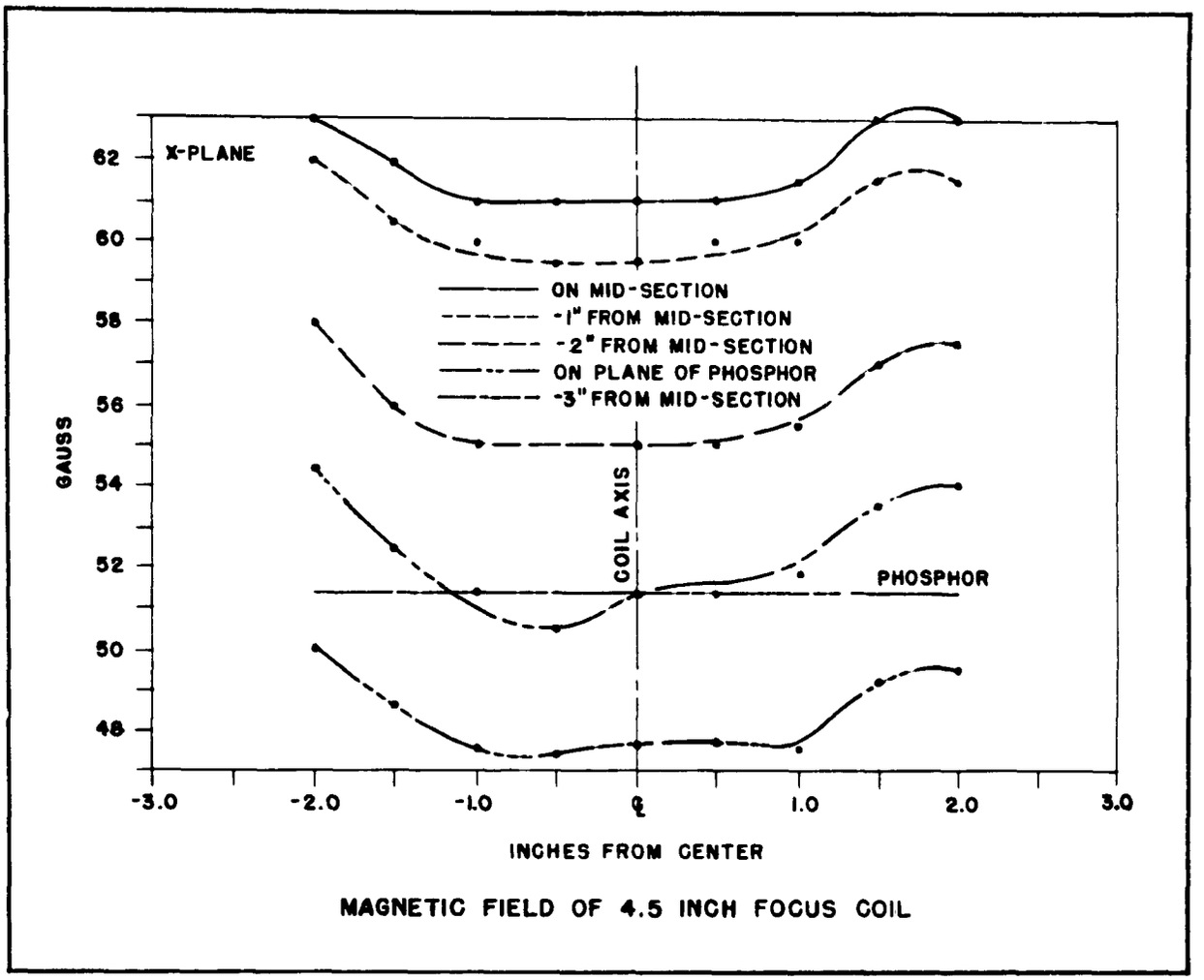

Figure 3-4. Same as Figure 3-3 on Phosphor Side Midsection

in a stored pattern of 500 lines per inch. This result is as expected, since the shutter screen is placed at the antinode of the focusing loop.

Figure 3-5b shows a simple resistive network which places the mesh at -10 kv and the photocathode about 25 volts less negative when the timer contacts close. When they open, it returns the spiral to normal operation.

The capacity of the shutter mesh to its surroundings is relatively low and a change of only about 1000 volts is needed for the exposure. With only a small power consumption, shutter exposures of 100 microseconds were attained in the experiments.

3.5 RESOLUTION MEASUREMENTS ON PHOTODIODES

Limiting resolutions were read by several observers on optically reduced RETMA charts. Complete aperture response curves were produced with the Westinghouse

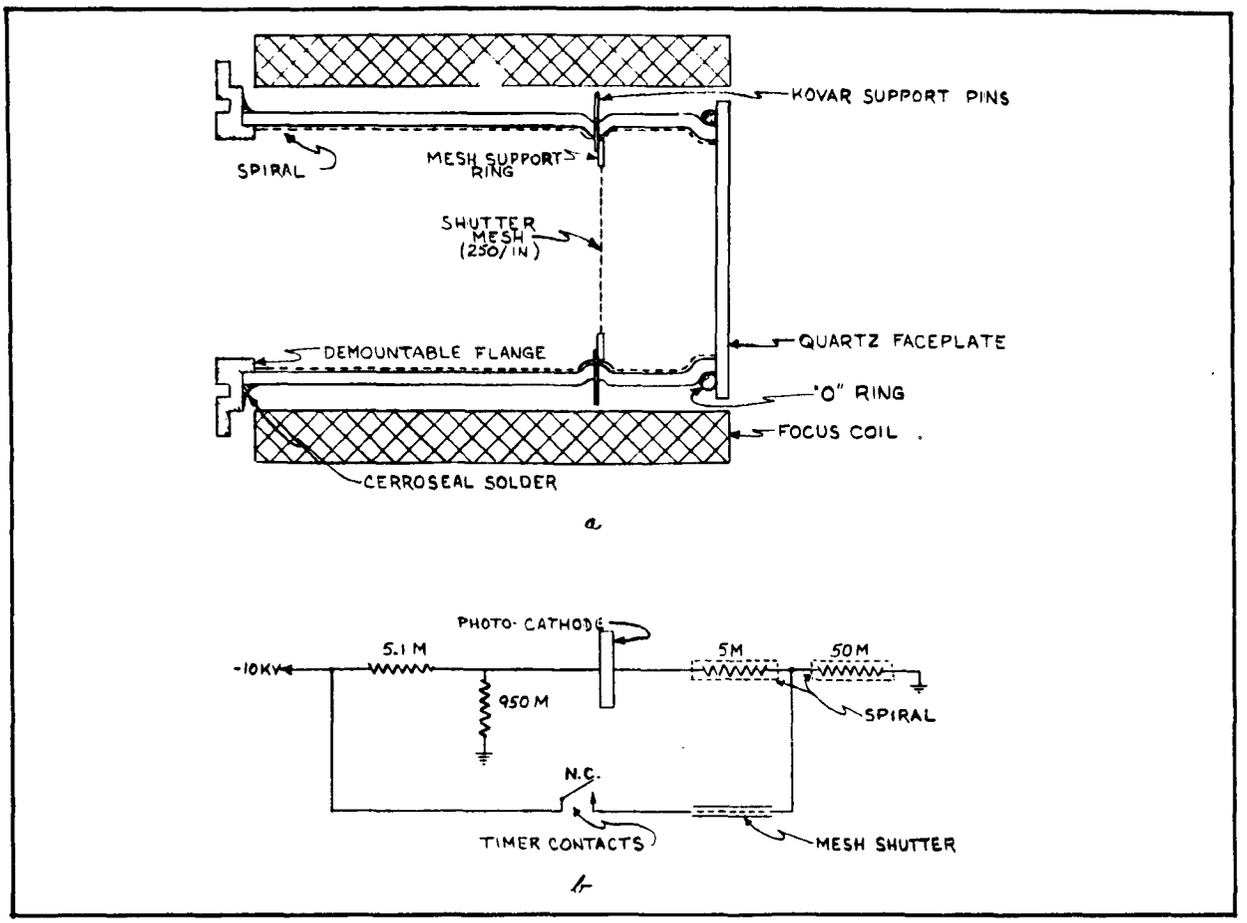

Figure 3-5. Electronic Shutter

diminishing bar pattern[1/] in procedures which were modified to the special purposes as shown in the following paragraphs. The limiting resolutions measured by observation always corresponded to a response between 3 and 5 percent on the aperture response curve.

3.5.1 Lens Resolution

The lenses used in all phases of the program were measured for their limiting resolution on the optical axis in the following way. The Westinghouse bar pattern was set up at a distance and the real optical image was observed by eye through a high quality microscope with 250X magnification. The distance was chosen in such a way that the image width of the smallest bars was near the limiting resolution. It was assumed and later found to be correct that the microscope resolution was nearly one order of magnitude better than the tested lenses. Therefore no correction was made here for the resolution by the microscope.

Table 3-2 shows the results of these measurements. Note that the limiting resolution was lower at higher f numbers, an outcome of the diffraction law. The highest resolutions were usually for one to two stops smaller than the largest lens aperture.

TABLE 3-2

LIMITING RESOLUTION OF OPTICAL LENSES

	Focal Length (mm)	Limiting Resolution (line pairs per mm)									
		f/1.9	2.7	3.5	4.5	5.4	8	11	16	22	32
Elgeet	76	-	-	268	268	268	161	102	61	34	-
Xenar	135	-	-	-	145	145	145	117	110	-	-
Zeiss Tessar	80	-	195	195	195	145	135	-	-	-	-
Zeiss Tessar	120	-	-	-	170	170	170	102	80	64	38
Zeiss Tessar	45	-	313	313	273	221	132	-	-	-	-
Kodak Anast.	13	460	650	460	354	275	200	-	-	-	-
Roussel	50	-	-	-	155	-	-	-	-	-	-
Ektanon	25.4	625	-	-	-	-	-	-	-	-	-
Brumberger	127	-	-	161	-	-	-	-	-	-	-

The whole aperture response curve of lenses was established by moving the Westinghouse pattern in front of a well illuminated slit. See figure 3-6. The lens system under examination made a known reduction of the test bars. The microscope with a 25X objective was well focused onto the real images and produced an enlarged image in the plane of the very fine slit (0.4 mil) in the microscope. A Westinghouse WX-7909 photomultiplier tube with an electron multiplication of 170,000 was installed on the ocular end. The signal from the tube was amplified and applied to a recorder.

The slit in the microscope was adjusted to be parallel to the bars, first by optical means, and then by rotating for maximum signal strength. The amplitudes of the bar signals on the recorder were measured and plotted against the computed bar width at the real image plane as in figures 3-7 and 3-8. A hand driven microscope stage with a potentiometer, a Densichron light recorder head on the microscope with amplifier, is shown in figure 3-9. The potentiometer was used for the positioning of an X-Y plotter. Note that all lens measurements were done on the optical axis of the lens only. The measurements in the next paragraph used images on the optical lens axis only.

3.5.2 Image Section Resolution

The setup for these measurements was similar to the one shown in figure 3-6 but with the addition of the photodiode and another lens (figure 3-10). The real image of

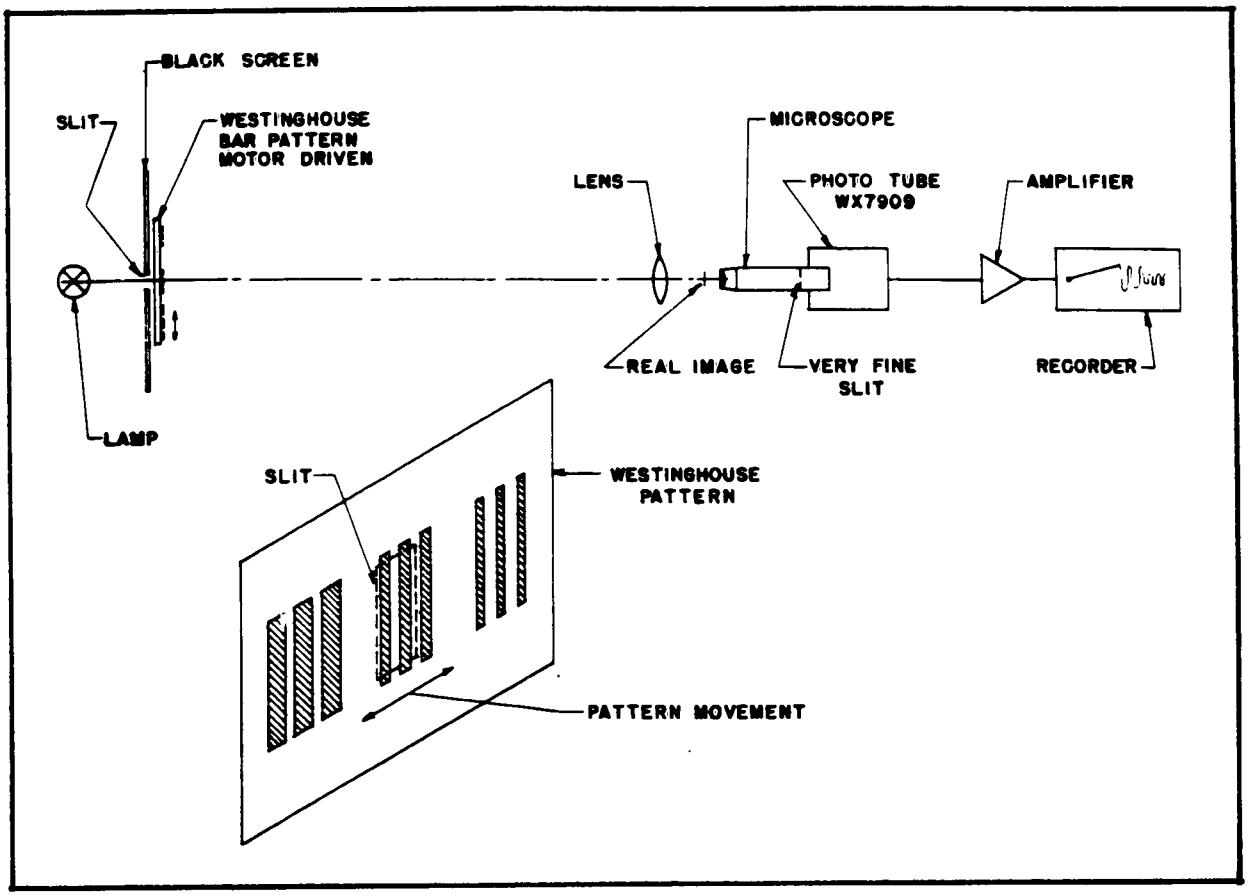

Figure 3-6. Lens Resolution Measurements

the bars was projected onto the photocathode of the photodiode. The reduction was computed from the lens equation and later verified with a cathedometer. The photoelectrons produced a 1 to 1 picture on the phosphor. The re-entrant exit window of the tubes is unfortunately so small in diameter that the microscope objective would not fit. Therefore an Elgeet lens was used as a relay lens to produce a 1 to 1 real image of the phosphor picture. The microscope was focused with its 25X objective onto this real image, and the light output through the slit in the microscope was recorded and plotted (as in paragraph 3.5.1). Off-axis measurements were made by moving the photodiode with its focus coil perpendicular to the optical axis. In this way all the lenses and the microscope were used on axis and did not change in aperture response (figure 2-2). Figure 3-11 shows the response as produced by the recorder. Table 3-3 shows the width of the bars in the groups of the Westinghouse bar pattern. The optical reduction at the photocathode was 15.7 times the reduced bar width which is also shown in table 3-3.

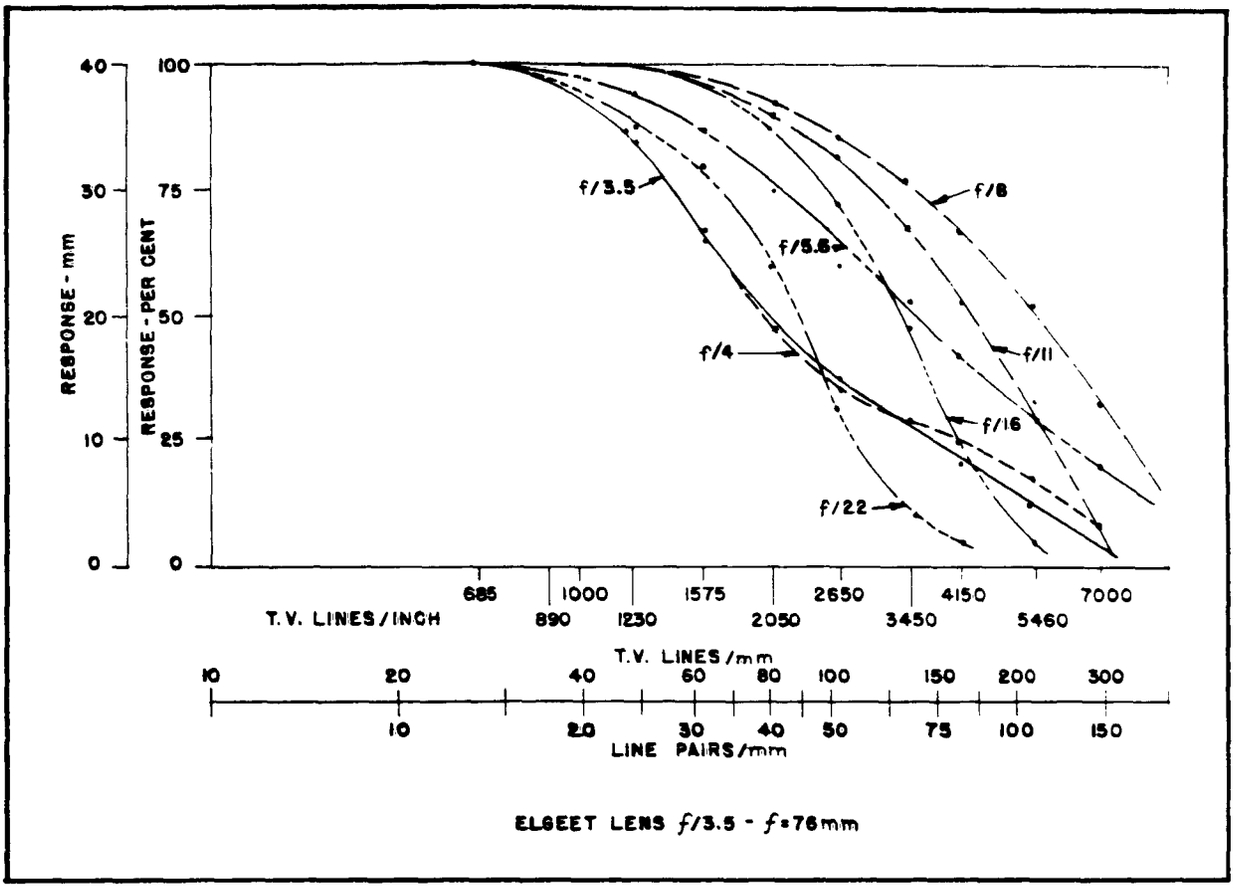

Figure 3-7. Square Wave Response of Elgeet Lens

In the last column of table 3-3 are the percent response for the corresponding bars as measured from the recorder strip and as later on used for plotting the "photodiode and lenses" square wave response on figure 3-12. The off-axis square wave aperture response of figures 3-13, 3-14, and 3-15 were done in the same way.

The off-axis curves were obtained by magnetically refocusing the pattern for optimum signal strength. For the points farthest out (1.375 inches) from the center, the focus current had to be reduced by about 2 percent. This can very well be seen on figure 3-2 which shows the field becoming stronger farther away from the axis. This refocusing does not bring the resolution to the high values of the center. The interaction with the electrostatic field, which is not everywhere parallel to the magnetic field, probably is the cause of this.

The center curve of figure 3-12 is the plot of the aperture response curve of the Xenar lens at f/5.6, the Elgeet lens at f/8, and the microscope together. The lower curve is the aperture response of all those optical devices plus the photodiode together as shown in figure 3-10.

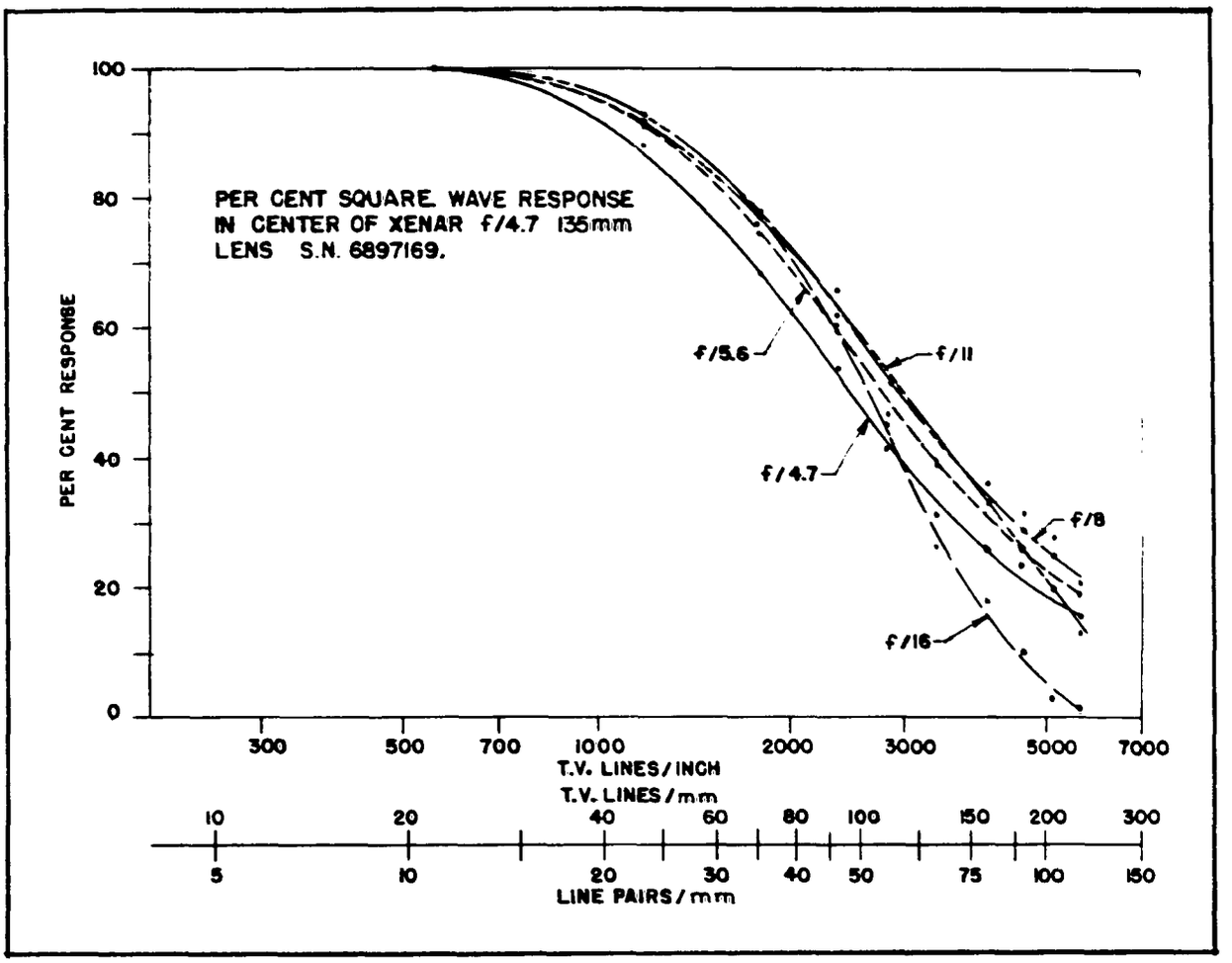

Figure 3-8. Square Wave Response of Xenar Lens

In Section 8 it is shown that the difference between using the sine wave response or the square wave (the Westinghouse pattern is the square wave) is not too significant as long as it is multiplied or divided not more than once. Therefore the ordinates of the combined curve were divided by the corresponding ordinates of the curve for the lenses along; this resulted in the curve labelled "photodiode alone."

Resolutions in the order to 4900 TV lines per inch or 98 line pairs per millimeter were observed by eye. The visually measured resolution was later confirmed by recording and plotting the aperture response curve on which the 5 percent response was at 4900 TV lines (98 line pairs per millimeter). On figure 3-12 it can be seen further that the limiting resolution of the photodiode alone (without the resolution limitation of the lenses) must be near 11,000 TV lines per inch or 220 line pairs per millimeter. No known electron beam from a gun is fine enough to produce picture with this high resolution.

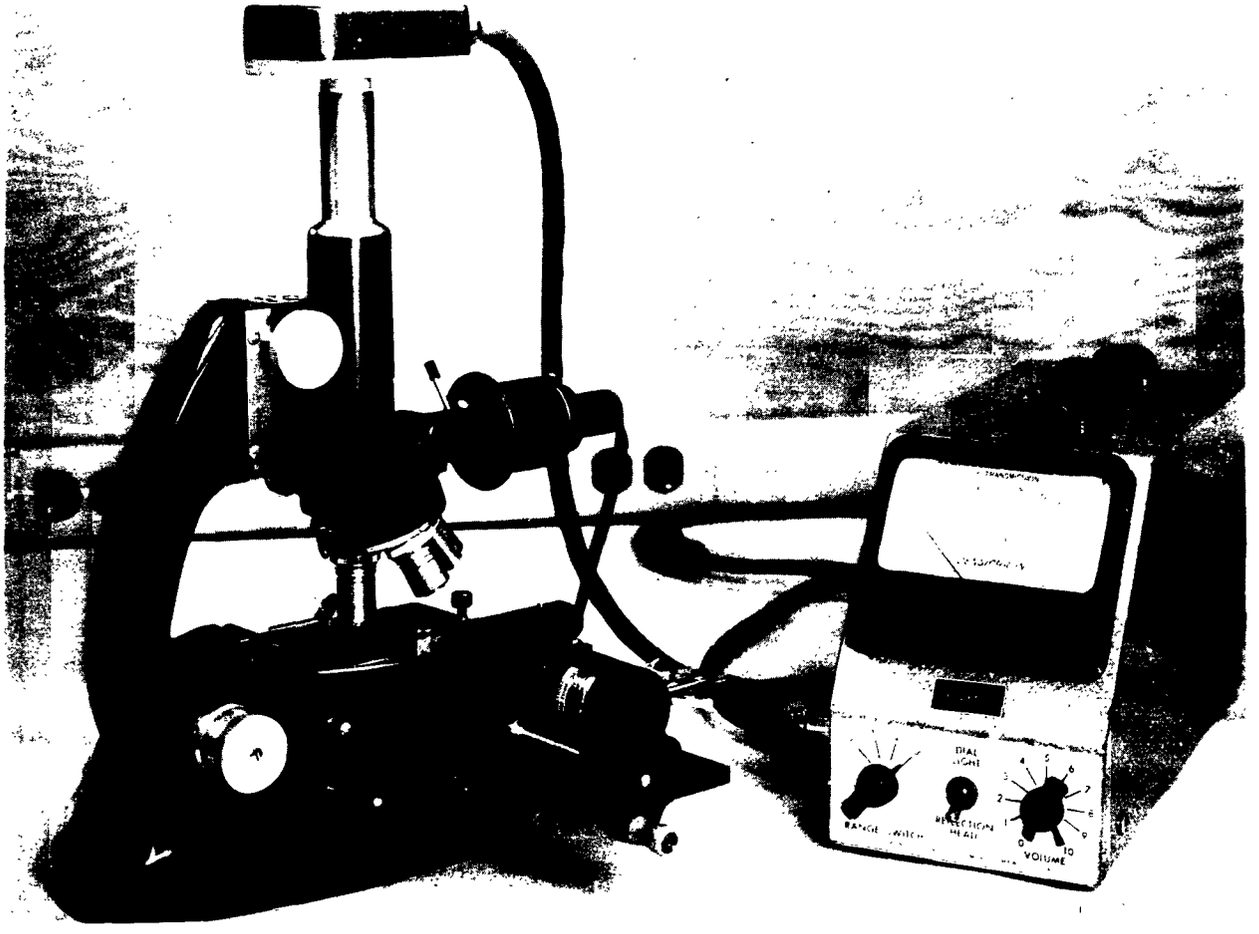

Figure 3-9. Microdensitometer for Response Measurements

The data of figures 3-12 to 3-15 can be replotted as in figure 3-16 to show a family of curves of resolution at a given square wave response as a function of radius from the coil axis.

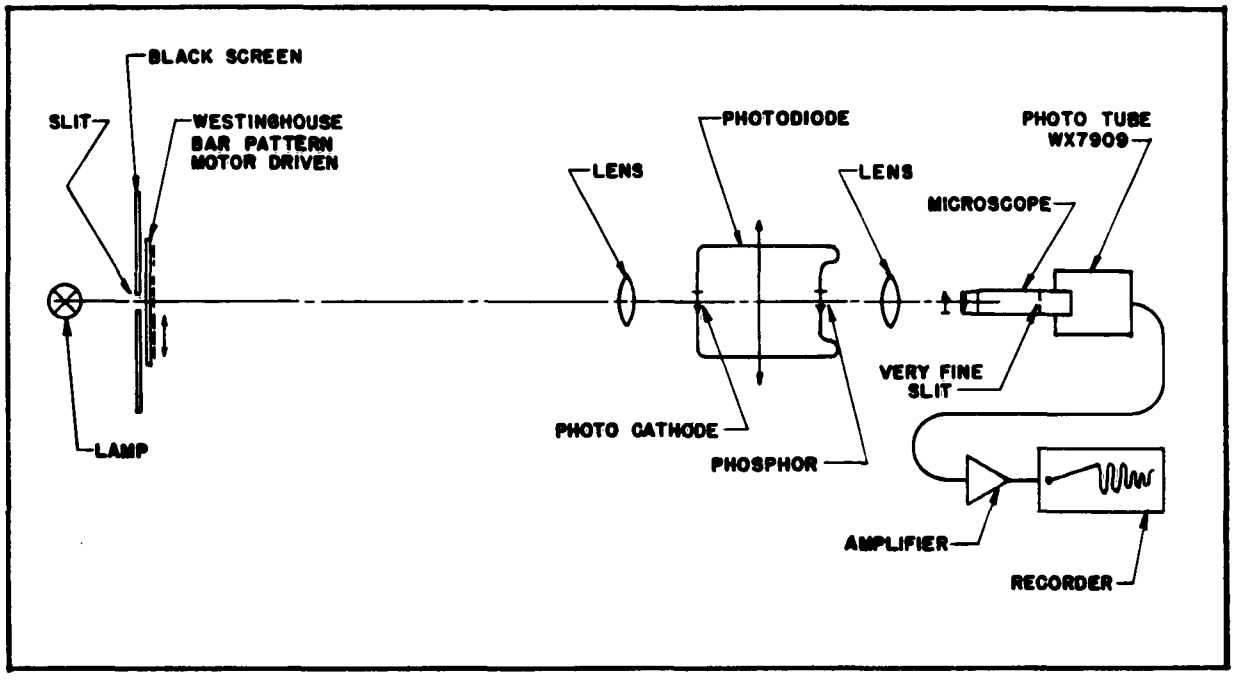

Figure 3-10. Image Section Resolution Measurements

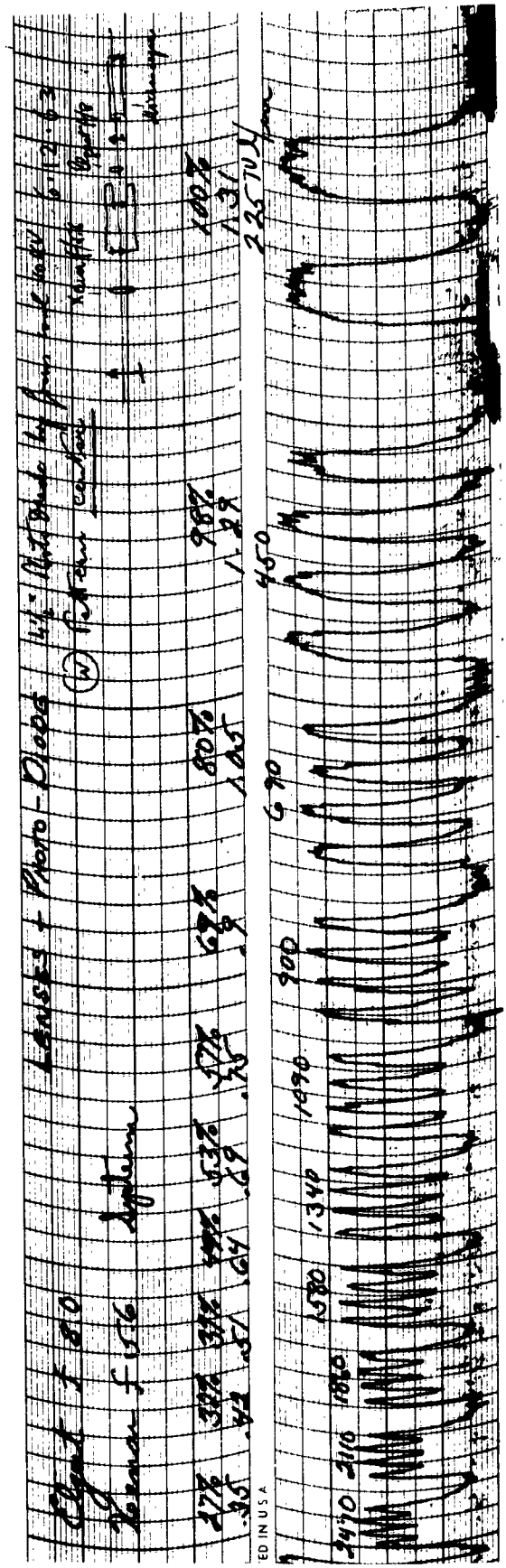

Figure 3-11. Recorder Trace of Bar Pattern, Photodiode Image

TABLE 3-3

TABLE FOR PLOTTING RESPONSE CURVE

Bar Group	Reduced (mils)	Reduced (mm)	15.7 Times Bar Width (mils)	15.7 Times Bar Width (μ)	TV Lines Per (inch)	TV Lines Per (mm)	Line Pairs Per (inch)	Line Pairs Per (mm)	Response (percent)
1	70.0	1.78	4.45	113.0	225	8.9	113	5.0	100.0
2	35.0	0.89	2.22	56.5	450	17.7	225	8.8	98.0
3	23.0	0.59	1.45	37.0	690	27.0	345	13.5	80.0
4	17.5	0.45	1.11	28.0	900	35.0	450	17.5	69.0
5	14.5	0.37	0.92	23.4	1090	43.0	545	21.5	57.0
6	11.8	0.3	0.75	19.0	1340	53.0	670	26.5	53.0
7	10.0	0.25	0.63	16.0	1580	62.0	790	31.0	49.0
8	8.5	0.22	0.54	13.7	1860	73.0	930	36.5	39.0
9	7.5	0.19	0.475	12.0	2110	83.0	1060	41.5	32.0
10	6.4	0.16	0.41	10.4	2470	97.0	1240	48.5	27.0

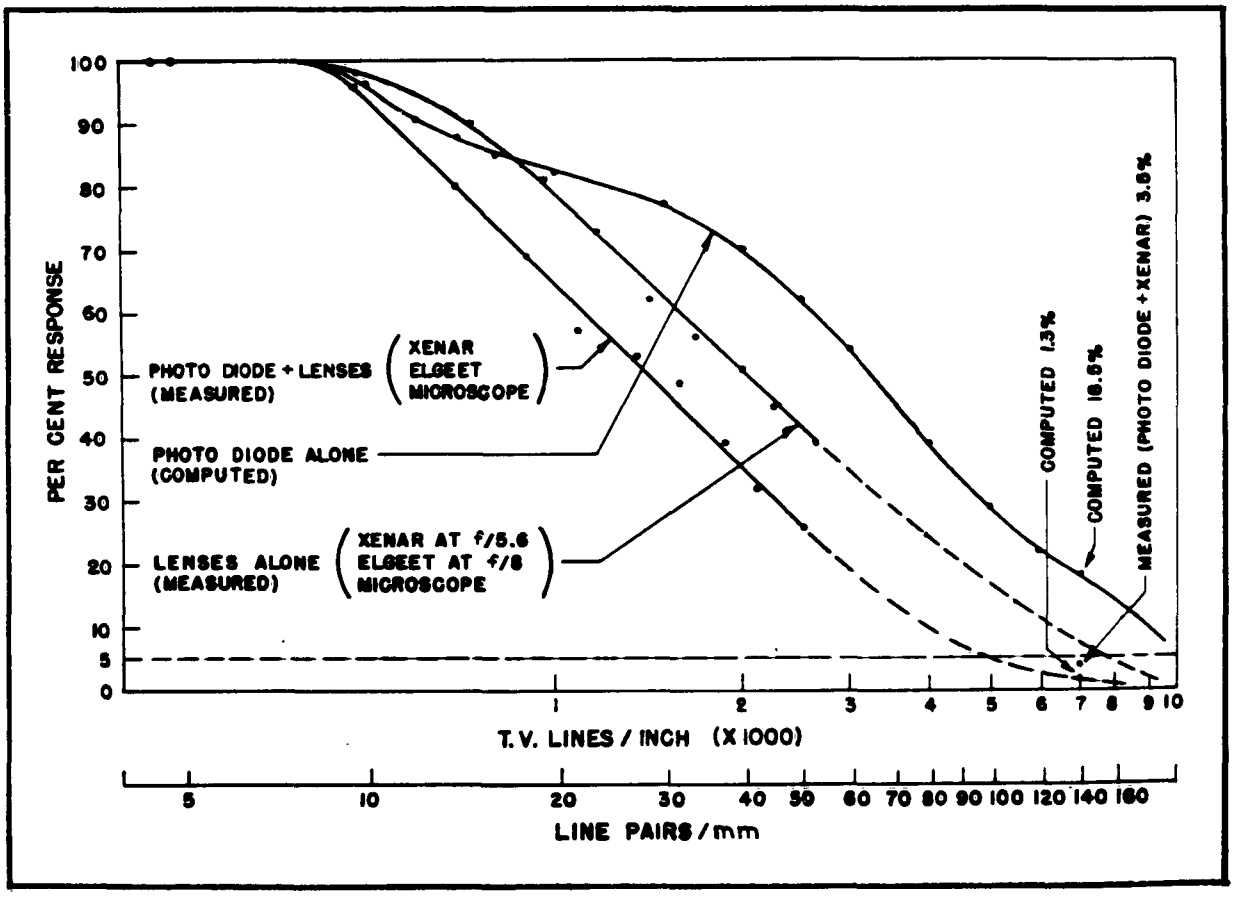

Figure 3-12. Square Wave Response for Photodiode. on Axis

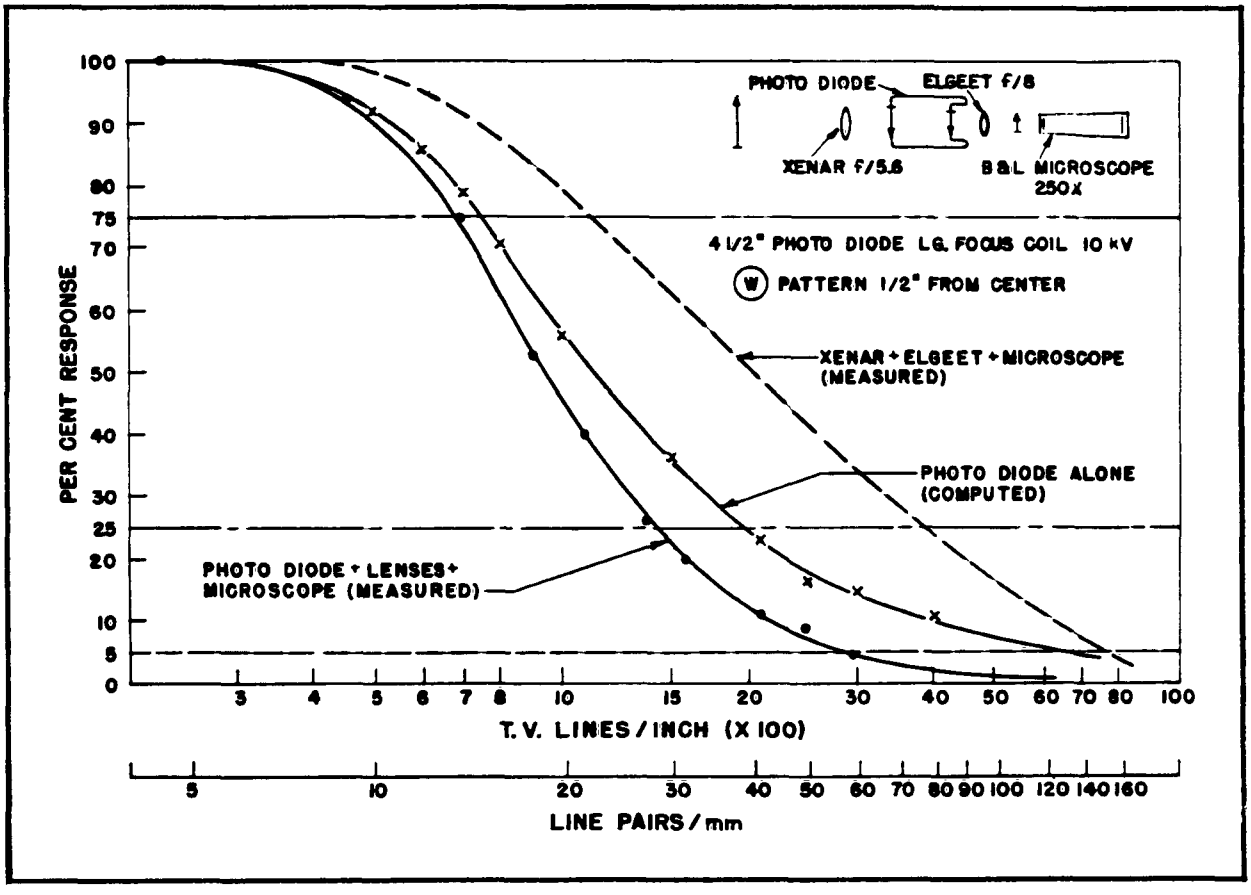

Figure 3-13. Square Wave Response for Photodiode 1/2 Inch From Center

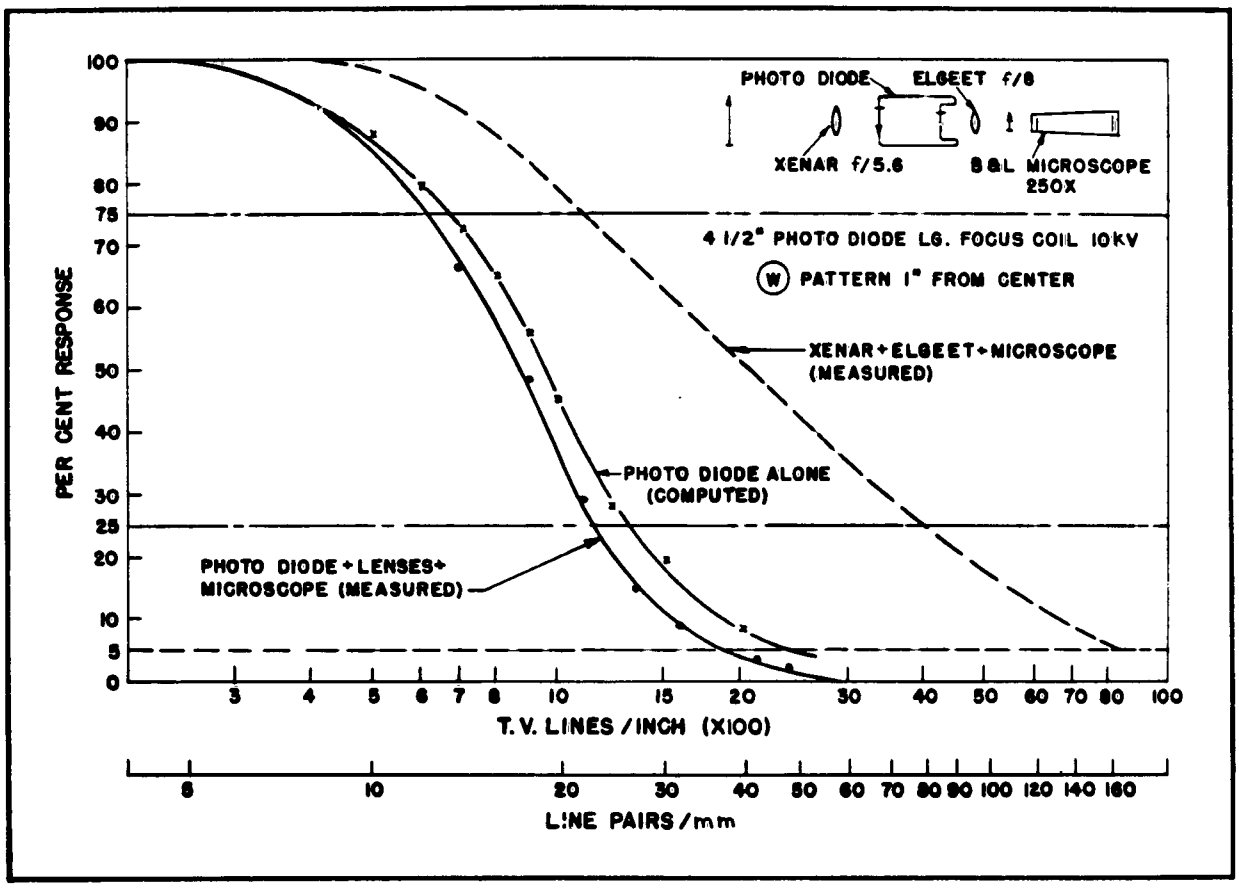

Figure 3-14. Square Wave Response for Photodiode 1 Inch From Center

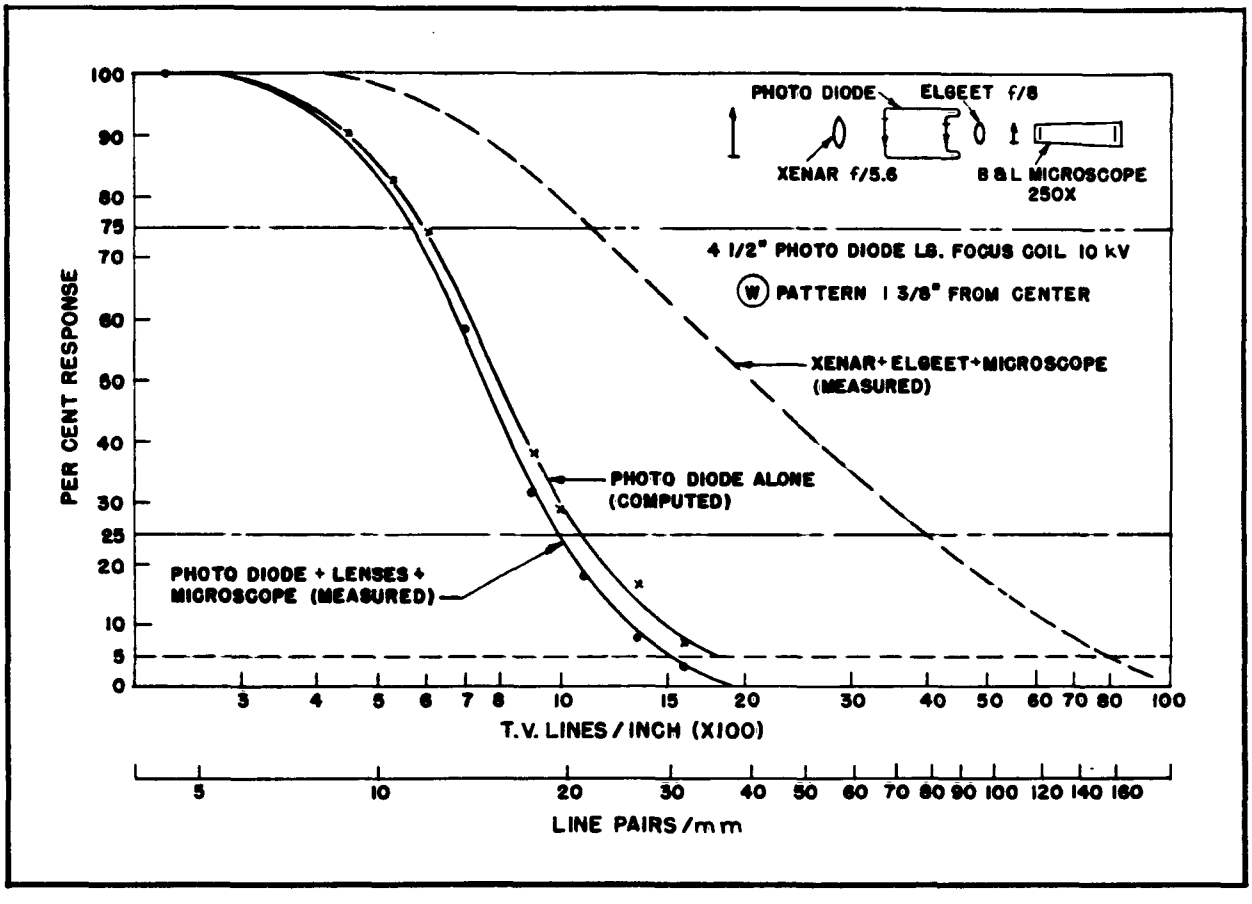

Figure 3-15. Square Wave Response for Photodiode 1-3/8 Inch From Center

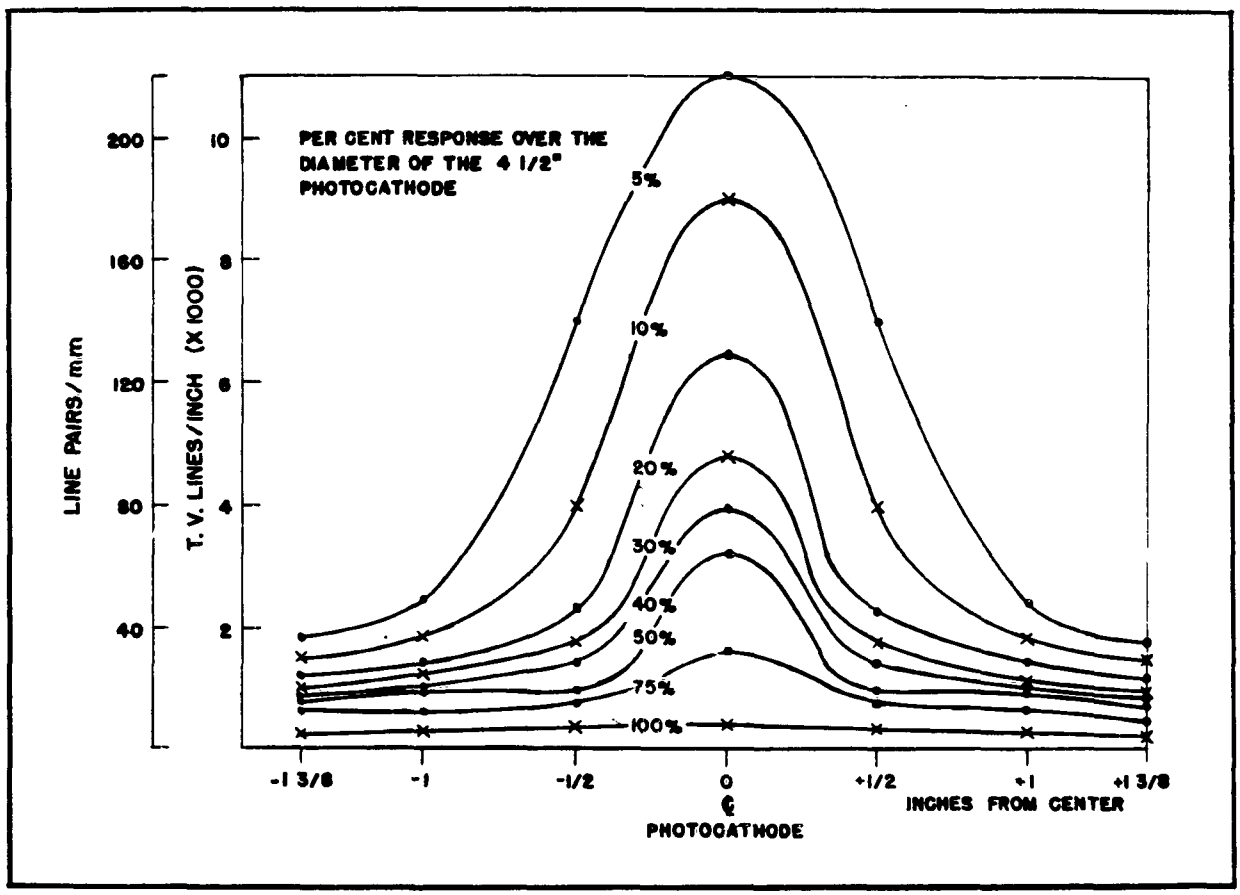

Figure 3-16. Photodiode Resolution Variation With Radius

4. STORAGE TARGET TAPE CHARACTERISTICS

4.1 DIELECTRIC STUDY

To facilitate selecting compounds having high specific resistance and low dielectric constants, it is desirable to compare the existing data on the dielectric constants and specific resistances of the various alkali and alkaline-earth halides and oxides which can be used in vacuum evaporation thin film studies. A desirable minimum for the volume resistivity, ρ, would be on the order of 10^{18} ohm-centimeter. Other desirable qualities include good evaporation characteristics and the capability of good adhesion to the substrate.

The dielectric constant, ϵ, of an insulator is the ratio of the capacitance, Cp, of a given set of electrodes with the material being studied as the dielectric to the capacitance, Cr, of the same electrode configuration with a vacuum as the dielectric. Methods of measuring ϵ are best described in ASTM Standards, Part II, 1961; pp. 859-912.

Electrical resistance, in particular volume resistivity ρ, is calculated from the formula

$$\rho = \frac{AR_v}{s}$$

where

R_v = sample resistance, in ohms

s = average thickness of sample

A = effective area of the electrodes

For approved methods of measurement refer to ASTM Standards Part II, 1961; pp. 988-999.

Generally speaking, a strong and rigid chemical bond in an oxide or halide will produce high resistivity and a small dielectric constant. This characteristic is also to be expected in a good insulator, according to E. Ryshkewitch[2]. One simple means of relating chemical bonding to electric properties is through a study of lattice energies.* According to an article by A. P. Nakhodnova[3], the electrical conductivity,

* Lattice energy is the energy required to separate the ions of a crystal to an infinite distance from each other.

dielectric constant, and tan δ generally all increase as the lattice energy decreases. For example, note the relationships between the lattice energy and the dielectric constants of various alkaline-earth oxides in the table below. The lattice energy is given in kilocalories per mole.

Compound	BeO	MgO	CaO	SrO	BaO
Lattice energy[4]	1080	936	830	784	740
Dielectric constant[5] ϵ	7.35	9.65	11.8	13.3	34.0

Unfortunately, no published data were available at the time of this report to correlate the hypothesis with the fluoride group, but there is no reason to believe that the pattern is not the same. Thus it has become possible to select a low dielectric constant compound from other groups in the periodic chart when the data are available.

A comparison of the negative heat of formation energy* ($-\Delta F_f$) of the compound with its dielectric constant indicates the periodicity shown in the following tables. The negative heats of formation are given in kilocalories per mole.

	LiF	NaF	KF	RbF	CsF
ϵ[2]	9.27	6.00	6.05	5.91	5.90
$-\Delta F_f$[6]	145.6	136	134.5	133.2	126.9

	BeF_2	MgF_2	CaF_2	SrF_2	BaF_2
ϵ[2]	<5.0	5.30	6.76	7.69	7.33
$-\Delta F_f$[6]	251.4	263.5	290.3	289.0	286

It appears that BeF_2 and the alkali halides and fluorides most nearly approach the requirements of a low dielectric constant. Although their specific resistances are not presently known, it must be assumed that they are very high since all of these compounds have high chemical bonding strengths.

* Formation energy is the negative heat energy of formation of the compounds from the elements.

The dielectric constants of the alkaline earth and alkali salts exhibit predictable trends according to their position in the periodic table with respect to ascending or descending atomic number. Exceptions are the fluorides and chlorides of lithium which have inordinately high dielectric constants. The exceptions probably occur because lithium salts deviate from the structure of the others in Group Ia of the periodic table. Note that in the alkaline earth group, the tendency is for the dielectric constant to increase with the increase in atomic number. However, the more electropositive ion (Be^{++}) has a low dielectric constant while in the Group Ia series, three of the alkalis have approximately the same value. This condition is probably explained by the fact that the crystal lattices of Na, K, Rb, and Cs salts are all cubic, while those of Li, Ba, Sr, Ca, and Mg are more complex and have entirely different lattice energies. In general, those salts with the most compact and stable cubic structure offer the best possibilities for low dielectric constant and high resistance.

Investigation of the resistivities and dielectric constants of the oxides and halides of the various atomic groups in the periodic table shows the choice of inorganic salts to be rather limited. Further investigation of the Group Ia and Group IIa salts shows that only a few chlorides and fluorides have good insulation properties and are suitable for vacuum evaporation. The chlorides are those of Na, K, Rb, and Cs and the fluorides are those of Be and Mg.

The only other suitable compounds might come from the oxides of Groups IIIa, IVb, Vb, and VIb. However, the evaporation characteristics of those compounds with the lowest dielectric constants are not good, and other means must be used to obtain them in thin films with good strength and high density. Also the oxides from these groups are particularly susceptible to poisoning by other elements, including common gases. The resistivities of these oxides decrease very rapidly with only a small contamination. In addition, it is extremely difficult to process these materials into their theoretically maximum density, purity, and resistance states. Ryshkewitch[2] gives a rather thorough treatment of the oxides of Al, Mg, Be, Ca and a few of the rare earths. The sampling of the resistivities and dielectric constants of the transitional oxides given in table 4-1 shows that generally they do not meet the requirements of the problem[2]. (See also figures 4-1 and 4-2.)

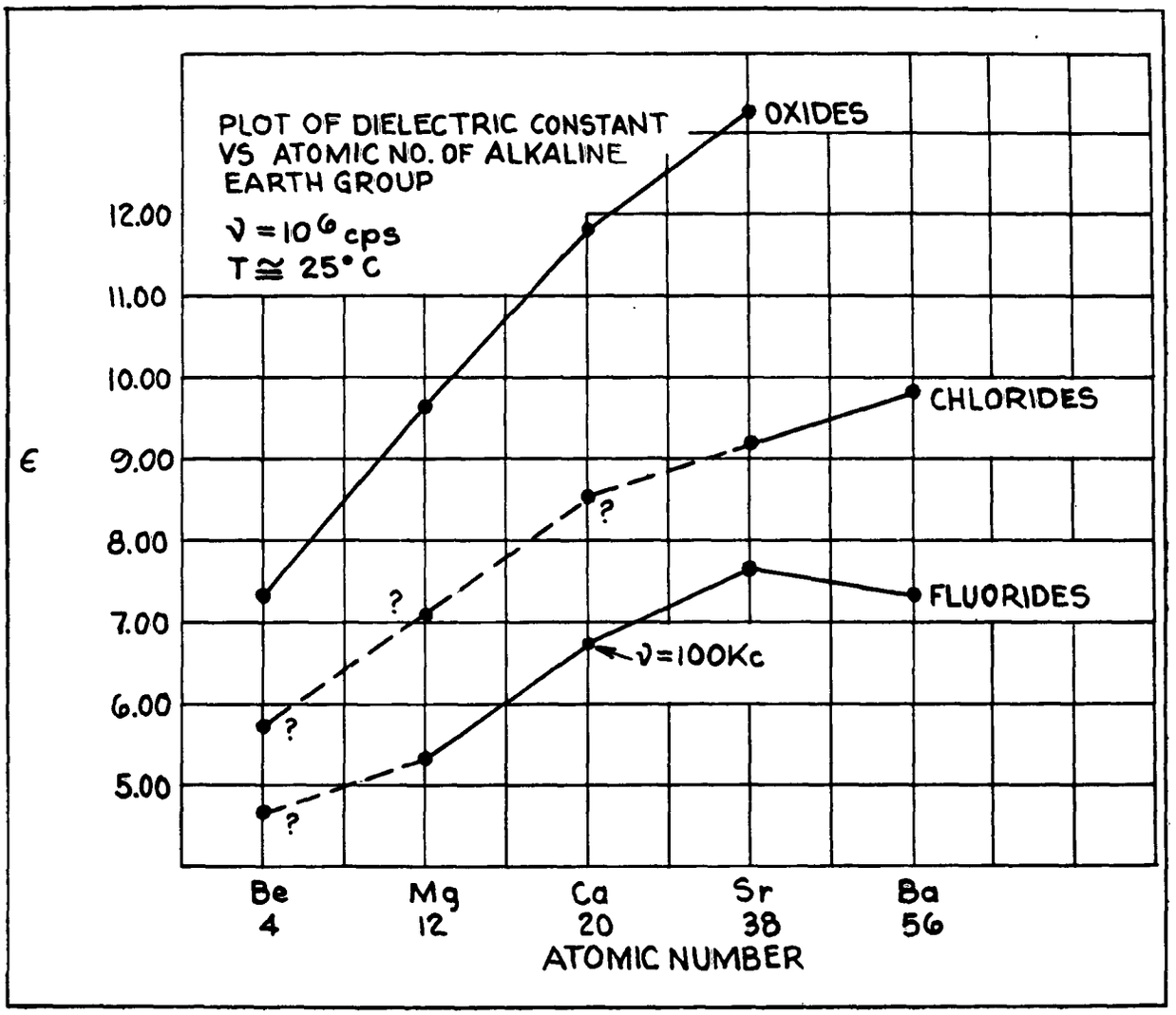

Figure 4-1. Dielectric Properties of Metal Salts

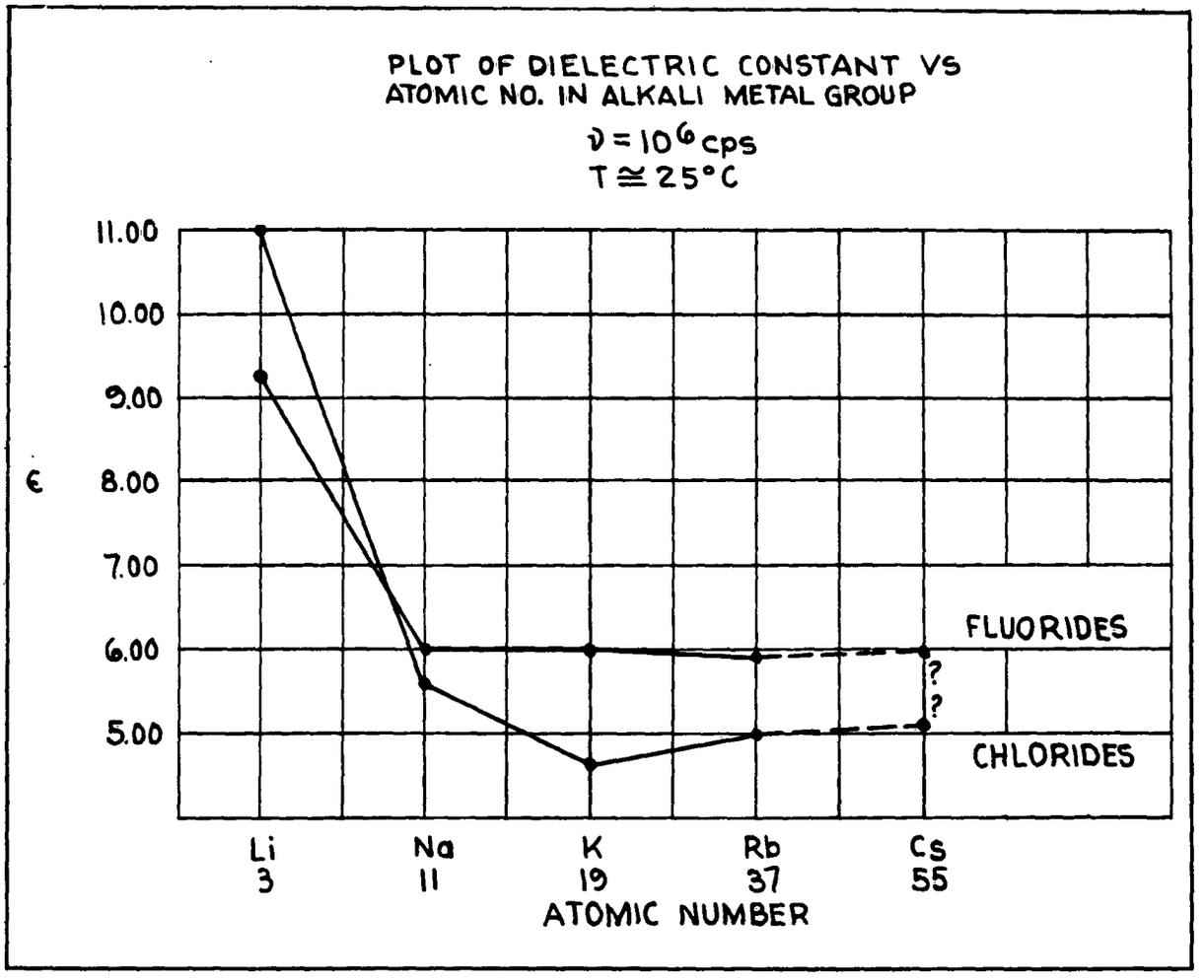

Figure 4-2. Dielectric Properties of Metal Salts

TABLE 4-1

TRANSITIONAL OXIDES

Oxide	Dielectric Constant	Specific Resistance
Ta_2O_5	11.6	
TiO_2 (Rutile)	100.0	
Cr_2O_3	12.0	
ZrO_2	12.5	3300 ohm-cm (697°C)
Ba_2SiO_4	13.0 (theoretical)	
CeO_2 (Ceria)	7.0	5×10^7 ohm-cm (500°C)
BeO	6.3 (Bur. of Stds)	10^8 ohm-cm (500°C)
Al_2O_3 (High Dens)	9.39	1.2×10^{13} ohm-cm (300°C)

Mention might be made of the work by Hass, Ramsey and Thun[7] on some of the rare earth oxides and fluorides used for evaporated films. Although the authors give no data for resistivity and dielectric constant, they do reach the following conclusions:

a. The oxides are usually condensed as nearly amorphous films.

b. The fluorides are usually condensed as large grains.

c. All films are hard and have excellent chemical and mechanical durability.

d. Amorphous film structures frequently are more influenced by small changes in deposition condition than are the well crystallized forms.

This information, too, indicates that .e fluorides and chlorides of Groups Ia and IIa are probably the best choices for vacuum evaporated films unless a choice can be made from such organic materials as polyethylene[8] (dielectric constant = 2.3 and resistivity = 10^7 to 10^9 ohm-cm), polystyrene[8] (dielectric constant = 2.7 and resistivity = 10^{17} to 10^{19} ohm-cm), or teflon[9] (dielectric constant $\approx$ 2.0 and resistivity $>10^{15}$ ohm-cm).

4.2 STORAGE TARGET CAPACITANCE

For computation of electron gain, measurements of the dielectric constant of the used material must be made. The dielectric constant of materials used for target storage surfaces can be computed using the following relationship:

$$C = \epsilon_o \epsilon A/S$$

where,

C = capacitance in farads

A = area of plates in meters^2

S = thickness of dielectric in meters

ϵ = dielectric constant

$\epsilon_o = 8.85 \times 10^{-12}$ farad/meter

The thickness, s, is measured during evaporation by observing the color of the light reflected from the interference film. The accuracy of this method of measuring dielectric films may be estimated by observing that an error in the determination of color from yellow to green for a second order film would only make a thickness variation of 0.05 micron out of a total thickness of 0.5 micron. This corresponds to a thickness error of approximately 10 percent. However, since the interference colors are vivid and easy to see after observing them a few times, it is felt that the accuracy and reproducibility of these methods is much better than at 10 percent. The area is measured on a traveling microscope and the capacitance on a 1 percent impedance bridge. It is believed that the total error of the measurement of capacitance will be less than 10 percent. The thickness range of the dielectric will be 0.2 to 1×10^{-6} meters, and the area 1 square centimeter or less.

The first capacitors of 1 square centimeter were shorted for all values of thickness. These were a 1 square centimeter spot on a larger area. A crossed stripe sandwich was tried next, but was still not successful in avoiding shorts. By reducing the width of the stripes to 2 millimeters and rigorously glow discharge cleaning the substrate, a measure of success was finally achieved.

Generally, the substrate which gave the best results was aluminum on glass. Other materials used were gold and chromium, the former to minimize oxide formation, the latter for better adhesion. Electropolished stainless and nichrome bases were also used with negative results.

Such thin film capacitors are characterized by voids, holes, cracks, and trapped dirt. Local areas (less than 1 square micron) can exhibit very high capacitance, but rather low voltage breakdown. After fabrications, the test capacitors are aged at

50 vac to burn away these thin areas and then the capacitance is measured. These measurements indicated an apparent value of ϵ between 15 and 20. Tests of signal writing speed, both in a demountable vacuum system and in sealed off tubes, made earlier in this program and published data on MgF_2 gave values of ϵ of approximately 5. It is quite probable that these first capacitance measurements included the anomalous side effects of the voids, cracks, etc, but which have little effect on tube operation.

Later measurements were made on samples formed by a first evaporation of an aluminum electrode on a glass substrate followed by a second evaporation of the dielectric. The second electrode was a foil pressed with a rubber dam against the dielectric. This bridged any small pinholes or thin spots in the dielectric. The average measurements of these dielectric constants were 5 for magnesium fluoride and 6.7 for calcium fluoride, in agreement with the writing speed measurements and published data for bulk material.

In the UV-gold photocathode demountable vacuum system both grating storage targets and flat continuous dielectric targets were discharged by secondary electron emission. Photoelectron current was separately measurable by a sensitive microammeter. Secondary emission ratio was measured by an experiment, as described in paragraph 4.4.2. Particular care had to be taken with the electron optics to prevent redistribution of secondary electrons. The primed target was exposed for well defined times and the discharge of the target surface (voltage drop) was measured by slowly making the cathode more negative. At the moment when the storage target became visible on the kinescope, the cathode potential was measured. The same method of measurement was used for both the priming voltage and the voltage after discharge. Therefore deviations by contact potentials and voltage drop in the cathode were cancelled out.

Discharge curves were plotted as function of time, and the initial rate of discharge used for computation to eliminate any effects of redistribution. These measurements showed that there is nearly no difference in capacitance per unit area between a uniform dielectric storage target and the grooved shape partially coated storage surface of the TVIST target. The capacitance of areas of the surface against the adjacent bare metal stripes seems to compensate somewhat smaller area of the dielectric surface. Typically, for a 0.4 micron thickness of magnesium fluoride on a grating target, taking the secondary emission ratio as 5.9 at the incident 440 volts, the capacitance per unit area was measured to be 106 $\mu\mu fd/mm^2$. Taking no account of

the grating structure but using the area normal to the electron beam, this indicates an effective dielectric constant of 4.8.

It is instructive from an information storage point of view to note the capacitance per unit area, measured at about 10^{-10} fd/mm^2. For maximum reading signal about 3 volts of stored signal is required. This corresponds to 2×10^9 e/mm^2. A minimum resolution element requires about 10 microns, this is about 2×10^5 e/element. This means that a signal-to-noise ratio of 600 is possible in the stored signal. The capacitance of such a 10-micron element is about 10^{-14} fd/element. These capacitances per unit area are important for the computation of writing speed, sensitivity, and erasing time.

4.3 STORAGE TIME

4.3.1 Time Constant

In experiments described in paragraph 6.3.4 aperture response curves were plotted both immediately after writing and again after 41 hours of storage time. Since these indicated no loss in resolution, the charge leakage can be assumed to be entirely through the thickness of the dielectric. The signal strength had reduced to 58 percent of the original during the 41 hours storage.

For a storage target which was primed to -16 volts against the metal base, the reading transfer curve for a reading cathode at -11 volts against base (figure 6-12) shows that a 42-percent loss in return beam strength corresponds to a reduction in the voltage across the dielectric from -16 to -14.6 volts only. From this fact, assuming the resistance to be independent of the voltage and assuming a dielectric constant of 5 for magnesium fluoride as indicated in 4.2 above, the resistivity is computed to be 3.8×10^{18} ohm-centimeter, which is in reasonable agreement with published values. The time constant of such a capacitor is computed to be 467 hours.

4.3.2 Cobalt-60 Irradiation

During the course of storage time measurements of a flip-over target storage camera tube, an attempt was made to determine the effect of a gamma radiation field on the decay of the stored image. An image was stored in a normal manner and the target was then left facing toward the photocathode. The optical lens was removed, the focus fields turned off, and the tube left under these conditions for 1/2 hour. After this time, the signal amplitude was measured with a line selector and A-scope and compared with the signal level of the original stored image. Exactly the same technique was used again with the exception that a 0.75 millicurie Co-60

source was placed against the photocathode for the same 1/2 hour storage time. This source produced a gamma radiation field of 52 milliroentgen per hour at the target 5 inches away. The total radiation during the 1/2 hour time was 26 milliroentgen. This computed value was varified within 10 percent by means of a geiger counter. There was no measurable difference in signal amplitude decay between the two tests.

4.4 PRESTORAGE GAIN

4.4.1 EBIC Gain

The UV-gold photocathode demountable vacuum system used in this experiment was the same as used in the measurement of storage target capacitance described in paragraph 4.2. This was not only convenient but reliable since confidence could be had in the voltage and current measurements, and the target capacitance had already been measured in the same equipment. The same procedure was used. The photoelectron current was measured with a sensitive microammeter. The primed target was exposed to the 10 Kev photoelectrons for well defined time intervals. The discharge of the voltage of the target surface was measured by slowly making the reading cathode more negative. At the moment when the storage target became visible on the kinescope,the cathode potential was measured. The same method of measurement was used for both the primed condition and the discharge condition. Therefore, the difference in the cathode voltages equalled the discharge voltage, deviations due to contact potentials and voltage drop in the cathode cancelling out. Discharge curves were plotted as a function of time. The initial rate of discharge was used for computation to eliminate the effects of variation of EBIC gain with voltage gradient, since the reading characteristics determine that only the first 3 volts discharge out of 12 volts is of interest for writing. Values of EBIC gain for magnesium fluoride were measured between 5.7 and 10, averaging about 7. More work needs to be done to determine the dependence of EBIC gain on dielectric thickness.

4.4.2 Secondary Emission Measurements

The system diagrammed in figure 4-3 was used to measure the secondary emission characteristics of a dielectric target between its first and second cross over points. The setup includes a demountable Pyrex Tee enclosure with an electrostatically focused and deflected reading or probe gun, a flood gun, an electrostatic collimating lens, and a target support plate behind a mesh.

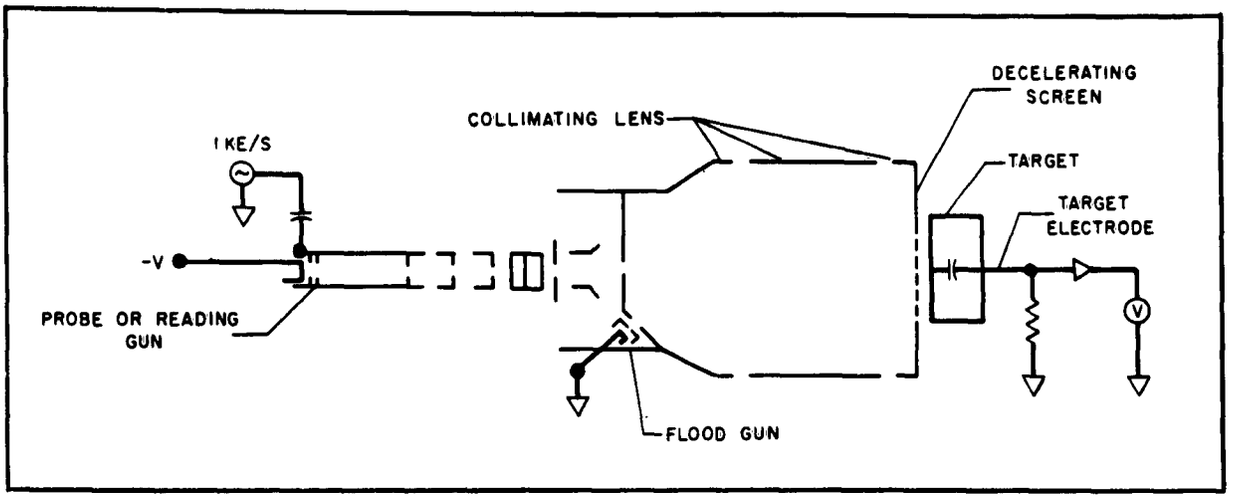

Figure 4-3. Secondary Emission Measurements

During the measurements the dielectric target surface is held at ground potential by setting the target electrode and the flood gun cathode at ground and having a high flood gun current density with respect to the probe gun current density. Then the probe gun cathode is made negative (from -50 to -400 volts) with respect to ground and even though it will tend to discharge the surface by secondary emission, the flood gun will concurrently recharge the surface and hold it at ground. Computations of the secondary emission ratio, δ, are made as follows: a 1-kc signal is put on the grid of the probe gun, then the resulting current through or away from the target is read at the target electrode after being amplified and passed through a narrow band filter tuned to 1-kc. The equation,

$$I_{primary} = I_{secondary} + I_{collected},$$

yields

$$1 - (I_{collected}/I_{primary}),$$

and $I_{collected}$ is negative between cross overs. Therefore, δ can be computed from the ratio of the amplitude of the 1-kc signal through the target to the amplitude of this signal in the primary beam incident on the target. Since the target is held at ground potential,the secondary emission characteristic is obtained by plotting, as a function of the primary beam's energy (proportional to the potential of the probe gun cathode), δ for that potential.

Using the equipment and techniques described above,the secondary emission measurements were made on nine target surfaces between first cross over and approximately 500 volts. These are tabulated in table 4-2; figure 4-4 shows secondary emission characteristic curves for the first 5 of these targets.

TABLE 4-2

SECONDARY EMISSION RATIO MAXIMA

Target No.	Substrate	Dielectric	Thickness, μ	Maximum	$V_{prim/max}$ (volts)
1	Al-flat	MgF2	0.40	6.43	330
2	Ni-flat	MgF2	0.34	6.55	350
3	Ni-grating	MgF2	0.34	5.90	430
4	Cu-flat	MgF2	0.40	5.50	330
5	Cu-grating	MgF2	0.40	5.32	330
6	Ni-flat	MgF2	1.0	5.35	340
7	Ni-grating	MgF2	1.0	3.26	370
8	Ni-flat	CaF2	0.30	5.40	470
9	Ni-grating	CaF2	0.40	7.10	480

This data were necessary to enable the quantitative measurement of dielectric constant and capacitance. The measure of EBIC gain was essentially a manner of comparing EBIC gain to secondary emission gain. These curves again were required to evaluate the EBIC gain from this ratio.

4.5 TAPE FABRICATION

4.5.1 Electroform Technique

Storage target substrates for flip-over target storage camera tubes with the required sawtooth cross section and groove numbers, about 240 per millimeter, have been fabricated. A high quality diffraction grating replica was purchased having the proper number of grooves per millimeter and the required groove shape. This diffraction grating was carefully mounted in a plastic frame and made conductive with a deposited thin conductive layer. This surface was then electroplated with a low stress nickel to a heavy rigid thickness of approximately 50 to 80 mils. The electroformed material was then removed from the diffraction grating, being then the submaster which is a faithful replica of the diffraction grating.

From this nickel submaster target, substrates could be produced by the same electroforming technique. These substrates were produced with thicknesses of only 20 mils. The material may be cut and trimmed by normal techniques to fit the purpose intended. Rigid target substrates have been made by this method in groove numbers from 40 per millimeter to as high as 720 per millimeter.

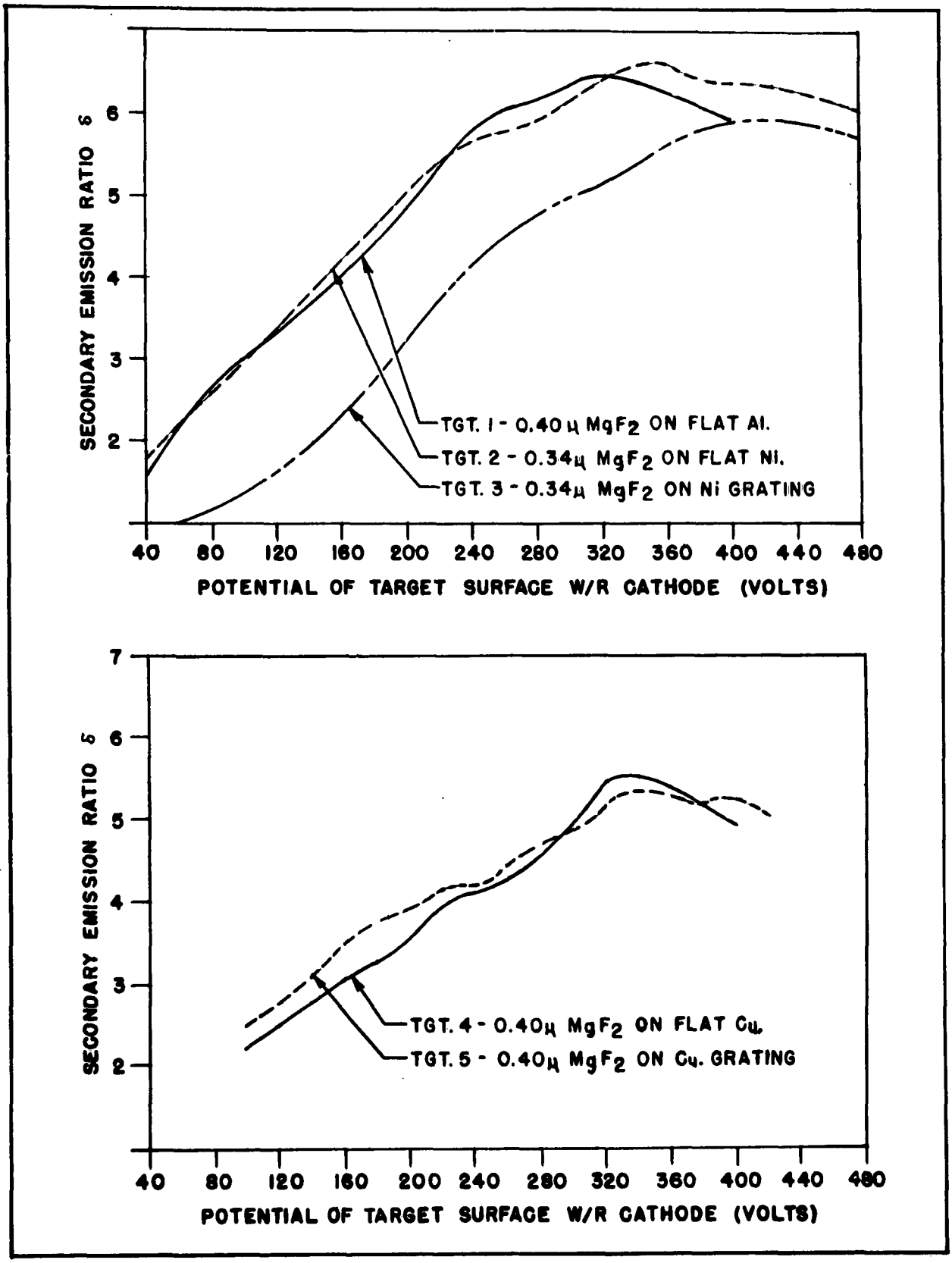

Figure 4-4. Secondary Emission Characteristic Curves

4.5.2 Frame Tapes

Several lengths of tape consisting of 2-inch square frames were made. These tapes were about 1-mil thick and approximately 18-inches long. Ten of the 20-mil rigid submasters were carefully machined and deburred to 2 inches by 2 inches. These plates were then carefully mounted with a contact adhesive under heat and pressure against ten 2-inch square by 1/2-inch thick steel blocks. These ten steel blocks with the diffraction grating mounted on one side were then mounted in a surface grinder in such a way that two of the opposite edges could be accurately ground plane and parallel. The blocks were then mounted in a line on a 3/4-inch steel bar in such a way that the plane parallel edges were contacted by the adjacent blocks. This produced a master of about 18-inches long and 2-inches wide which was then used for making a single heavy electroformed submaster. From this submaster many 18-inch lengths of 1-mil thick nickel tape were produced. This technique was worked out to prove the feasibility of the manufacture of frame tape. The method could be easily adapted to a continuous drum production of frame tape by mounting the blocks around the periphery of the large drum.

4.6 TAPE DRIVES

Means for moving the tape within the demountable vacuum systems have been very simple and relatively crude, being simply a rod through a double O-ring seal (refer to figure 6-1). For a sealed off tube with an alkali photocathode a much more sophisticated drive mechanism is required. Several attributes are important to it. It must be bakable to 450°C, of low vapor pressure, and capable of being thoroughly outgassed. It must be vacuum tight, not just of low leakage. Long life, many rotations before failure, and nonmagnetic operation are desirable. It must operate smoothly to maintain high resolution in the direction of motion for cases where writing or reading is being done during the motion. To allow the effective use of a flywheel on the motor to keep this smoothness, a fair gear reduction is desirable. Good acceleration of the massive tape requires a high torque.

Magnetic drives are available, being essentially motors with a thin, nonmagnetic metal, vacuum wall in the air gap. These radiate large magnetic fields that would be difficult to shield and would upset the magnetic focus fields. They also have low torque, and they are relatively bulky.

Several metal bellows type vacuum drives have been made which use cranks to nutate the bellows and transfer the rotational motion into the vacuum chamber. Several ball bearings try to make this operate smoothly but there is doubt as to the

tightness and backlash these permit. The bellows life is questionable. At least one crank bearing is inside the vacuum, in addition to the reel bearings.

Recently a new drive mechanism has become available which seems to be the most promising. It is marketed by American Shoe Machinery Corporation as a harmonic drive for tape (film and magnetic tape in present applications). It comprises a planetary type gear inside the reel, concentric with this is a drive gear (too small a diameter to engage) mounted on a thin, flexible, metal, vacuum wall. After tube processing, the drive mechanism is inserted inside this thin, metal, vacuum wall cylinder. This mechanism, in air, comprises the motor with an elliptical cam fastened to its shaft. The major axis of the cam is just too long to fit inside the thin metal cylinder so it stretches it out of shape, into an elliptical cylinder - just enough to engage the gear teeth adjacent to the ends of the major axis. Since the number of teeth on each gear is different, rotation of the cam produces a differential rotation of the reel. This drive seems to satisfy all the requirements listed, but it remains to be evaluated by actual test.

5. READING SECTION AND ELECTRON GUN

5.1 READING GUN IMPROVEMENT

The high-resolution reading gun as used in all of the demountable guns on the ultraviolet system as well as all of the 3-inch and 4.5-inch flip-over target storage camera tubes have been greatly improved. The addition of smaller limiting apertures and pure nickel shaved cathode structures has helped to reduce the spot size considerably. The gun was then operated with grid G_1 at a small constant positive potential with respect to the cathode. This also gave a reduction in spot size. Since it was found that electrical alignment of the gun after installation in a tube was extremely critical, special fixturing had to be designed to ensure positive mechanical alignment of the gun elements before assembly.

The return beam multiplier assembly was improved by the addition of another multiplier stage bringing the stages to a total of six. It was demonstrated that the overall gain was improved by a factor of 2 to 3 over that obtained with a standard image orthicon five multiplier return beam assembly. These gun-multiplier assemblies have been very reliable and have given little trouble in most of the sealed off tubes which were constructed.

5.2 READING BEAM MEASUREMENTS

5.2.1 Slit Target Tube

High-resolution gun characteristics and beam diameters are determined using a slit target tube. A sketch of this tube and the test setup are shown in figure 5-1. The tube consists basically of an image orthicon with a different gun assembly. Part of the image section is replaced by a Faraday cage assembly directly behind the target. The target consists of a thin gold covered copper foil with two slits of known width and separation.

Focused electrons from the cathode are deflected across the target perpendicular to the slits. They pass through the slits and are collected in a Faraday cage. These collected electrons contribute to the signal pulses which can be made visible on the oscilloscope as two sharp signal peaks above the noise. Knowing the physical distance between the two pulses, it is possible to determine how wide these pulses are at any amplitude. This is a direct measure of the beam diameter.

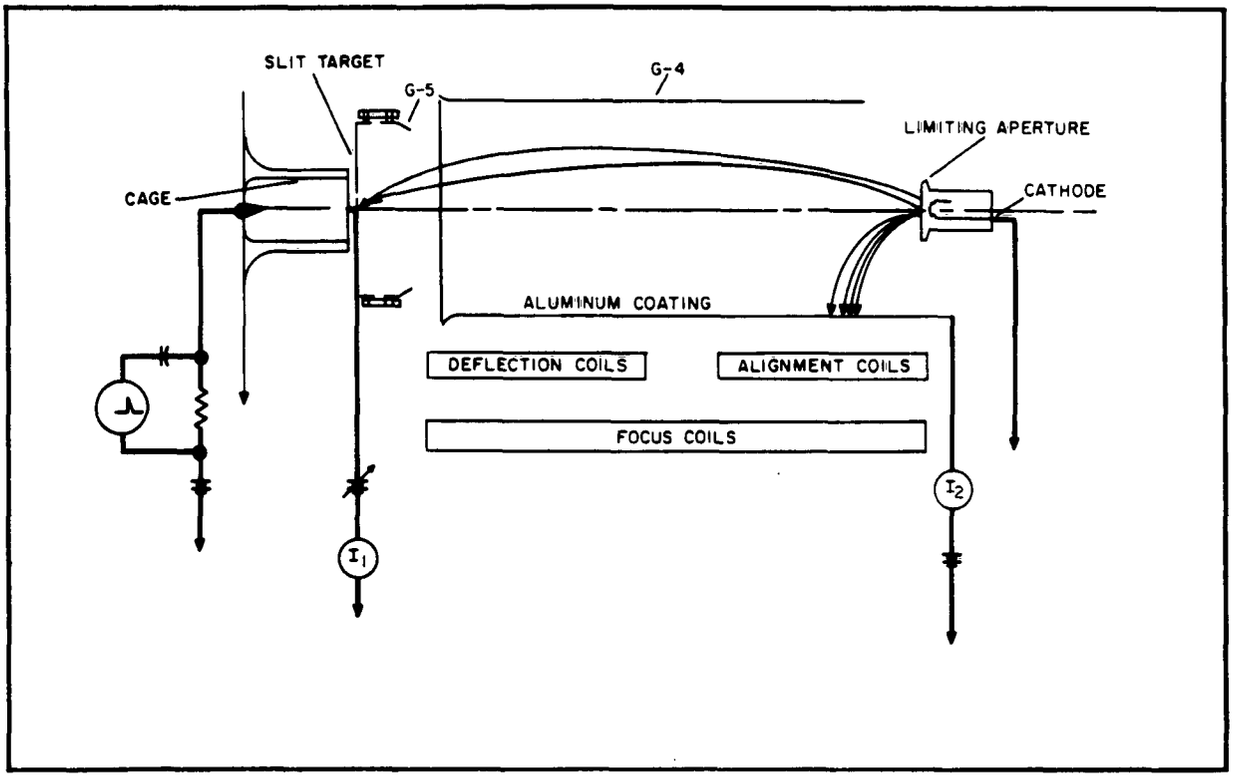

Figure 5-1. Schematic of Slit Test Tube

To determine the total current in the beam, magnetic deflection, focus, and alignment fields are turned off, and the cathode current passing through the limiting aperture is measured as I_2 collected at grid G_4. With the magnetic fields, the beam is focused and deflected across the target and the beam diameter is measured as described above. Alternatively, the target may be biased to turn back electrons which have axial velocities less than a prescribed value.

The results of the above measurements are listed in table 5-1. A sample photograph of an oscilloscope trace achieved with the gun in tube E0187 is shown in figure 5-2. The beam diameter at the 50-percent point on this photograph was 0.39 mil. Two separate forms of operation were used to plot the histograms shown in figures 5-3 and 5-4. The gun geometries of the tubes are the same for all the histograms and include those indicated in table 5-1. These figures are the results of 16 different measurements. Eight measurements made with the cathode grounded and eight measurements with the cathode negative with respect to a grounded grid, G_2. The smallest spot sizes and the highest beam current densities were obtained with the second mode of operation. Since these are the same tubes, the consequence is that negative operation creates a different lens arrangement such that the spot size is

TABLE 5-1

HIGH RESOLUTION GUN TESTS

Tube No.	Cathode or Grid	Beam Current I_b (μa)	Spot Size (mil)	Current Density (amps/cm^2)
E0188	Cathode ground	0.6	0.520	0.44
H.R. Partial	G_1 + 3.5v	1.0	0.520	0.73
Pure Ni Cathode	Cathode neg.	1.0	0.467	0.89
E0186	Cathode ground	0.2	0.520	0.096
H.R. Partial	G_1 +	0.7	0.520	0.49
Pure Ni Cathode	Cathode neg.	0.4	0.390	0.47
E0178	Cathode ground	0.1	0.516	0.076
H.R. Partial	G_1 +			
Pure Ni Cathode	Cathode neg.	1.0	0.512	0.76
E0177	Cathode ground	1.0	0.769	0.33
Orthicon Partial	G_1 +			
Pure Ni Cathode	Cathode neg.	1.0	0.515	0.76
E0185	Cathode ground	1.0	0.925	0.23
Orthicon Partial	G_1 +			
Pure Ni Cathode	Cathode neg.	1.0	0.675	0.43
E0173	Cathode ground	0.5	0.515	0.37
H.R. Partial	G_1 +			
Shaved Impure Ni	Cathode neg.	1.0	0.515	0.75
E0170	Cathode ground	0.1	0.500	0.084
H.R. Partial	Cathode neg.	0.8	0.508	0.61
Shaved Pure Ni				
E0187	Cathode ground	0.78	0.515	0.58
H.R. Partial	G_1 +	1.0	0.563	0.64
Shaved Pure Ni	Cathode neg. G_2 ground	1.0	0.388	1.3

diminished. Most of the spot sizes were in the range of 0.5 to 0.6 mil and the spread is toward the higher spot sizes. However, several tubes had beam diameters significantly less than this value. As expected, the current density spread is toward the higher densities when the cathode is operated in the negative mode.

In the analysis of the beam size as measured from the slit target tube, it is necessary to make a correction for the width of the slit used in the target. This slit width is only 0.2 mil; however, since this is a significant percentage of the actual beam size, it is necessary to make a correction for this width. The sine wave response of the slit may be computed according to the usual (sin X)/X formula where $X = \pi f w/2$,

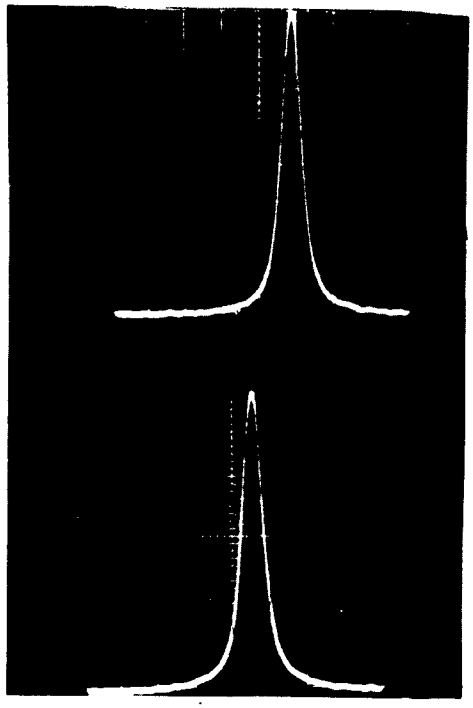

$I_{BEAM} = 1\mu A$; SCALE: 0.13 MIL PER SMALL DIVISION ;
50 % BEAM DIAMETER : 0.39 MIL.

Figure 5-2. Beam Current Density Distribution, Tube E0187

f is spatial frequency in lines per inch, and w is the slit width in inches. The beam aperture response as derived from measurements on the slit target tube is actually the aperture response of the beam in combination with the 0.2-mil slit used to measure it. The response of the beam alone may be obtained by taking a point-by-point quotient of the combination and the slit response.

The results of this procedure are shown in figure 5-5. The correction for the finite slit width is shown to be quite small. It is evident that the slit is adequately narrow for resolving the very fine beam, yet this was not expected because the slit width appeared coarse in relation to the sharp peak of the aperture response. The adequacy of the slit may be partially explained by the fact that the lowest spatial frequency at which complete cancellation can occur is 10,000 lines per inch, at which one sine wave line pair or two lines appear across the width of the slit. Better evidence is shown in figure 5-6, in which a gaussian aperture response closely matching the original observed aperture response near the peak is shown along with the

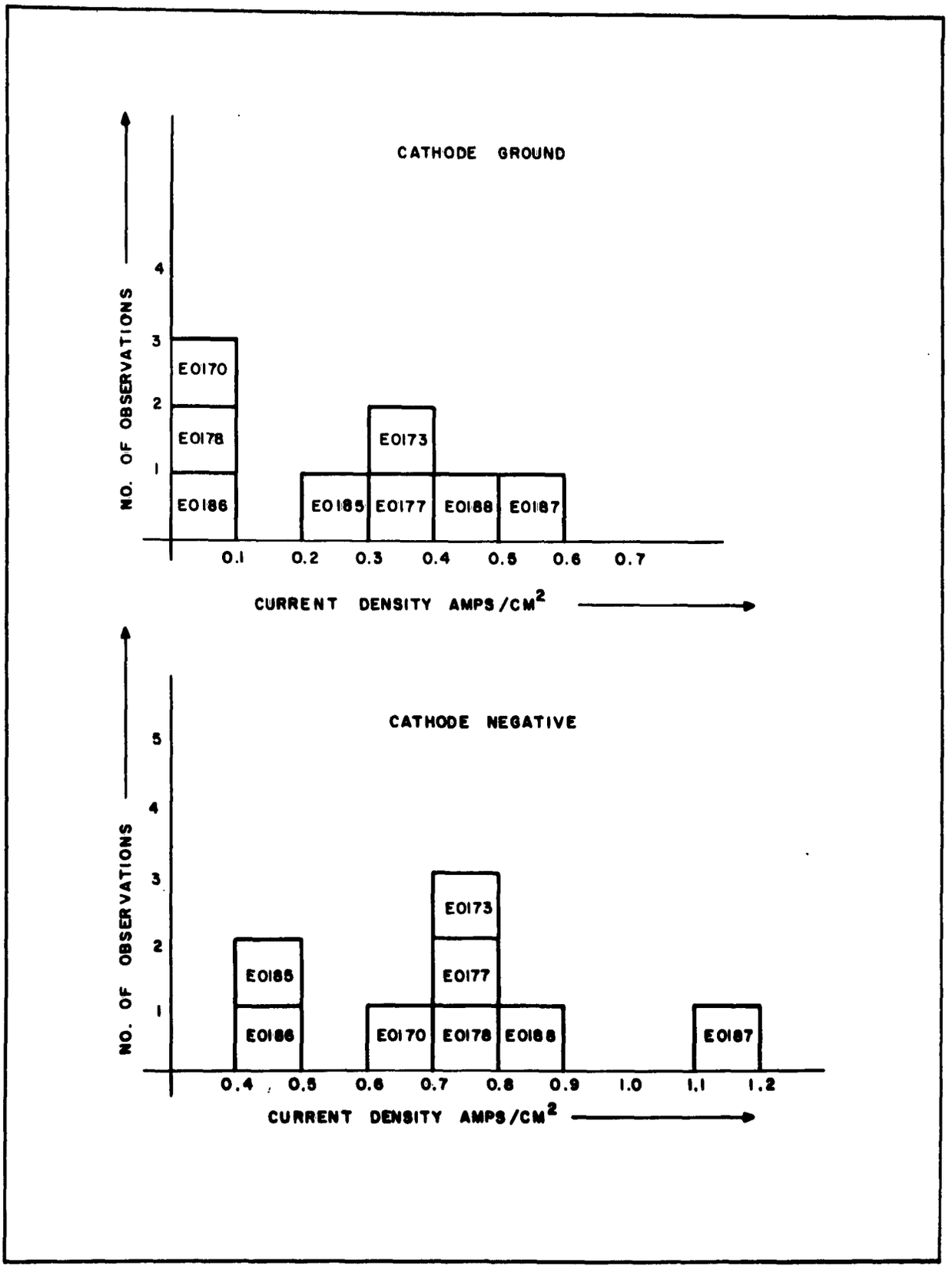

Figure 5-3. Beam Current Density Observations

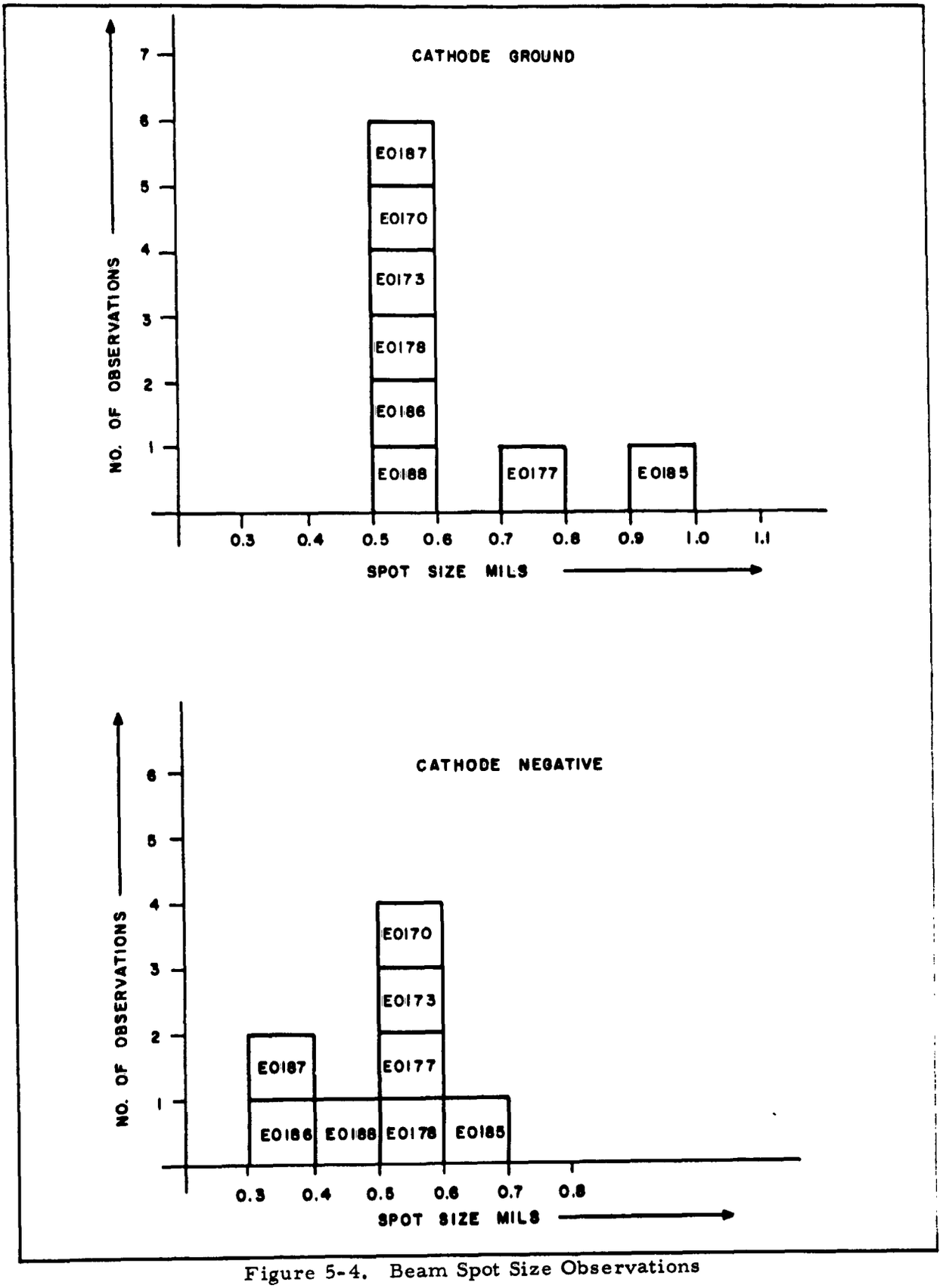

Figure 5-4. Beam Spot Size Observations

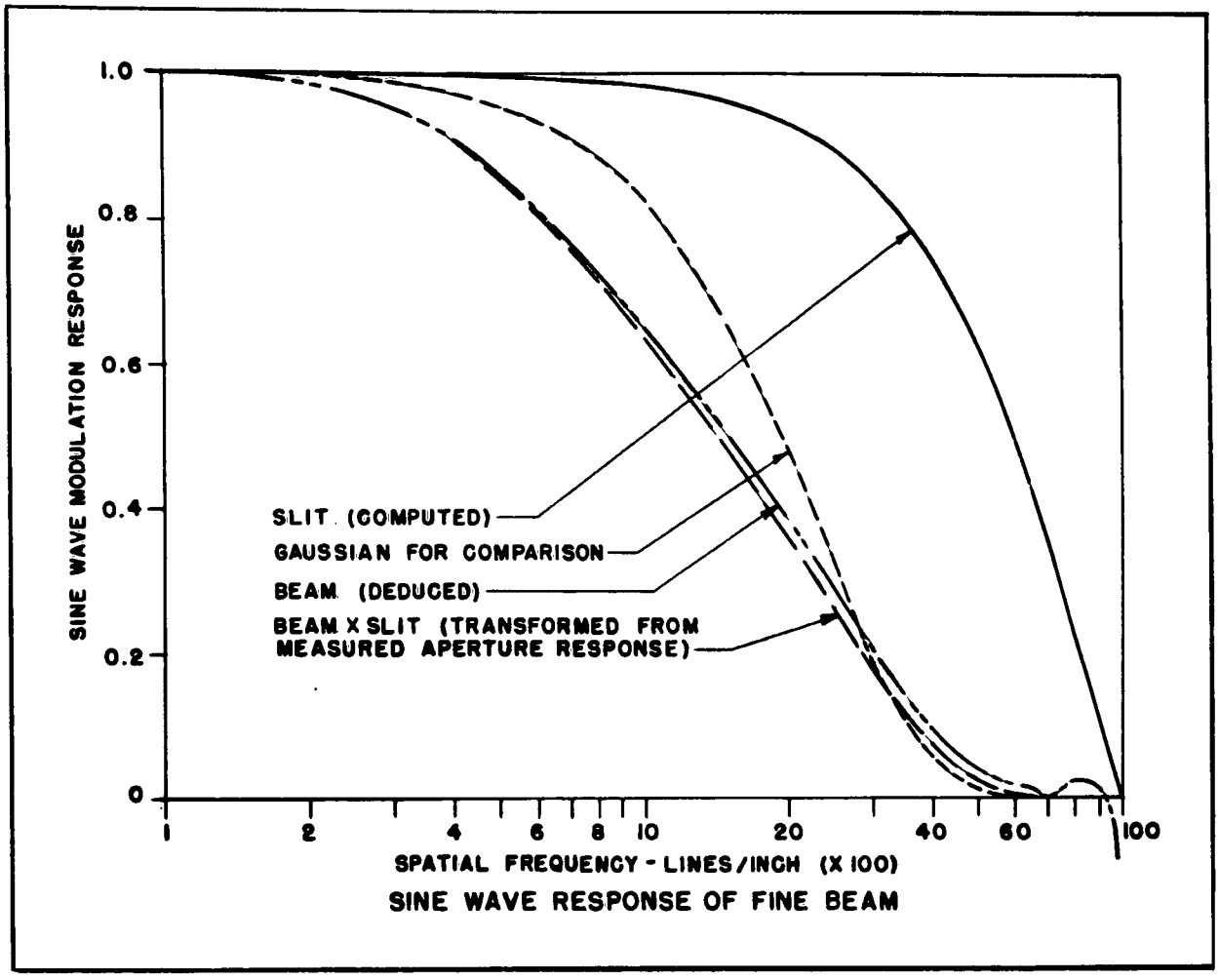

Figure 5-5. Correction of Beam Aperture Response For Slit Width

aperture response of the combination of the gaussian and a zero-point 2-mil slit (convolution of gaussian and slit). The two agree so closely that it is difficult to show both on the same plot, thus the slit is demonstrated as being quite adequate for resolving this sharp gaussian response.

A more complete discussion of aperture response and a combination of individual aperture responses is given in Section 8.

5.2.2 Monoscope Tube and Westinghouse Pattern

Measurements of beam size in terms of aperture response were made in a different way on specially built monoscope tubes. The monoscope target that was installed in these tubes was fabricated in the following way. Using aluminum over gold, the work function difference of these metals as well as the slight charges stored on the aluminum oxide result in high differential modulation of a beam of slow electrons.

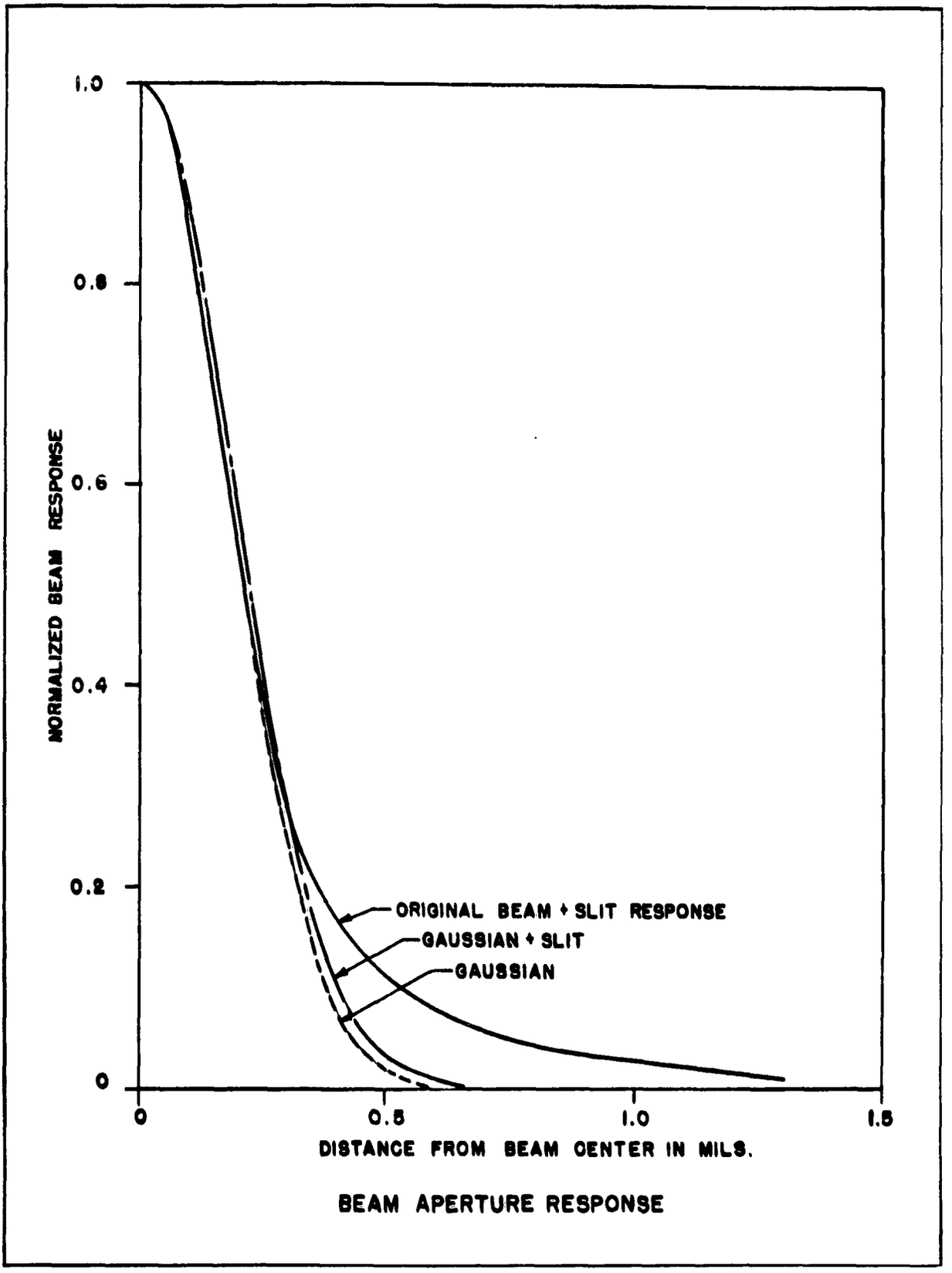

Figure 5-6. Convolution Integral of Gaussian and Slit

Several 0.75-inch diameter glass discs were made with a chromium base evaporation, a gold film, and an aluminum top layer 500-Angstroms thick. A complete Westinghouse diminishing bar pattern, reduced to approximately 1 x 6 millimeters, was photoetched into the aluminum all the way down to the gold layer. The smallest gold bars measured on a pattern of this type under the microscope showed a width of 8 microns interspaced by aluminum bars 14 microns wide. This pattern was then mounted in the target position normally occupied by the target in this standard flip-over target test tube.

This target was scanned at right angles to the bars and the output of the return beam multiplier was amplified and displayed on an A-scope. Only one horizontal scan line was displayed at a time to keep the noise at a low level. Since it was found that the signal was bandwidth limited by the video amplifier, the 6-millimeter length of the pattern was underscanned in sections of 2.1-millimeter lengths. A typical oscilloscope display is shown in figure 5-7. In this example the measurements were made with the cathode 7 volts negative with respect to the target. The same measurements were repeated for cathode potentials of -10 and -15 volts. The higher cathode potentials produced higher signals but the percent response remained constant.

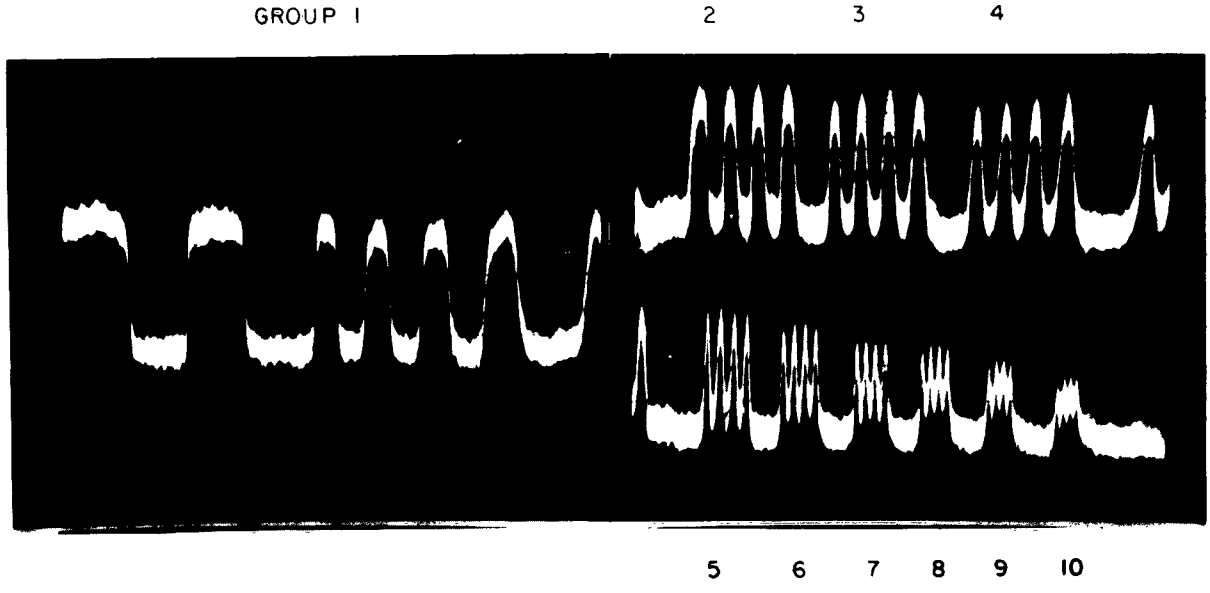

Figure 5-7. A-Scope Bar Pattern Signal From Monoscope Tube

A beam aperture response curve plotted from this information is shown in figure 5-8. The 50-percent response is at approximately 1400 lines per inch and the limiting 5-percent resolution is better than 6000 TV lines per inch.

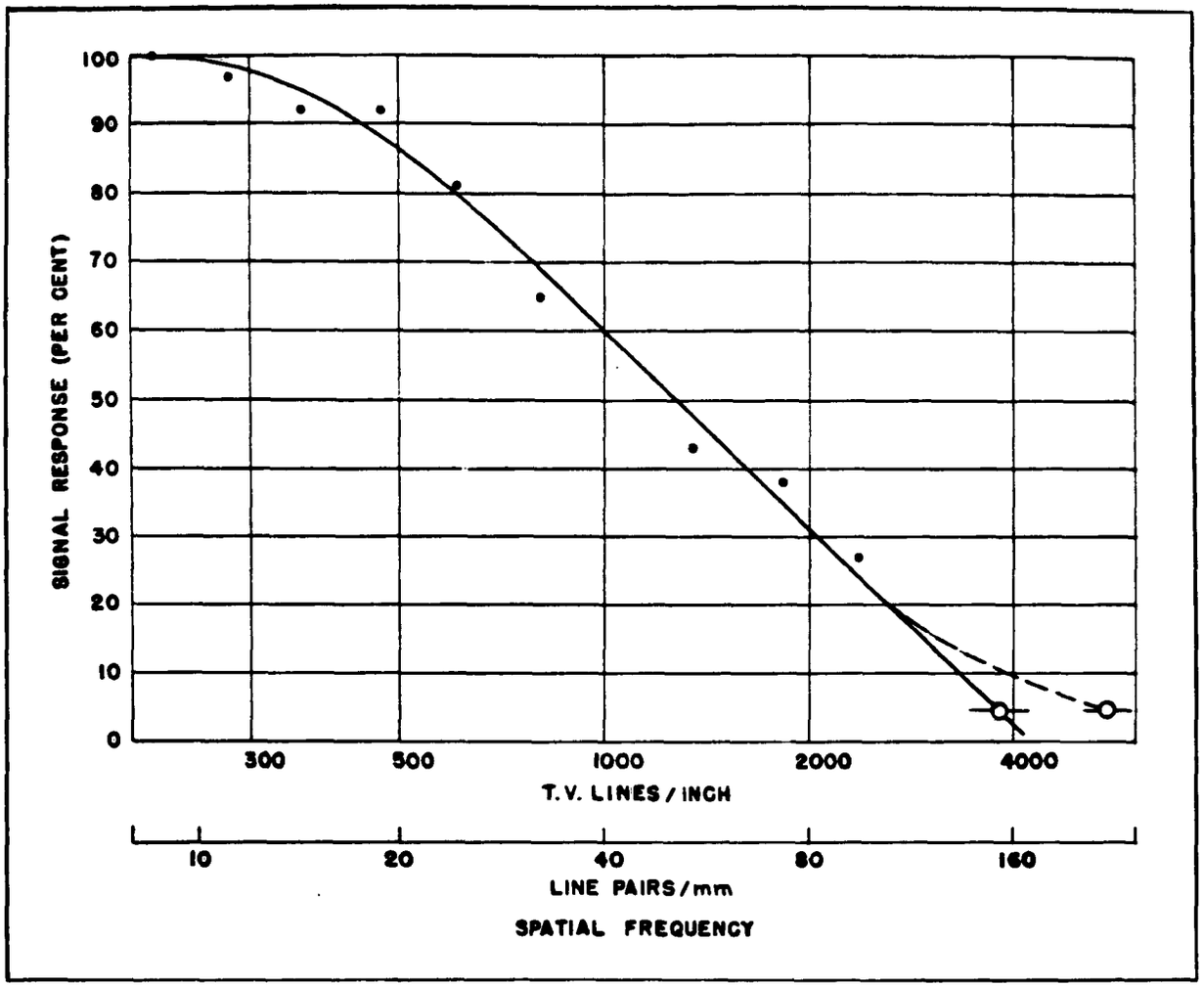

Figure 5-8. Aperture Response Curve: Reading Beam Spot and Amplifier Monoscope With Westinghouse Bar Pattern in Al on Au

From the measured beam diameter of about 0.4 mil at the 50-percent point, the response at this level could be expected to be 2500 TV lines per inch in first approximation. However, the convolution of the base of the gaussian curve together with amplifier bandwidth limitation bring the 50-percent response down to approximately 1400 TV lines per inch. Moreover, in the last three bar groups the etching process produced aluminum bars which were 24, 33, and 65 percent wider than the corresponding gold bars. For purposes of simplicity in plotting the aperture response curve, the arithmetic mean values between the bar widths were used.

6. CAMERA STORAGE TUBE

6.1 ULTRAVIOLET DEMOUNTABLE VACUUM SYSTEM

6.1.1 Operation

The ultraviolet system is a demountable header machined from stainless steel and designed to mount three individual tubes. These may be the prime-erase gun, the read gun and the writing gun, or the image section. The header is designed to take several different inserts depending on the type of target that is to be tested. The tubes are sealed to a stainless steel O-ring flange by an ultrasonic soldering procedure using a low melting point indium alloy. This flange along with its tube is then mounted to the main housing. The whole assembly, figure 6-1, is carried on top of a 4-inch vacuum station which is capable of producing a vacuum within the header of approximately 2×10^{-6} millimeter of mercury.

The normal method of operation includes a spiral image section but since regular alloy photocathodes cannot be used in a demountable system which is periodically let down to standard air pressure it was necessary to use an evaporated coating of pure gold with 50 percent transmission. This type of photocathode has excellent corrosion and oxidation resistance, and is very successful as a photoemitter when used with ultraviolet radiation of less than 2500 angstroms. This shortwave length requires that the gold photocathode be deposited on a quartz plate. The quartz plate is sealed to the outside end of the spiral photodiode envelope by means of an O-ring. In this way the photocathode may be easily removed and re-evaporated at any time. A small mercury vapor tube about 3-inches long and 1/4 inch in diameter is used as the ultraviolet source. A 6-inch parabolic reflector, used to collimate the light from this tube, was made by cutting off the faceplate of a standard automobile headlight seal beam unit. This combination results in an extremely high intensity short wavelength ultraviolet source suitable for photoelectric writing from the gold photocathode.

A pattern for storage experiments is usually produced by evaporating a heavy coating of aluminum through a very fine mesh screen on top of the gold photocathode. This produces a pattern which occludes the emission of photoelectrons from that area.

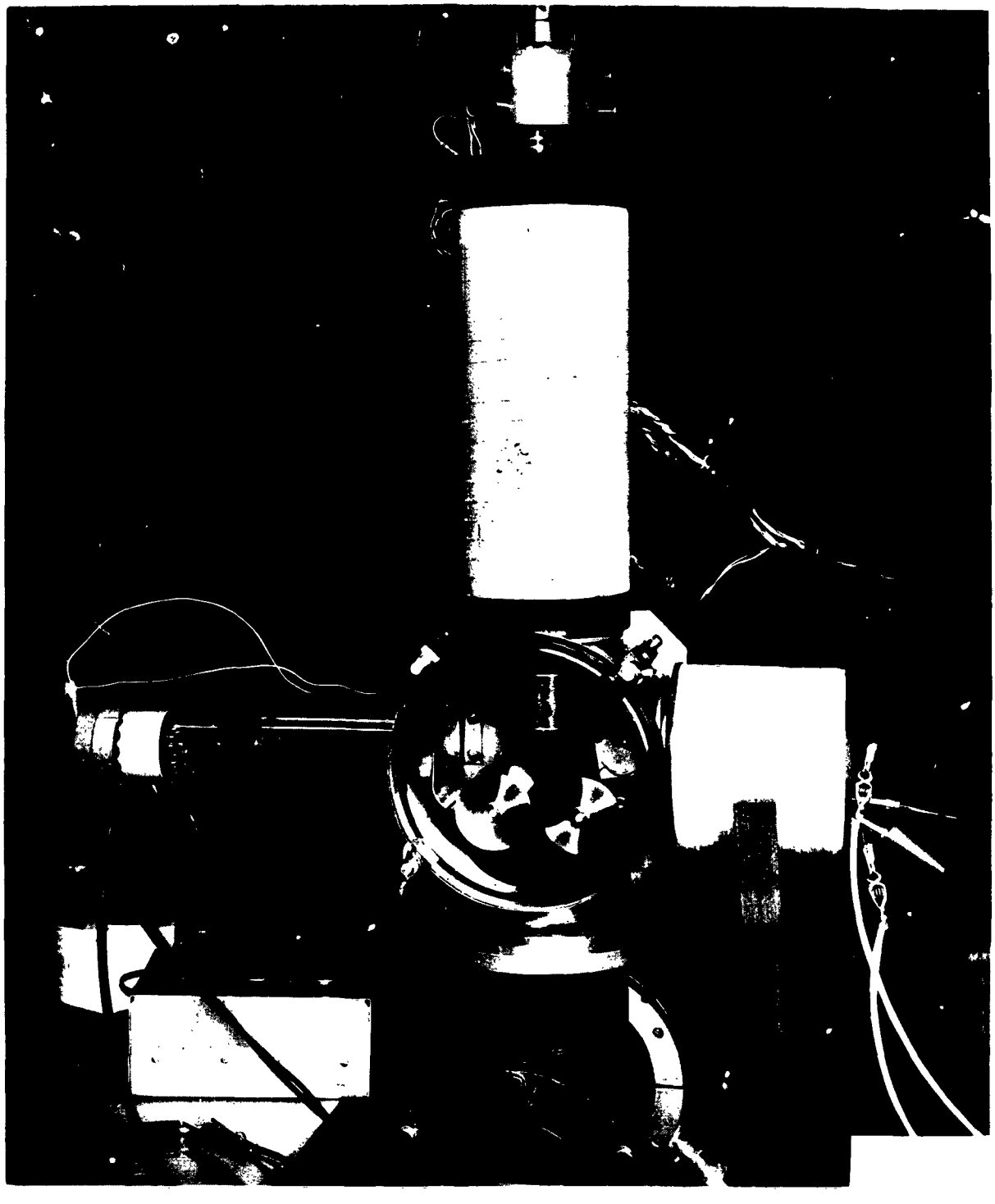

Figure 6-1. Ultraviolet Demountable System

This pattern is then focused onto the target under test by means of the 10 kv accelerating field and the magnetic field surrounding the image section.

6.1.2 Rigid Target Testing

An insert was designed for the testing of rigid targets which can mount as many as seven targets at one time. The usual procedure, however, is to use one of the positions to hold a phosphor which is used for focusing the written image. This insert may be rotated by means of a manipulator outside the vacuum chamber so that each target can be presented to the area in front of each tube in quick succession. The targets are normally grounded through the contact with the arms of the insert and are held to the arms by small stainless steel clamps.

6.1.3 Tape Testing

A second insert is available for testing the length of target tape. A photograph of this insert is shown in figure 6-2. This insert is operated by means of two shafts which project through the side wall through two O-ring sealed vacuum manipulators. The device is stainless steel and includes reels large enough to hold 100 feet of normal TVIST tape. The guide is simply a polished and formed piece of stainless steel over which the tape slides from one reel to another. There are three flat surfaces in the focal plane of each tube so that the tape may pass through these surfaces in succession. A Helmholtz coil is included to extend the magnetic focusing field properly through and beyond the tape.

6.2 FLIP-OVER TARGET TEST TUBE

6.2.1 Construction

The so called flip-over target storage camera tube was conceived as a research tool to test the compatibility of materials and components within a sealed off tube, and also to determine tube parameters as they would be on a final camera tube. The flip-over target test tube consists essentially of an entire TVIST system in a single envelope about the same size and physical shape as an image orthicon camera tube. There is one important exception, however, the target does not consist of a moving tape as described for the TVIST system. Instead the target is a small rigid piece of this tape material suspended in the center of the tube in such a way that it can be rotated to face either the image section or the reading section. A schematic drawing of this tube is shown in figure 6-3 and a photograph of a typical tube is shown in figure 6-4. The front of the tube contains the image or writing section consisting of an alkali photocathode, a spiral or 10 cylinder accelerator system, and the target assembly. The rear half of the tube contains the high resolution TVIST reading gun and a

Figure 6-2. Tape Transport Insert for Demountable Vacuum System

six multiplier return beam assembly in place of the standard five multiplier assembly. There is no prime or flooding gun included. This function being assumed by the reading gun.

The fabrication and processing of this tube has been an invaluable aid in determining problems encountered in the fabrication of a complete TVIST camera tube. Incompatibility of materials was a tremendous problem in the beginning but has since been solved.

Flip-over target test tubes were designed and built in two basically different types. These were the 3-inch and the 4.5-inch tubes. Both tubes had some samples which used a 10-cylinder accelerator and some used a spiral accelerator. All of the tubes

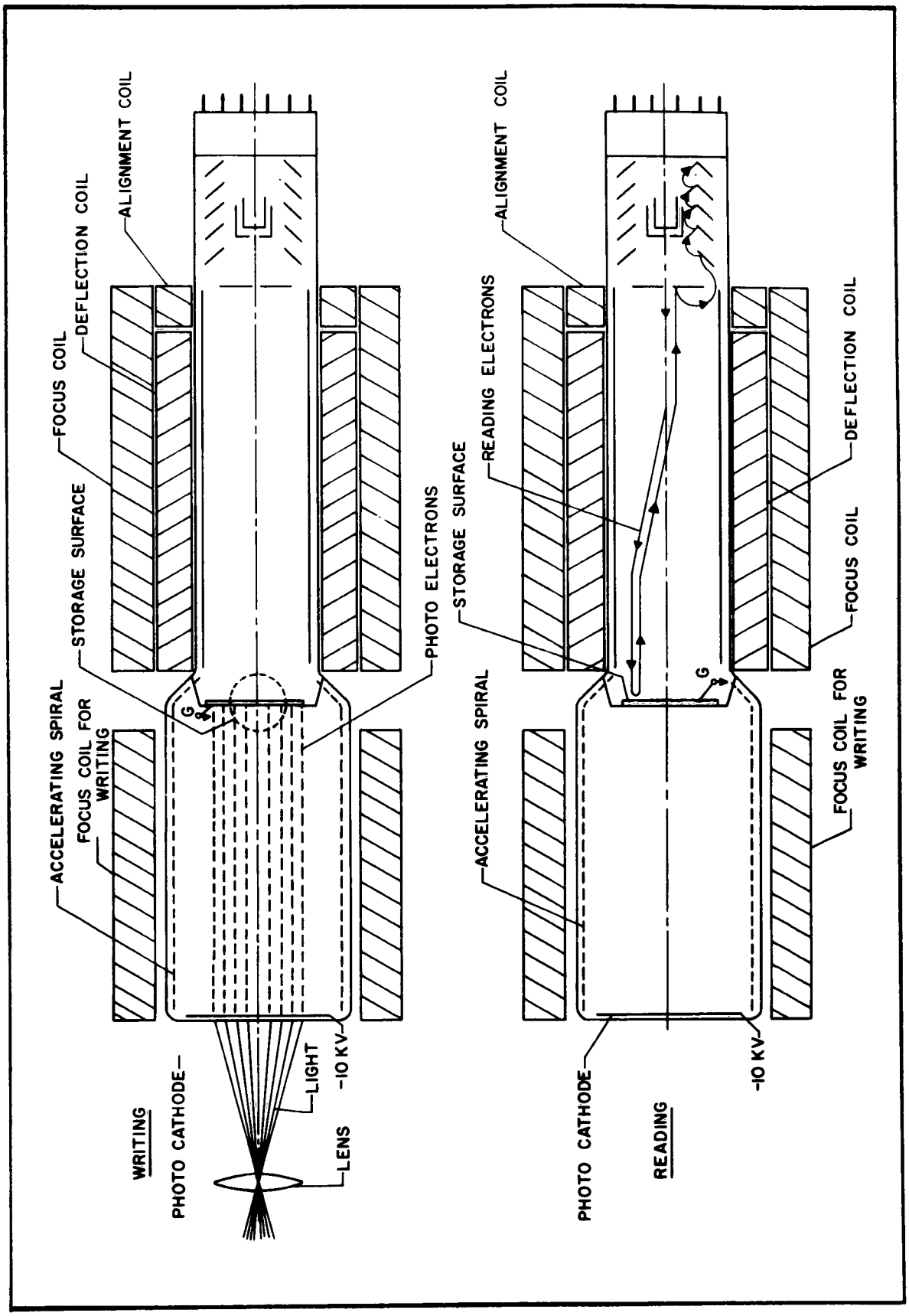

Figure 6-3. Flip-Over Target Storage Camera Tube Schematic

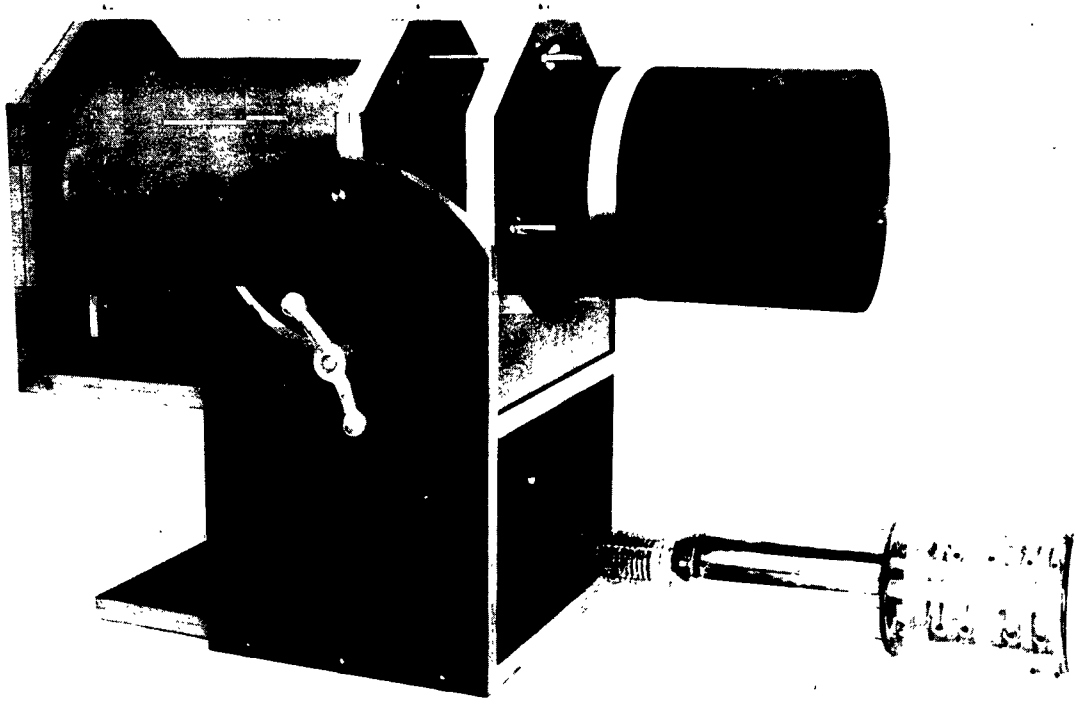

Figure 6-4. Flip-Over Target Storage Camera Tube

included the TVIST WX-4787 high resolution reading gun, as well as the standard 6000 line per inch electroformed nickel target. The photocathodes were either bialkali or trialkali surfaces. In the early stages it was feared that photosurfaces having a large amount of free cesium would be incompatible with long time storage on the TVIST surface. However, this fear was proven to be unfounded when trialkali photosurfaces were used successfully.

The basic configuration of the flip-over target tube is that of a standard image orthicon camera tube. However, the image section part of the flip-over target tube bulb has been lengthened by nearly a factor of two. It includes a faceplate which is not an integral part of the bulb but is presealed to a kovar flange which is then heli-arc welded to a kovar flange sealed to the front edge of the image bulb. This was necessary to permit the making of the spiral accelerator on the interior surface of the image section bulb. Kovar buttons are brought out through the side of the image section bulb for making contact to the spiral.

The target in the 3-inch flip-over target tube consists of a 1.6-inch diameter 20 mil thick standard TVIST electroformed grating mounted on a pivot to allow it to rotate 180 degrees against two stops. One stop allows the target to face the reading

gun and the other stop allows the target to face the photocathode. The target is weighted in such a way that it may be positively rotated to these two stable positions by means of a 180 degree axial rotation and a slight longitudinal tilt. The target shaft is electrically connected to the pivot mounting by means of a small hair spring so that electrical connection to the target is never lost. This mounting assembly is then electrically connected and mechanically supported on the shoulder socket pins.

The 4.5-inch flip-over target tube is electrically identical to the 3-inch tube. The mechanical difference consists of a larger envelope size as well as a target which is 2.5-inches square of which 54-millimeters square are useful for storage.

The cradles which were designed to hold the deflection assemblies for the 3-inch and 4.5-inch flip target tubes were built entirely from nonmagnetic material to avoid any magnetic field distortion either in the focus or deflection fields. These assemblies were made extremely heavy and rigid so that basic errors in mechanical alignment could be overcome. A slight flexing of the mechanical mounting can become extremely critical when working with resolutions in excess of 3000 lines per inch. The cradle was designed in such a way that the entire focus coil deflection and assembly could be rotated about its own longitudinal axis. The coils were provided with a handle and stops adjustable so that the rotational limits could be accurately determined. This entire assembly was then mounted into a clevis arrangement so that the device could be tilted forward and aft. Thus the required motions for rotating the target from read to write position were obtained. The video preamplifier and return beam multiplier power supply is located in a small box which fastens to the base of the coils and has a socket which connects to the base of the reading gun assembly. The shoulder connections from the tube are made through a socket located within the focus coil. The negative 10 kilovolts used in photoelectron acceleration writing is connected directly to the kovar which contacts the photocathode at the front of the image section. The tube as a whole can be surrounded by several layers of magnetic shielding material to cut down the influence of outside stray magnetic fields. A photograph of the complete 4.5-inch assembly is shown in figure 6-4.

6.2.2 Magnetic Field Measurements

A commercially built coil assembly was purchased for the 4.5-inch flip-over target tubes. This device includes deflection and focus coils as well as the shoulder socket connections necessary to make contact to the target of the tube. There are four separate and individual coils in the Marconi yoke for focusing. The current

through these coils may be individually varied so that the combination of the four produces a focus field which is as uniform as possible throughout the length of the tube. Since the 4.5-inch flip-over target test tube is somewhat longer than the standard 4.5-inch image orthicon configuration and since the requirements for a uniform field are much more severe in this case, it was necessary to design an extending coil to fit on the front of the deflection focus yoke to extend the field uniformly in the vicinity of the photocathode.

A magnetic field comparison between the 3-inch and 4.5-inch focus coils was made. Figure 6-5a shows the focus field of the 3-inch tube which was used to measure the previously reported 3800 TV lines per inch. Since the focus fields of the 4.5-inch yoke are actually made up of five separate coils, the fields were adjusted by means of shunts to give a shape as shown in figure 6-5b. The proper reading field for the 3-inch tube is 80 gauss and the proper field for the 4.5-inch tube is 60 gauss. These values agree quite closely with the plotted fields. As can be seen, the field uniformity of the 4.5-inch tube is better than that of the 3-inch tube.

The magnetic field contributed by a typical 4.5-inch spiral accelerator having a resistance of 10 megohms and an accelerating voltage drop of 10 kilovolts was computed to be a maximum of 6.5 milligauss on axis.

6.3 PERFORMANCE

Most of the following performance data were taken in the flip-over target test tube as being most indicative for a sealed-off camera tube with alkali photocathode.

6.3.1 Reading Transfer Characteristics

An experimental study of the noncharging-nondestructive readout process was carried out. Figures 6-6 through 6-11 show teledeltos electric field plots of a typical TVIST target cross section. These figures also show computed electron trajectories for the particular charge conditions involved. For all the plots it was assumed that the target dielectric had been primed to -16 volts with respect to the metal base and the reading cathode gun was held at -11 volts with respect to the target base. Successive figures have the uniform target prime charge decreased by the writing process from -16 volts to -15, -14, -13, -12, and -11 volts respectively. These figures show that the return beam is calculated to change by the different voltage levels from 100 percent to 8.3 percent. Also, experimental measurements were made to determine the return beam modulation as a function of the potential on the dielectric

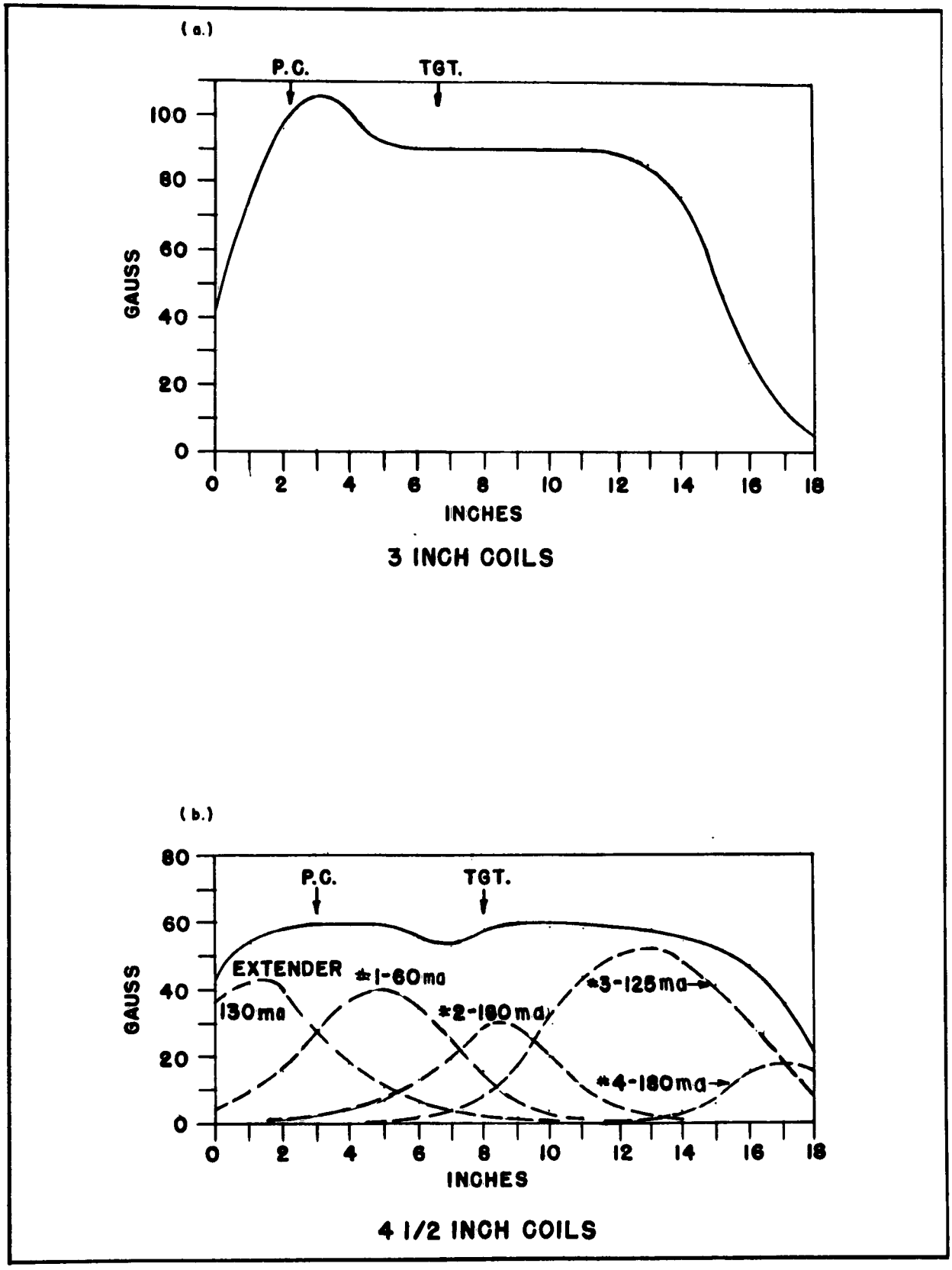

Figure 6-5. Magnetic Field Distribution, Focus Coil

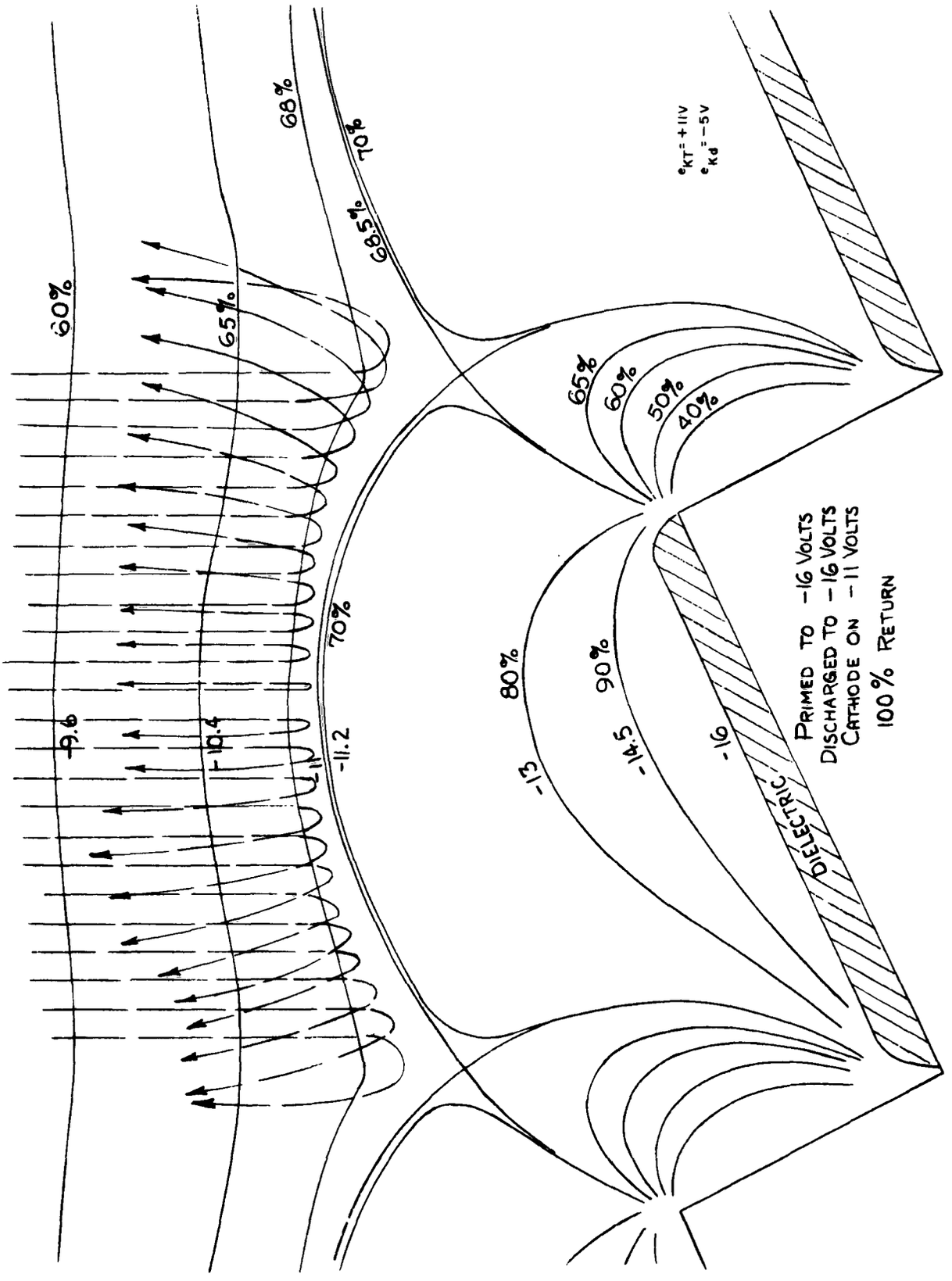

Figure 6-6. Teledeltos Electric Field Plot Showing Electron Trajectories

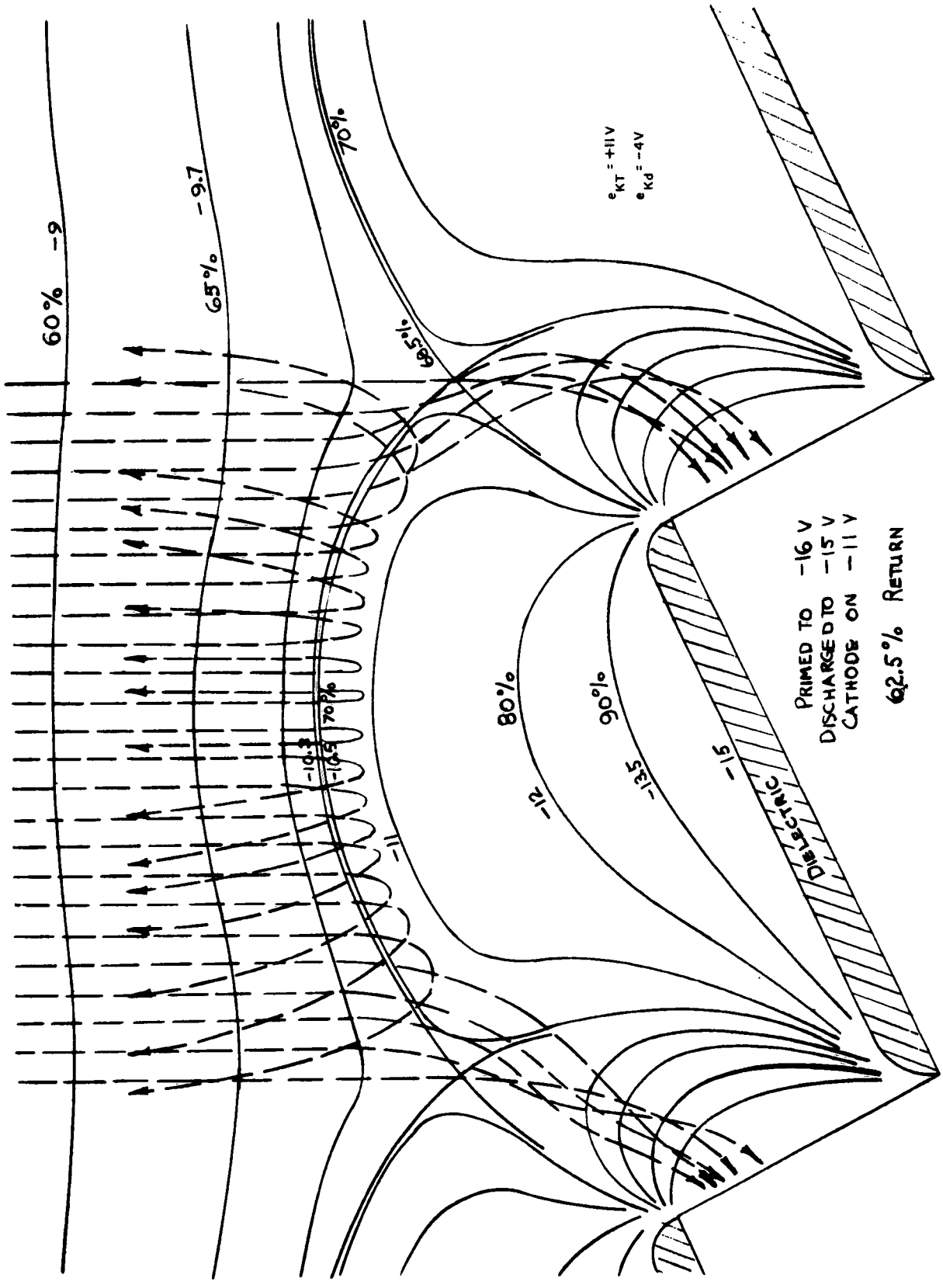

Figure 6-7. Teledeltos Electric Field Plot Showing Electron Trajectories

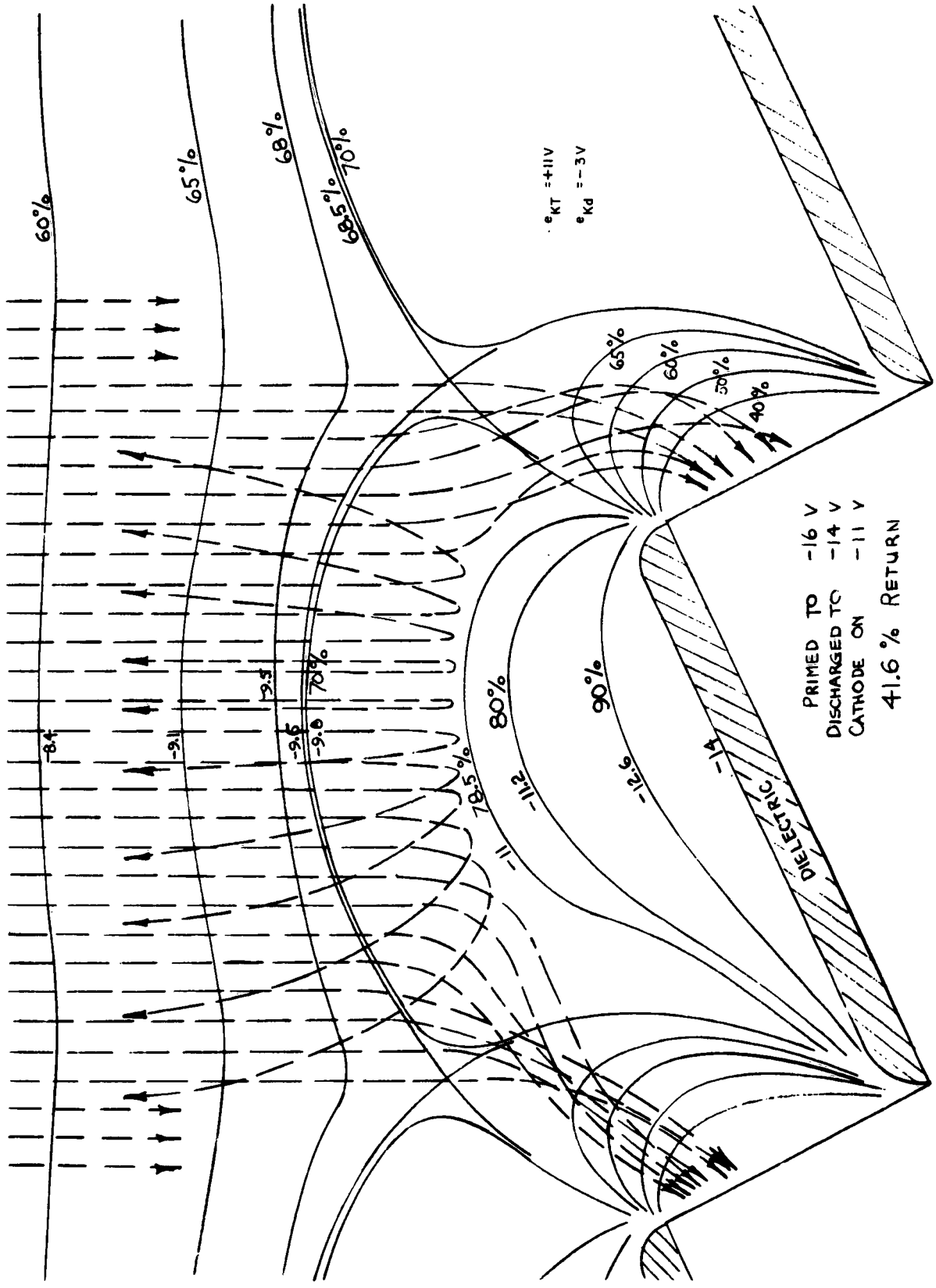

Figure 6-8. Teledeltos Electric Field Plot Showing Electron Trajectories

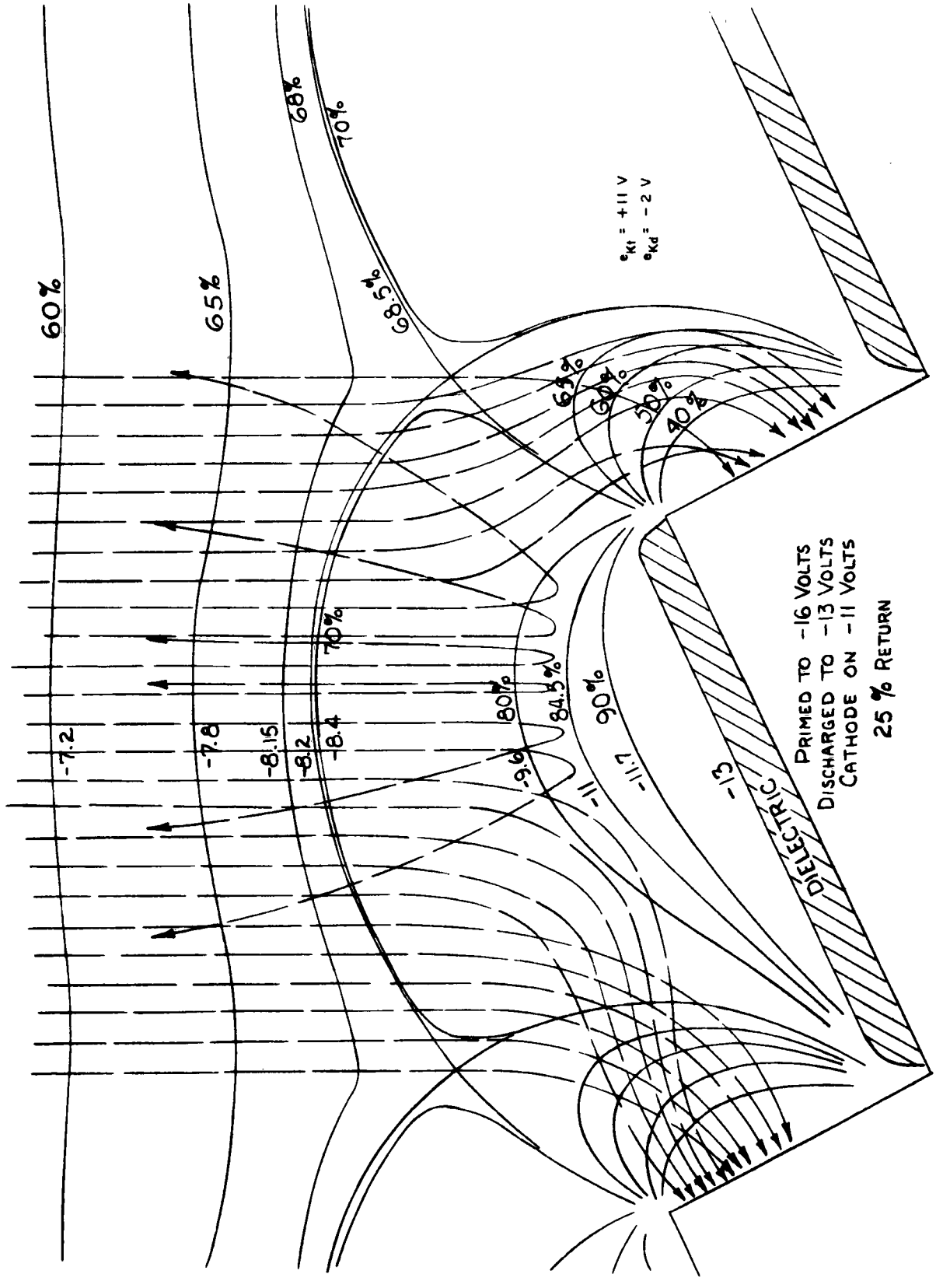

Figure 6-9. Teledeltos Electric Field Plot Showing Electron Trajectories

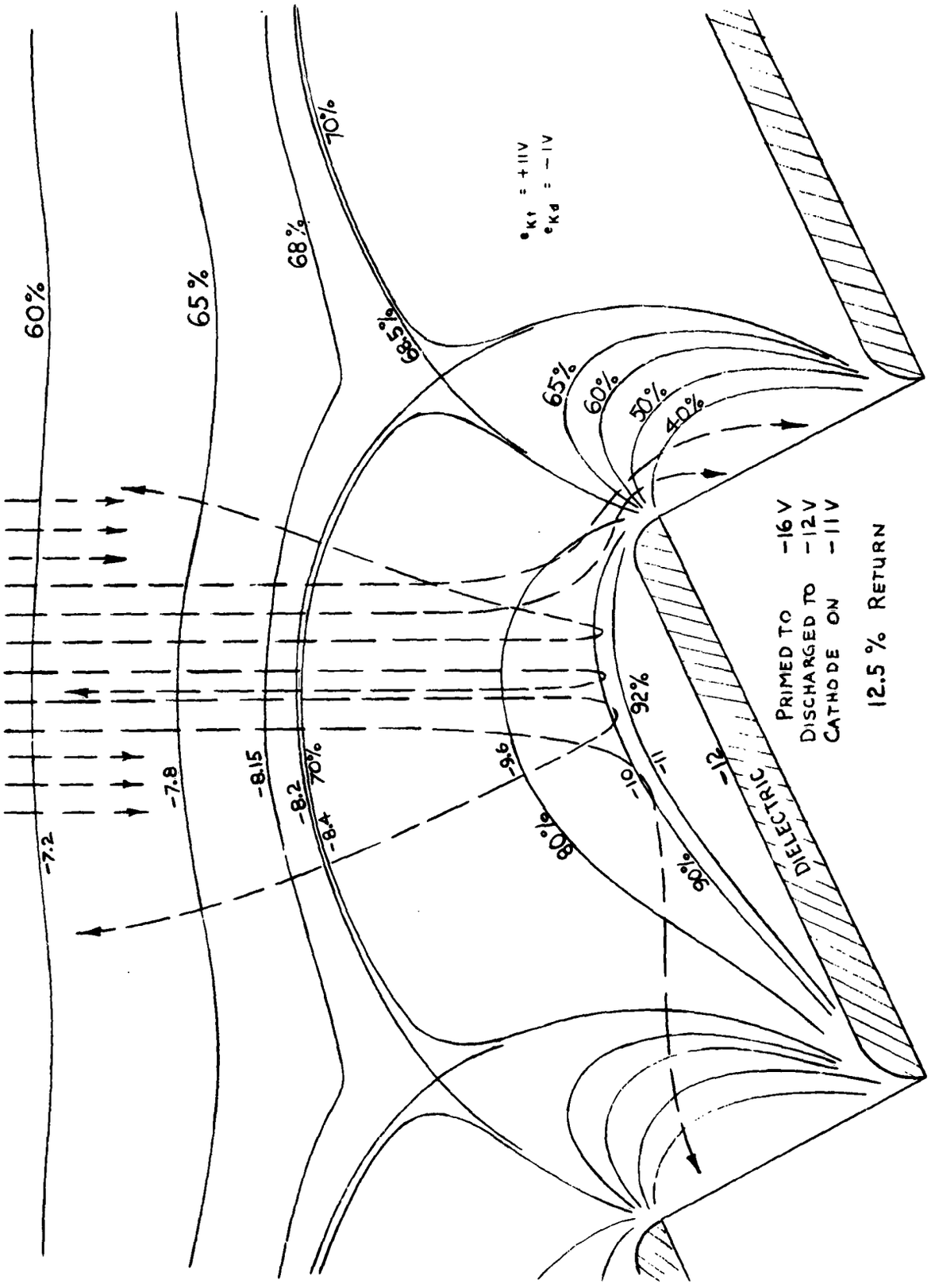

Figure 6-10. Teledeltos Electric Field Plot Showing Electron Trajectories

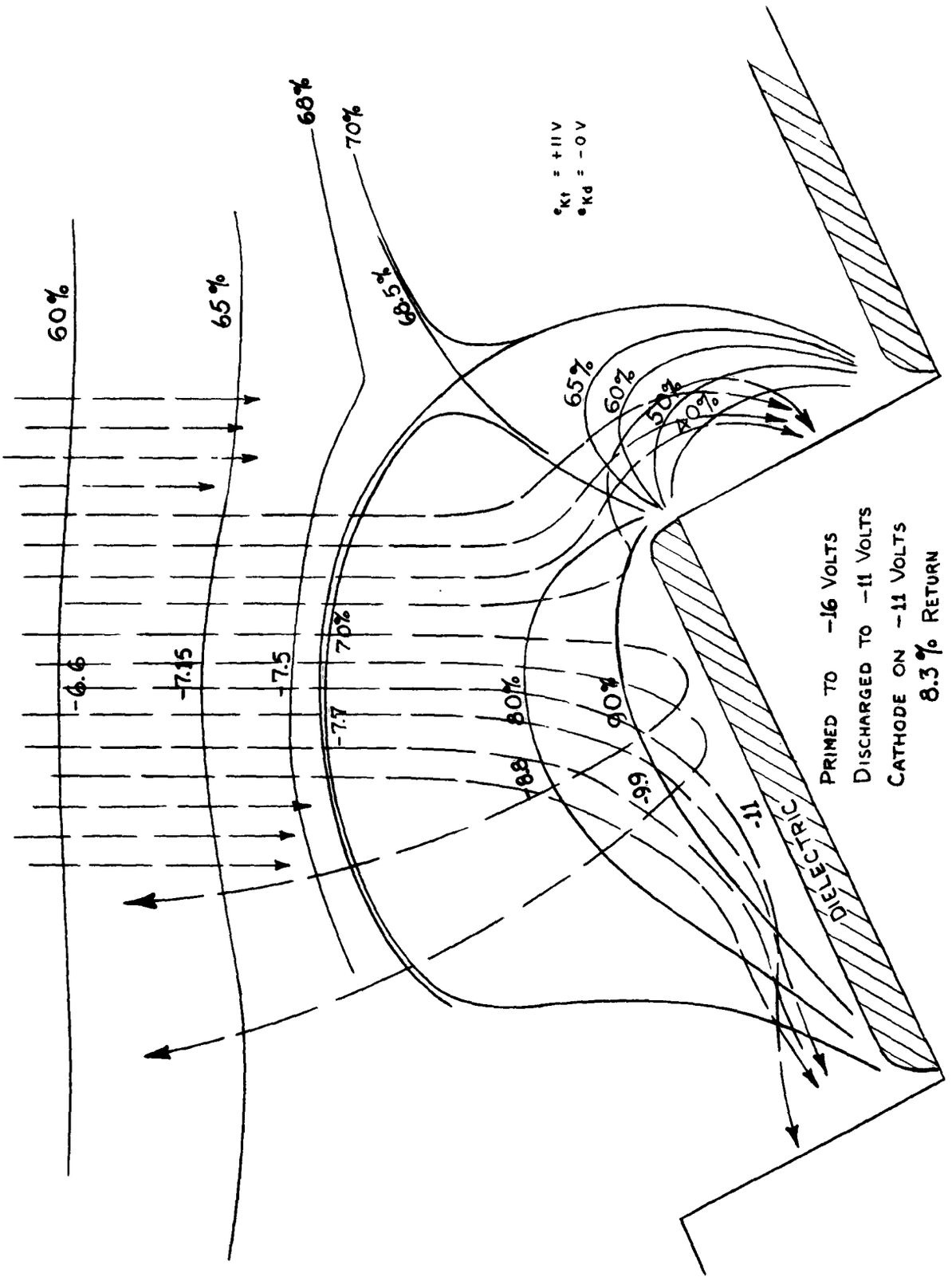

Figure 6-11. Teledeltos Electric Field Plot Showing Electron Trajectories

surface with respect to the cathode (e_{kd}) and also of the potential on the target base with respect to the cathode (e_{kt}). For noncharging-nondestructive reading a varying portion of the primary reading beam is collected by the bare slopes of the target grooves. This portion of the primary beam depends on e_{kd} and e_{kt} and constitutes the modulation of the return beam. The measurements for figure 6-12 were made with a constant primary beam of 50×10^{-9} amperes. The curve for e_{kt} = +11 volts is commonly used for readout for storage experiments. The dielectric surface had been primed to -16 volts with respect to the target base and an electrostatic pattern was produced by writing (discharging) part of the surface charge. For reading the cathode is set to -11 volts with respect to target base (e_{kt} = +11 volts).

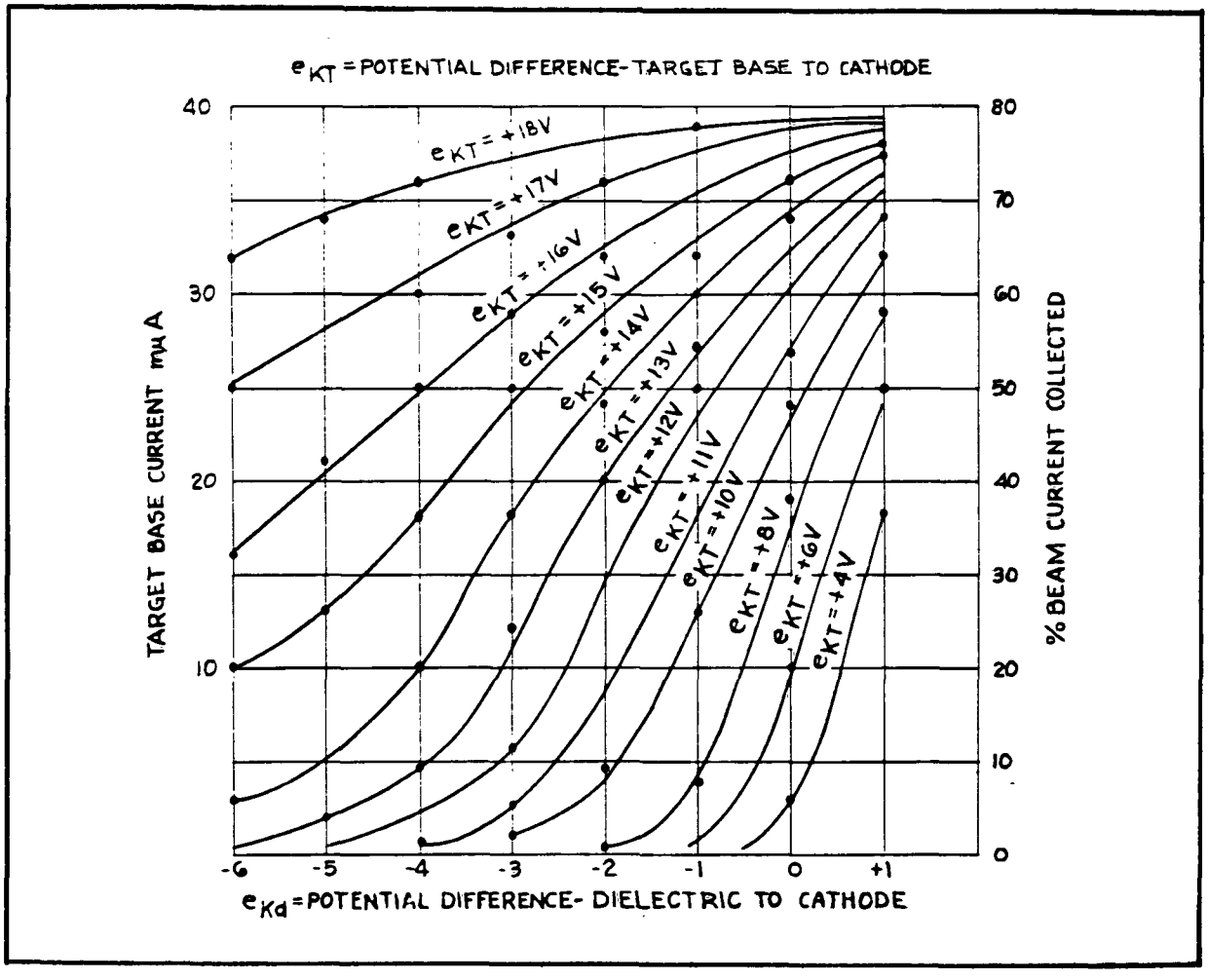

Figure 6-12. Reading Transfer Characteristics, Beam Current 0.05 Microampere

For a linear transfer only the straight part of the curve e_{kt} = +11 volts is used. For nondestructive readout, this curve can be used only to where e_{kd} = 0 (points further to the right on this curve will have electrons landing during readout, these electrons will produce a change in the storage pattern). The writing (exposure) is continued to the point where the potential pattern on the dielectric lies between -3 volts and zero with respect to the reading cathode. This potential range on the dielectric surface modulates the return beam more than 60 percent.

Figure 6-13 shows a reading transfer curve which was taken from a later tube which had an S-20 photocathode. The cathode potential in this case was -11 volts with respect to the target base. The theoretical curve on the left is the reading transfer curve which was derived from the teledeltos field plots and electron trajectory traces. The points of the measured and experimentally derived transfer curves are shifted 2.5 volts to the left. This shift takes into account the contact potential of the cathode and the bare base nickel of the grooves in vacuum. The voltage drop of the cathode current through the barium oxide coating is also included in this 2.5-volt shift. For a comparison with the theoretically derived curve, both conditions, the contact potential and the voltage drop, have to be algebraically added to the measured cathode potentials. The ordinates of the theoretically derived curve were reduced by 13.3 percent. This reduction compensates for electrons lost during priming and those which were not accounted for in the theoretical determination. It can be seen that the experimentally measured curve matches the theoretically derived curve quite closely when reasonable corrections are applied.

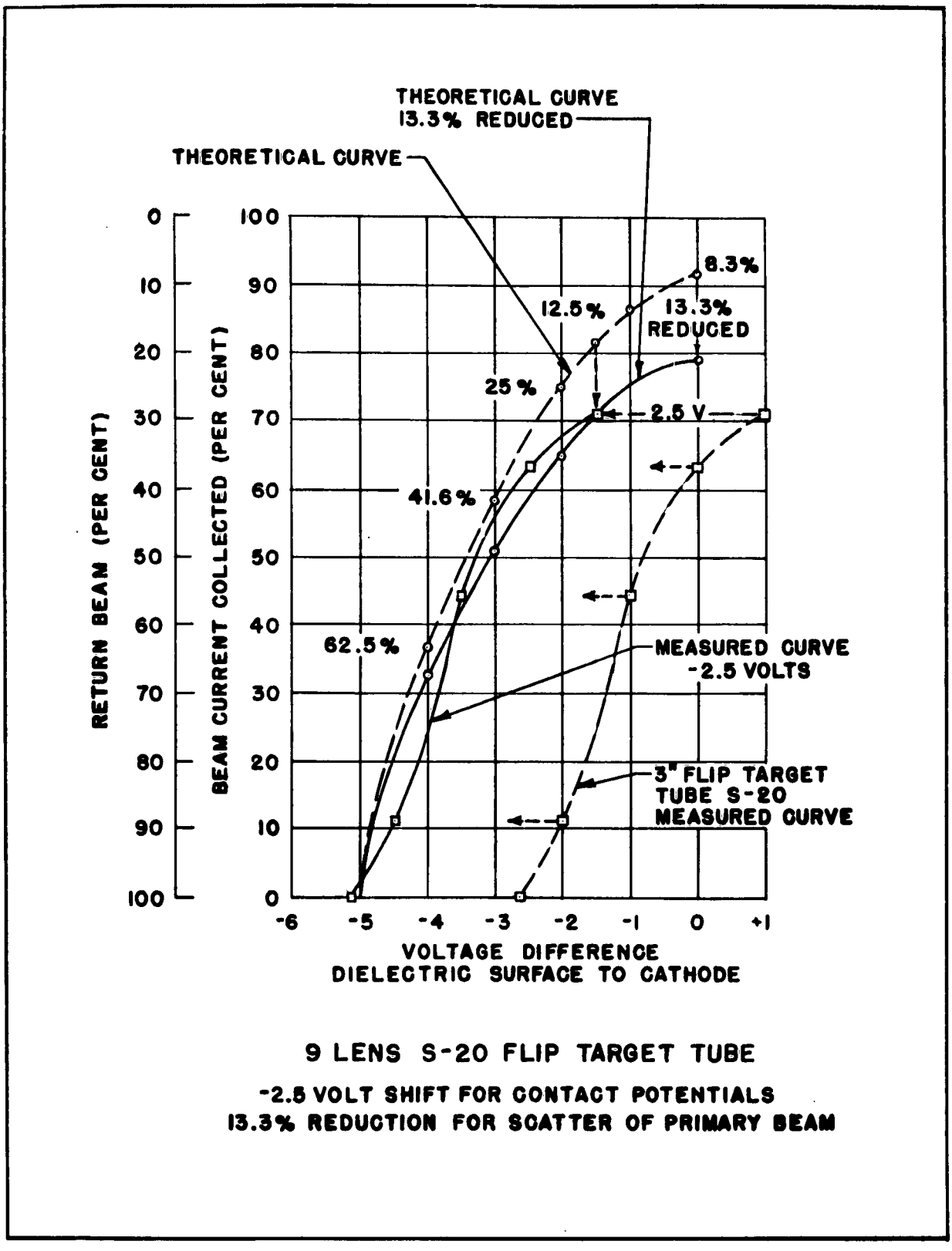

Figure 6-13. Reading Transfer Theoretical Curve
Comparison of Experiment and Theory

6.3.2 Sensitivity

A practical measure of sensitivity for a typical flip-over target test tube was obtained by making photographic light measurements with a Western photovoltaic exposure meter on typical test patterns and average scenes.

With a 9-microampere per lumen bialkali photocathode flip-over target test tube, it was found that the optimum exposure at f/8 was approximately 1/5 of a second with an average scene brightness of about 25 candles per square foot on a low contrast picture, or 0.6 meter-candle-seconds average exposure. The corresponding ASA value given on the exposure meter is approximately 10 to 12. Measurements of highlight brightness on a RETMA test pattern transparency show a value of 150 candles per square foot. The proper exposure for this condition turned out to be 1/25 second at f/4.7, or 2 meter-candle-seconds for the highlight. This again corresponds to an ASA of approximately 10 to 12.

The 50 percent contrast aerial photograph was stored on a tube with a 50 microampere per lumen trialkali photocathode with an average exposure of 0.8 meter-candle-seconds and showed 8 shades of gray in the hard copy film photo of the display kinescope. This indicates an exposure index of about ASA 9. It is known that the storage dielectric on this tube was too thick for proper EBIC gain; this would explain its low exposure index despite the higher photocathode response.

A theoretical analysis of overall camera tube sensitivity was given in the Technical Documentary Report ASD-TDR-62-990, dated 30 November 1962, Appendix A.

6.3.3 Resolution

The aperture response indicating the resolution of the whole TVIST system is composed of the following apertures:

a. Optical lens

b. Transformation of light energy into photoelectrons

c. Magnetic focusing of the photoelectrons in an accelerating electrostatic field

d. EBIC (or secondary emission) writing

e. Storage of the electrostatic charge pattern

f. Reading beam diameter, magnetic focusing, and deflection

g. Reading process (nondestructive)

h. Target disturbance

i. Return beam

j. Amplifier

k. Display kinescope CRT spot diameter, focusing, and deflection

l. Recording of display, camera lens

m. Recording of display, film

Photos of the kinescope display of stored pictures involve all of these apertures. Aperture response curves taken from bar pattern signals from the amplifier involve only the first ten apertures.

6.3.3.1 Standard 30 Frames Per Second, 525 Line Raster, Underscanned

6.3.3.1.1 RETMA Chart Measurements. - In figure 6-14 a photo of the kinescope display of a stored RETMA chart portion is shown. The figures along the wedges correspond to the TV lines per height of the test chart. The charts were optically reduced by a camera lens focusing it onto the photocathode such that the chart height of the image was known. The ratio of the figure corresponding to the point where the wedge was still resolved to the chart height in inches is then the resolution in TV lines per inch on the storage target. The RETMA chart was optically reduced to 0.192 inch on the photocathode and on the storage surface. In the figure only a portion of the chart was underscanned at 30 frames per second with an 8 mc display. The pattern can be resolved down to "725." Therefore the limiting resolution is 725/0.192 = 3800 TV lines per inch or 75 line pairs per mm storage surface.

6.3.3.1.2 Westinghouse Bar Pattern, 30 Frames Per Second. - This pattern is shown in figure 6-15. It is composed of nine sets of bars and permits aperture response measurements or visual resolution measurements in each corner and side as well as the center of the picture. In our work frequently only one diminishing bar pattern group was used, placed in the area of interest and of a size appropriate to the resolution limit measured.

This is the pattern used in paragraphs 3.5 and 5.2.2. For determining the aperture response curves on the flip-over target test tubes, the procedure was somewhat modified.

The pattern was optically reduced 17.5 times and the image focused onto the photocathode. The photoelectrons were accelerated with 10 kv for EBIC writing and the test pattern stored on the storage surface. As before the storage target was underscanned with a 525 line raster at 30 frames per second with an 8 mc amplifier. A line selector A-scope displayed the read output on only one horizontal scanning line perpendicular to the stored bars. In figure 6-16 the aperture response curves for 4 different storages and readouts are plotted. Their 5-percent response point (limiting resolution) is around 3800 TV lines per inch or 75 line pairs per mm.

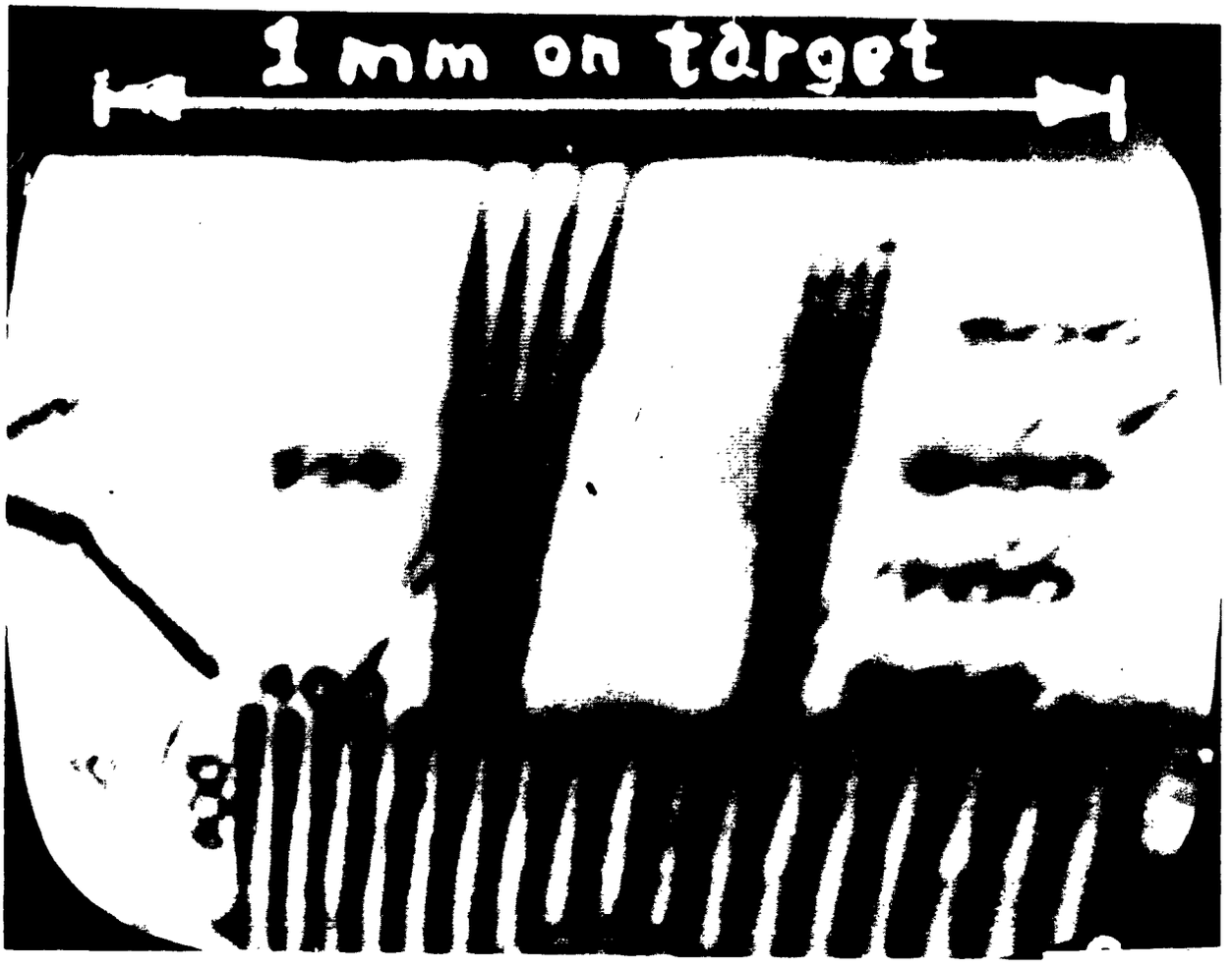

Figure 6-14. Display of Underscanned Stored Picture, RETMA Chart 0.192-Inch High

6.3.3.2 Slow Scan Measurements

By scanning the stored picture with 9000 lines (7500 active lines; 1500 lines during vertical retrace blanking) only once in six seconds (five seconds scan, 1 second vertical return) a factor of 5 x 30 x 525/900 = 9 is gained in bandwidth over the conventional 525 lines at 30 frames per second scan. The unit to produce this slow scan is described in Section 7. A chart of nine Westinghouse patterns arranged as in figure 6-15 was optically reduced to a picture size of 0.8 x 0.6 inch with a diagonal of one inch on the photocathode and the storage surface of a 3-inch diameter flip-over target test tube. The entire picture was scanned.

6.3.3.2.1 Westinghouse Bar Pattern, Resolution Uniformity. - The stored bar patterns 1 to 6 were successively displayed on the line selector A-scope and a Polaroid picture of each bar group was taken. (See figure 6-16a.) Three groups of experiments

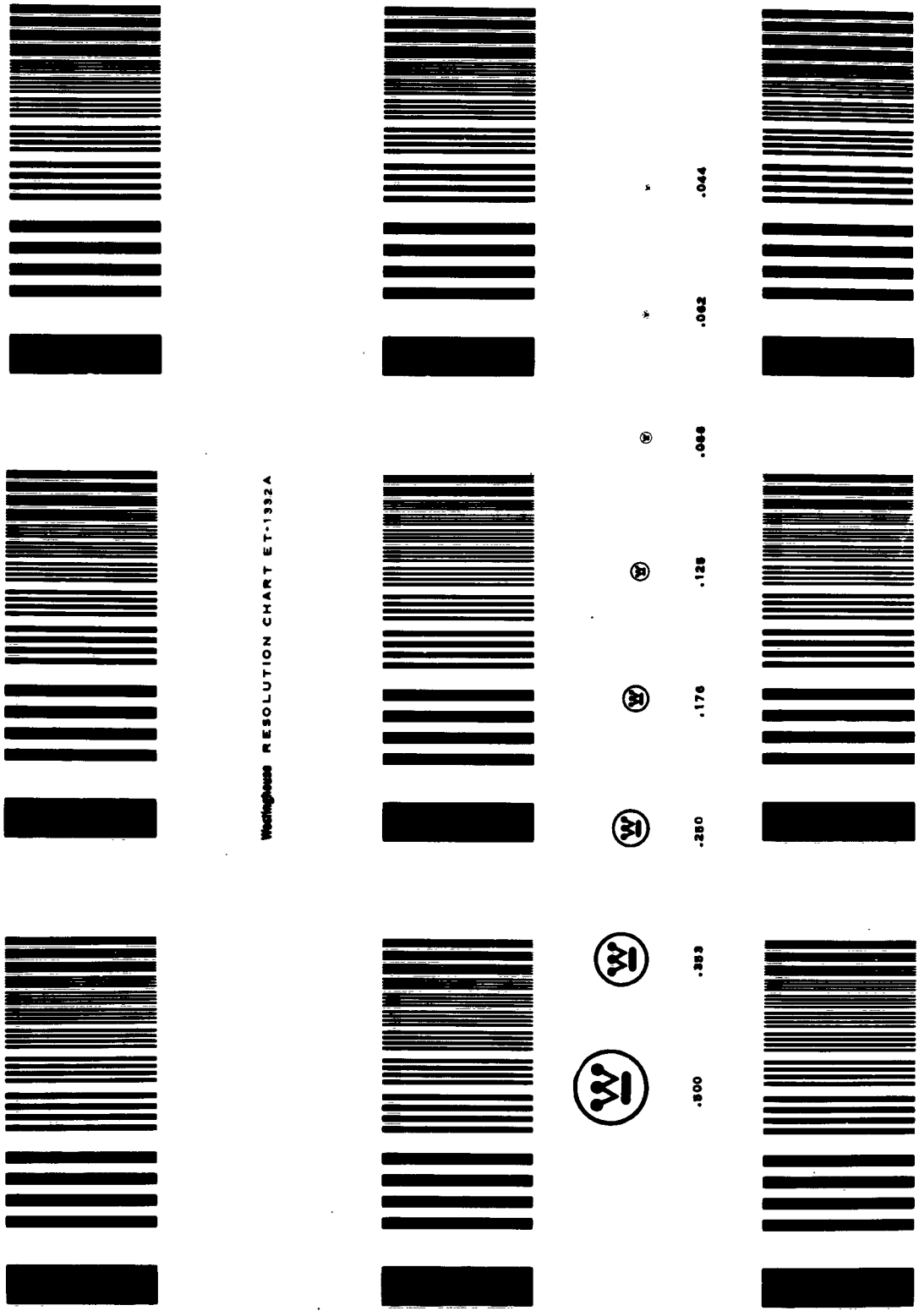

Figure 6-15. Westinghouse Bar Pattern 9.38 Inches by 7 Inches

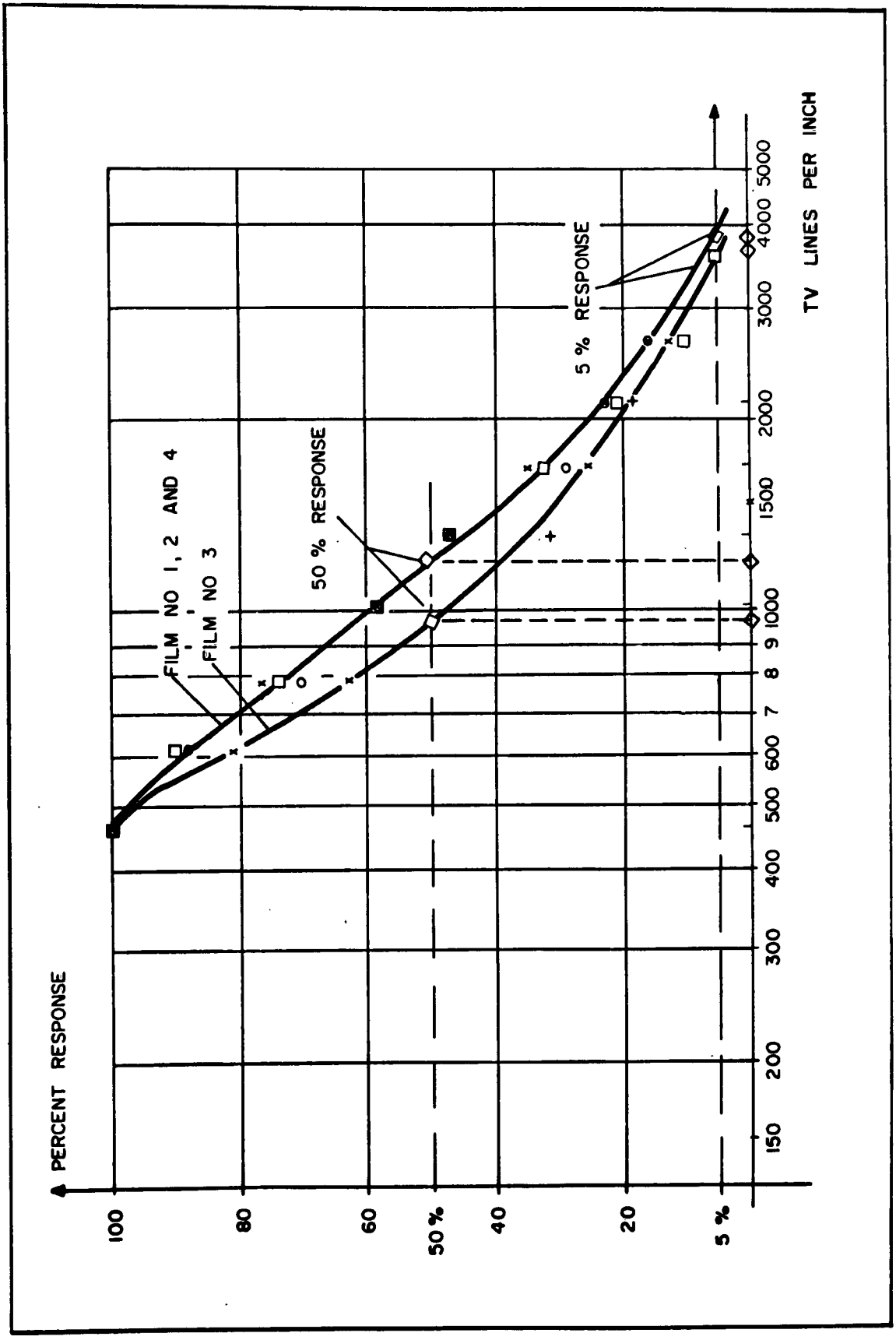

Figure 6-16. Square Wave Response Curve, Westinghouse Bar Pattern Underscanned 30 Frames Per Second

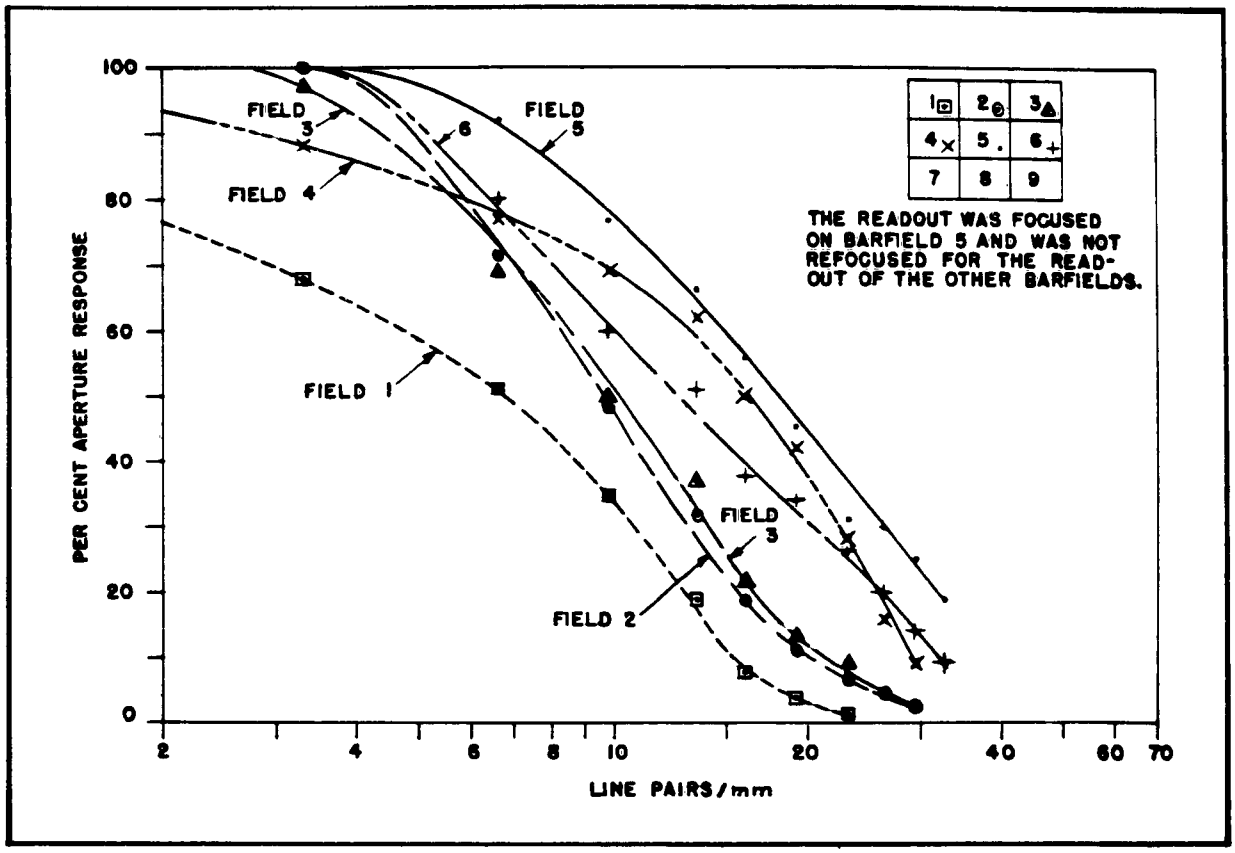

Figure 6-17. Square Wave Response Variation Over Picture Area, Center Focus

were made which demonstrate the necessity of dynamic focusing of the reading beam. In the first group the aperture response of the bar fields 1 to 6 was recorded by setting the readout focus to an optimium for the center bar field No. 5 and then reading all other bar fields with the same focus setting. The aperture response curves were plotted for each bar field in figure 6-17. Bar field 5 has the highest resolution and fields 4, 6, 3, 2, and 1 follow in this sequence. In the second group an optimum average focus for bar fields 2 and 5 was set for the reading, and all fields were read with the same focus setting. The resulting aperture response curves are plotted in figure 6-18. In the third group the reading was focused for optimum for each bar field in simulation of dynamic focusing for optimum. These show the highest resolutions (figure 6-19), but there is still an appreciable loss towards the periphery which cannot be improved by dynamic focusing of the reading beam. This must be due to the large loss of resolution towards the periphery in the image section as shown in paragraph 3.5.3.

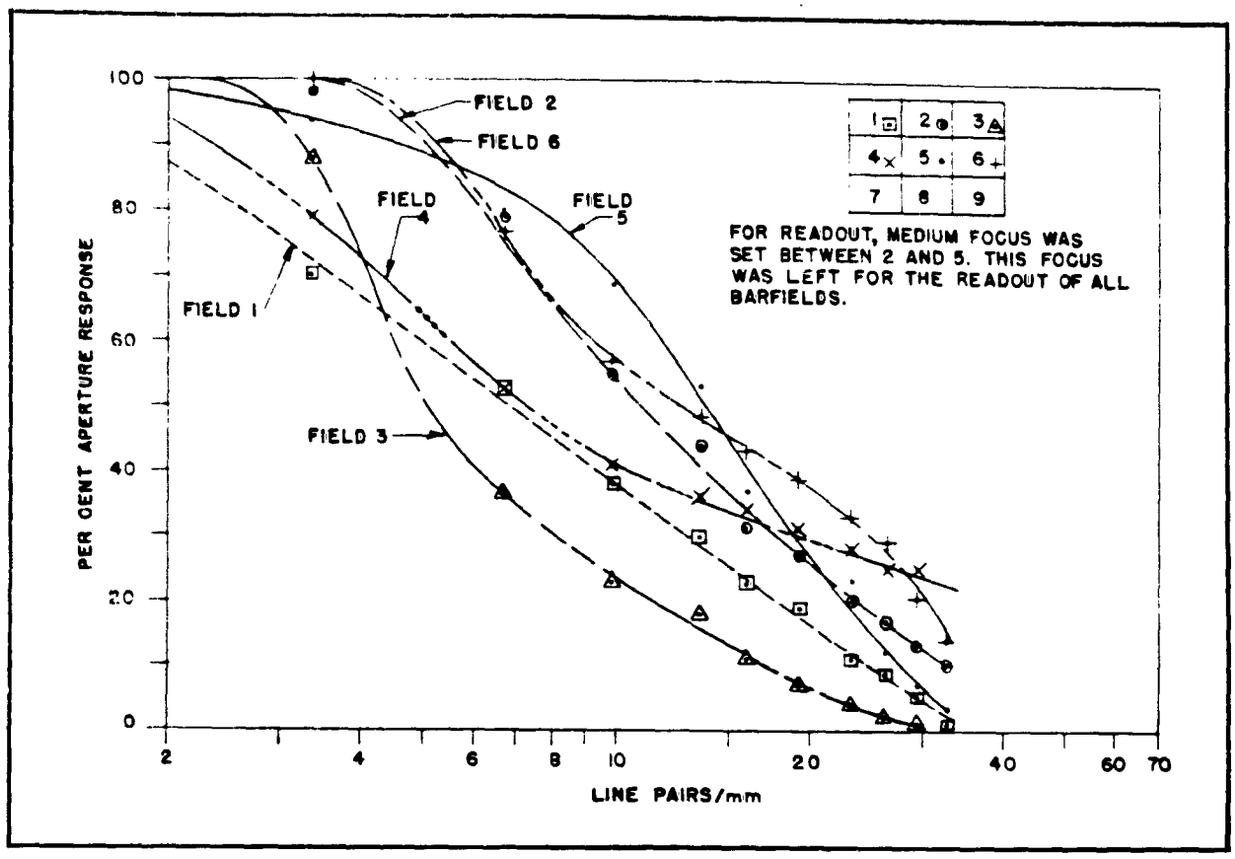

Figure 6-18. Square Wave Response Variation Over Picture Area, Mid Focus

All these curves indicate no 50-percent response worse than 5 line pairs per mm and some as great as 20 line pairs per mm. Limiting resolution at 5-percent response is nowhere less than 18 line pairs per mm and in the center it is as great as 50 line pairs per mm.

6.3.3.2.2 Aerial Photograph. - A 3-foot square aerial photograph of a portion of Wright-Patterson Air Force Base was provided by the ASD Reconnaissance Laboratory. It had been specially printed on semimatte paper to have a maximum contrast ratio of 50 percent in reflectance. There were three 50-percent contrast Air Force test patterns and two gray wedges of different slopes set into the photo. This photo was reduced optically 51 times by a Xenar f/4.7, 135 mm lens with its aperture set at f/8 (see figure 3-8). The image size was 0.7 inch x 0.7 inch with a one inch diagonal. Table 6-1 is included as an aid to figures 6-20a through 6-20g.

Several such photographs were taken on 4 x 5 inch Panatomic X photographic cut film in a Crown-Graphic camera. These were each developed in 3 to 1 diluted

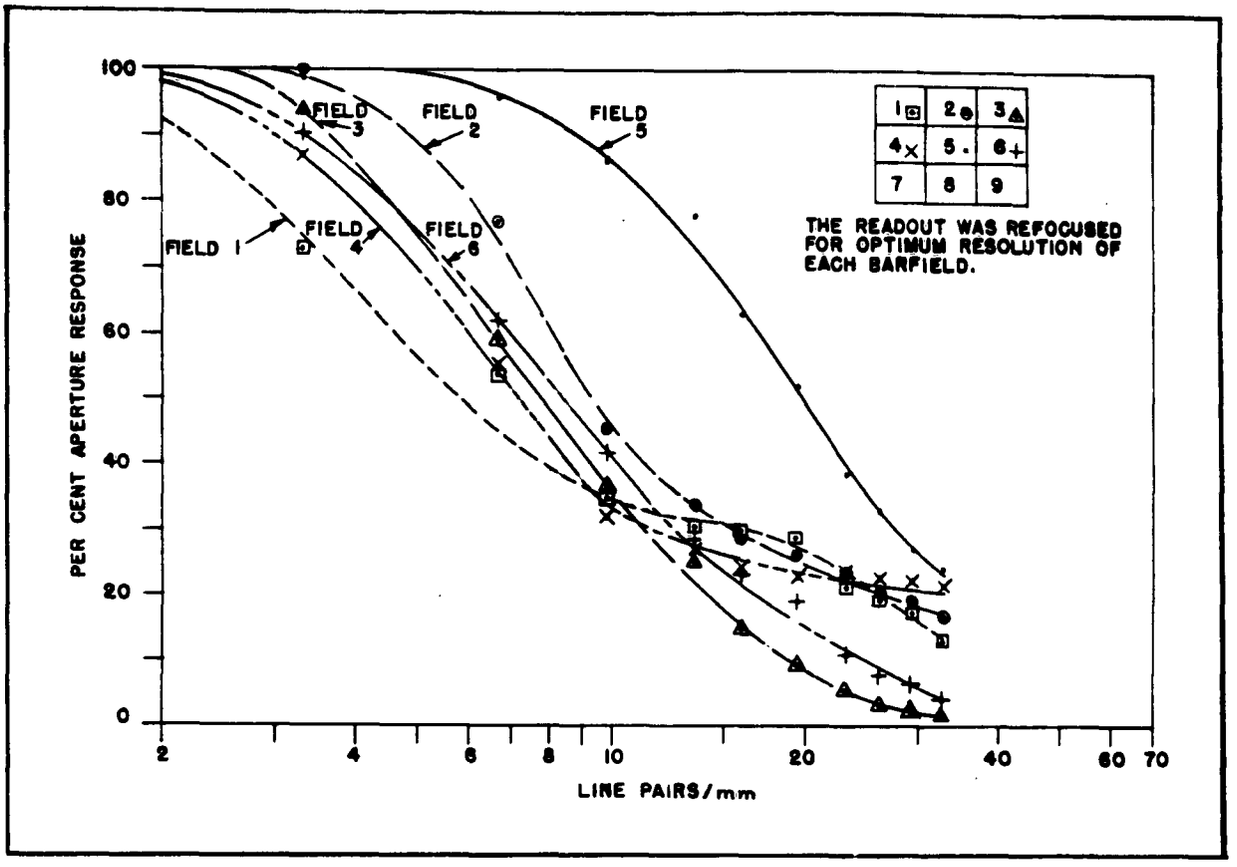

Figure 6-19. Square Wave Response Variation Over Picture Area, Dynamic Focus

Microdol for 22 minutes, and the best negative was chosen. Figure 6-20a is a 4.2X positive enlargement of this 0.7 x 0.7 inch negative image.

With the same lens and optical arrangement forming the 0.7 x 0.7 inch optical image on the photocathode, a charge pattern was stored on the grating target storage camera tube. Figure 6-20b was produced by reading the entire 0.7 x 0.7 inch stored picture on the slow scan unit, displaying it on the kinescope on a 2.8-inch square raster and photographing the kinescope on 4 x 5 inch Polaroid P/N type 55 cut film to form a 3-inch square photo. Note that this then is essentially a 4.3X negative enlargement of which figure 6-20b is a positive contact print.

Comparing these two the photographic enlargement shows 30 line pairs per mm limiting resolution, no blemishes and a better gray scale. The stored picture has 23 line pairs per mm resolution and an enhanced contrast which has limited the gray scale. These resolution measurements are made on the AF test pattern at one edge of the picture. The three negative AF test patterns on the ground along the south of

runway 27 can be seen, but not resolved on both, but are more pronounced on the stored picture because of its higher contrast.

Figure 6-20c is a portion of a 14X enlargement of the photographic negative. Figure 6-20d is a positive print of a Polaroid negative which was obtained by underscanning the 0.7 x 0.7 inch charge pattern on the storage target by a factor of 3.5X with a 0.21- x 0.21-inch square raster. This was displayed on the kinescope 2.8-inch square and photographed 3-inch square for a total 4 x 3.5 = 14X enlargement.

The photograph shows better gray scale and a limiting resolution of 34 line pairs per mm. The stored picture does not resolve the AF pattern since it is just out of the chosen reading gray scale, but the runway numbers can be read indicating better resolution than the previous 23 line pairs per mm.

In figure 6-20e that portion of the photographic negative, which shows the AF test pattern near the center of the aerial photograph is enlarged 51X.

For comparison figure 6-20f shows the same inset AF test pattern on the same stored charge pattern. It was read still again, but this time underscanned 11.9X with a 0.059-inch square 5-second raster, followed by a 48X kinescope enlargement and a 1.04X photographic enlargement for a total 51X enlargement.

The heavy grain on the photograph makes the sixth step of the first bar group the limit of resolution at 51 line pairs per mm, with the entire pattern at very low contrast. The stored picture shows the first step of the second bar group at 64 line pairs per mm; the whole pattern is of good contrast, clear and free from noise though there is a strong disturbance pattern from scratches (not grating grooves at 240 per mm) on the storage target. This shows that even for a low contrast scene, the high resolution charge pattern has been stored. It may be read if the reading data rate is low enough and if the display kinescope and its photographic recording has sufficient resolution.

Note that this AF test pattern shows that the resolution is the same in all directions. Thus, there is no loss in resolution that can be ascribed to leakage or electrostatic interaction along the grating grille lines, even after the half hour of storage time required to perform this experiment.

6.3.3.2.3 RETMA Chart, Resolution Uniformity and Gray Scale. - The RETMA test pattern of figure 6-21* was reduced to 0.8 x 0.6 inch on the photocathode and the storage surface, displayed on the slow scan unit and photographed from the kinescope

* Figures 6-20 through 6-21 are comparisons between Photography and TVIST (on slow scan), 50-percent contrast, aerial picture 3 x 3 feet.

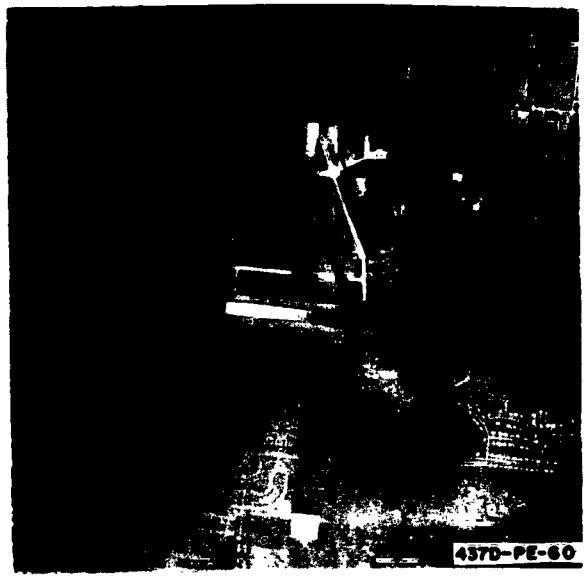

Figure 6-20a. Photographed on 0.7 x 0.7-Inch Negative, Enlarged 4.3 X to 3 x 3 Inches

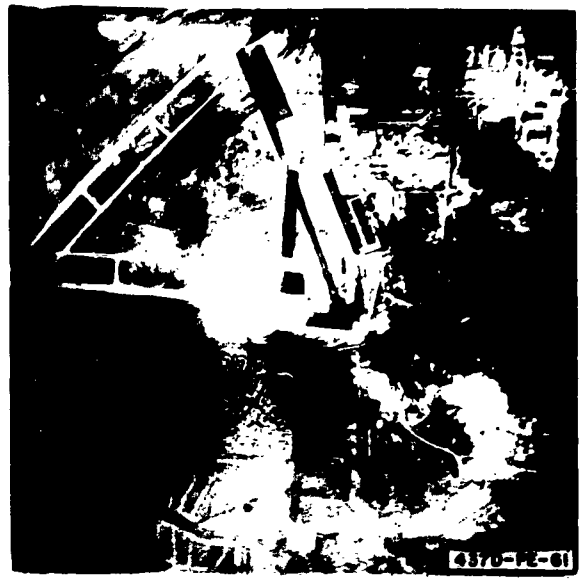

Figure 6-20b. Stored on 0.7 x 0.7-Inch Area, Readout With Slow Scan Unit, Display enlargement 4 X; Photographic enlargement 1.07 X; total 4.3 X

Figure 6-20c. Part of Above Photograph Enlarged 14 X

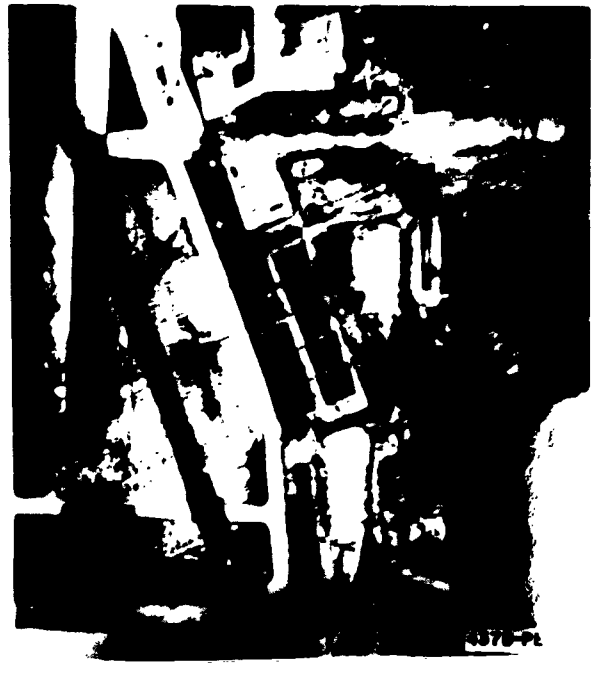

Figure 6-20d. Same Storage as Above; Underscanned 3.3 X, Display enlargement 4 X; Photographic enlargement 1.07 X; Total 14 X.

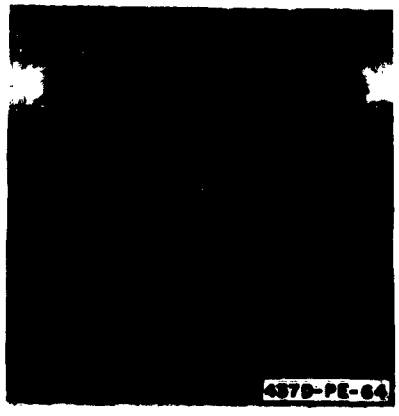

Figure 6-20e. Part of 6-20a 51 X Enlarged

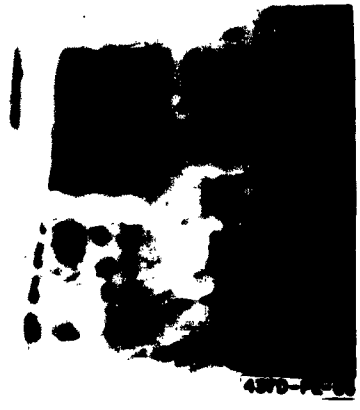

Figure 6-20f. Same Storage As 6-20b, Underscanned 11.9 X Display enlargement 4X; Photographic enlargement 1.07X; Total 4 x 1.07 x 11.9 = 51X

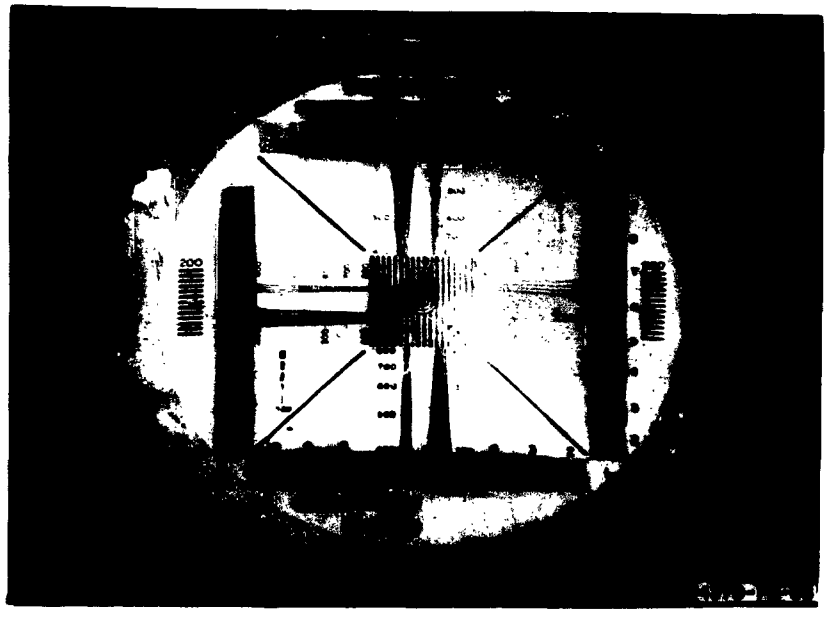

Figure 6-21. Kinescope Display of REMTA Chart, 0.8 x 0.6-Inch Raster

TABLE 6-1

TECHNIQUE DATA TO FIGURE

Figure 6-20	Process		Optical Reduction	Full 3- x 3-Foot Chart Size Reduced to		Scanned Raster Size in Mils	Magnification			Total
	Photography	Stored, Displayed and Photographed		On Negative (inch)	On Storage Target (inch)		Display	Photographic	Underscan	
a	✓		51 X	0.7 x 0.7				4.30 X		4.3 X
b		✓	51 X		0.7 x 0.7	700 x 700	4 X	1.07 X	1.0 X	4.3 X
c	✓		51 X	0.7 x 0.7				14.00 X		14.0 X
d		✓	51 X		0.7 x 0.7	210 x 210	4 X	1.07 X	3.3 X	14.0 X
e	✓		51 X	0.7 x 0.7				51.00 X		51.0 X
f		✓	51 X		0.7 x 0.7	59 x 59	4 X	1.07 X	11.9 X	51.0X

display. The resolution can be seen clearly down to 800 which means that it must be much in excess of 800/0.6 = 1330 TV lines per inch, or 26 line pairs per mm. Simultaneously, the corner resolution is 10 line pairs per mm, and 8 steps of gray can be counted. The several "200" groups at 5 line pairs per mm are everywhere on the chart at very high contrast.

6.3.3.2.4 Aperture Correction. - All of the experiments described in this report were done with no aperture correction in the amplifier. This was done purposely since the intent was to determine the performance of the storage camera tube alone without the benefits of any subsequent circuit sophistication. If any at all were employed, it would be difficult to draw a line where to stop, and all the data would have to be qualified by what circuitry was used and how much. However, it is of interest to demonstrate that some such circuit modification is able to improve the system performance. Addition of aperture correction adjusted for the storage camera tube aperture response gives the expected results. Figure 6-22 shows the A-scope display at the output of the amplifier without and with aperture correction for comparison. The input signal was the stored signal from the center bar field No. 5 of the Westinghouse Bar Pattern. Figure 6-23 is a plot of the two aperture response curves which result, showing the improved response at mid frequency and the more rapid fall off as is common when this technique is applied to amplifiers. The 50-percent response has been improved from 17 line pairs per mm to 31 line pairs per mm, while the 10-percent response can still be estimated at about 40 line pairs per mm.

6.3.4 Storage Time

Measurements were made on the slow scan system to determine if resolution was affected by long storage times. These experiments were done in the following way.

The Westinghouse diminishing bar pattern was imaged on the photocathode and stored in the target in the usual manner. This stored image was then read with a single scan and displayed on a line selector oscilloscope. The oscilloscope was photographed and the peak signal amplitude for each line group was measured on the photograph. The aperture response was then plotted on a logarithmic scale shown in figure 6-24. After a storage time of 41 hours, the same stored charge pattern was read again with a second scan and photographed on the A-scope in the same manner. This aperture response was then plotted on the same graph by the dotted line.

The signal amplitude decay at the 100-percent level was approximately 42 percent. It was found that when this curve was normalized to 100-percent, that there was little

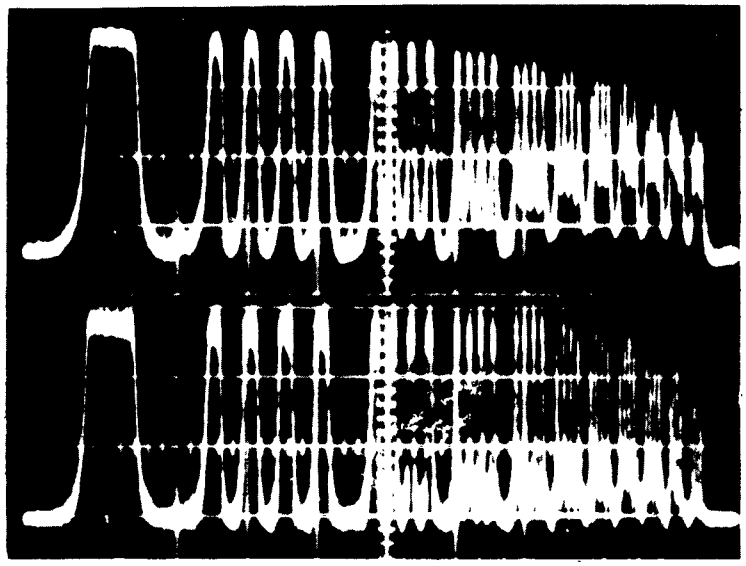

Figure 6-22. A-Scope Display, Westinghouse Bar Pattern No. 5 (Center), at Amplifier Output

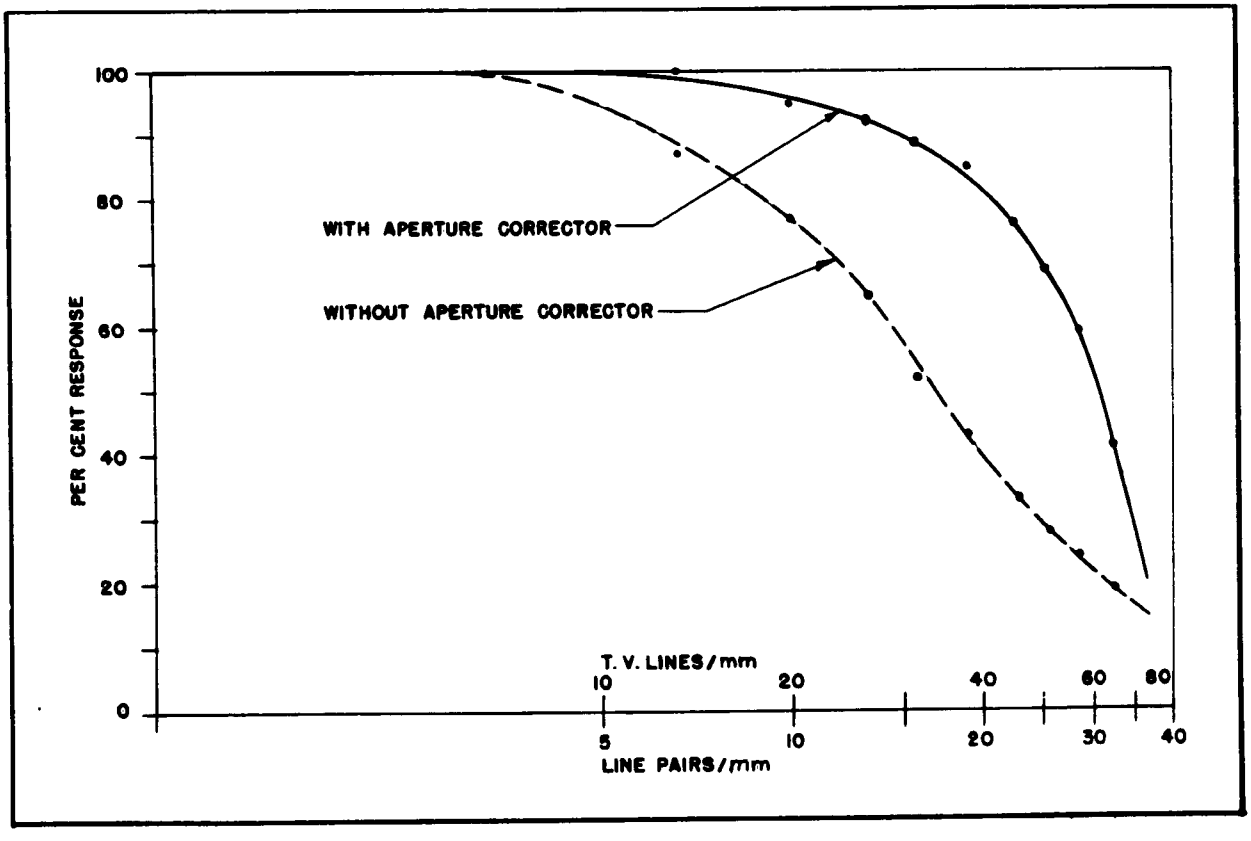

Figure 6-23. Square Wave Response Curve With and Without Aperture Corrector. Note Peaking of Aperture Response.

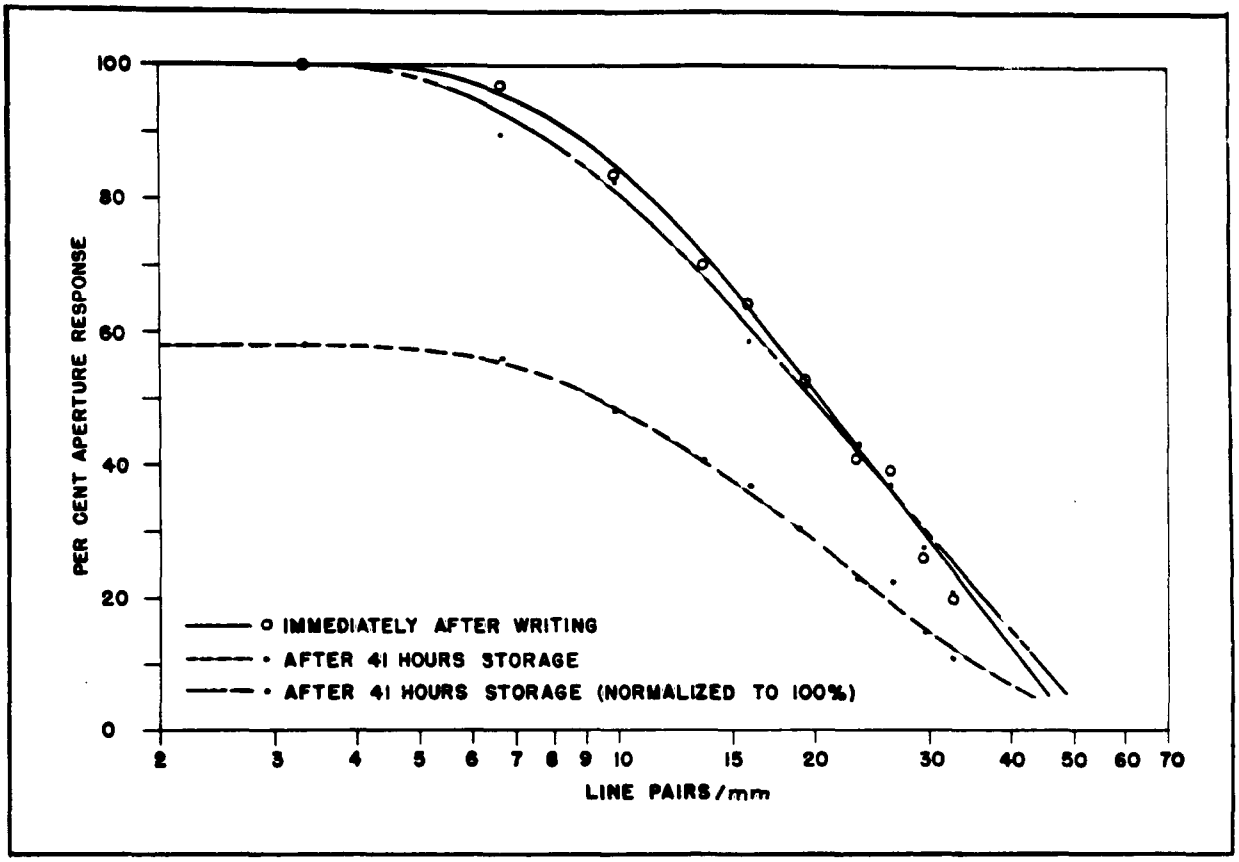

Figure 6-24. Square Wave Response Before and After 41-Hour Storage

if any degradation in resolution due to the long storage time. This is shown by the close matching of the two curves as indicated on the graph.

Storage times of as long as 80 hours have been observed frequently on a TVIST system. These storage times show a contrast decay at the 100-percent level of approximately 60 percent.

7. SLOW SCAN DISPLAY UNIT

7.1 DESIGN PHILOSOPHY

Sweep rates were chosen to avoid the complications of special amplifiers or high reading beam currents to display the very high resolution of the stored patterns. A raster of 7500 scan lines over a 5-second frame time requires only 8-mc bandwidth for the display of a 5000 by 5000 TV element raster with minimum loss of amplitude information. Measured values of the limiting resolution of the electronic display system show values in excess of 4800 TV lines per raster side.

The block diagram of figure 7-1 shows the essential elements of the system. The synchronizing generator feeds the two deflection circuits and the blanking section of the video amplifiers. Direct current filaments had to be used in the deflection circuits to reduce stray 60-cycle coupling. The power supplies are also common to many of the circuits and are not shown here.

The high resolution of the TVIST system and the fact that neither the vertical or horizontal rates are synchronized to the power line dictates that special shielding provisions had to be made. The power supplies and all power filament and line regulating transformers are housed in one cabinet while the deflection, video, and other active circuits are housed in a second cabinet 25 feet from the first cabinet. The kinescope, Westinghouse WX-4647-P11 is placed in a triple shield consisting of a 15-pound steel face shield, a simple SAE 1010 neck shield, a Mumetal main shield, an outer shield of SAE 1010 steel, a rear steel spun cover, and a faceplate steel tube which also acts as a stray light shield.

It was originally proposed that a fast mode, 20 frames per second of about 70 actual scan lines, would be used for set up purposes. However, in actual use, this mode is seldom employed since it tends to store retrace lines.

7.2 CIRCUIT DESIGN

7.2.1 Synchronizing Generator

The synchronizing generator, figure 7-2, consists of a crystal oscillator (30 kc) which feeds a train of eight phantastrons to produce the horizontal and vertical synchronizing pulses. Phantastrons are used because the output leading edge is slave to

the input trigger. The vertical jitter is less than 50 microseconds and the horizontal jitter is less than 0.04 microsecond.

7.2.2 Video Test Oscillator

A crystal oscillator (figure 7-3) operating at 1.2 mc feeds selected frequency multipliers and a squaring circuit to generate square waves at 3.6 mc, 2.4 mc, 1.2 mc, 600 kc, 300 kc, 150 kc, 30 kc while the 30-kc signal is also used as an external trigger to the 58B1 synchronizing generator. In this way, very low jitter signals for video testing are made which are precisely tied to the horizontal synchronizing pulses.

7.2.3 TVIST Video Preamplifier

The preamplifier and multiplier net are contained in a small aluminium box mounted at the socket end of the TVIST camera tube. See figure 7-4. The basic circuit uses a 6BQ7 cascoded to a 6DK6 amplifier feeding the 12AV7 cathode follower. The bandwidth is 11 mc and the voltage gain is 54.

7.2.4 TVIST Video Post Amplifier

This circuit consists of a cascade of 6DK6 - 6U8 (pentode) and 6DK6 - 6CL6 to feed the kinescope grid. The triode section of the 6U8 and 6AL5 comprises key clamp. The video chain was tested using the output of the 58B15 test oscillator through an attenuator. It displayed good contrast at 3.6 mc (or 4800 TV lines/raster side). The postamplifier is shown in figure 7-5.

7.2.5 TVIST Slow Scan

This chassis drives both the kinescope and the orthicon deflection coils. The vertical synchronizer triggers a monostable multivibrator which feeds an operational integrator to generate the vertical sawtooth which drives the pair of transistorized operational amplifiers with high feedback to produce the linear currents to the vertical coils. Switches select appropriate time constants for operation at the 20-frame per second set-up rate or the 5 seconds per frame operating rate. The horizontal synchronizer triggers a monostable multivibrator which gates a 6U8 bootstrap integrator to generate the horizontal sawtooth. The output circuit is a common audio amplifier using an extended range output transformer having a 500-ohm output which provides a reasonably good match to the deflection coils. Figure 7-6 is a schematic of the TVIST slow scan.

7.2.6 TVIST Blanking

As shown in figure 7-7, horizontal and vertical synchronizing signals are fed to monostable multivibrators to generate the blanking gates. A cathode follower pair

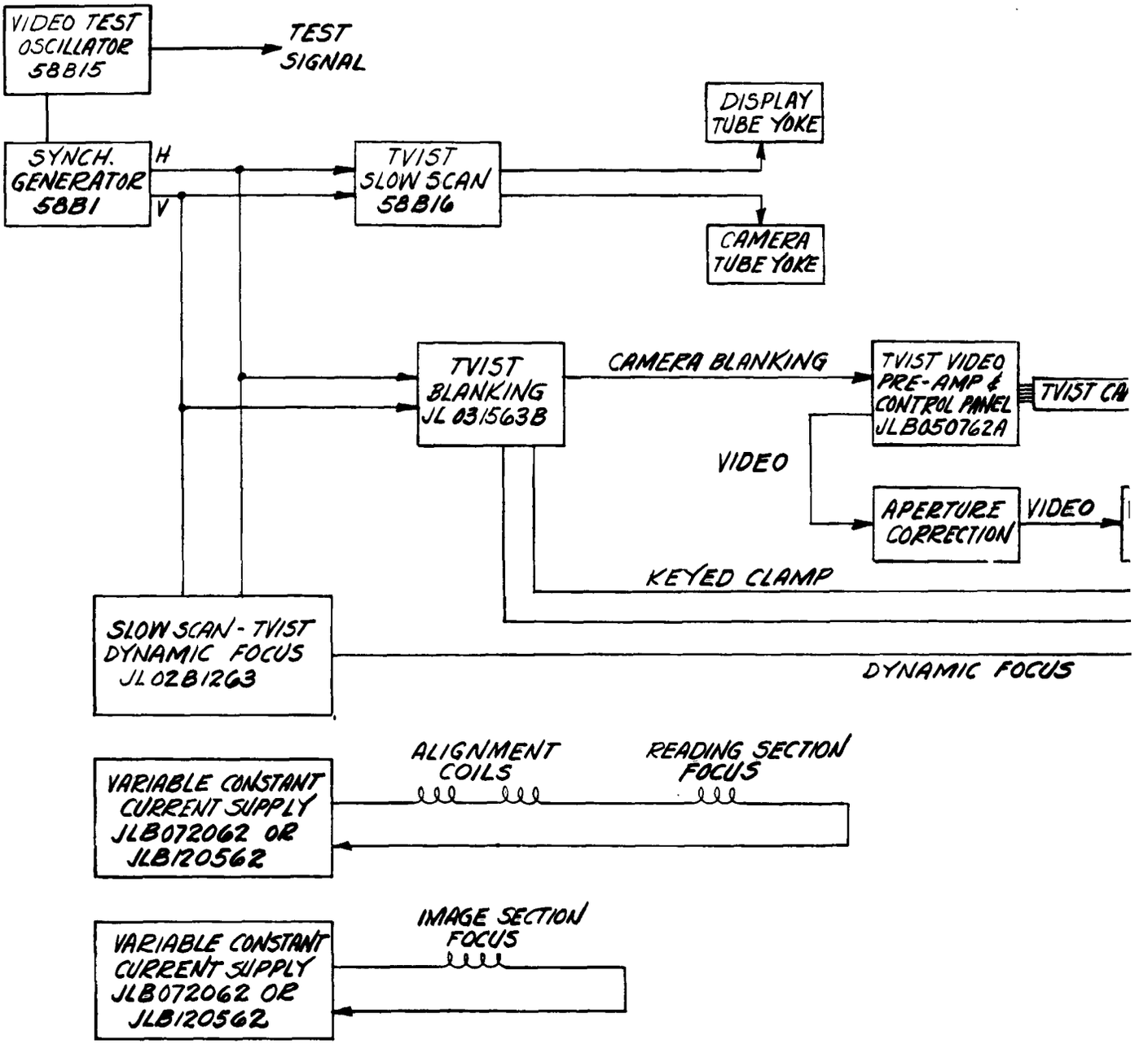

Figure 7-1. TVIST Slow Scan Bl

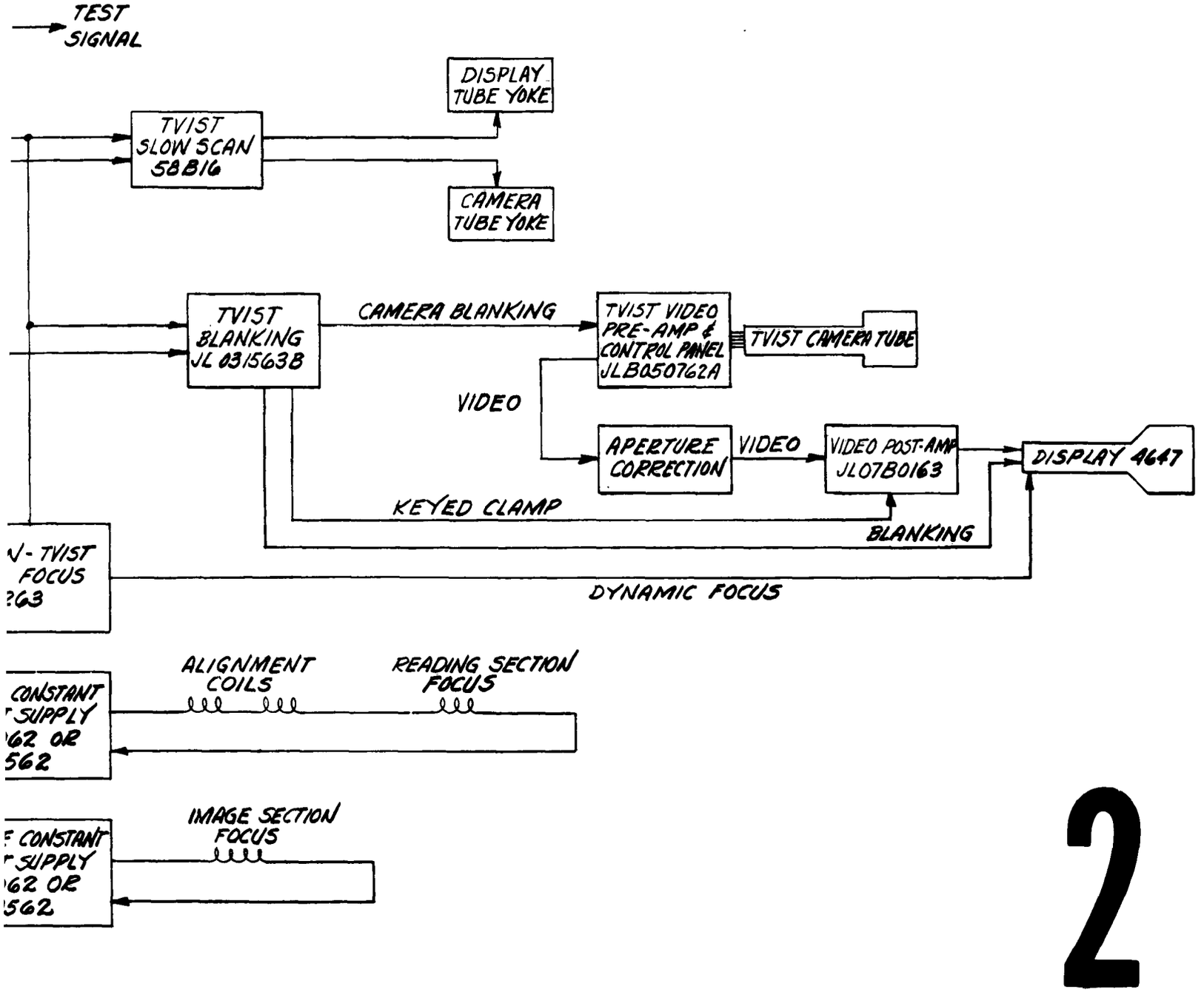

Figure 7-1. TVIST Slow Scan Block Diagram

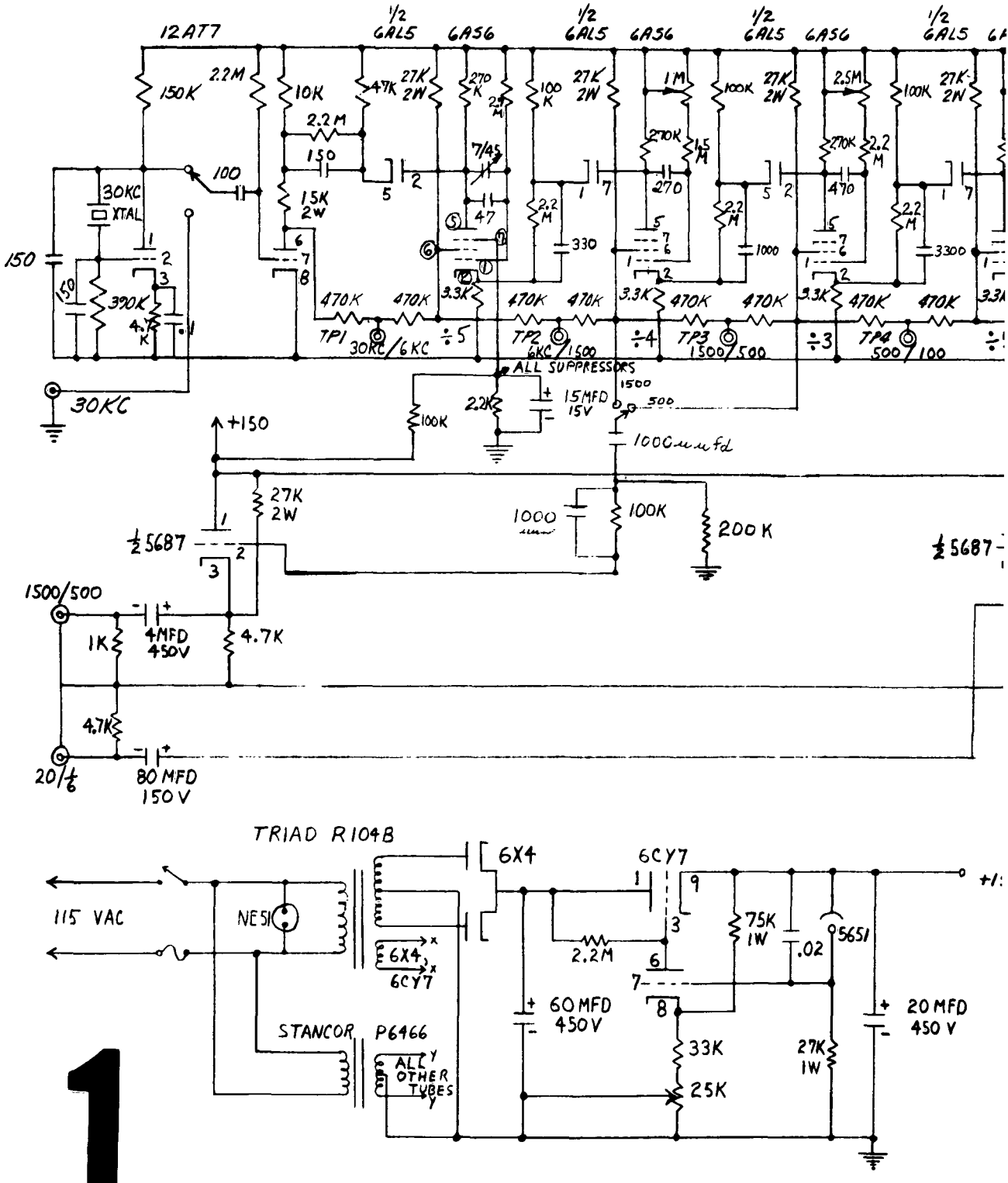
12AT7
1/2 6AL5
6AS6
1/2 6AL5
6AS6
1/2 6AL5
6AS6
1/2 6AL5
150K
2.2M
10K
47K
27K 2W
270 K
100 K
1M
100K
2.5M
150
100
30KC XTAL
15K 2W
7/45
47
330
270
1000
3300
390K
4.7 K
470K
3.3K
TP1 30KC/6KC ÷5
TP2 6KC/1500 ÷4
TP3 1500/500 ÷3
TP4 500/100
ALL SUPPRESSORS
30KC
+150
2.2K
15MFD 15V
1500
500
1000 mmfd
27K 2W
1000 mmf
200 K
½5687
1500/500
1K
4MFD 450V
4.7K
20/½6
80 MFD 150V
TRIAD R104B
115 VAC
NE51
6X4
6CY7
2.2M
75K 1W
.02
5651
60 MFD 450V
20 MFD 450 V
33K
25K
27K 1W
STANCOR P6466
ALL OTHER TUBES

1

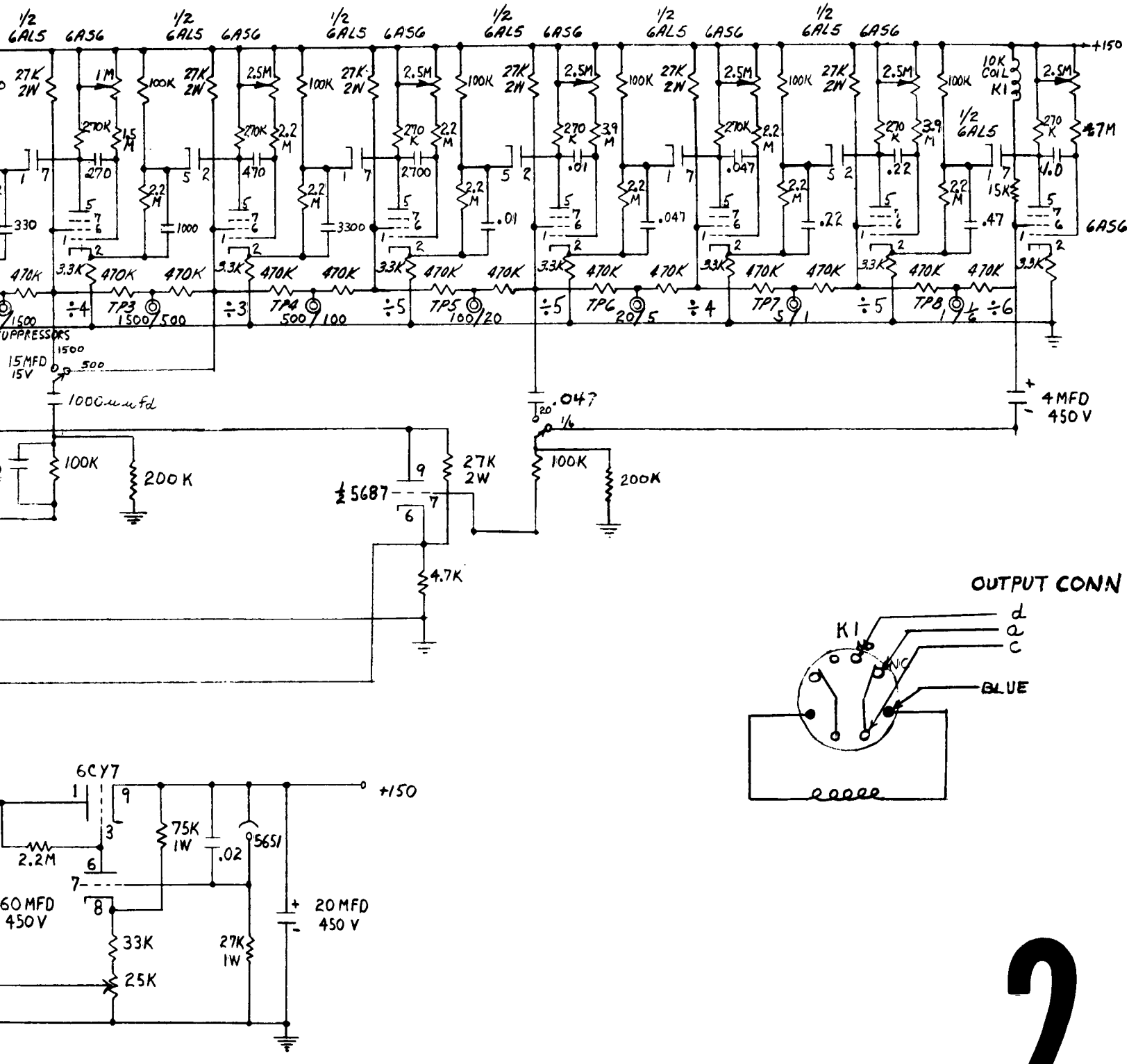

Figure 7-2. Slow Scan Synchronized Generator

2

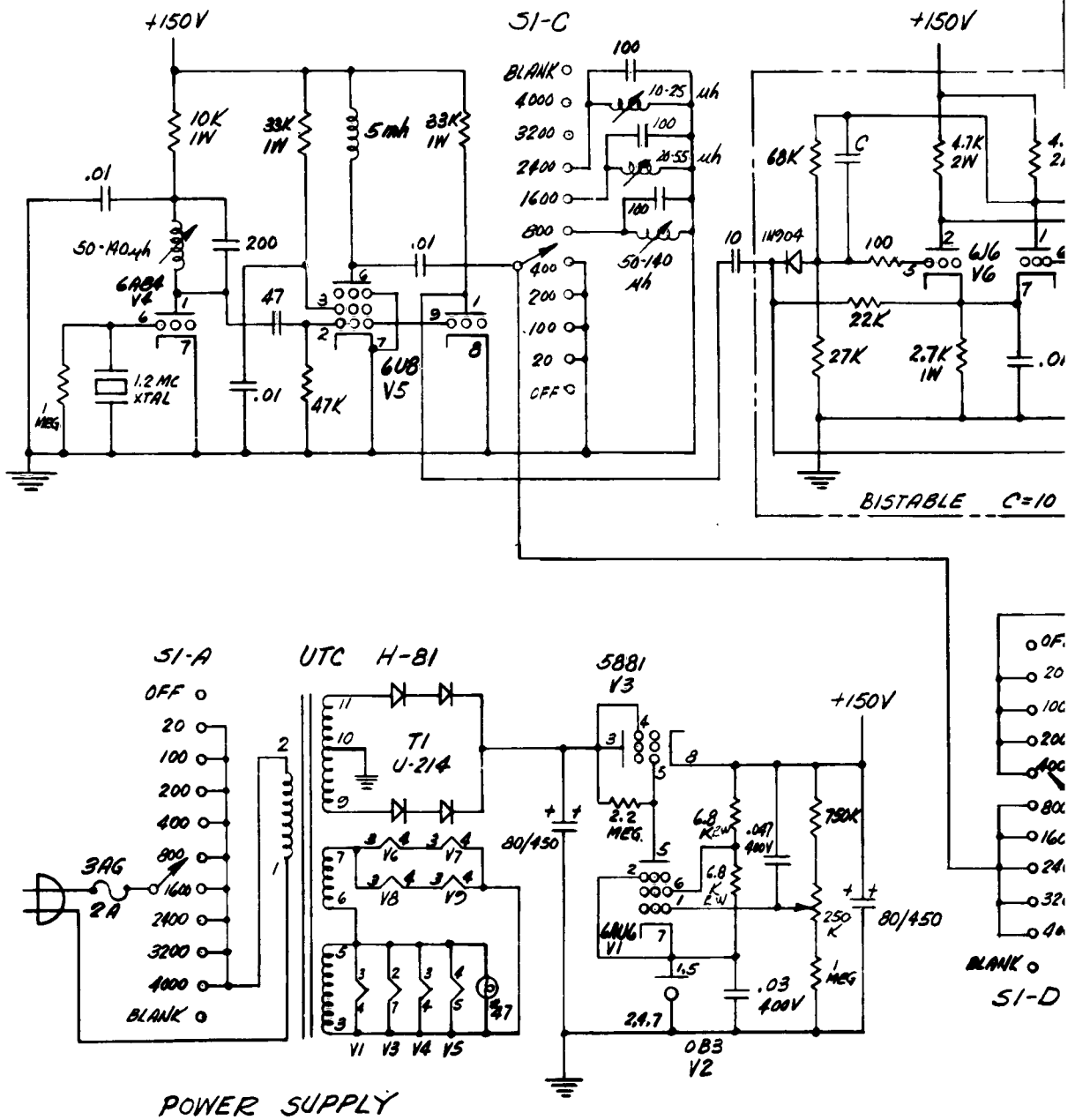

POWER SUPPLY
150 V. OUTPUT @ 75 MA.

1

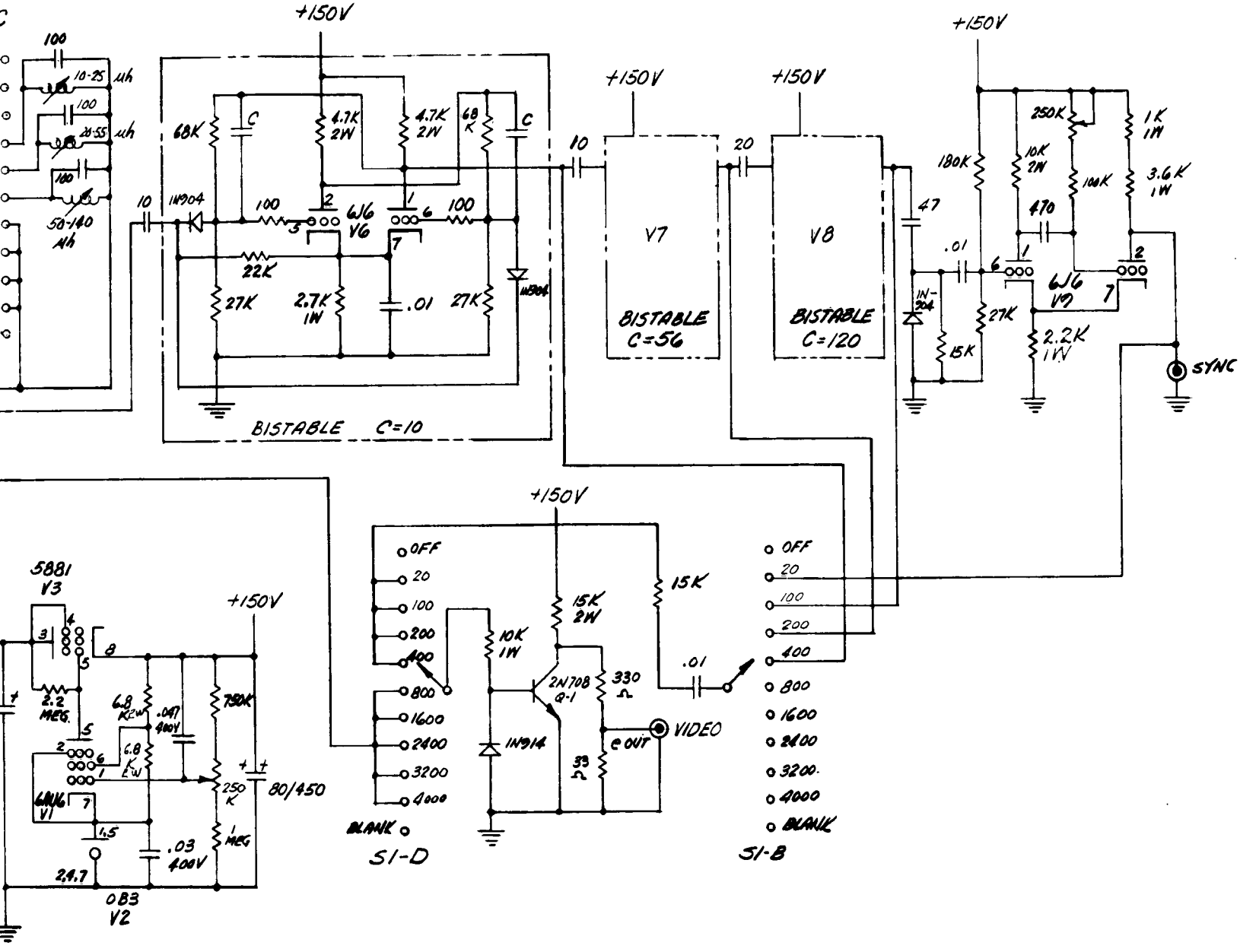

Figure 7-3. Video Test Oscillator Schematic

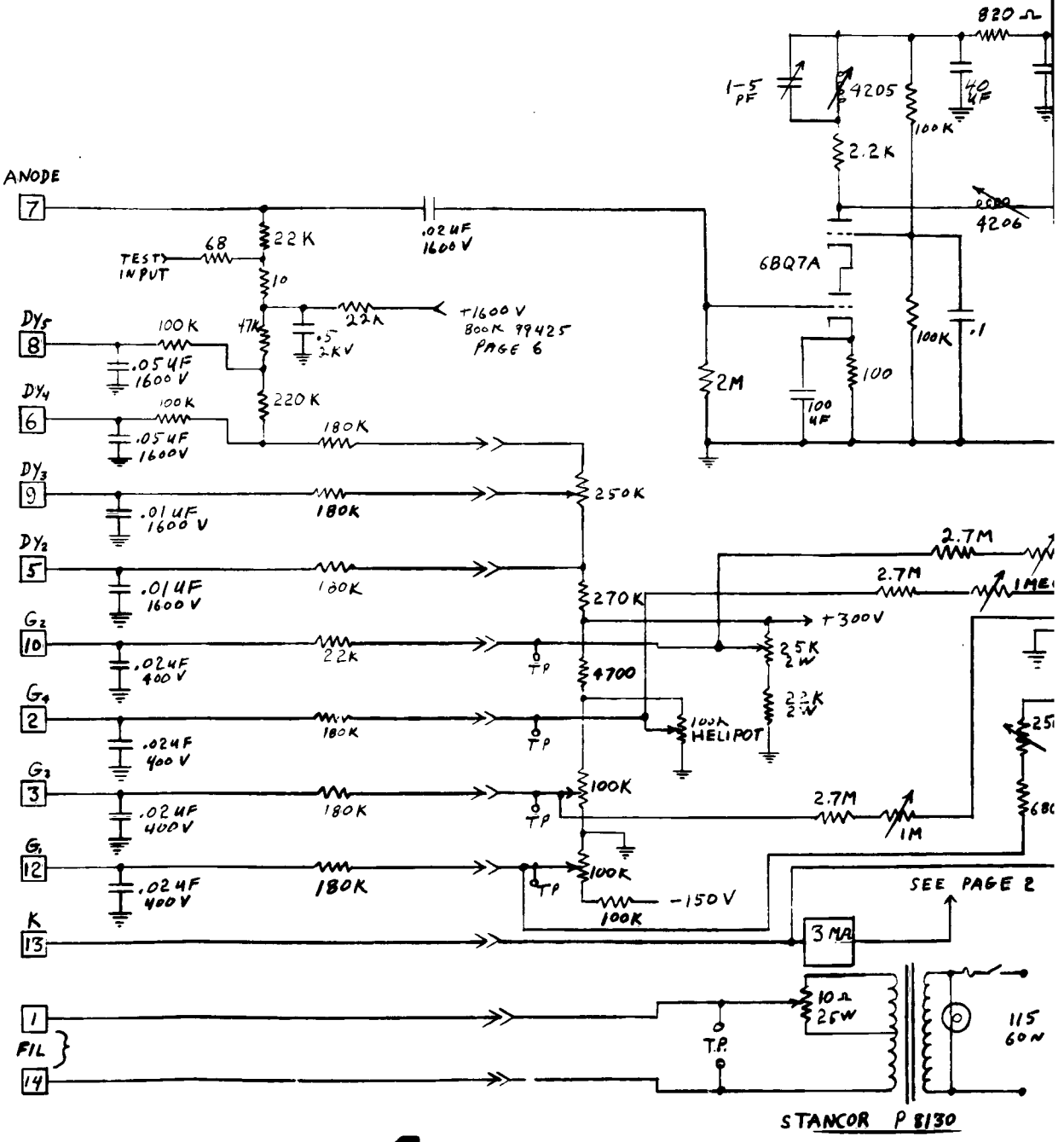
ANODE
7
.02 UF 1600 V
22 K
68
TEST INPUT
10
DY5
8
100 K
47K
.5 2KV
22K
+1600 V 800K 99425 PAGE 6
.05 UF 1600 V
DY4
6
100 K
220 K
.05 UF 1600V
180 K
DY3
9
250 K
.01 UF 1600 V
180K
DY2
5
.01 UF 1600 V
180K
270 K
G2
10
.02 UF 400 V
22k
TP
4700
+300V
2.5K 2W
22K 2W
G1
2
.02 UF 400 V
180K
TP
100K HELIPOT
G3
3
.02 UF 400V
180K
TP
100K
2.7M
1M
G1
12
.02 UF 400V
180K
TP
100K
-150V
100K
K
13
3 MA
SEE PAGE 2
1
FIL
14
T.P.
10Ω 25W
115 60 W
STANCOR P 8130
820Ω
1-5 PF
4205
40 UF
100K
2.2K
4206
6BQ7A
2M
100K
.1
100
100 UF
2.7M
2.7M
1ME
25
68
1M

1

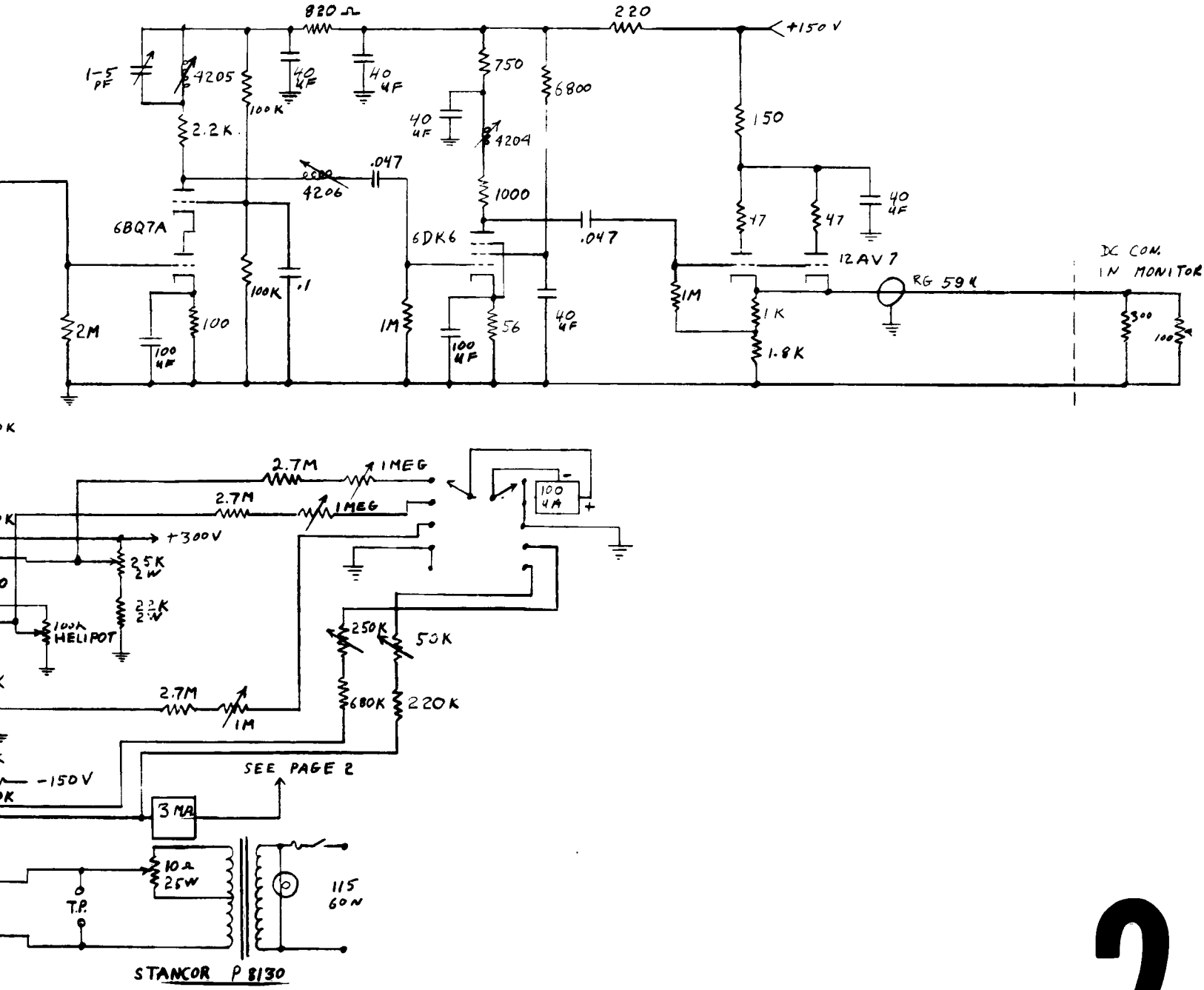

Figure 7-4. TVIST Video Slow Scan

2

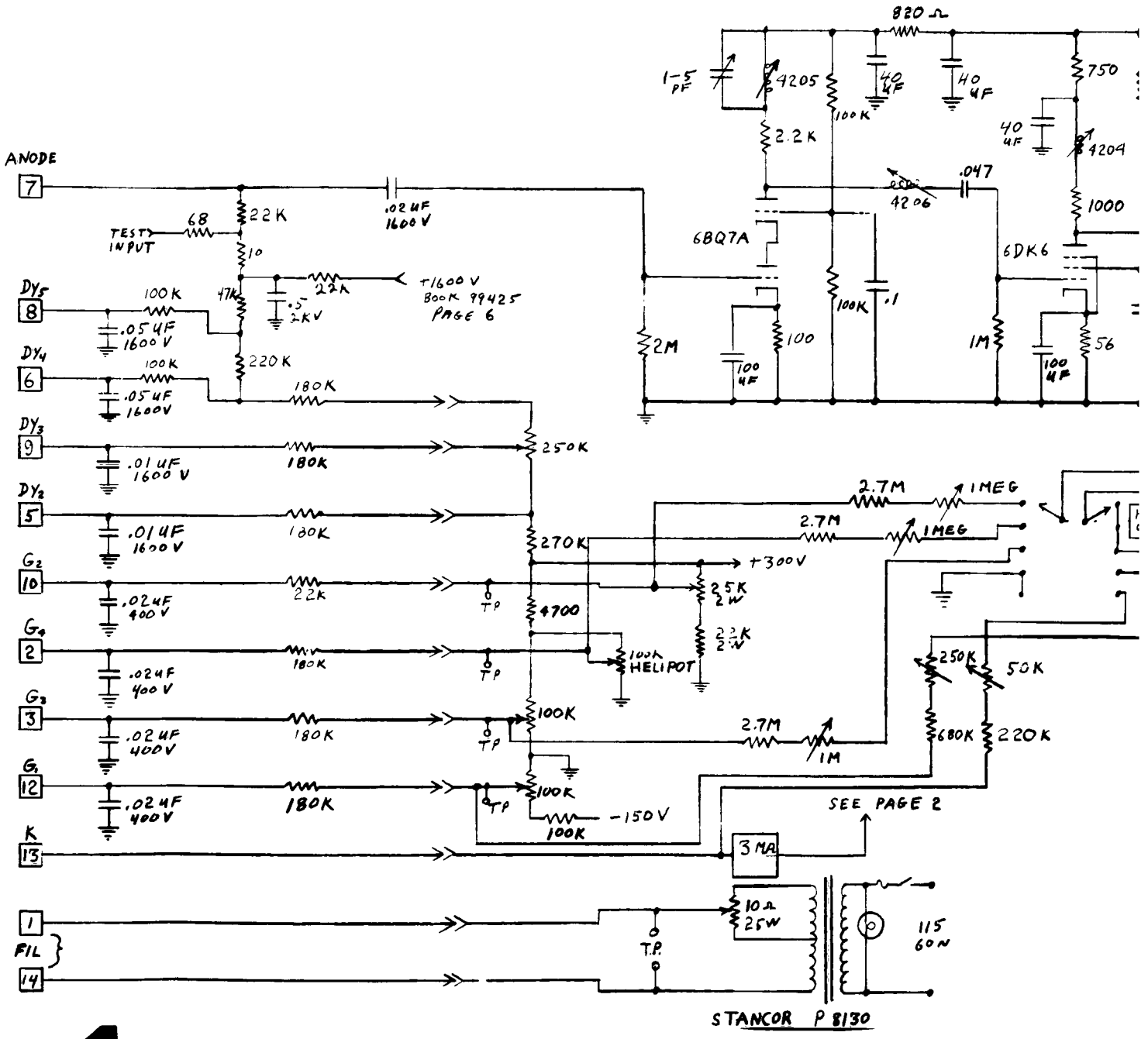
ANODE
7
68
22K
.02 UF
1600 V
TEST INPUT
10
+1600 V
BOOK 99425
PAGE 6
DY5
8
100K
47K
22K
.5
2KV
.05 UF
1600 V
DY4
6
100K
220K
180K
.05 UF
1600V
DY3
9
.01 UF
1600 V
180K
250K
DY2
5
.01 UF
1600 V
180K
270K
G2
10
.02 UF
400 V
22K
TP
4700
+300V
25K
2W
G4
2
.02 UF
400 V
180K
TP
100K
HELIPOT
22K
2W
G3
3
.02 UF
400V
180K
TP
100K
G1
12
.02 UF
400V
180K
TP
100K
-150V
K
13
3 MA
1
FIL
14
T.P.
10Ω
25W
115
60W
STANCOR P 8130
820Ω
1-5 PF
4205
100K
40 UF
40 UF
750
2.2K
40 UF
4204
.047
4206
1000
6BQ7A
6DK6
100K
.1
2M
100
1M
56
100 UF
100 UF
2.7M
1MEG
2.7M
1MEG
250K
50K
680K
220K
2.7M
1M
SEE PAGE 2

1

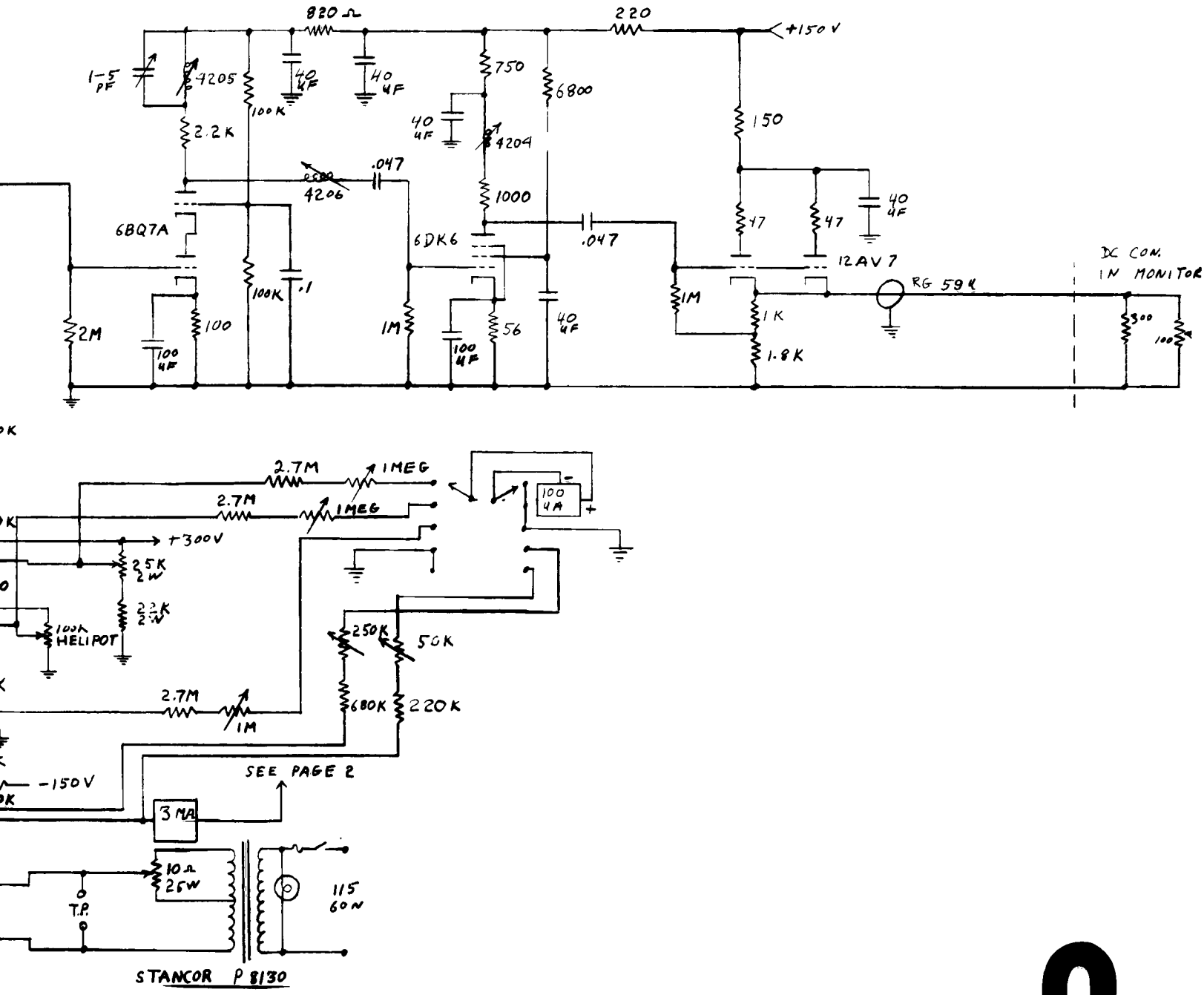

Figure 7-4. TVIST Video Slow Scan

2

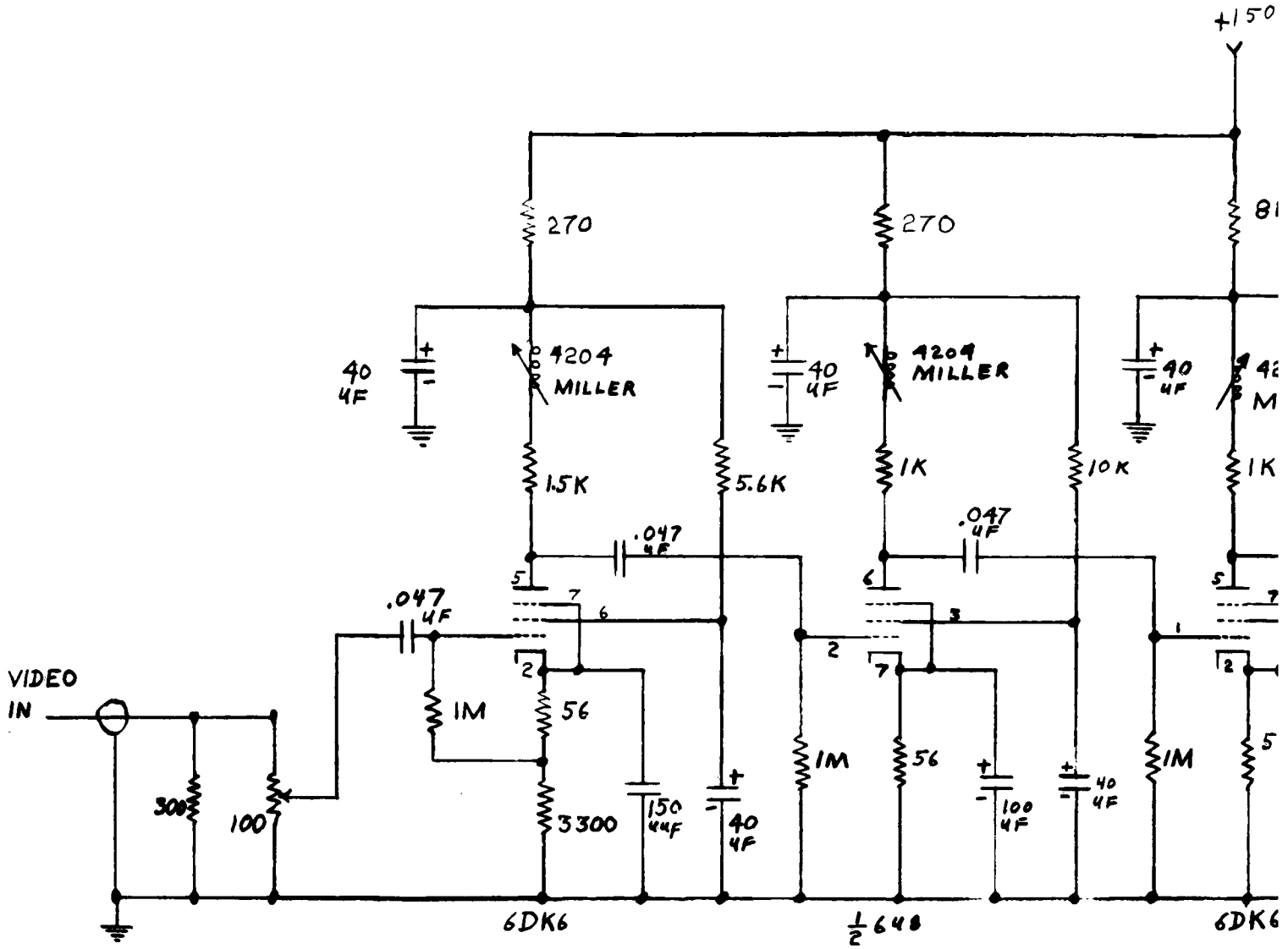
+150
270
270
40 4F
4204 MILLER
4209 MILLER
40 4F
40 4F
1.5K
5.6K
1K
10K
1K
.047 4F
.047 4F
.047 4F
VIDEO IN
1M
56
3300
150 44F
40 4F
300
100
1M
56
100 4F
40 4F
1M
6DK6
½ 6U8
6DK6

1

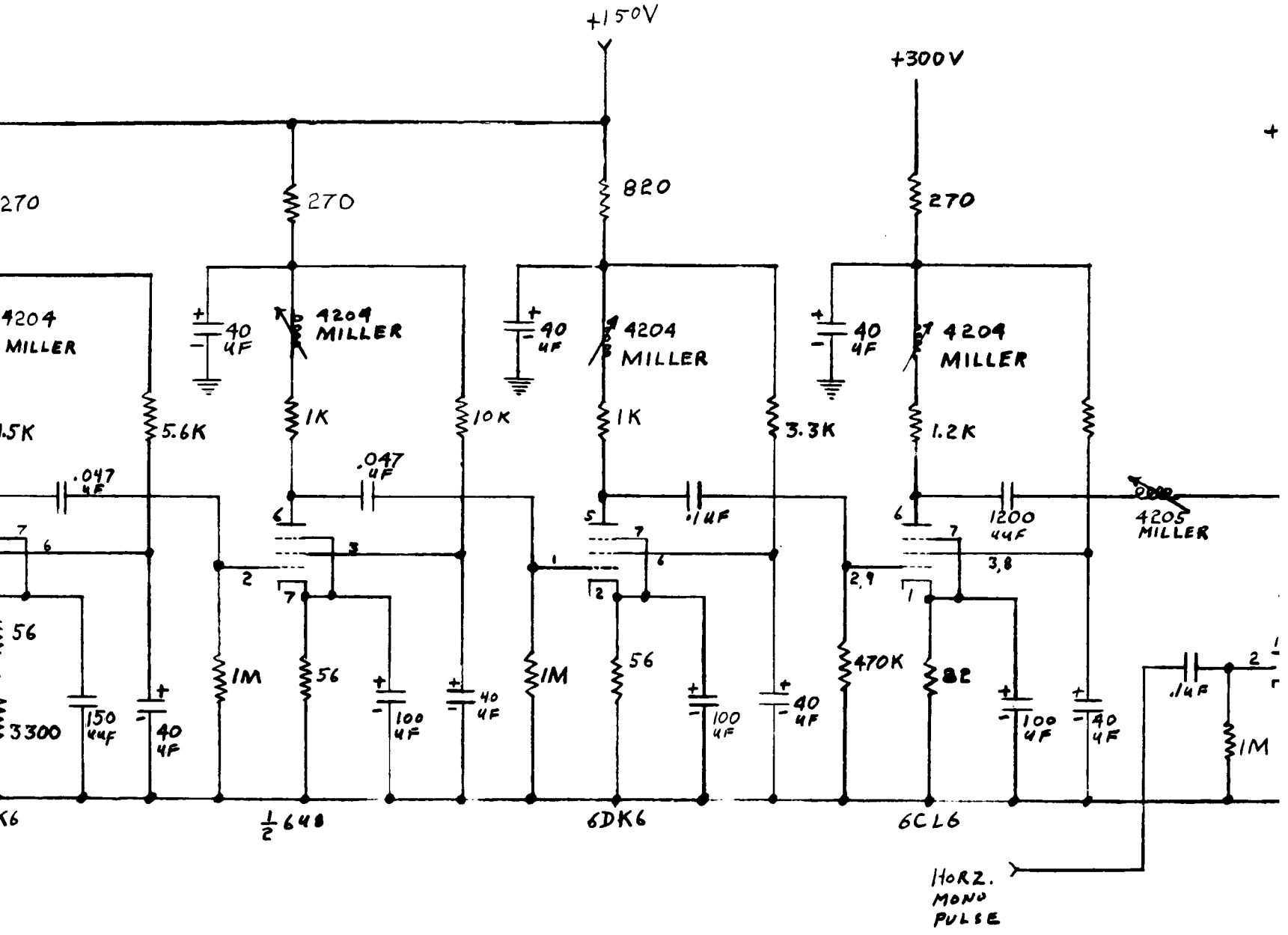
+150V
+300V
270
270
820
270
4204 MILLER
4204 MILLER
4204 MILLER
4204 MILLER
40 uF
40 uF
40 uF
5.6K
1K
10K
1K
3.3K
1.2K
.047 uF
.047 uF
.1 uF
1200 uF
4205 MILLER
56
3300
150 uF
40 uF
1M
56
100 uF
40 uF
1M
56
100 uF
40 uF
470K
82
100 uF
40 uF
.1 uF
1M
1/2 6U8
6DK6
6CL6
HORZ. MONO PULSE

2

Figure 7-5.

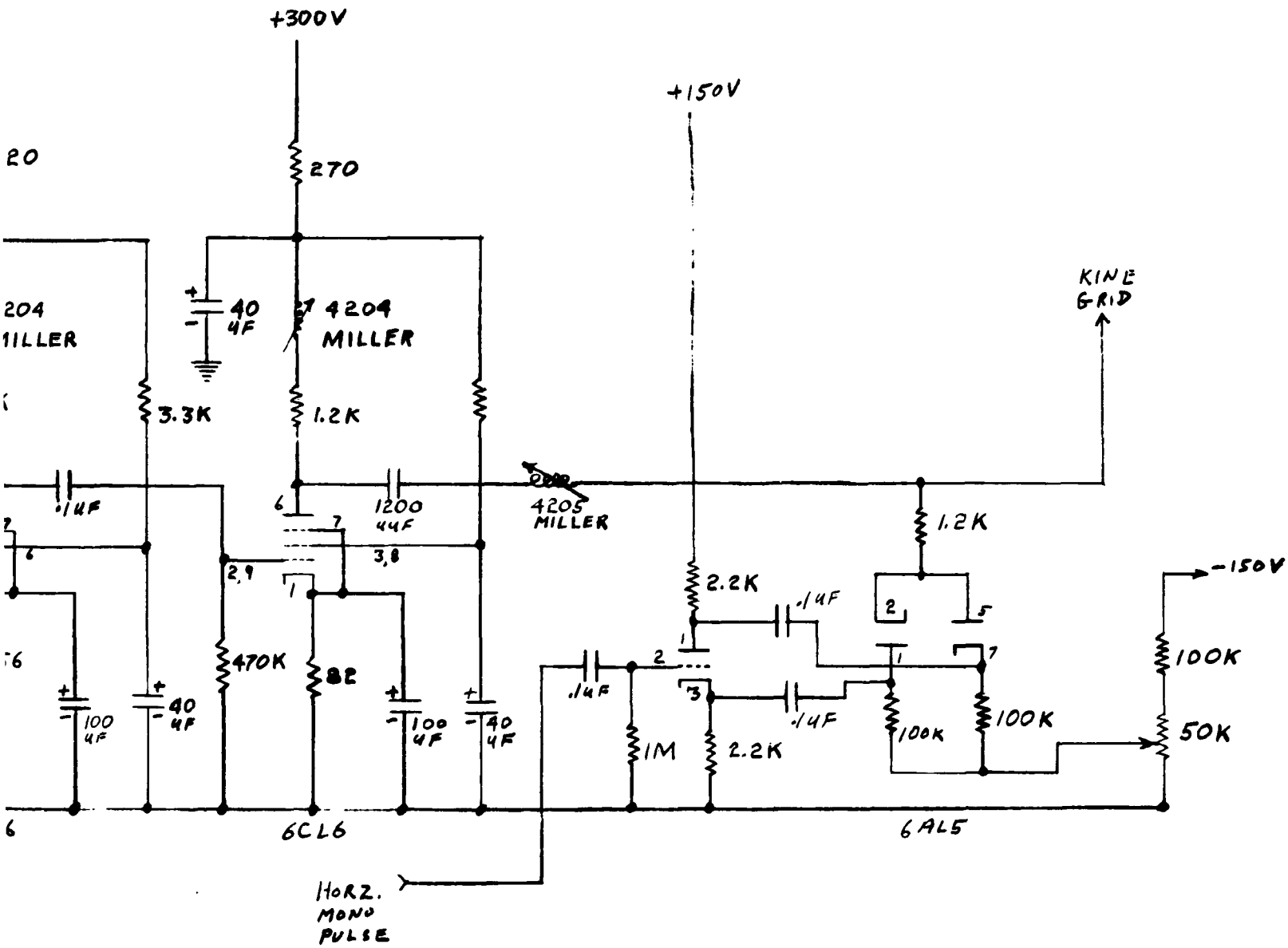

Figure 7-5. TVIST Slow Scan Video Post

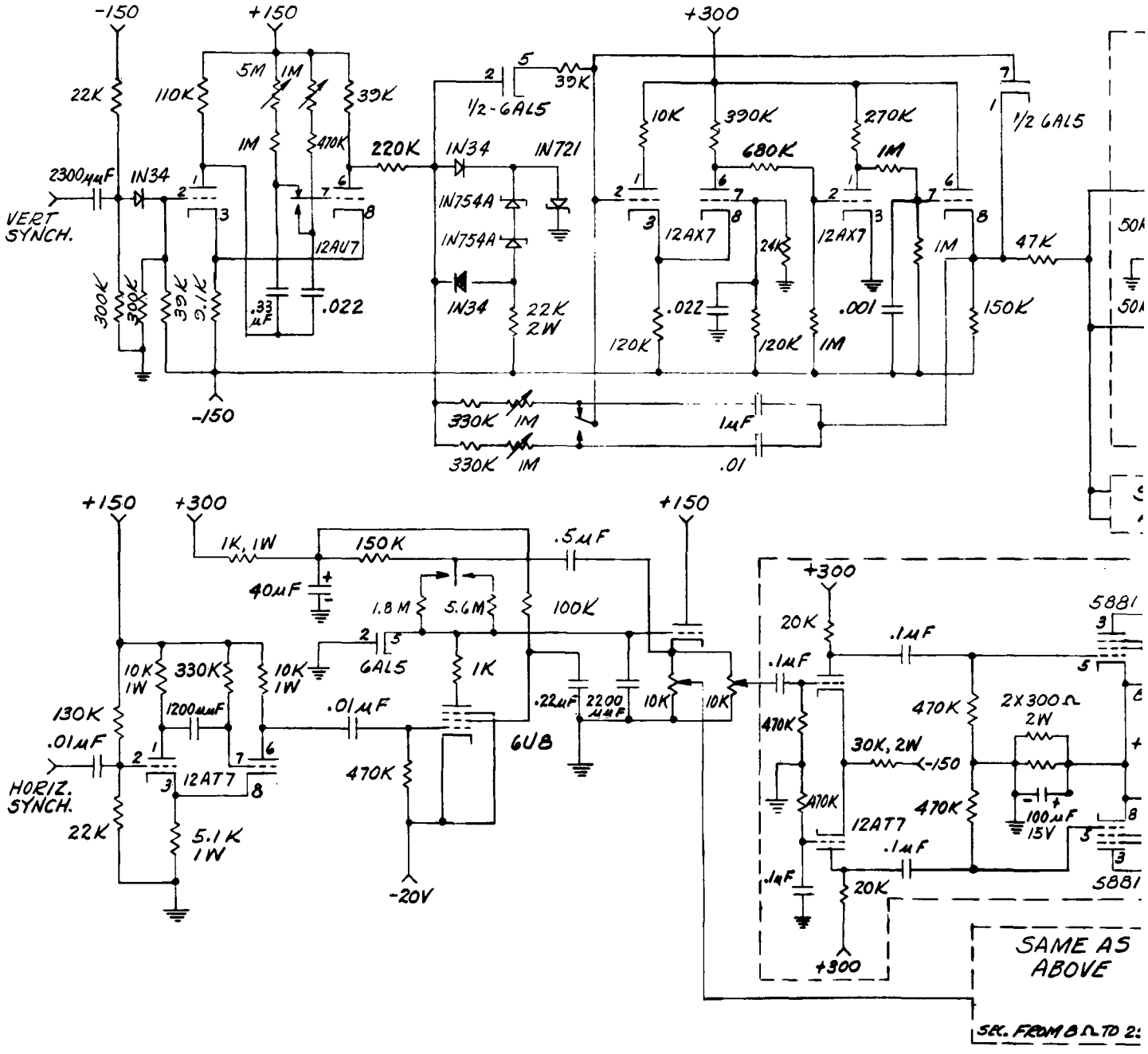
-150
+150
+300
22K
110K
5M
1M
39K
1M
470K
220K
2300μμF
IN34
VERT SYNCH.
12AU7
300K
300K
39K
2.1K
.33 μF
.022
-150
2
5
39K
1/2-6AL5
IN34
IN721
IN754A
IN754A
IN34
22K 2W
10K
390K
680K
270K
1M
12AX7
24K
12AX7
.022
120K
120K
1M
.001
1M
47K
150K
1/2 6AL5
330K 1M
330K 1M
1μF
.01
+150
+300
1K, 1W
150K
.5μF
40μF
1.8 M
5.6M
100K
10K 1W
330K
10K 1W
1200μμF
.01μF
6AL5
1K
.22μF
2200 μμF
10K
10K
130K
.01μF
HORIZ. SYNCH.
12AT7
22K
5.1K 1W
470K
6U8
-20V
+150
+300
20K
.1μF
.1μF
470K
470K
30K, 2W
-150
470K
12AT7
.1μF
.1μF
20K
+300
2X300Ω 2W
100μF 15V
470K
5881
5881
SAME AS ABOVE
SR. FROM 8Ω TO 2:

1

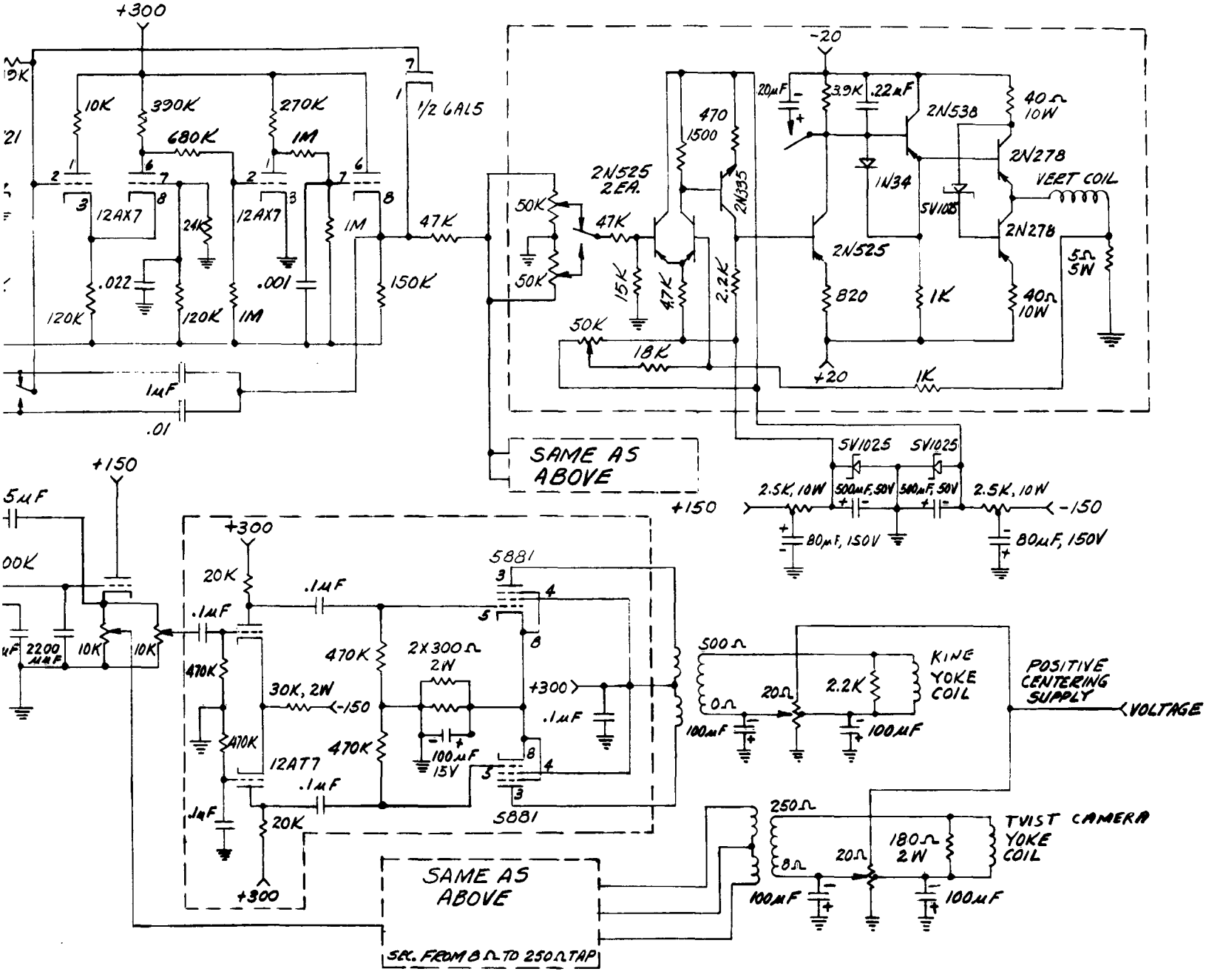

Figure 7-6. TVIST Slow Scan

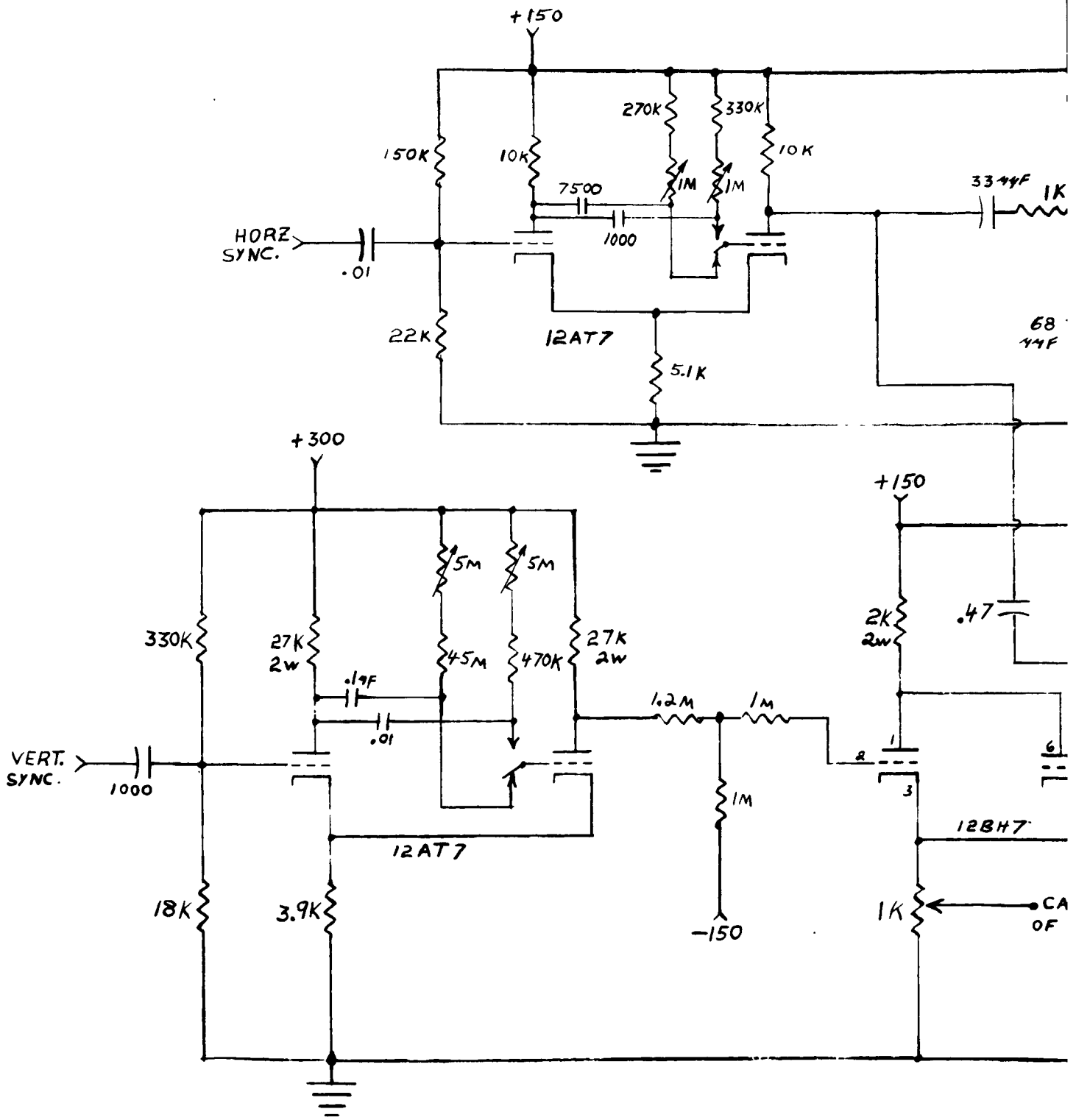
+150
270K
330K
10K
150K
10K
1M
1M
7500
1000
HORZ SYNC.
.01
22K
12AT7
5.1K
+300
5M
5M
330K
27K 2w
45M
470K
27K 2w
.19F
.01
1.2M
1M
VERT. SYNC.
1000
1M
12AT7
18K
3.9K
-150
+150
2K 2w
.47
12BH7
1K

1

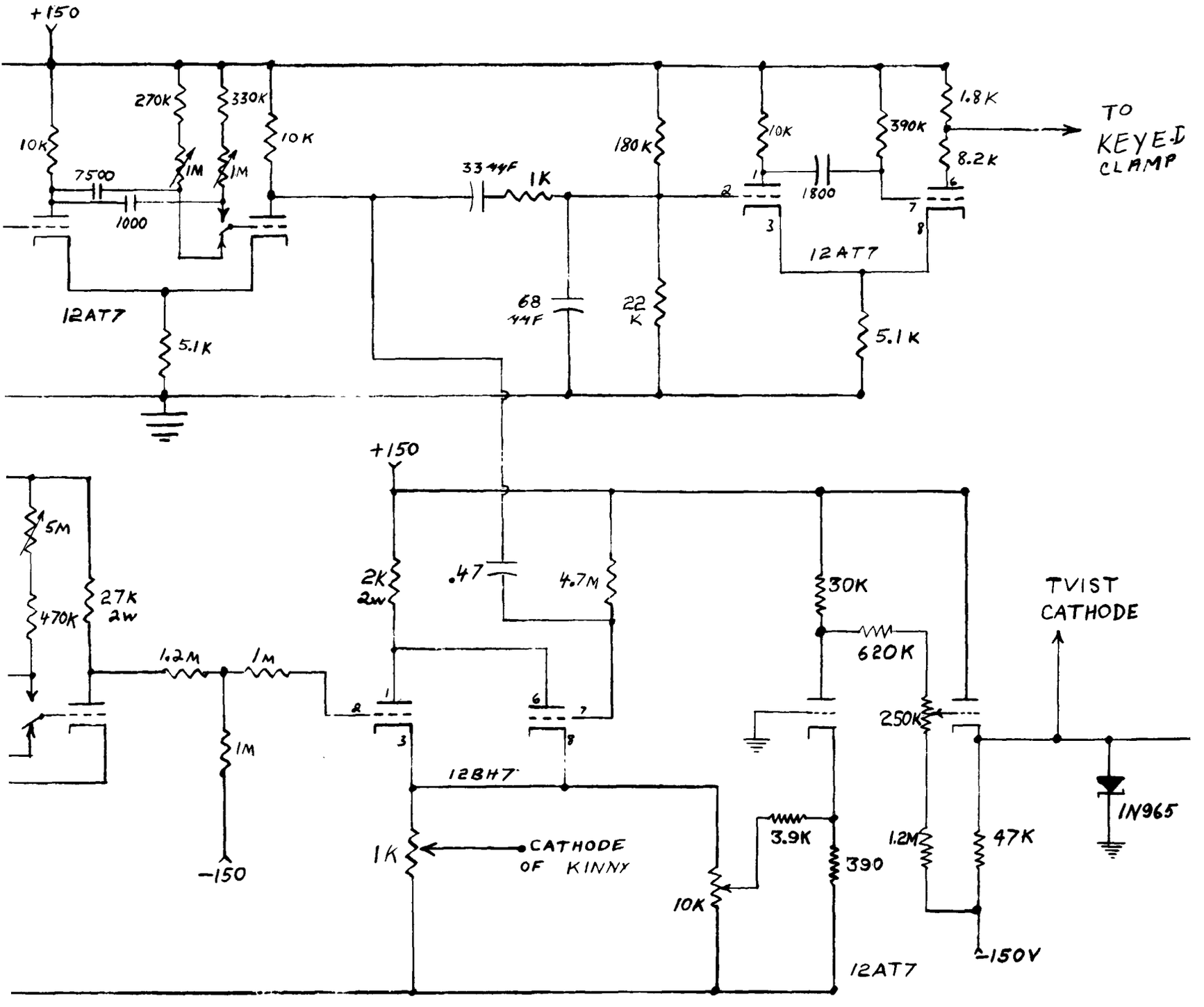

2

Figure 7-7. TVIST Bl

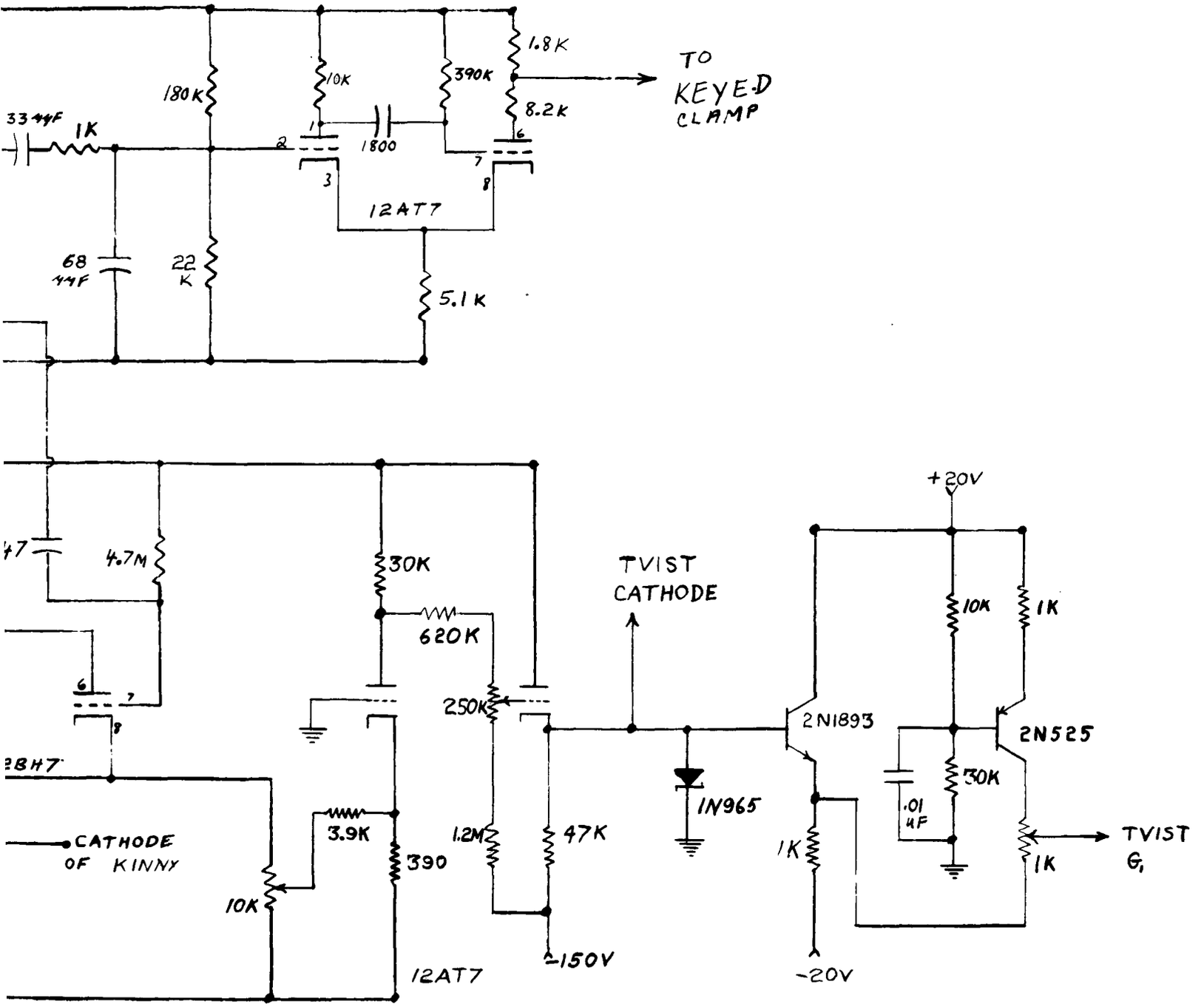

Figure 7-7. TVIST Blanking Slow Scan

mixes these gates and feeds the kinescope cathode and a grounded grid amplifier and cathode follower to feed the TVIST camera tube cathode. This signal also feeds an emitter follower and bias circuit to feed the G1 of the TVIST tube. The horizontal gate also feeds an RC delay and a gate generator to produce the key clamp gate within the time of blanking gate.

7.2.7 Dynamic Focus

The TVIST dynamic focus is shown in figure 7-8. With the exception of the NU7235 focus voltage shunt regulator, this circuit was not often used. The purpose of the circuit is to generate the dynamic focus parabolas for the kinescope. In practice, at slow scan rates, it is extremely difficult to set it up in any way to achieve real benefit.

7.2.8 Aperture Corrector

The aperture corrector, figure 7-9, consists of a transistorized video amplifier feeding the delay line and the two transistor mixer difference amplifier and an emitter follower. The circuit peaks at 2.5 mc to peak the high frequencies without phase shift. The effect of the aperture corrector on the measured spatial frequency response is shown in the photographs of the oscilloscope displaying the response to stored Westinghouse bar pattern (figure 6-22) and the plot of the relative response, figure 6-23.

7.2.9 High Voltage Power Supplies

Power oscillators are used in the high voltage supplies. Except for rectifier and amplifier polarities, the +15-kv and -10-kv circuits are the same. The appropriate control grid of the 6U8 error amplifier compares the high voltage via a 900-megohm meter multiplier resistor to the 87-volt reference. The pentode section of the 6U8 feeds the 12B4 which is a shunt for the screen voltage of the power oscillator tube. At -10 kilovolts, the ripple is less than 0.1-v rms and the short time regulation less than 2 volts. This close regulation is dictated by the high resolution requirements of the system. See figure 7-10 for more detail.

7.2.10 Low Voltage Supply

This is a series regulated supply for the high voltage supply, figures 7-11 and 7-12 respectively. The special transformer was made by winding high voltage wire on the primary core (secondary removed) of a 6.3 V-10A transformer.

7.2.11 Power Supply 10 to 15 kv

This supply, shown in figure 7-12, is similar in design to those described in the high voltage power supplies, figure 7-10. This supply was used for the photodiode tests and is self-contained in a portable case which also includes the power supply of

7.2.12 Variable Constant Current Supply

A differential amplifier compares the cathode voltage of a pair of triode connected 5881's to a -87-volt reference. The amplified and inverted error voltage is applied to the 5881 grids. This circuit, figure 7-13, will provide constant current of 50 to 120 ma (with small internal adjustments) to the load, providing the voltage drop across the load is less than 225 volts. This is used to supply the orthicon or TVIST camera tube focus coil.

7.2.13 Variable Constant Current Supply

The variable constant current supply is the same as shown in figure 7-13 except that 6550's are used in place of the 5881's, and a larger transformer is used. See figure 7-14. It is capable of supplying up to 190 ma of regulated current and is used for the 4.5-inch thicon coils or for certain special tests on the standard orthicon or flip target apparatus.

7.2.14 Filament Supply

A regulated filament supply was built to eliminate 60 cycle filament noise such as in the deflection chassis. See figure 7-15. The elimination of this source of deflection jitter was required to achieve the proper reading of the stored images. The circuit is a simple transistorized series regulator using a nichrome surge limiter and a brute force filter.

7.2.15 1600 Volts Power Supply

This is a regulated power oscillator used to produce the +1600 to +1800 voltage for the reading beam electron multipliers. Figure 7-16 shows the power supply.

7.2.16 Regulated Utility Power Supply

This is the basic rack supply used for powering the other units. It consists of a number of rectifier and series regulators to provide the required regulated power. See figure 7-17.

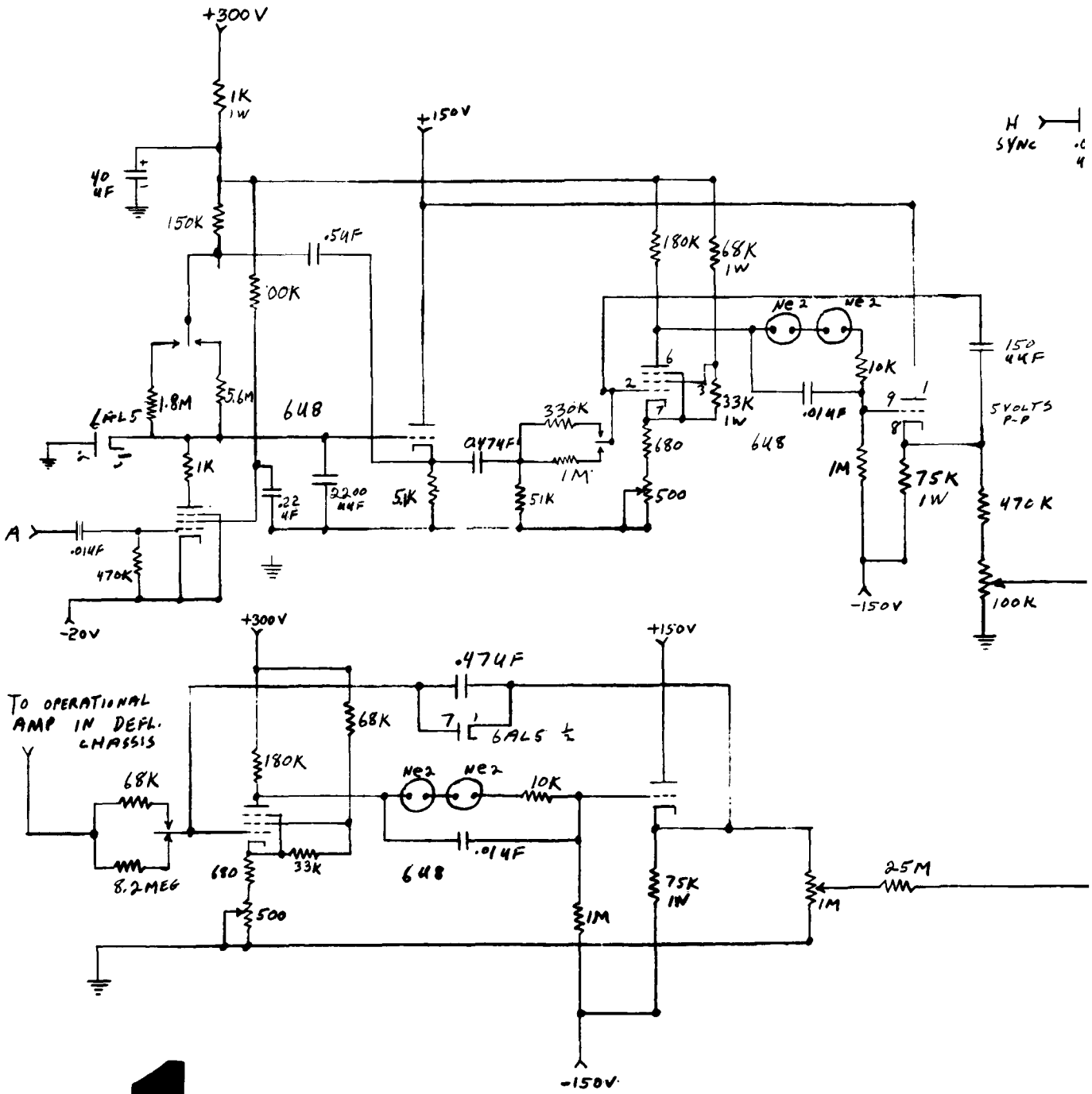
+300 V
1K 1W
40 uF
150K
.5uF
100K
+150V
180K
68K 1W
Ne 2
Ne 2
150 uuF
10K
1.8M
5.6M
6AL5
6U8
330K
33K 1W
.014F
5 VOLTS P-P
.0474F
680
1M
500
51K
5K
.22 uF
2200 uuF
1K
A
.014F
470K
-20V
75K 1W
470K
100K
-150V
H SYNC
+300V
+150V
.474F
TO OPERATIONAL AMP IN DEFL. CHASSIS
68K
6AL5
180K
Ne2
Ne2
10K
68K
8.2MEG
680
33K
.014F
6U8
75K 1W
25M
1M
500
1M
-150V

1

Fi

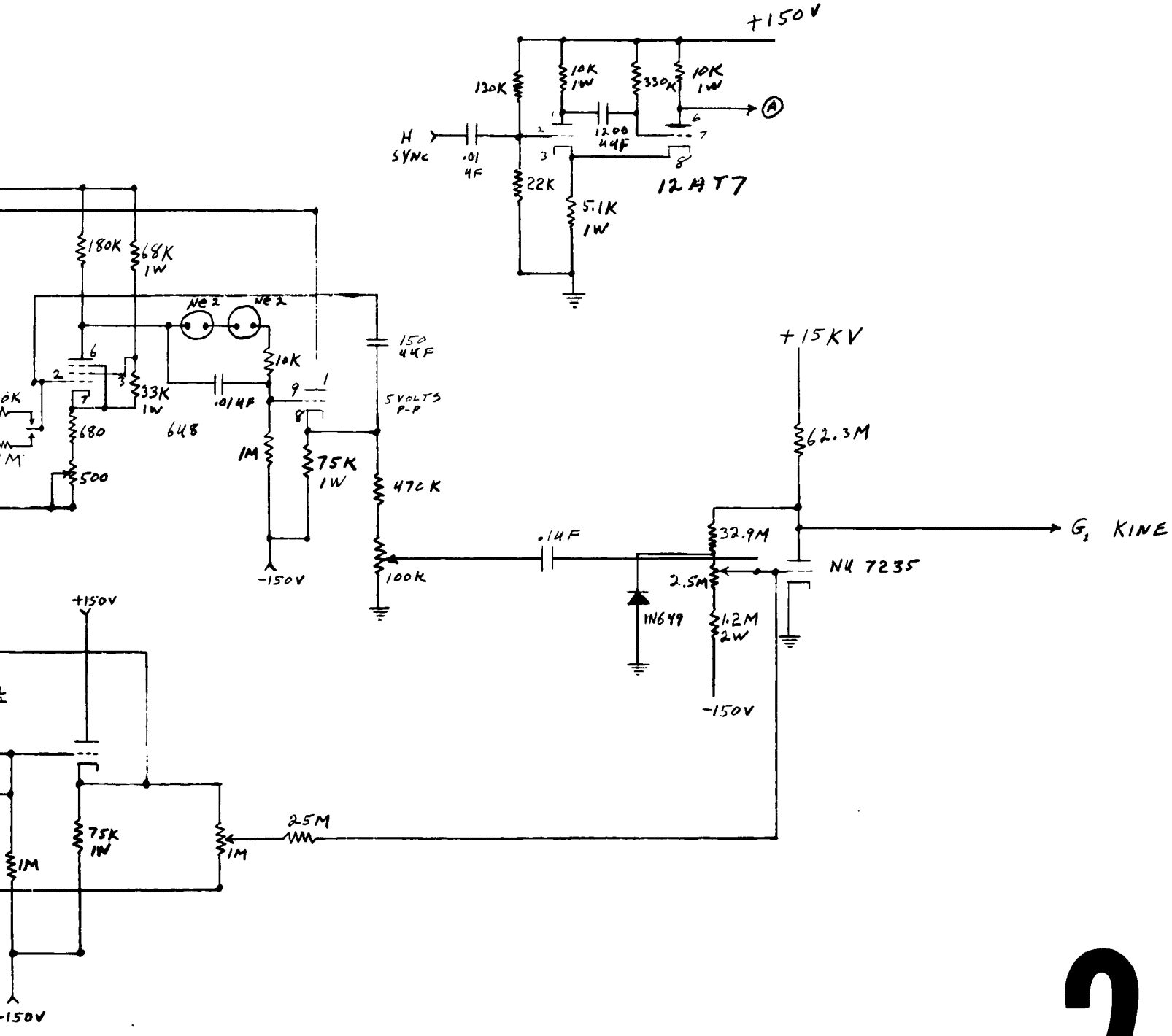

Figure 7-8. Slow Scan - TVIST Dynamic Focus

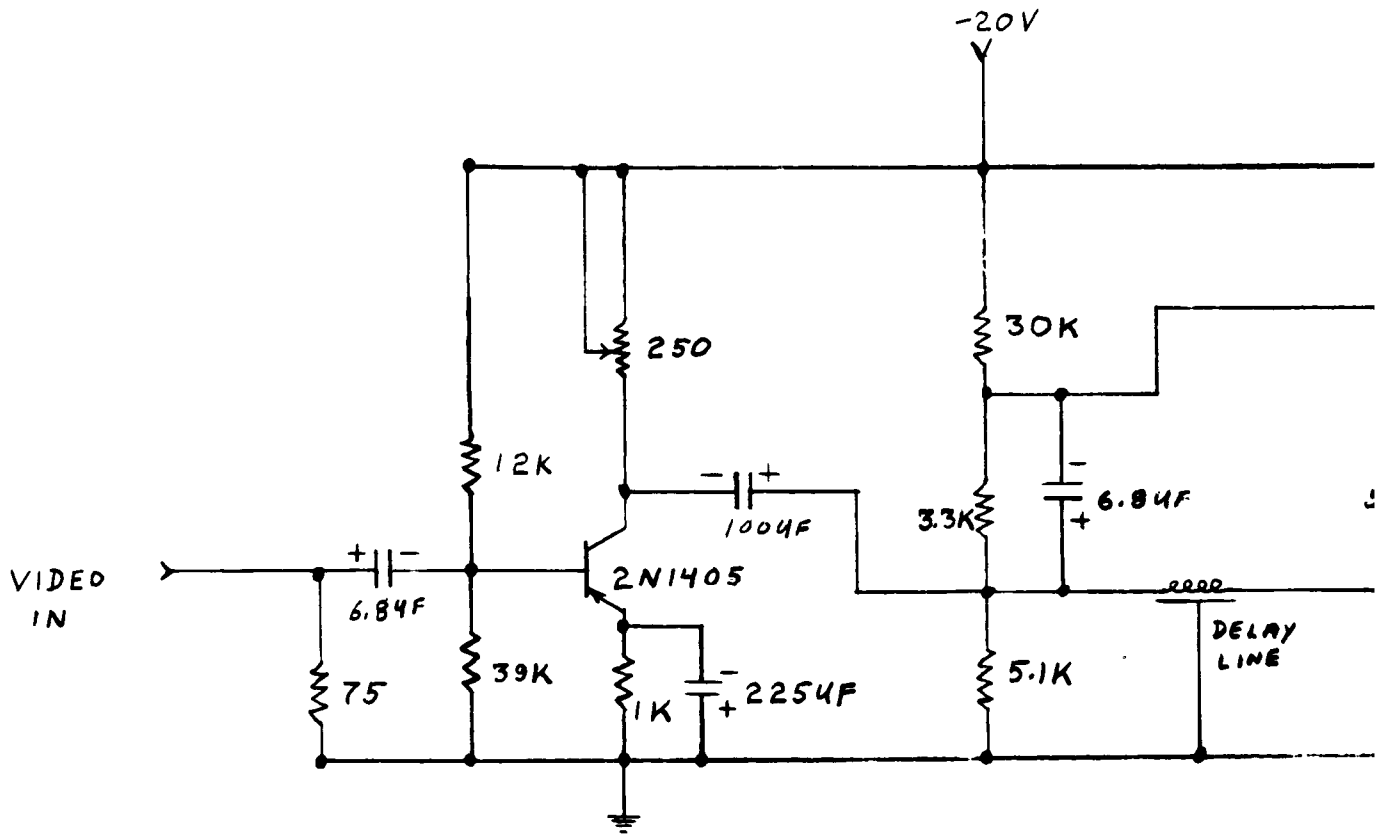

DELAY LINE

Z_o = 87 OHMS

DELAY = 170×10^{-9} SECONDS

f_c = 12 Mc.

1

Figure

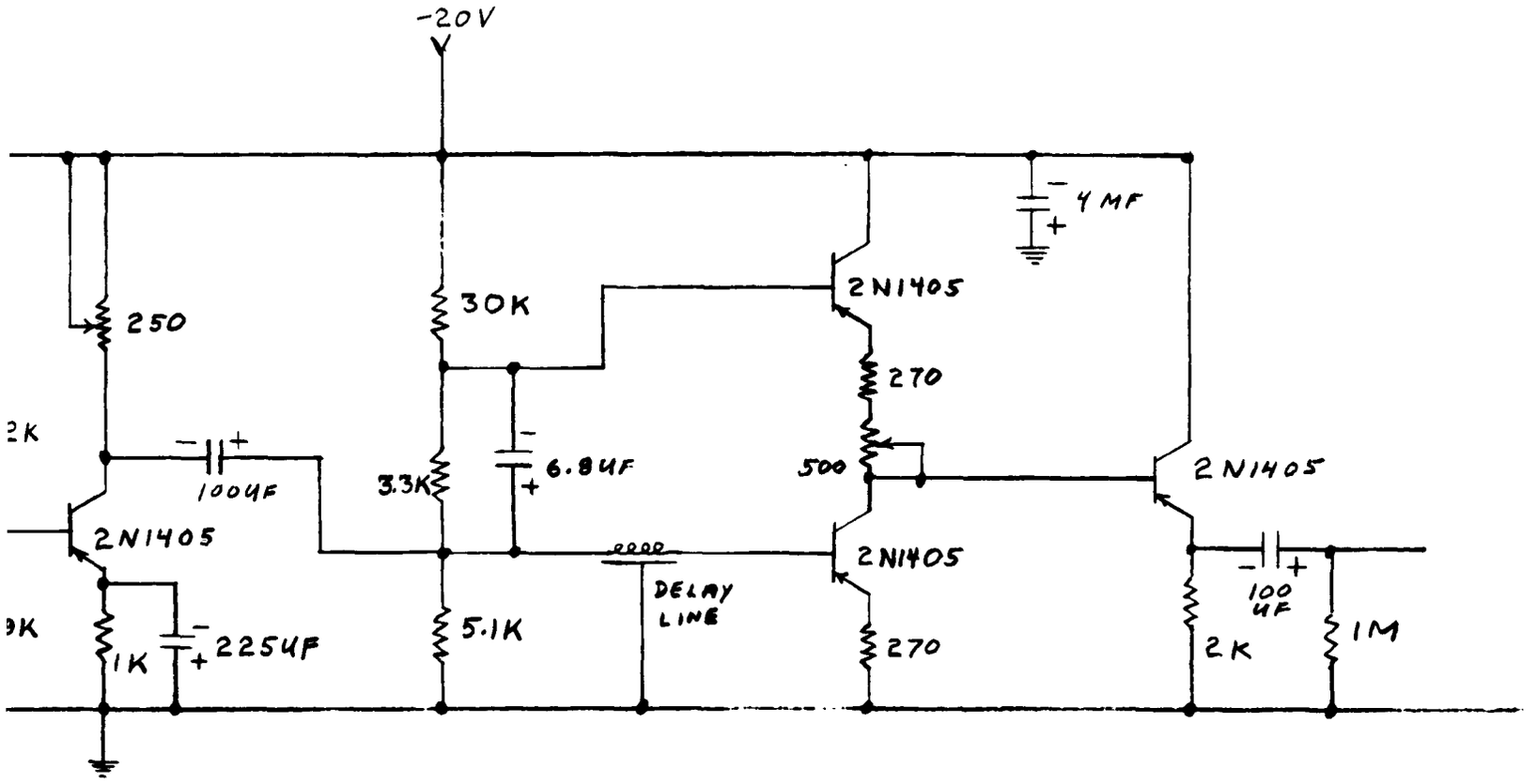

DELAY LINE

Z_o = 87 OHMS

DELAY = 170×10^{-9} SECONDS

f_c = 12 Mc.

Figure 7-9. Aperture Correction

2

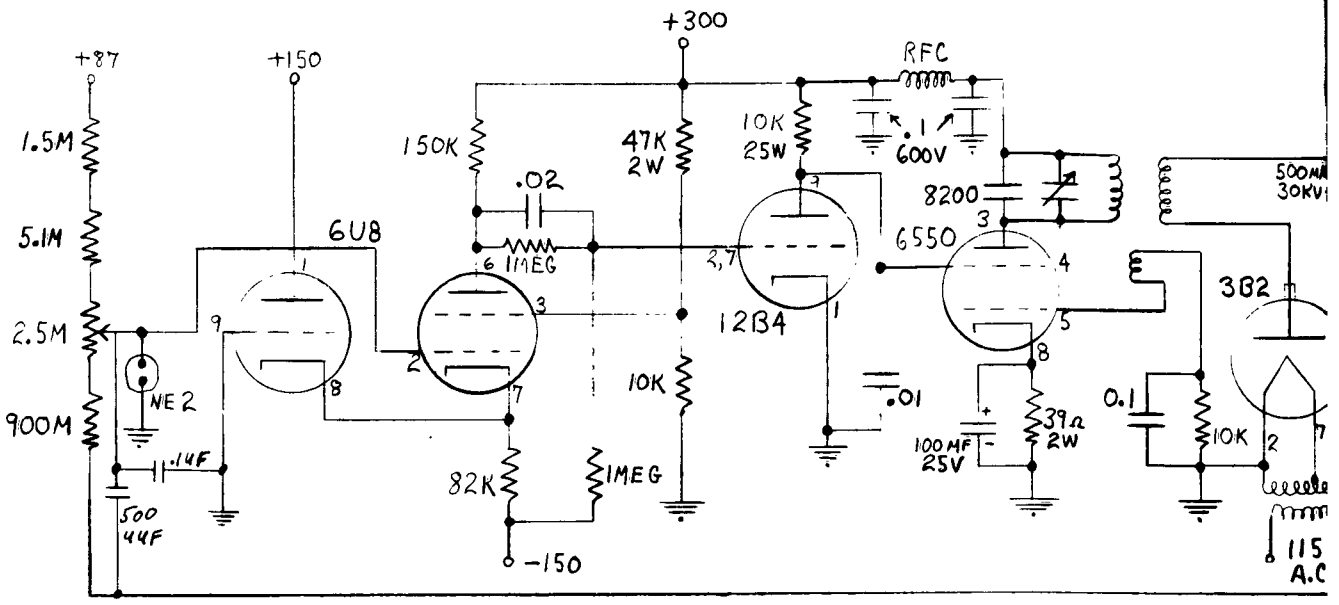
+87
+150
+300
RFC
1.5M
5.1M
2.5M
900M
150K
.02
47K
2W
10K
25W
.1
600V
8200
6550
6U8
1MEG
12B4
3B2
NE2
.01
10K
39Ω
2W
100MF
25V
0.1
.14F
500
44F
82K
1MEG
-150
115
A.C

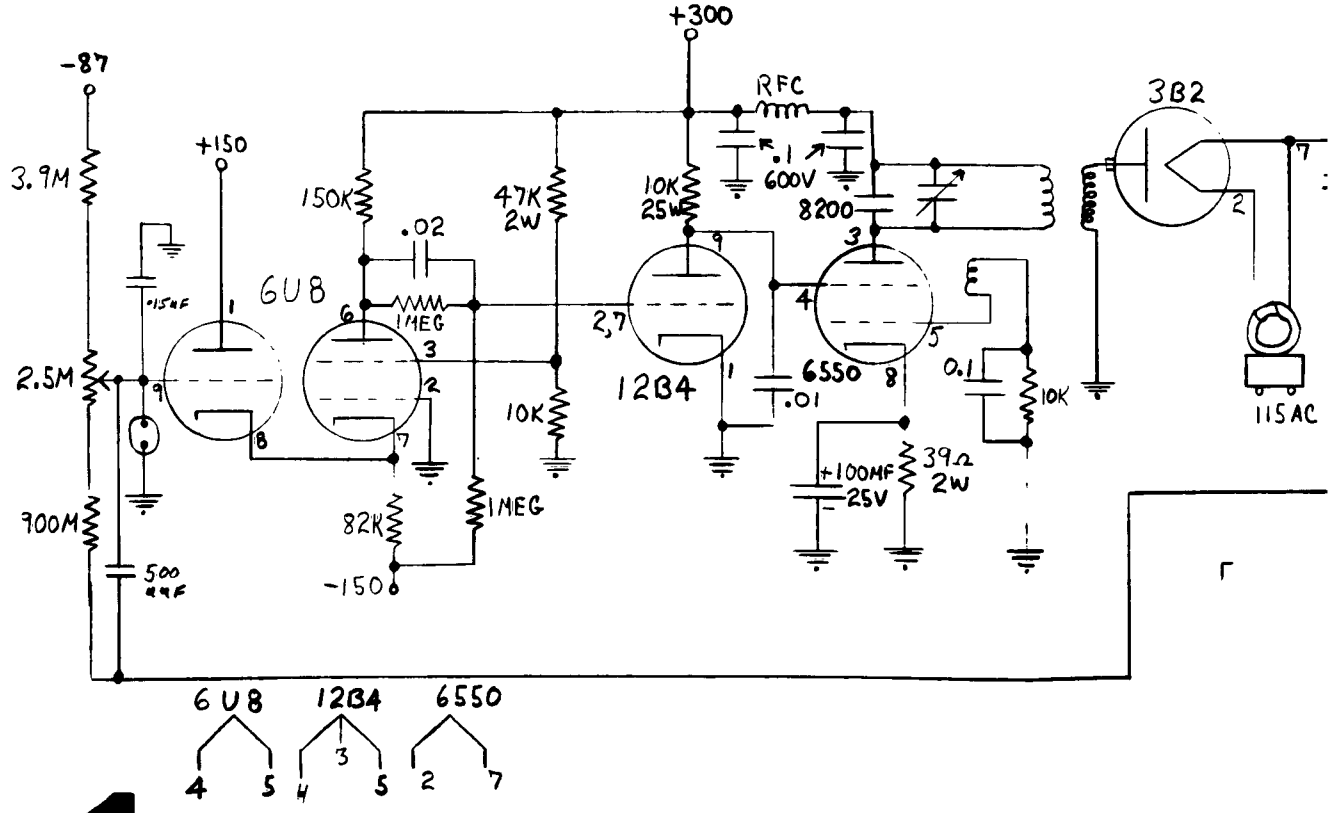
-87
+150
+300
RFC
3B2
3.9M
2.5M
900M
150K
.02
47K
2W
10K
25W
.1
600V
8200
6U8
1MEG
12B4
6550
.01
0.1
10K
39Ω
2W
+100MF
25V
82K
1MEG
-150
115AC
500
44F

6U8
12B4
6550
4
5
4
3
5
2
7

1

Figur

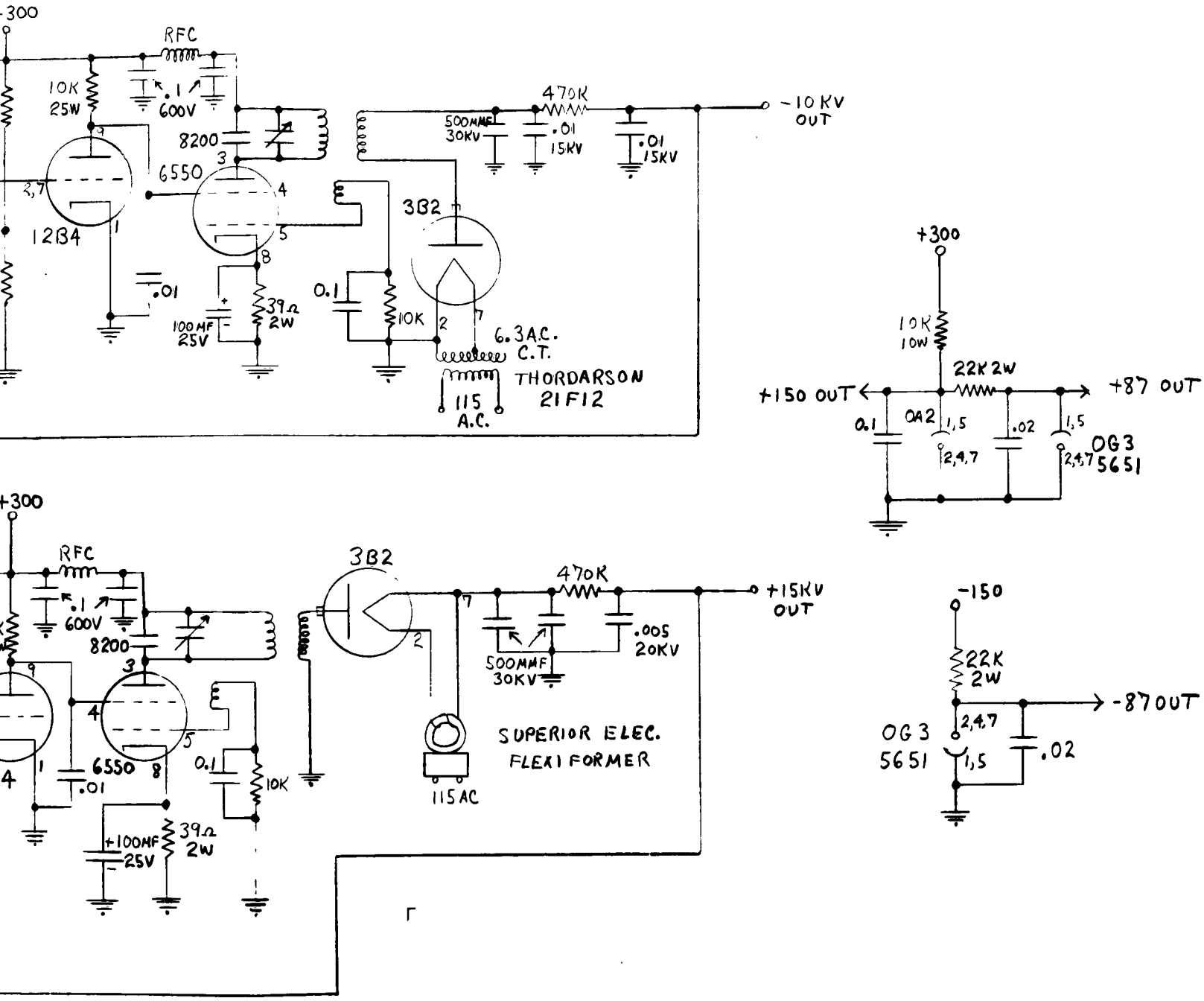

Figure 7-10. Power Supplies +15, -10 Kilovolts

2

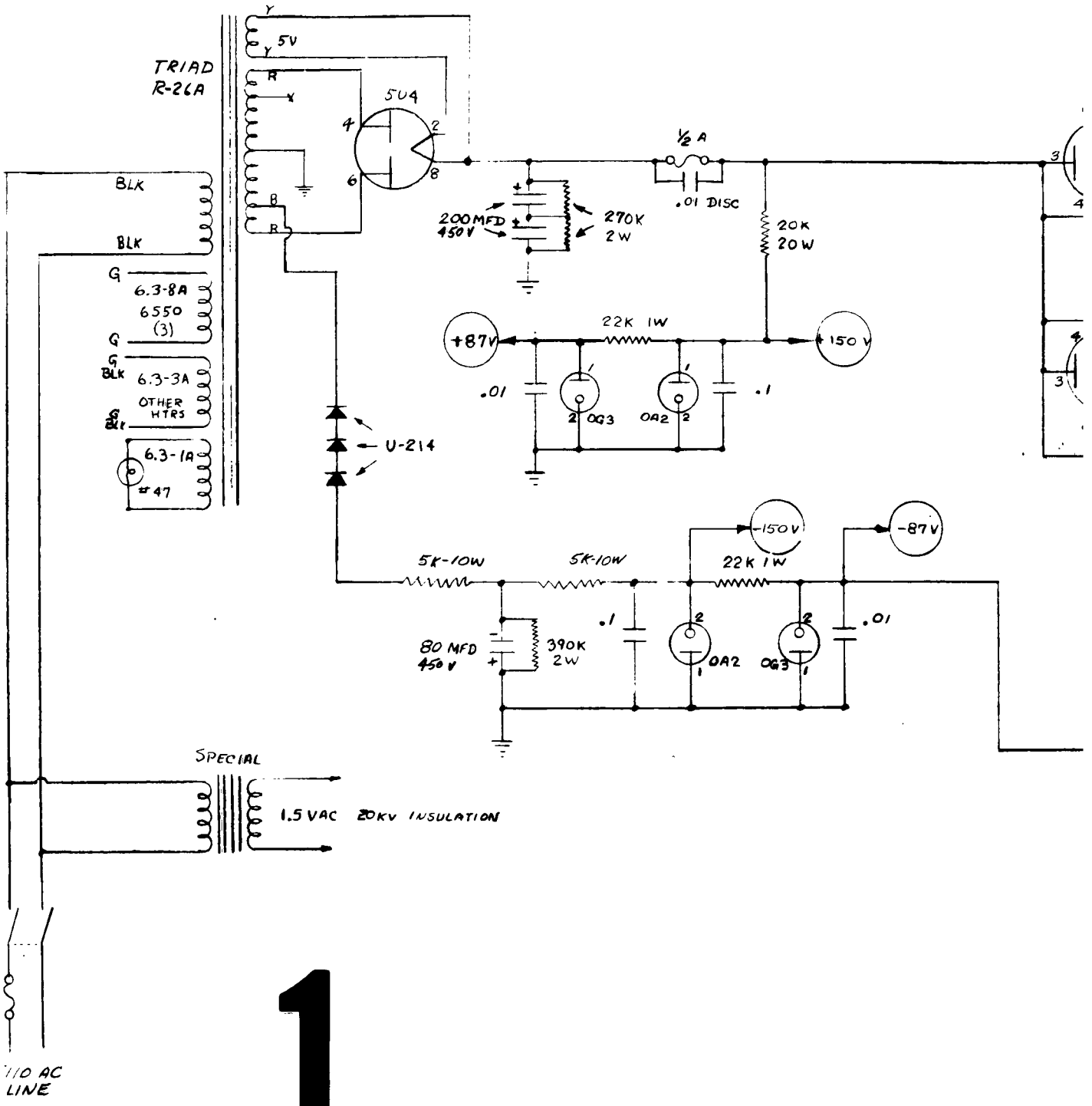

Figure 7-11. Low V

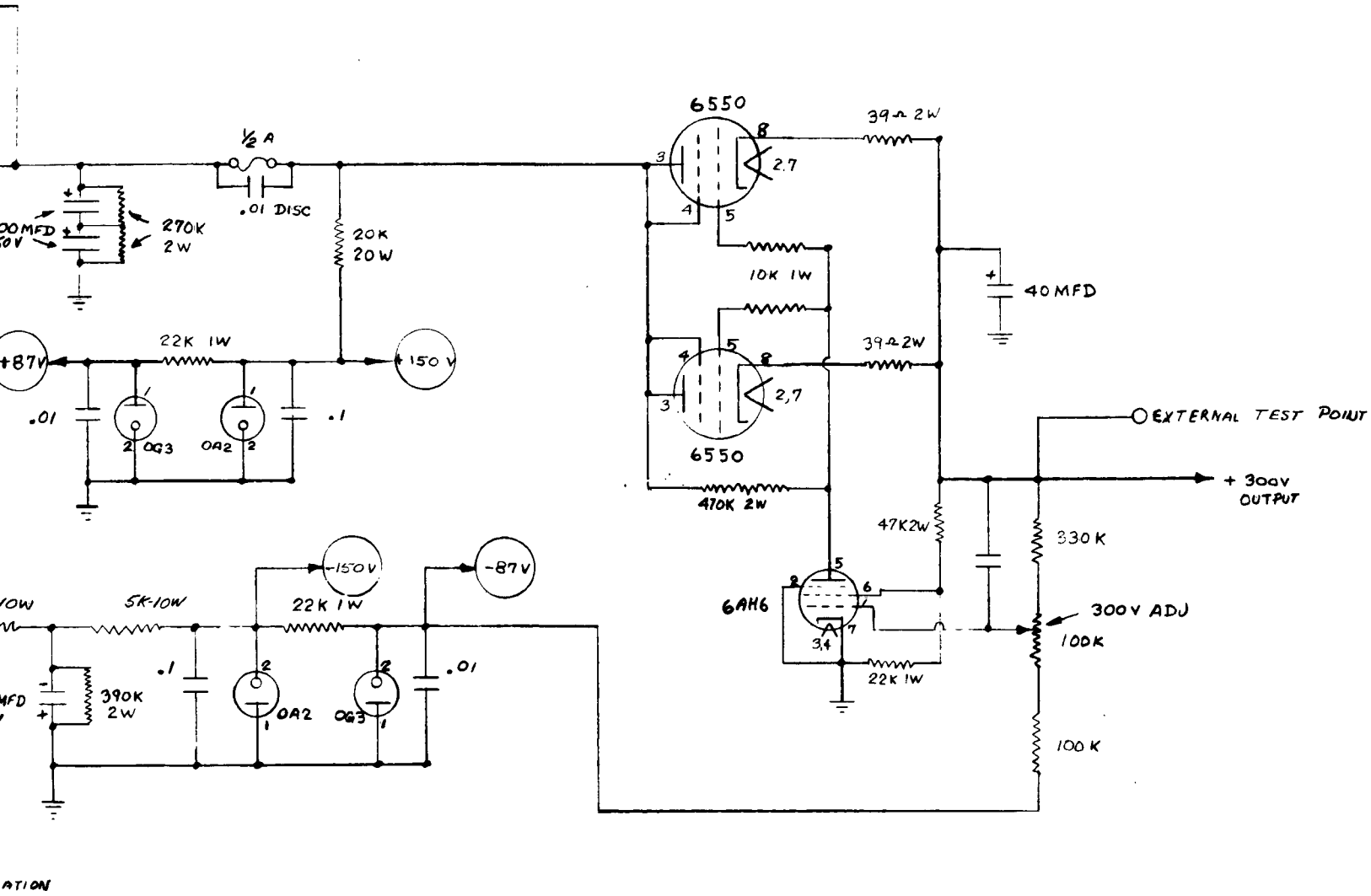

Figure 7-11. Low Voltage Supply for 10-to 15-Kilovolt Supplies

SUPPLY SHOWN CONNECTED FOR <u>POSITIVE</u> OUTPUT

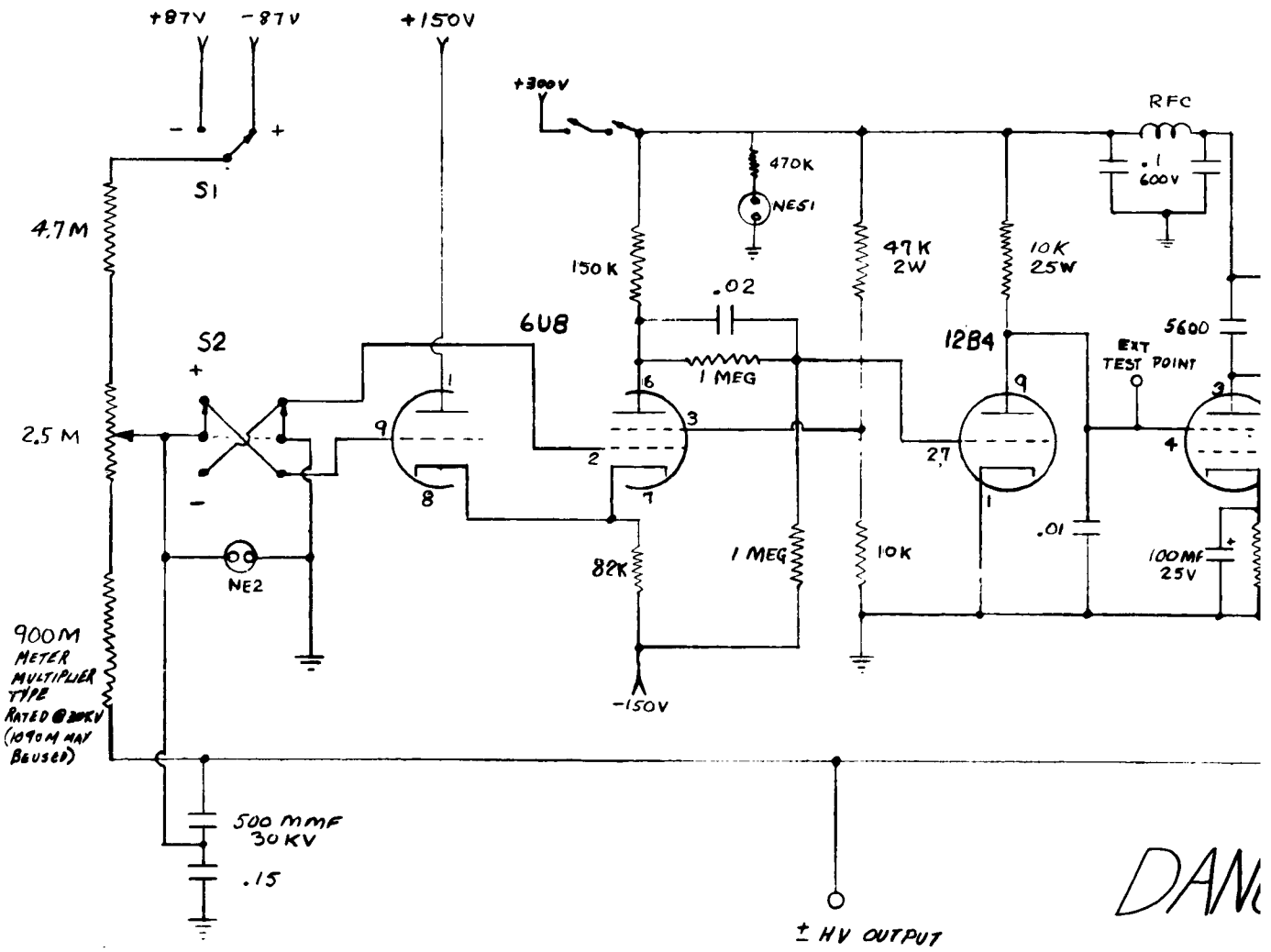

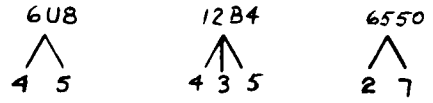

Figure 7-12. 10-to 15

POSITIVE OUTPUT

TO REVERSE POLARITY

1. REVERSE S1
2. REVERSE S2
3. REVERSE FLEXIBLE LEADS NEAR 1B3

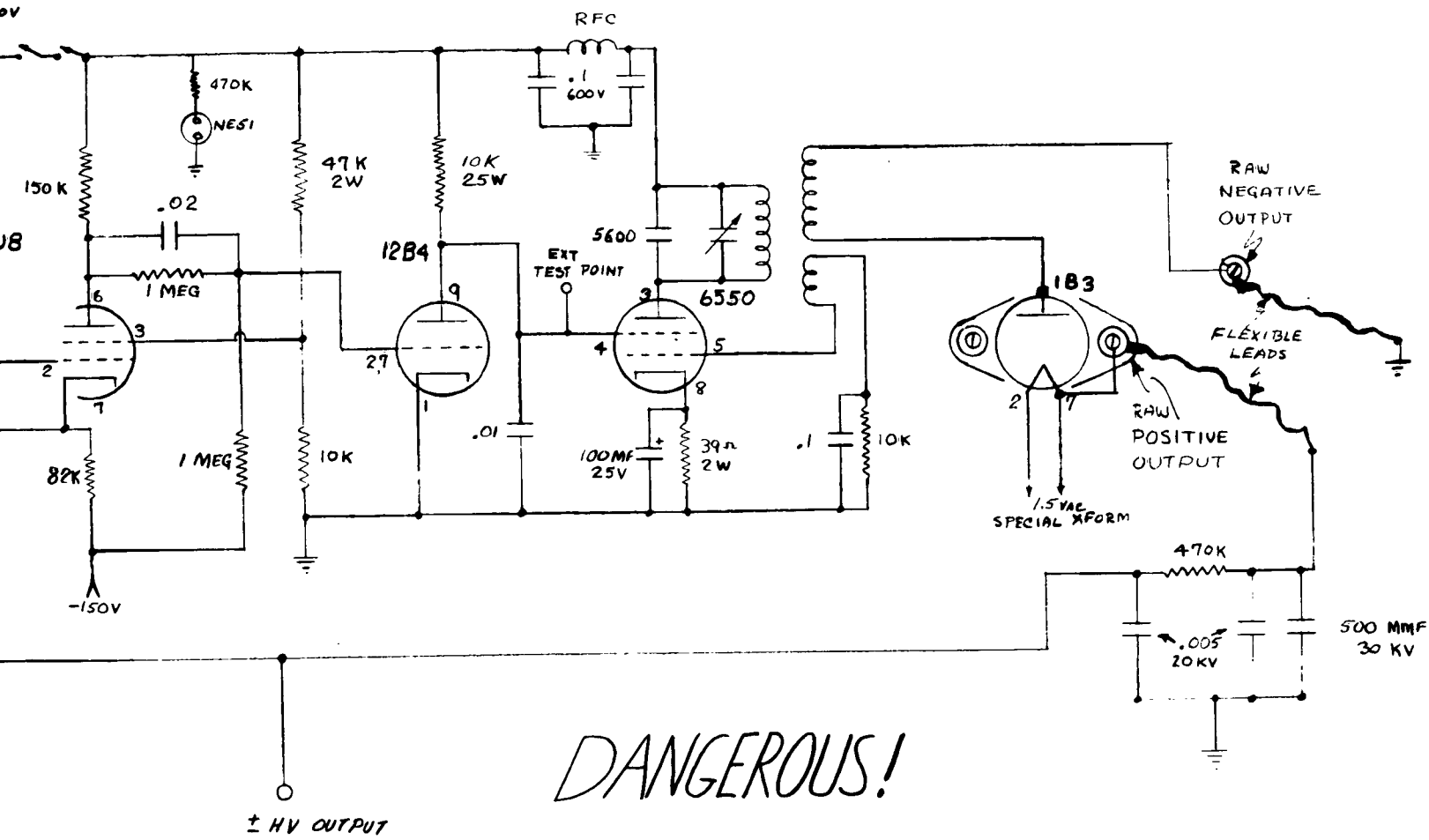

12B4 6550

Figure 7-12. 10-to 15- Kilovolt Power Supply Reversible Polarity

2

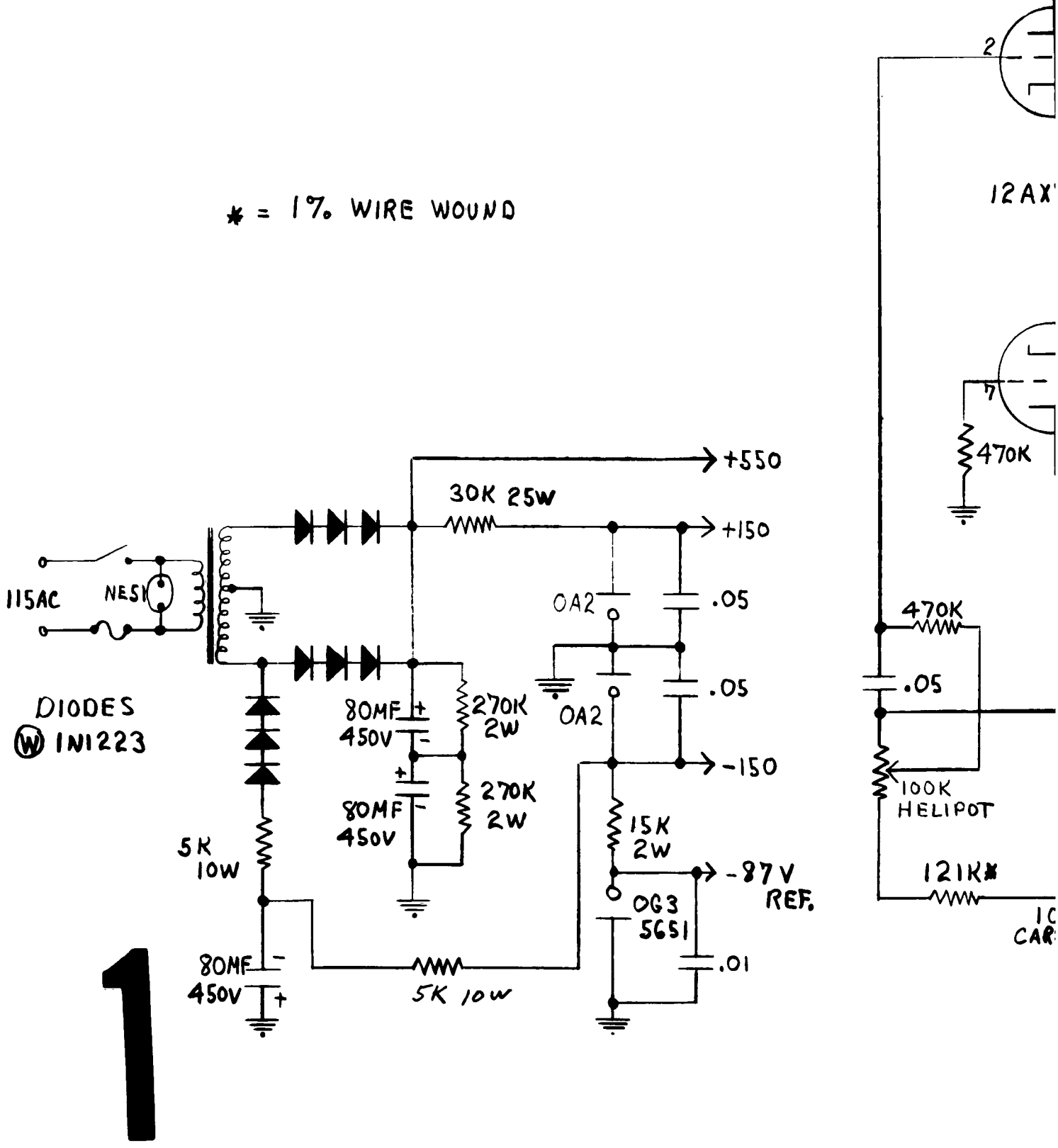
* = 1% WIRE WOUND
+550
30K 25W
+150
115AC
NE51
OA2
.05
.05
OA2
DIODES
Ⓦ 1N1223
80MF
450V
270K
2W
80MF
450V
270K
2W
-150
15K
2W
5K
10W
-87V
REF.
OG3
5651
.01
80MF
450V
5K 10W
1
2
12AX
7
470K
470K
.05
100K
HELIPOT
121K*

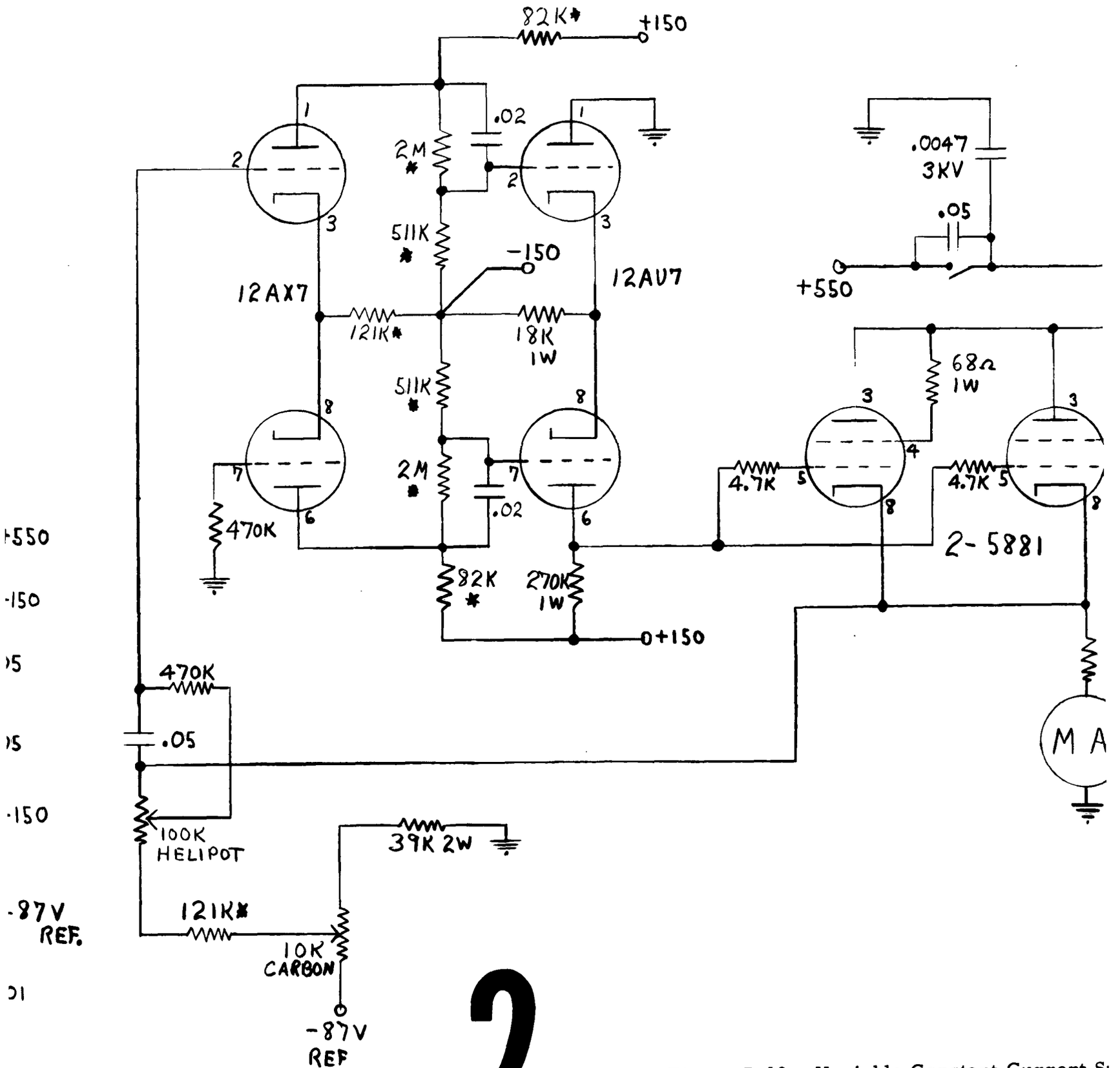

2

Figure 7-13. Variable Constant Current S

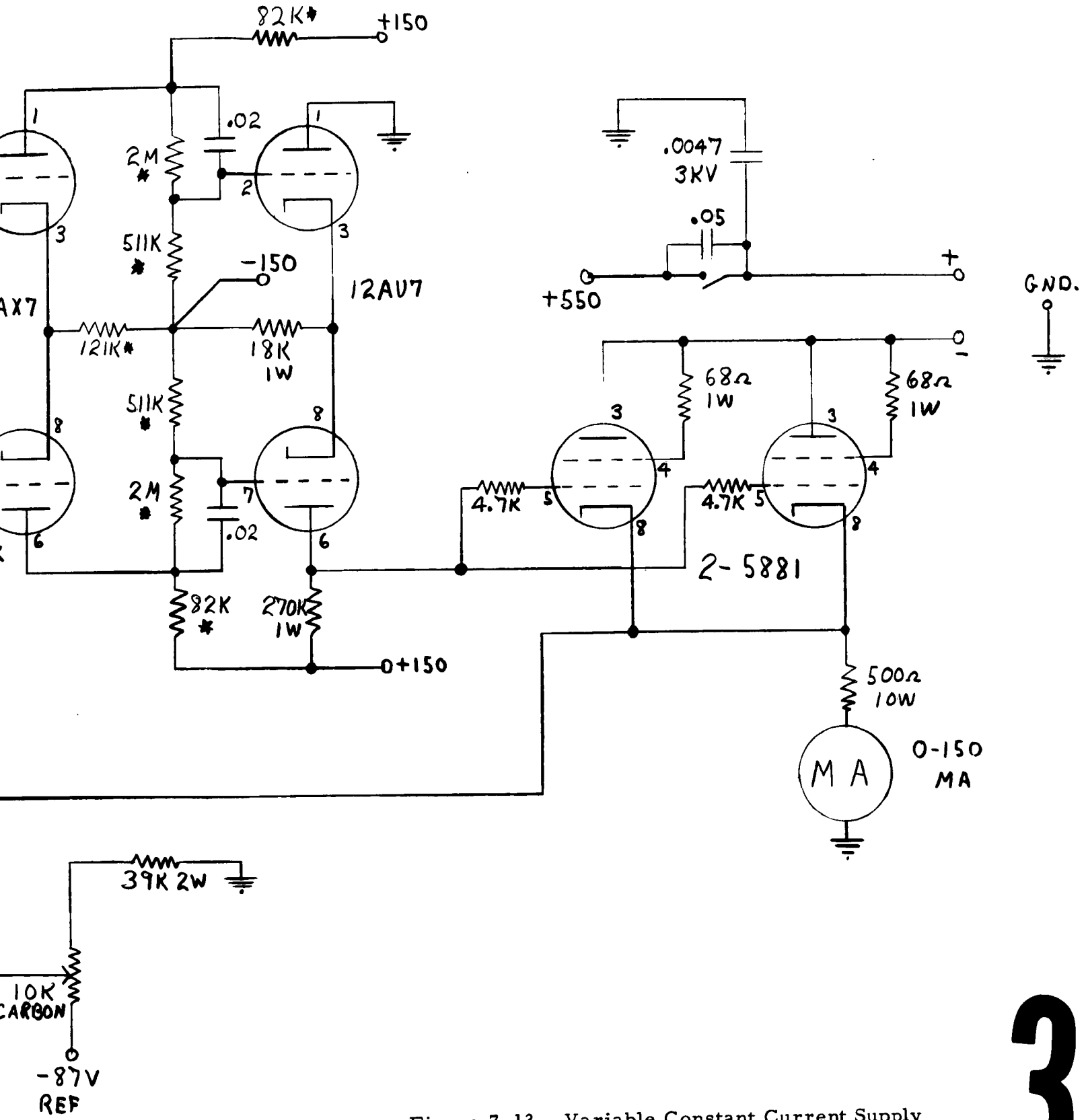

Figure 7-13. Variable Constant Current Supply

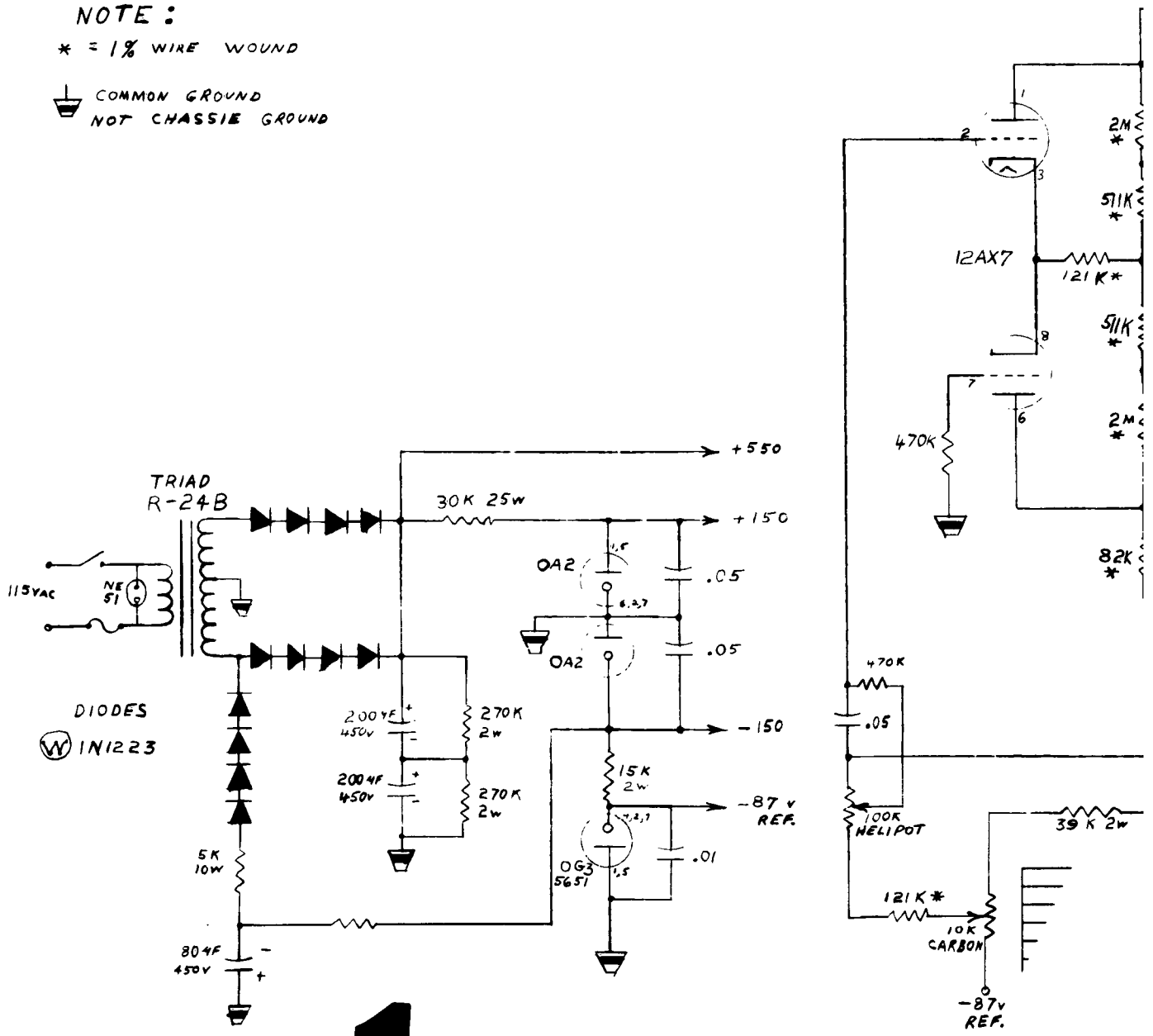
NOTE :
* = 1% WIRE WOUND
COMMON GROUND
NOT CHASSIE GROUND
TRIAD
R-24B
115VAC
NE 51
DIODES
IN1223
30K 25w
+550
+150
-150
-87 v REF.
OA2
OA2
.05
.05
.01
200 MF 450v
200 MF 450v
270K 2w
270K 2w
15K 2w
5K 10W
80 MF 450v
OG3 5651
12AX7
2M
511K
121K*
511K
2M
470K
82K
470K
.05
100K HELIPOT
39K 2w
121K*
10K CARBON
-87v REF.

1

Figur

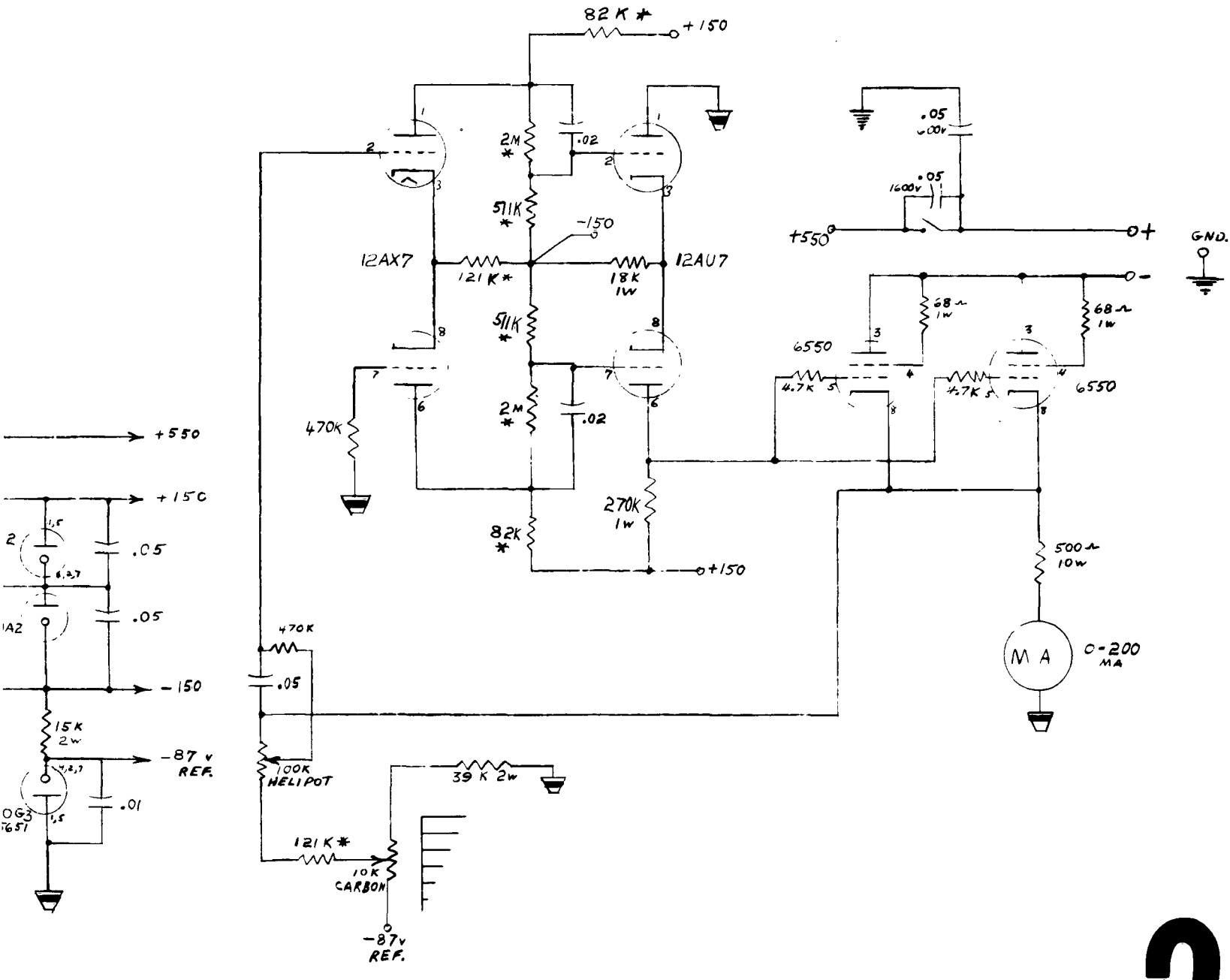

Figure 7-14. Variable Constant Current Supply

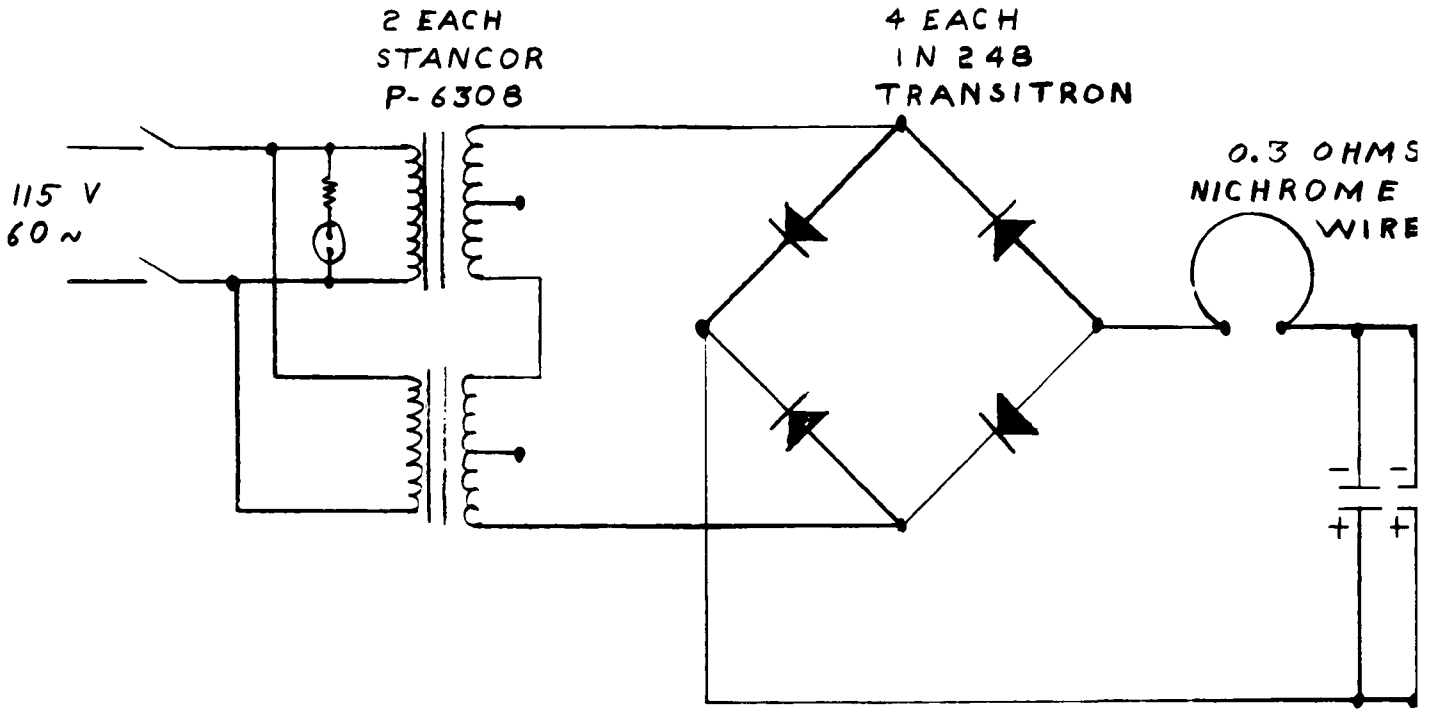

RANGE 4 TO 8 VOLTS
0 TO 10 AMPERES

REGULATION 10% } @ 7AMPS
P-P RIPPLE 1.5% } 7VOLTS

1

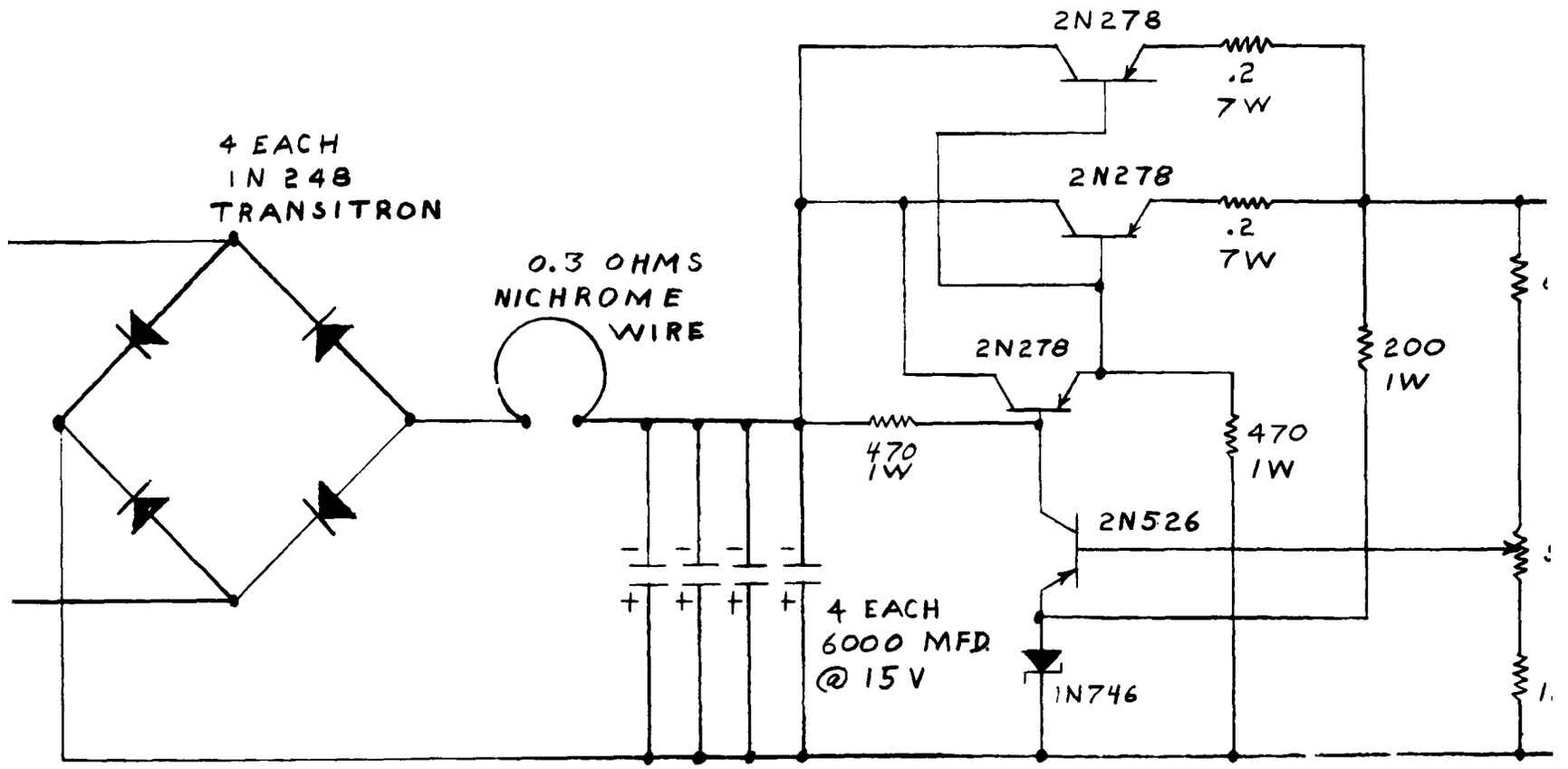

OLTS

AMPERES

'AMPS
'VOLTS

2

Figure 7-15. Slow Scan Filament Su

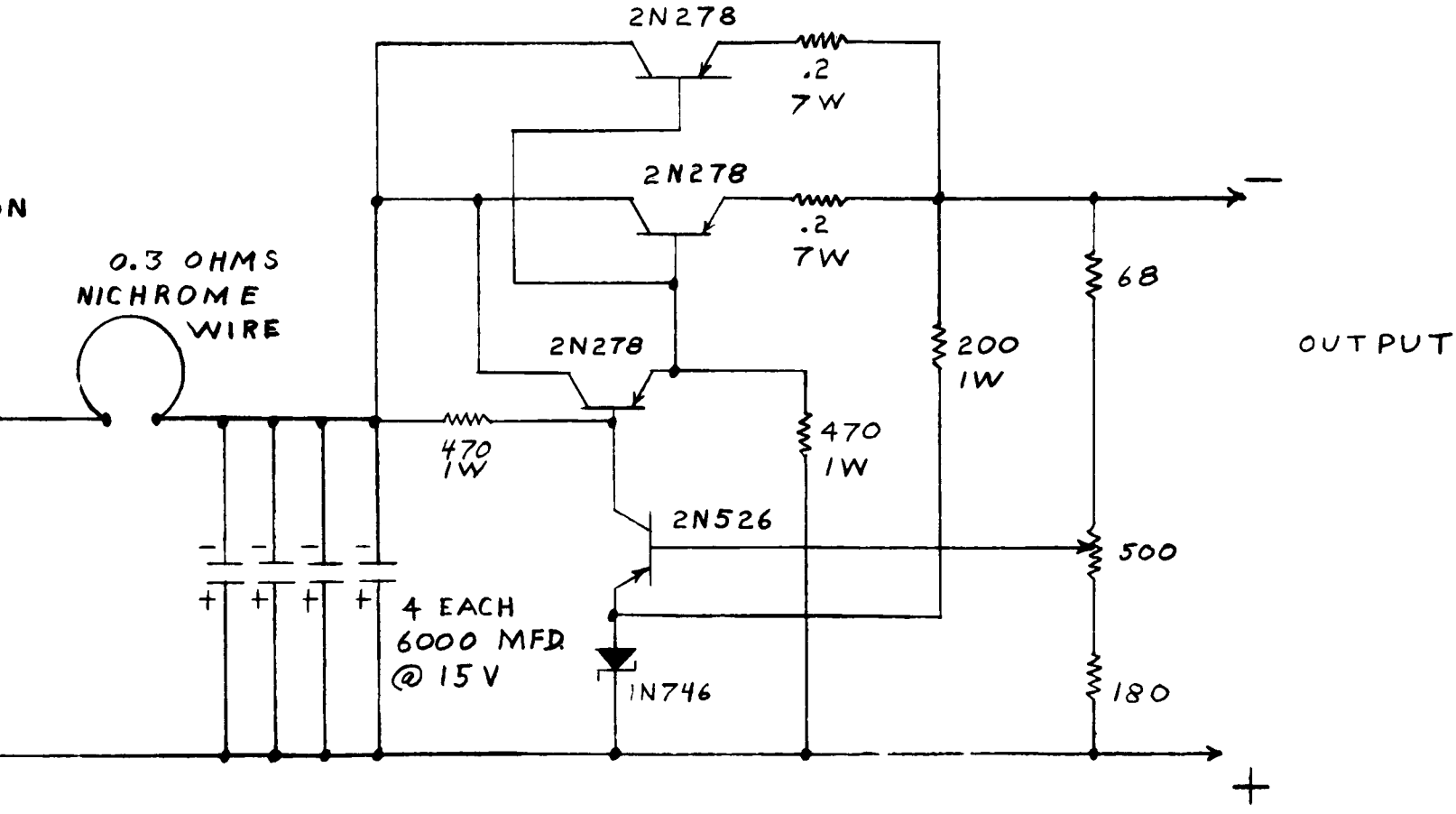

Figure 7-15. Slow Scan Filament Supply

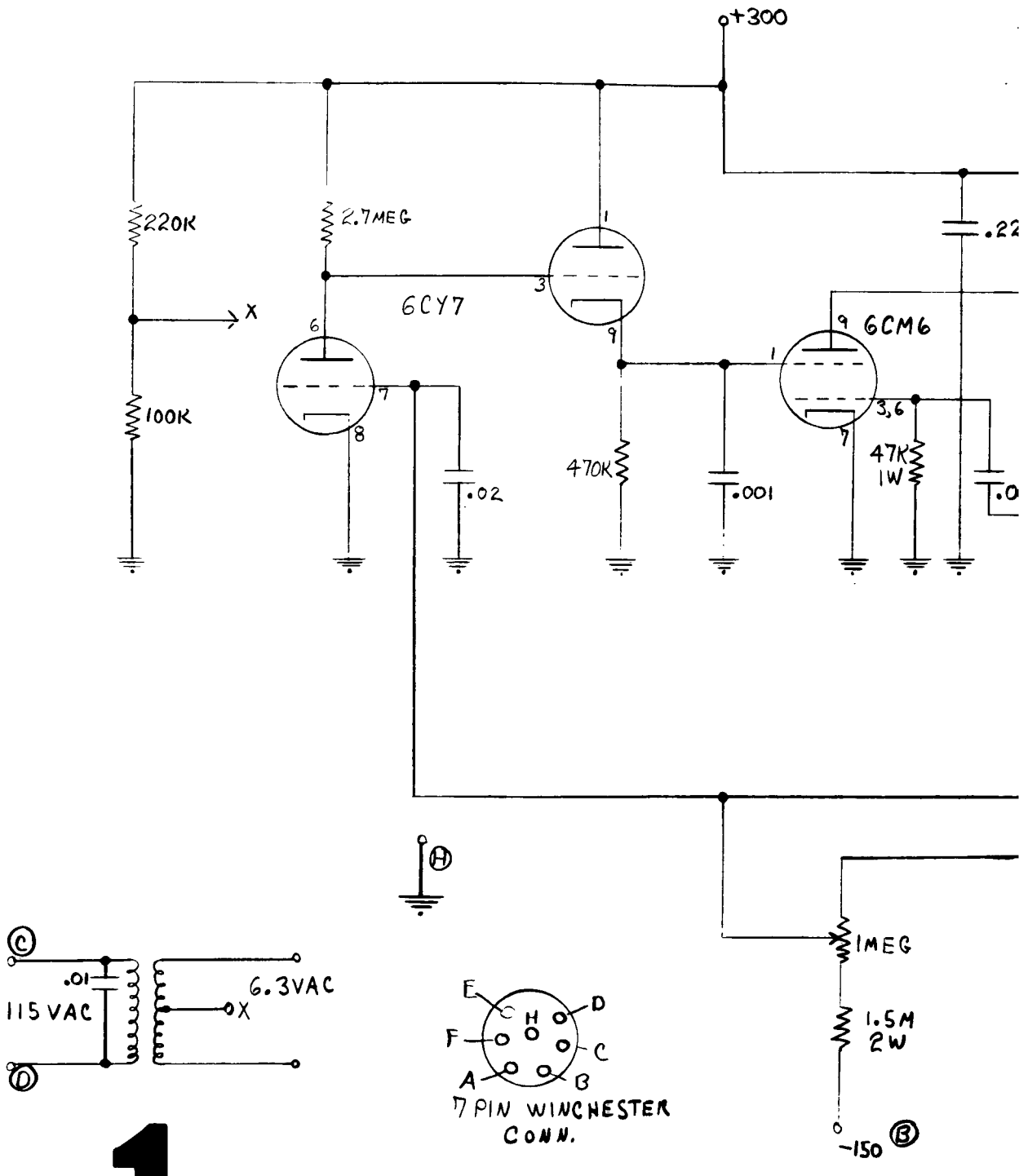
+300
220K
2.7MEG
X
6CY7
6CM6
100K
.02
470K
.001
47K
1W
.22
.0
A
1MEG
1.5M
2W
-150
B
C
115 VAC
.01
6.3VAC
X
D
E
H
D
F
C
A
B
7 PIN WINCHESTER
CONN.

Figure 7-16

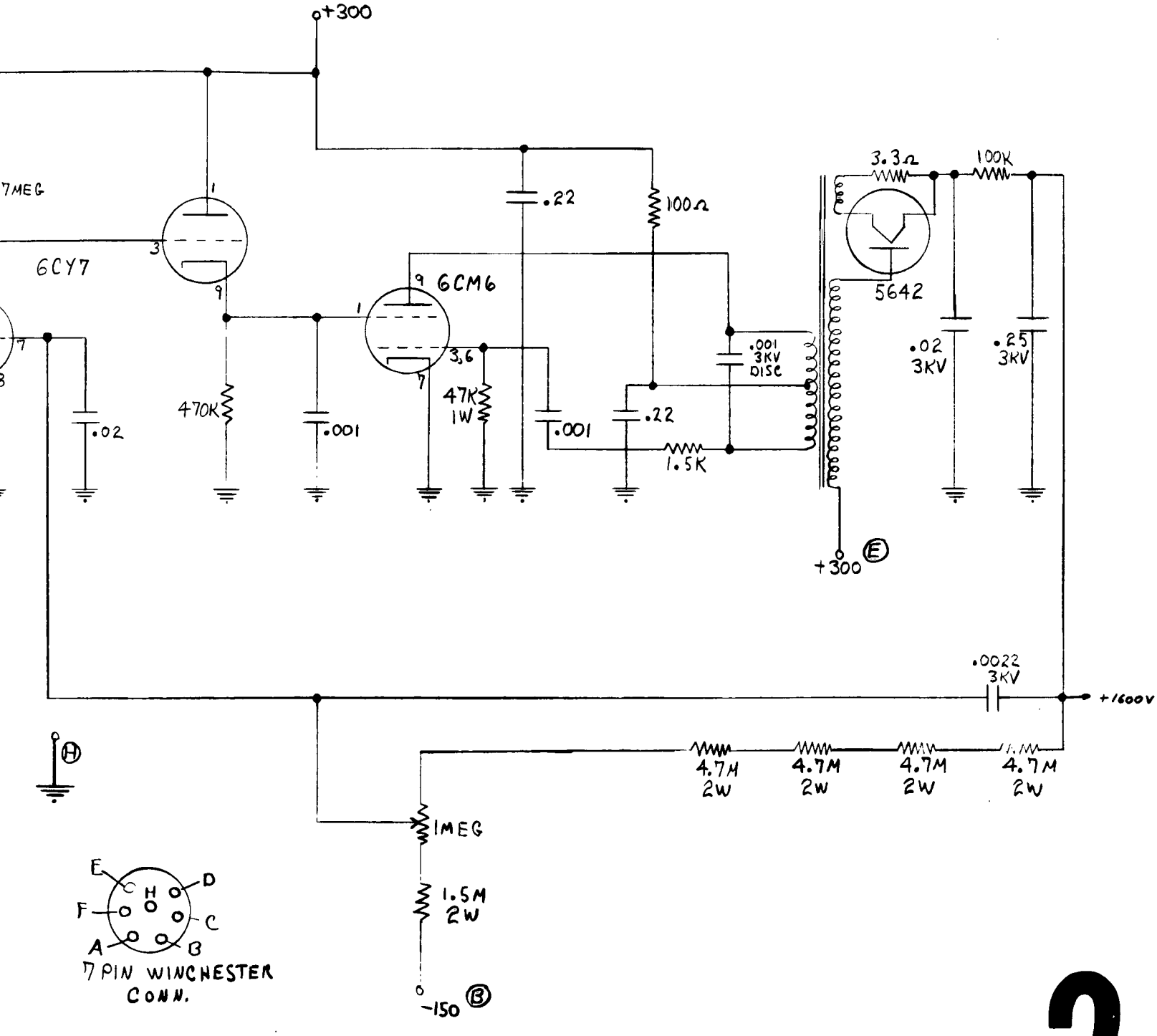

Figure 7-16. Power Supply 1600 Volts DC

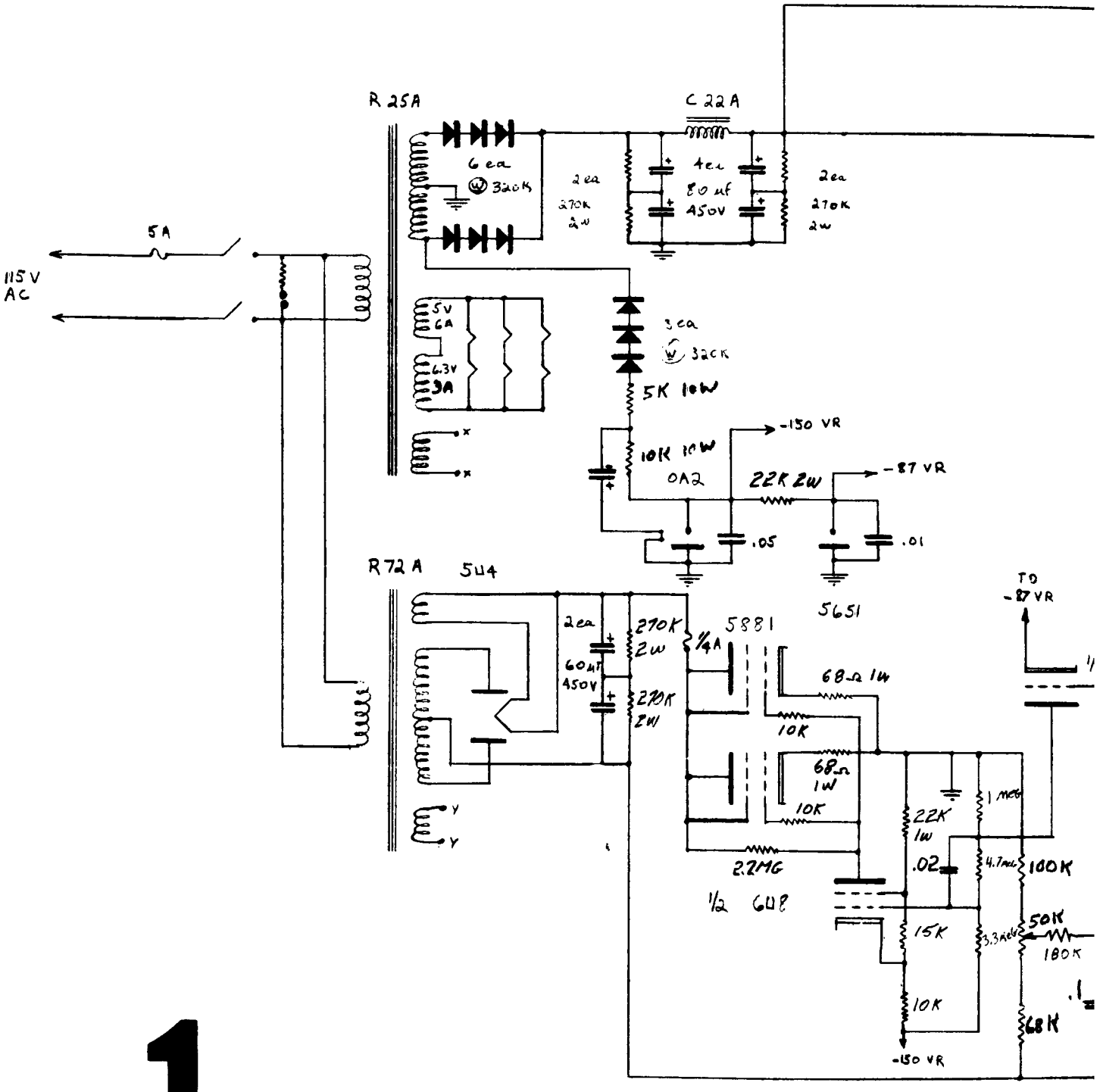
R 25A
C 22A
6 ea
320K
2 ea
270K
2W
4 ea
80 uf
450V
2 ea
270K
2W
5A
115 V
AC
5V
6A
6.3V
3A
3 ea
320K
5K 10W
10K 10W
-150 VR
0A2
22K 2W
-87 VR
.05
.01
5651
R 72 A
5U4
2 ea
60 uf
450V
270K
2W
270K
2W
1/4A
5881
68Ω 1W
10K
68Ω
1W
10K
2.2MG
1/2 6U8
22K
1W
1 meg
.02
4.7meg
100K
50K
180K
15K
3.3meg
10K
68K
-150 VR
TO
-87 VR

1

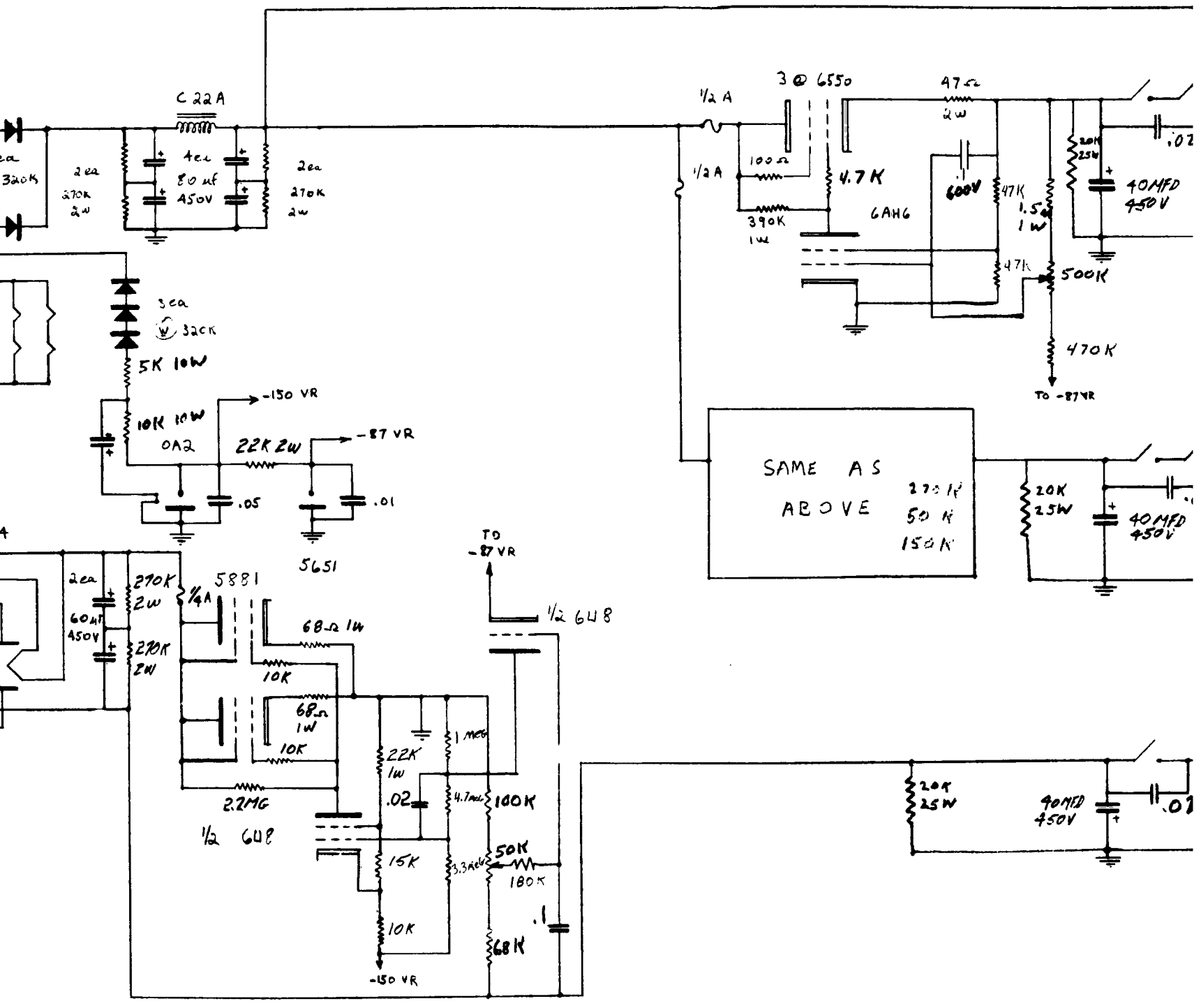

2

Figure 7-17. Regulated Utility Power Su

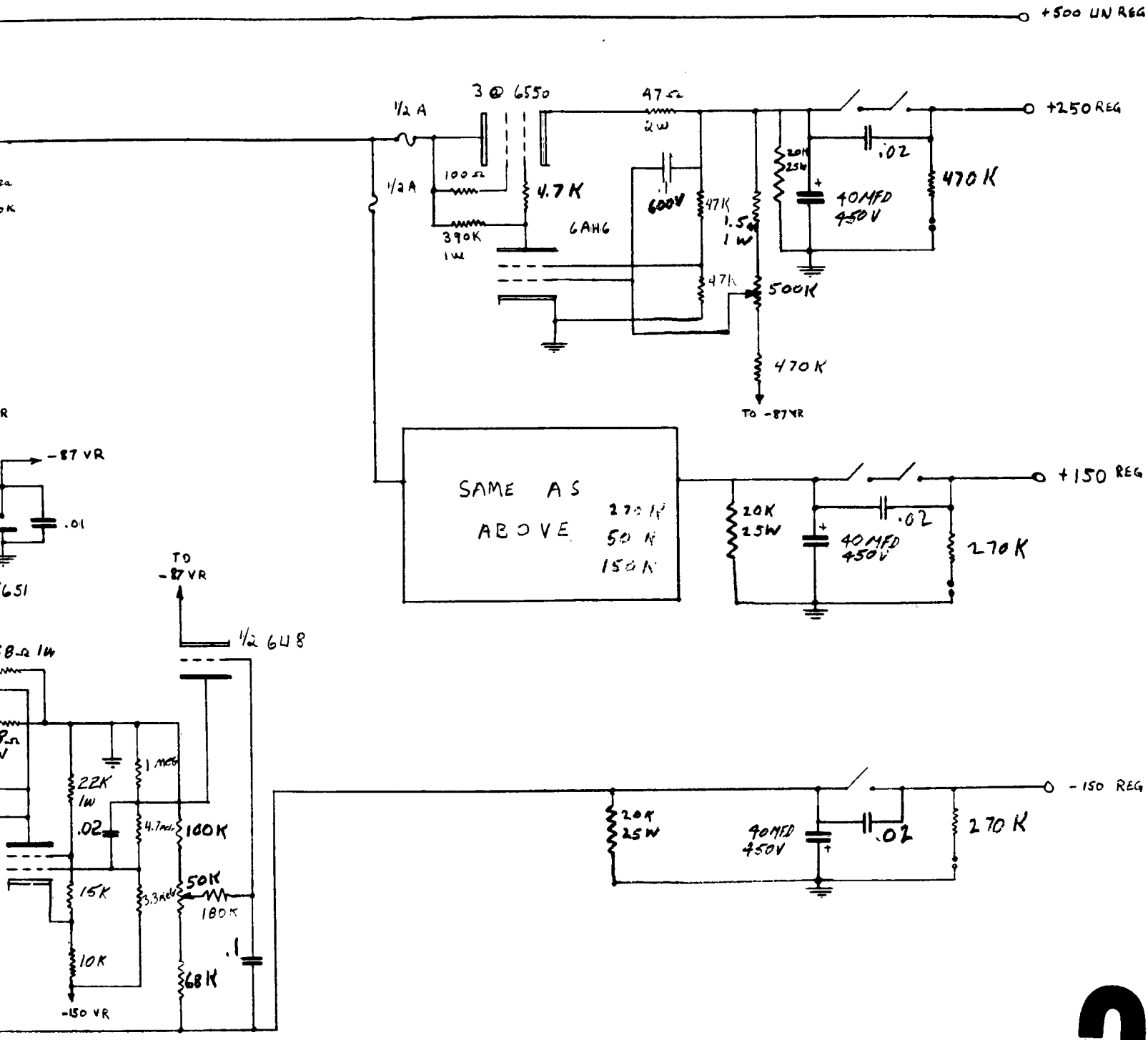

Figure 7-17. Regulated Utility Power Supply

3

8. APERTURE RESPONSE ANALYSIS

8.1 INTRODUCTION

The resolution of any part or combination of parts of an imaging sequence may be expressed as an aperture response, a sine wave response, or a square wave response. In any given case, one of these three responses is usually easiest to measure. Thus, aperture response is relatively simple to measure for the scanning beam of an electron gun under development, sine wave response is easiest to measure for an electronic circuit, and square wave response is most easily measured for a camera tube or combination of imaging parts where the input is a light image.

These three resolution response functions are well known and will not be formally defined here. A line image input is implied for each: a single very narrow bright line for aperture response, an array of parallel lines varying sinusoidally in brightness for sine wave response, and an array of parallel black and white bars of equal width for square wave response. Figures 8-1 and 8-2 show a matching set of response curves. Figure 8-1 is the aperture response curve for a television resolution measurement; it is basically a plot of the A-scope trace itself when the input is a single bright line perpendicular to the scan direction. Aperture response curves often resemble gaussian normal error curves because many resolution degrading processes involve statistical spread. For example, the electrons of a focused beam aim at a point but scatter like shot. A perfect gaussian distribution has actually been used for the illustrative curves of figures 8-1 and 8-2. Although few practical curves fit such a distribution precisely, the shapes, slopes, and general comparative characteristics depicted are grossly typical of most measured curves.

Figure 8-2 shows the corresponding sine wave and square wave response curves. Each is a plot against input image spatial frequency of the output amplitude, as may be observed on an A-scope. The output amplitude is normalized to unity at the lower frequencies where amplitude response typically holds constant. For the particular gaussian case treated here, the sine wave response curve is also gaussian, as would be seen more clearly if the spatial frequency abscissa scale used in figure 8-2 were

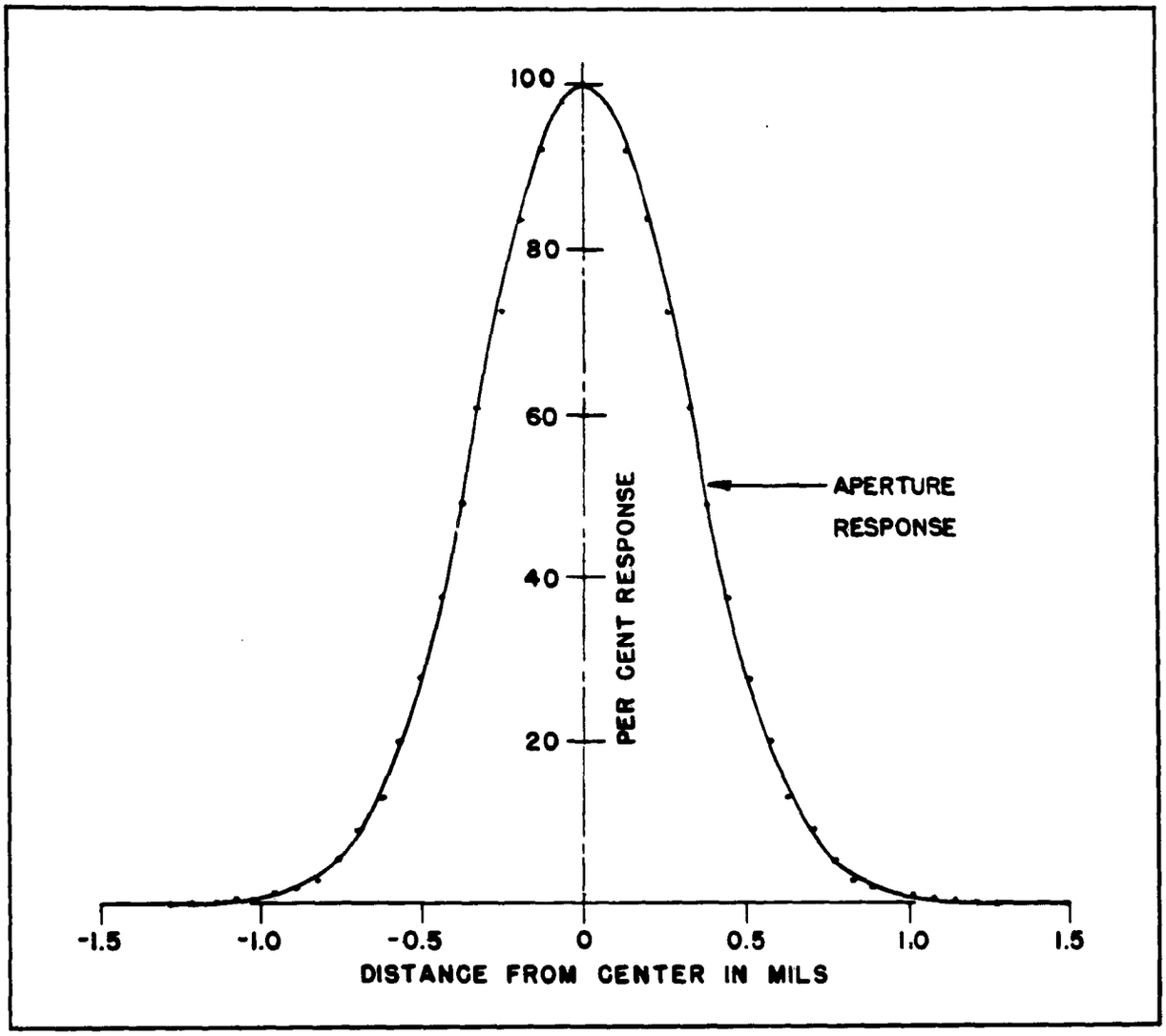

Figure 8-1. Resolution Response Functions

linear instead of logarithmic. However, this perfect correspondence of shape is unique to the gaussian case, and it typically does not hold for practical measured curves.

In figure 8-2 the square wave response curve rises higher than the sine wave response curve, in the ratio of $4/\pi = 1.273...$ for the upper two thirds of the frequency range. At lower frequencies, the ratio drops to 1 as the two curves come together. This is a general characteristic of all reasonably well behaved response curves. It relates to the mathematical odd-integer harmonic nature of the square wave. A square wave of unit amplitude has a sine wave fundamental of amplitude greater than unity, namely $4/\pi$. So to speak, a square wave contains more sine

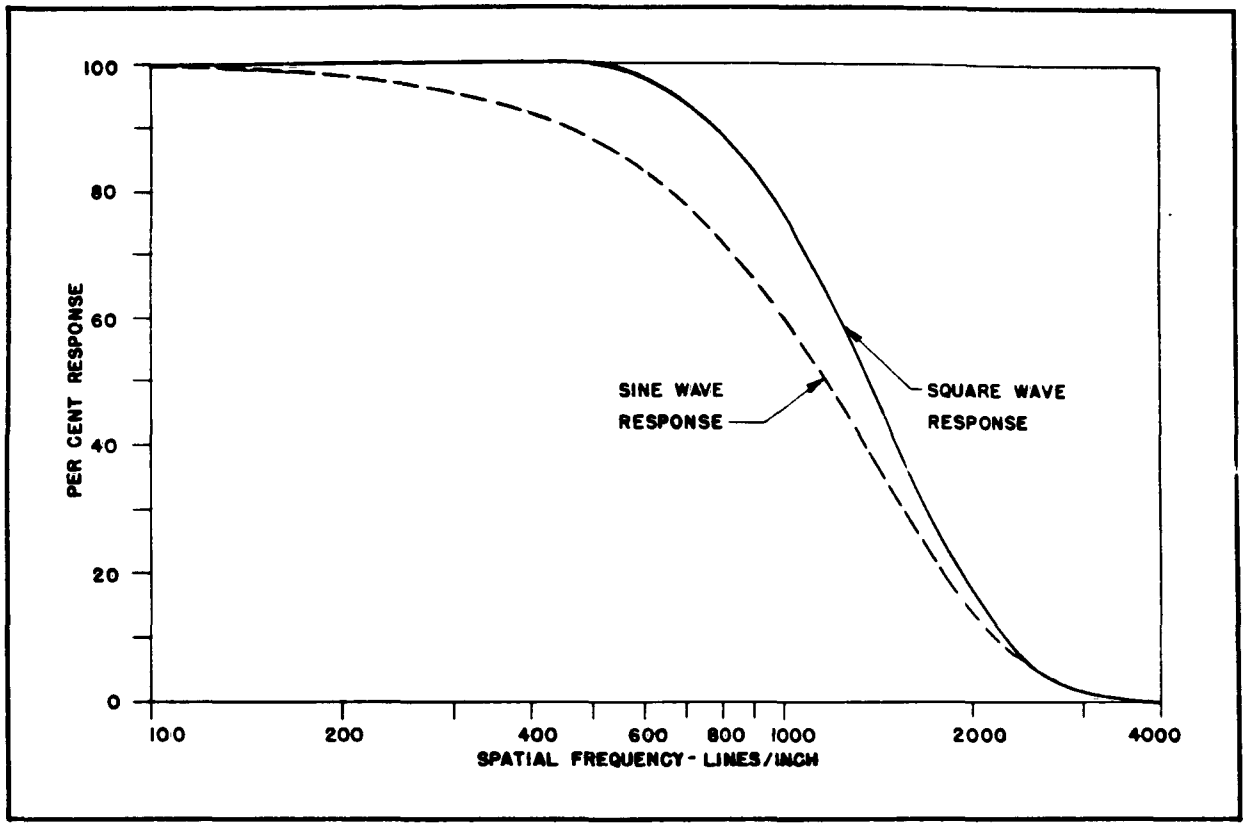

Figure 8-2. Resolution Response Functions

wave fundamental than a sine wave itself. Only this fundamental of the square wave is transmitted from the upper cutoff frequency down to one-third of the cutoff frequency, and within this frequency range the square wave response is 27 percent higher than the sine wave response.

For the general comparative statements of the last paragraph, the qualifying statement is included that the response curves be reasonably well behaved, as they usually are in practical measurements. By this it is meant that the sine wave or square wave response curve should drop smoothly from unit response at low frequency to zero response at high frequency, with no abrupt discontinuities or obvious resonances along the way. Freak cases can be concocted that are not very well depicted by the statements of the last paragraph. For example, a circuit sine wave response curve consisting of only a single resonant frequency, f_r, would convert to a very strange square wave response consisting of a series of resonant spikes at frequencies f_r, $f_r/3$, $f_r/5, \ldots$, with amplitudes $4/\pi$, $-(4/\pi)/3$, $(4/\pi)/5, \ldots$. By the strict mathematical definition of square wave response, the alternate spikes would even have to be plotted negatively.

Each of the three response functions may be transformed mathematically to either of the other two. In principle, the transformation is perfect, independent of the particular shape of the curve involved. The difficulty of making the transformation varies considerably with which transformation is required. Of the six possible transformations, four will be considered more important here. Of these, transformation from aperture response to sine wave response is by far the most difficult and tedious. The converse transformation from sine wave to aperture response is of intermediate difficulty. The easiest is transformation from sine wave to square wave response, followed closely by the converse from square to sine wave. The remaining two of the six, from aperture to square wave and conversely, are usually best done by intermediate transformation through the sine wave response.

Transformation to the sine wave response is ideally best for all situations involving analysis of combinations of parts in an imaging sequence because the point by point (frequency by frequency) product of the sine wave responses of the parts is equal to the sine wave response of the combination. By theory, this important product rule holds perfectly for sine wave responses, whereas neither it nor any other simple combination rule holds for aperture or square wave response functions. The sine wave response product rule holds "forward and backward" for products and for converse quotients. Thus, if the sine wave response curves are known from measurement for a combination of two parts and for one of the parts, then the sine wave response of the other part may be obtained by taking the point by point quotient for the combination and the known part. In this way the product rule may be reapplied many times in succession to combine and to separate out the responses of different parts, until the response of a part that cannot be measured directly is finally deduced.

In theory, the product rule does not hold for direct use with square wave responses. This is unfortunate, since in many instances the square wave response curve is by far the easiest to measure. The temptation is great to take the point by point product of two measured square wave response curves and to call the result the square wave response of the combination. Strictly considered, this is wrong. However, the point is now made that the error introduced by this false application of the product rule is not necessarily large. Specifically, the error so introduced varies from 27 percent to none at all for any single combining of two curves. If three curves are so combined, the maximum error is $(4/\pi)^2$; for four, it is $(4/\pi)^3$; and so on.

The theory behind this 27-percent maximum error can be readily seen by considering the case of falsely combining two nearly identical square wave response curves. In the upper frequency range where the error is greatest, each square wave curve runs higher than the sine wave curve by the factor 1.273.... The false square wave product is then higher than the sine wave product by the factor $(1.273...)^2$, whereas the true square wave response of the product is higher by only 1.273.... Therefore, the false square wave product is higher than the true square wave product by the factor $1.273...^2/1.273... = 1.273...$. This is the maximum discrepancy. At lower frequencies the ratio drops to 1. Further, this maximum 27-percent discrepancy at higher frequencies occurs only if the two curves combined are nearly identical. If the two curves are well separated, as when a lens of excellent resolution is combined with a camera tube of much lower resolution, the frequency range important to the combination tends to correspond to the lower frequency part of the curve of better resolution, where its sine and square wave responses approach unity at a ratio of 1. In the limit, the second factor of 1.273... drops to 1, and no discrepancy remains.

For these reasons and for others that will be brought out later, it is recommended that the false square wave product should often be used, though always with caution, as a reasonable approximation. This recommendation has been followed often during the present project, and the resulting product curves appear in paragraph 5.1.3.2 of this report. In the analysis that follows immediately, however, the mathematically correct complete transformations are used.

8.2 PHOTOELECTRIC STORAGE COMBINATION RESPONSE

The analysis processes described above have been applied to the combination at the heart of the photoelectric information storage system by which resolution to 3800 lines per inch has been demonstrated. The final results are summarized in figure 8-3. The transformation details by which starting curves for this figure were obtained will be described later.

The dashed curve in figure 8-3 labeled "Total Combination" is the sine wave response for the combination of four parts, transformed from a direct square wave measurement of the combination, as plotted in figure 6-16. The four parts are (a) the optics, (b) the electron optical imaging section, (c) the storage tape action itself, and (d) the new very fine reading beam. This is the combination with which 3800 lines per inch is observed. Resolution by other parts like the amplifier circuit and the reading monitor is made negligible by underscanning the tape.

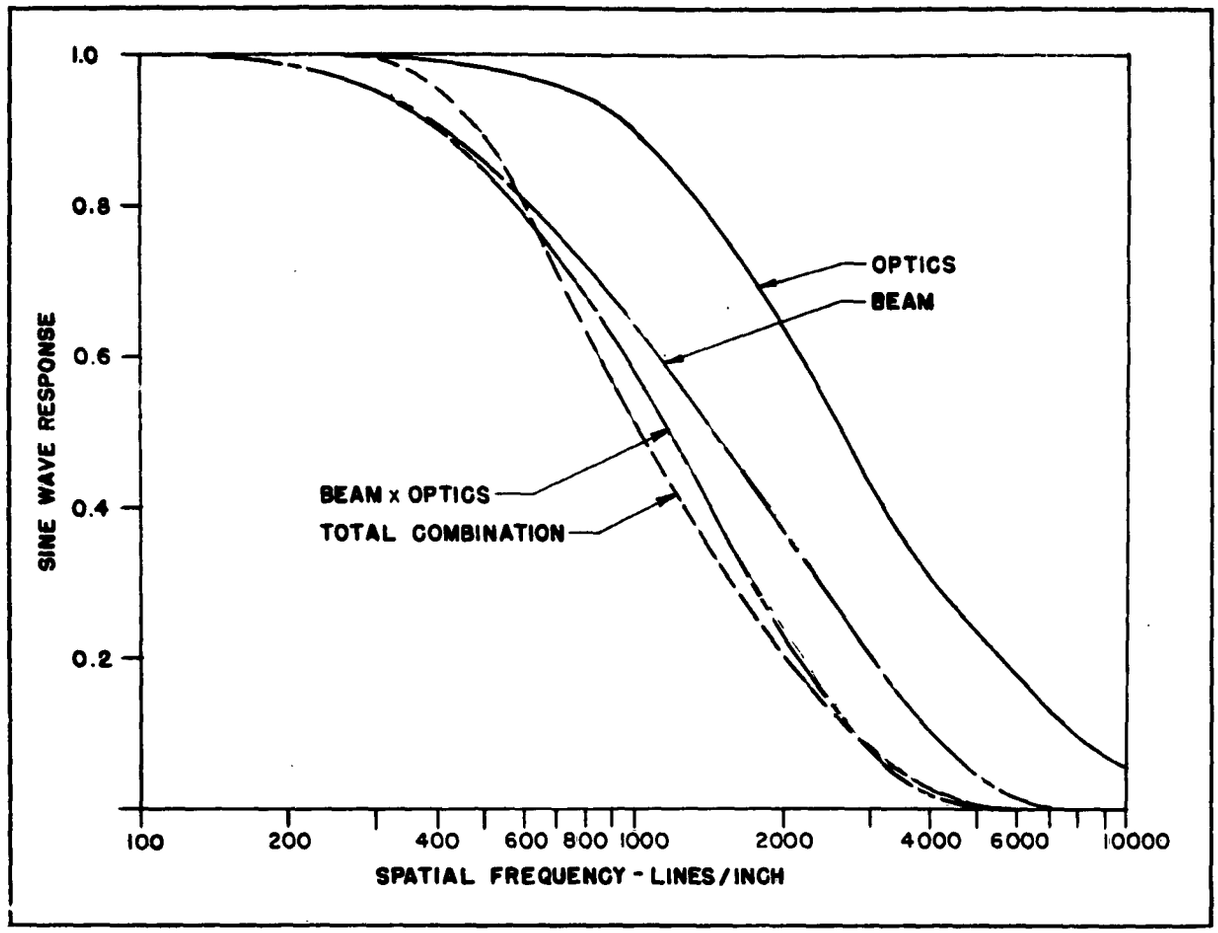

Figure 8-3. Comparison of Combination and Product of Parts

The curves in figure 8-3 marked "Optics" and "Beam" are the sine wave responses for parts (a) and (d), transformed respectively from a directly measured square wave response of the optics, figure 3-8, and a directly measured aperture response of the beam, figure 5-2. The subproduct for the combination of these two parts is marked "Beam x Optics." No measurements exist for the product of (b) and (c), or of (c) alone. A later measurement, figure 3-12, pertaining to (b) alone was made after this analysis was complete and is not now included. It is consistent with the statements that follow.

In principle, the curve for the Total Combination in figure 8-3 should fall below that for Beam x Optics at all spatial frequencies, and the quotient of the two should represent the sine wave response of (b) times (c). It is seen, however, that the Total Combination curve incorrectly rises higher in limited frequency range around 400 lines per inch. This is experimental error. The important fact is that the two

curves agree to within 10 to 15 percent over essentially all of the frequency range, or to within reasonable limits of measurement accuracy. The difference that must exist is so slight that it is pointless to try to use it for precision determination of the resolution of (b) times (c). The conclusion is that the resolution of (b) times (c) is very high, with a curve that probably lies between the curves shown here for the beam and optics.

8.3 READING BEAM RESPONSE

The directly measured aperture response of the new fine beam is shown in the A-scope photograph of figure 5-2. A plot of careful measurements of this aperture response with a traveling microscope is shown in figure 8-4. Strictly, this response is that of the beam in combination with the 0.2-mil slit used to measure it, and the effect of the slit must be corrected out. The aperture response of the beam and slit in figure 8-4 is transformed to its equivalent sine wave response marked "Beam x Slit" in figure 5-5 as will be discussed further below. The computed sine wave response of the slit alone is also shown in this figure. The point by point quotient is the sine wave response of the beam alone and is marked "Beam." This is the curve that was used for the beam in figure 8-3.

The results of figure 5-5 were surprising in two ways. First, the correction for the finite slit width is quite small. It is evident that the slit is adequately narrow for resolving the very fine beam. Yet this was not expected because the slit width appeared coarse in relation to the sharp peak of the aperture response. The adequacy of the slit may be partially explained in retrospect by the fact that the lowest spacial frequency at which complete cancellation can occur is 10,000 lines per inch, at which one sine wave line pair, or two lines appear across the width of the slit. Better evidence is shown in figure 8-5 in which a gaussian aperture response closely matching the original observed aperture response near the peak is shown along with the aperture response of the combination of the gaussian and a 0.2-mil slit. The two agree so closely that it is difficult to show both on the same plot. Thus, the slit is demonstrated as being quite adequate for resolving this sharp gaussian response.

The second surprise is that the original aperture response cannot be approximated by a simple single gaussian curve. Figure 8-5 shows clearly that a gaussian that fits the upper portion of the original curve is much too narrow to match also in the lower regions. This is also shown in figure 5-2, where the sine wave equivalent of the same gaussian aperture is included for comparison as a finely dotted line. It is often stated that most of the processes by which images are degraded correspond roughly

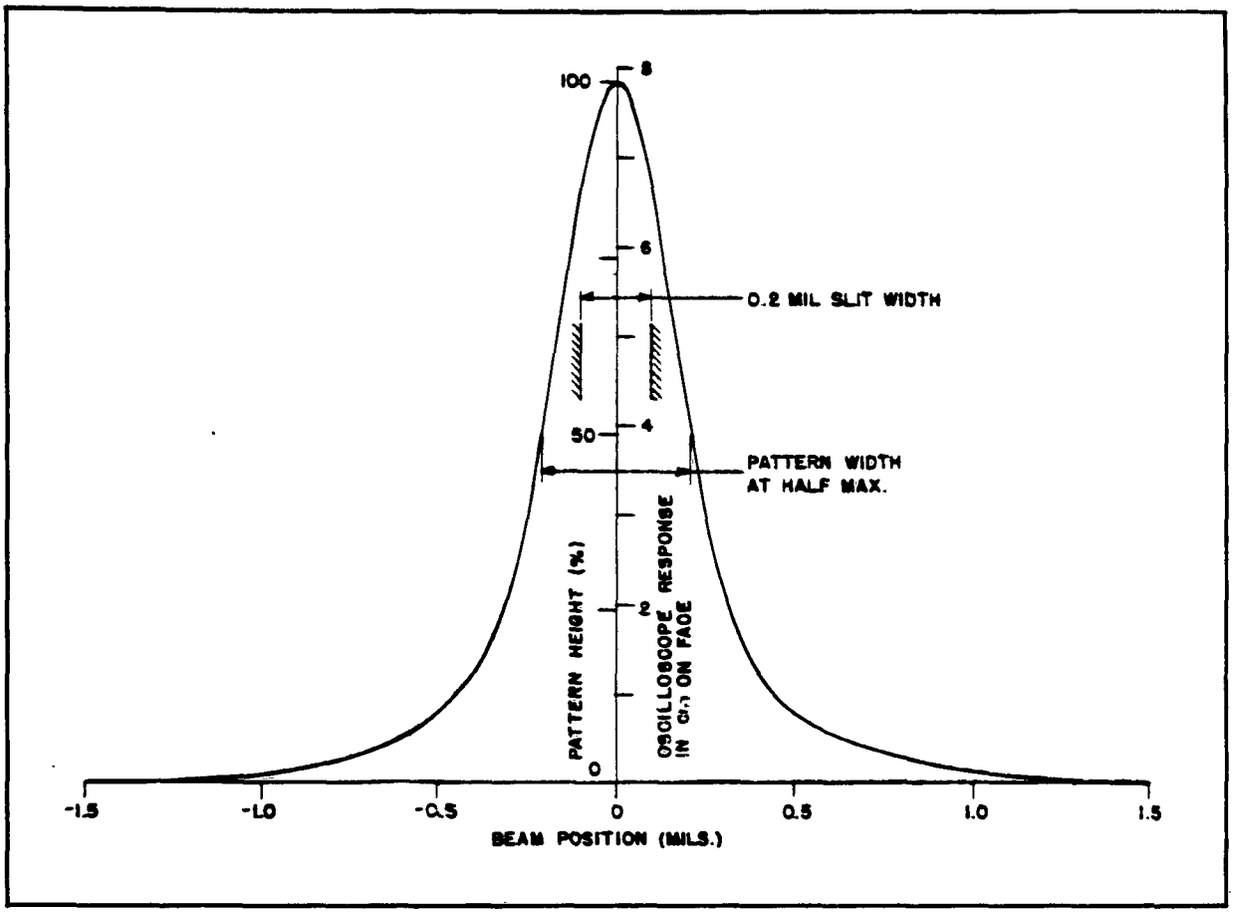

Figure 8-4. Reading Beam Current Density Distribution

to normal error curve processes, resulting in gaussian aperture responses. Accordingly, a gaussian response curve is sometimes fitted to a single measured point. The present case illustrates that the results can be very misleading.

In addition, it should be stated that the original aperture response curve can be closely approximated by the additive sum of two gaussian curves (not product). It is likely that this is physically significant and that the second broad low gaussian required corresponds to a secondary action within the gun. However, it is possible that it reflects only the mathematical capability of a small series of gaussian curves to represent a large variety of curves of this general shape.

The accuracy of the sine wave response curve for the beam alone is believed to be high. A small rise in the curve near 8500 lines per inch approximately matches minor perturbations noted in the original oscillograms, presumably due to circuit ringing. This rise is deleted in the curve as used in later combinations.

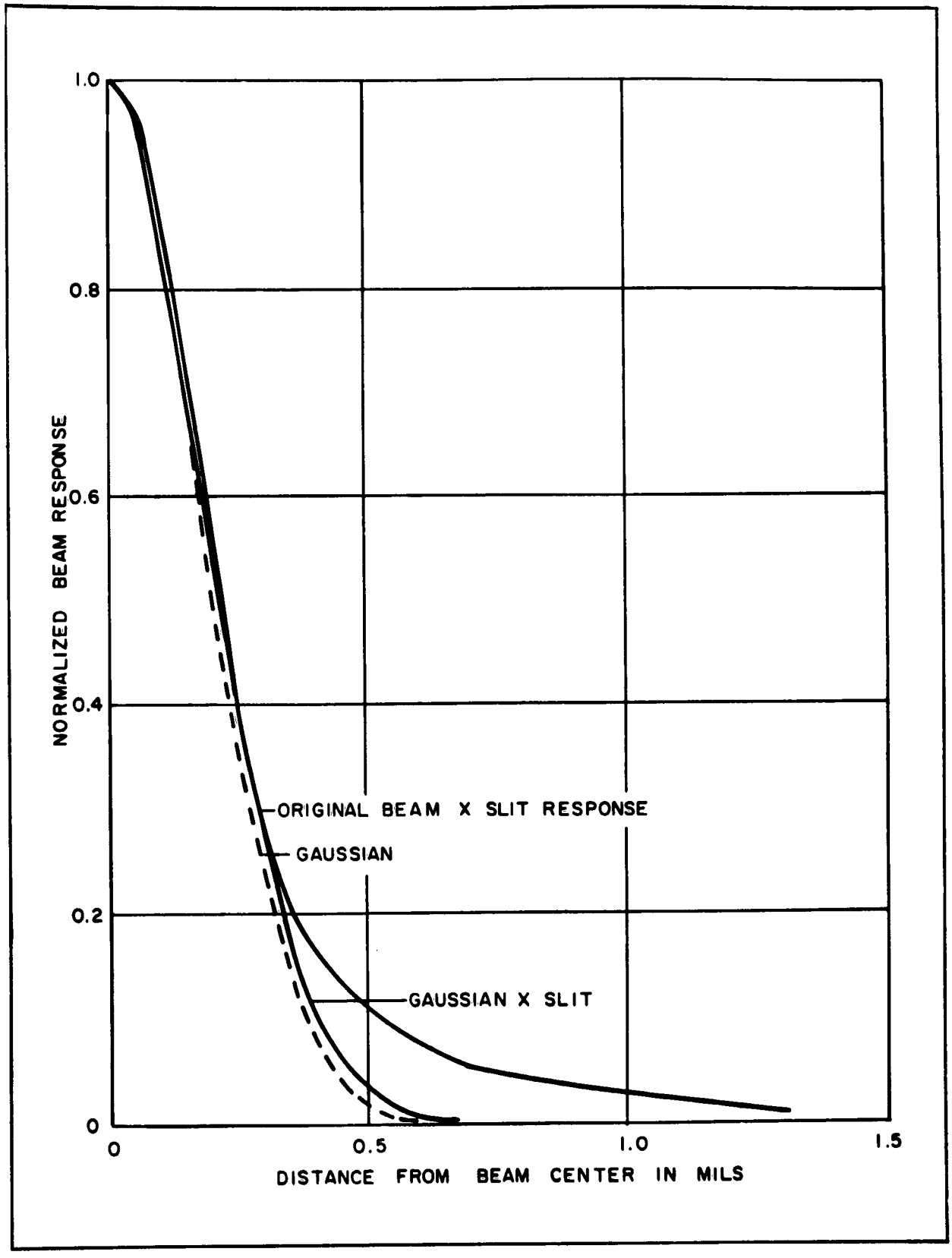

Figure 8-5. Beam Aperture Response

8.4 TRANSFORMATION OF THE BEAM RESPONSE

As was stated above, the observed aperture response of the beam and slit was transformed to the Beam x Slit sine wave response of figure 5-5. It has been mentioned that this transformation from aperture response to sine wave response is inherently tedious and difficult. The method used was derived from the Fischer-Hinnen method (Johnson, "Mathematical and Physical Principles of Engineering Analysis," page 258). The aperture response was imagined to repeat at 5-mil intervals. A Fourier cosine series of 25 terms was then fitted to this periodic curve by the approximation method devised, with harmonics at spatial frequencies of 400, 800, 1200,..., 10,000 lines per inch. The amplitudes of these harmonics are shown as A_1, A_2,... in table 8-1. A constant term, $1/2\ A_0$, is also obtained, such that the Fourier series with this added constant term represents the original aperture response function. Twice this constant, or A_0, represents the relative sine wave response at zero frequency, and the sine wave response at all frequencies is normalized to this response, to obtain a_0, a_1, a_2,... in table 8-1 as the normalized sine wave response of Beam x Slit.

The exact method used is described in a memo by A.R. Gedance. Two defects in the method are apparent. First, it involves taking more points from the lower less significant portion of the aperture response than from the upper part. Second, the method is extremely sensitive to arithmetic slips in a way that is not easily checked. To illustrate, the 24th harmonic is obtained early in the process. An error here affects values obtained later for the 12th, 8th, 6th, 4th, 3rd, 2nd, and 1st harmonics. It is thought that the transformation can best be performed in the future by computer programming.

The transformation computations were done with the use of trigonometric tables and a standard desk calculator. The tabulations occupy about a dozen pages. Frequent rechecks were necessary to locate and eliminate errors. It is recommended that future computations for this more difficult transformation be performed by computer programming. Preliminary inquiries suggest a cost under $50 for initially setting up and checking such a programmed transformation, and a cost under $25 for each later transformation. Actual computer performance time might be 5 minutes.

In table 8-1 the sine wave response of the slit is also given. This was computed according to the usual $(\sin x)/x$ formula, where $x = \pi fw/2$, f is spatial frequency in lines per inch, and w is slit width in inches. The sine wave response of the beam alone is shown in the last column and is the quotient of values in the preceding two columns.

TABLE 8-I

BEAM RESPONSE TRANSFORMATIONS

Harmonic Spatial Frequency (lines/in.)	Beam x Slit*	Beam x Slit**	Slit+	Beam++
(0)	$-A_0/2 = 0.876$	$a_0 = 1.000$	1.000	1.000
400	$A_1 = 1.589$	$a_1 = 0.907$	0.997	0.910
800	$A_2 = 1.254$	$a_2 = 0.716$	0.990	0.724
1200	$A_3 = 0.995$	$a_3 = 0.568$	0.976	0.582
1600	$A_4 = 0.793$	$a_4 = 0.453$	0.958	0.472
2,000	$A_5 = 0.634$	$a_5 = 0.362$	0.935	0.387
2,400	$A_6 = 0.494$	$a_6 = 0.282$	0.908	0.311
2,800	$A_7 = 0.363$	$a_7 = 0.207$	0.876	0.237
3,200	$A_8 = 0.275$	$a_8 = 0.157$	0.830	0.189
3,600	$A_9 = 0.202$	$a_9 = 0.115$	0.800	0.144
4,000	$A_{10} = 0.136$	$a_{10} = 0.077$	0.757	0.102
4,400	$A_{11} = 0.091$	$a_{11} = 0.052$	0.711	0.073
4,800	$A_{12} = 0.065$	$a_{12} = 0.037$	0.662	0.056
5,200	$A_{13} = 0.039$	$a_{13} = 0.022$	0.611	0.036
5,600	$A_{14} = 0.026$	$a_{14} = 0.015$	0.558	0.027
6,000	$A_{15} = 0.017$	$a_{15} = 0.010$	0.505	0.019
6,400	$A_{16} = 0.014$	$a_{16} = 0.008$	0.450	0.018
6,800	$A_{17} = 0.003$	$a_{17} = 0.001$	0.391	0.004
7,200	$A_{18} = 0.004$	$a_{18} = 0.002$	0.341	0.006
7,600	$A_{19} = 0.008$	$a_{19} = 0.005$	0.287	0.016
8,000	$A_{20} = 0.008$	$a_{20} = 0.005$	0.234	0.019
8,400	$A_{21} = 0.008$	$a_{21} = 0.004$	0.183	0.024
8,800	$A_{22} = 0.004$	$a_{22} = 0.002$	0.133	(0.017)
9,200	$A_{23} = 0.001$	$a_{23} = 0.001$	0.086	(0.009)
9,600	$A_{24} = -0.004$	$a_{24} = -0.002$	0.042	(-0.048)
10,000	$A_{25} = -0.004$	$a_{25} = -0.002$	0.000	$(-\infty)$

* Amplitudes to fit original observed aperture response.

** Normalized sine wave response.

\+ Sine wave response from $\frac{\sin x}{x}$.

++ Sine wave response from $\frac{\text{Beam x Slit}}{\text{Beam x Slit}}$.

8.5 TRANSFORMATION BETWEEN SINE AND SQUARE WAVE RESPONSE

The results of several transformations from the square wave response curve to the sine wave response curve have been used above, and the converse transformation will presently be used below. The complete processes for accomplishing these transformations will now be given. The reason for including such detail is that this will allow one to judge more fully whether the extra time required for transformation from observed square wave data to sine wave data is justified. This judgment should also take into account whether the transformation process introduces new curve characteristics that act to obscure interpretation of the original measured data.

Let y_f be the sine wave response at spatial frequency f. The corresponding square wave response Y_f is the composite amplitude response to a square wave of unit amplitude, measured at the center of the resulting output waveform. By the standard Fourier series for a square wave, this is:

$$Y_f = (4/\pi)\,(y_f - y_{3f}/3 + y_{5f}/5 - y_{7f}/7 + \ldots)$$

Here the terms of the series alternate regularly between negative and positive, and there are no missing terms.

Consider for illustration the curves of figure 8-2. Assume that the sine wave response curve is known and that transformation to the square wave response curve is desired. The actual transformation for three spatial frequencies is as follows, with the response values taken from the figure.

f = 400 lines/inch	f = 800 lines/inch	f = 1200 lines/inch
$y_f = 0.923$	$y_f = 0.722$	$y_f = 0.487$
$-1/3\ y_{3f} = -0.162$	$-1/3\ y_{3f} = -0.019$	•
$1/5\ y_{5f} = 0.027$	•	•
$-1/7\ y_{7f} = -0.003$	•	•
Sum = 0.785	Sum = 0.703	Sum = 0.487
$Y_f = (4/\pi)\,(0.785)$	$Y_f = (4/\pi)\,(0.703)$	$Y_f = (4/\pi)\,(0.487)$
= 0.999	= 0.895	= 0.620

A dozen such points is, of course, quite adequate for plotting purposes. Note that the process becomes progressively easier for points of higher spatial frequency, as the higher harmonic terms become negligible. Above a certain frequency (here,

about 1200 lines/inch) even the third harmonic drops out, leaving the ratio of the two responses at $4/\pi = 1.273...$ for all higher frequencies. Conversely at the low frequency end, computation becomes progressively more tedious. For example, at f = 200 lines/inch, eight terms through the fifteenth harmonic are required in the example above. Clearly, it is wise to avoid starting at too low a frequency. The limiting series at very low f, $1 - 1/3 + 1/5...$, converges only very slowly to $\pi/4$.

The illustration above may be misleading in that the start is not a series of measured points. It is necessary actually to draw a best adjusted curve from measured points and then to work from this curve. Otherwise, an excessive number of points would have to be measured to supply values for all the harmonic frequencies involved.

The even more important converse transformation from square wave response to sine wave response will now be considered. Coltman and Altar have shown (JOSA 44, 470) that the transformation equation, which holds perfectly mathematically, is:

$$y_f = (\pi/4)\,(Y_f + Y_{3f}/3 \qquad - Y_{5f}/5 \qquad +...)$$

It is very important to know that the higher terms do not behave in a manner that is immediately apparent as being smooth and regular. There are occasional missing terms and peculiar reversals of sign. Thus, the ninth harmonic is missing; in the derivation, the third harmonic also brings with it a reverse ninth harmonic, which cancels with the regular ninth harmonic. The full series of constants for successive terms are: 1, 1/3, -1/5, 1/7, 0, 1/11, -1/13, -1/15, -1/17, 1/19, 1/21, 1/23, 0, 0, -1/29, 1/31, 1/33, -1/35, -1/37, -1/39, -1/41, 1/43, 0, 1/47, 0, -1/51, -1/53, -1/55, 1/57, 1/59, -1/61, 0, 1/65, -1/67, 1/69,.... The sum of this series is $4/\pi$. Obviously, terms high enough to get into the peculiar region are only rarely needed, for low frequency transformations.

Consider again the curves of figure 8-2. Assume now that the square wave response curve is known from measurement and that transformation to the sine wave response curve is desired. The transformation for three points is as follows:

f = 400 lines/inch	f = 800 lines/inch	f = 1200 lines/inch
$Y_f = 1.000$	$Y_f = 0.896$	$Y_f = 0.619$
$Y_{3f}/3 = 0.206$	$Y_{3f}/3 = 0.024$	$Y_{3f}/3 = 0.001$
$-Y_{5f}/5 = -0.034$	•	•

f = 400 lines/inch	f = 800 lines/inch	f = 1200 lines/inch
$Y_{7f}/7 = 0.004$		
Sum = 1.176	Sum = 0.920	Sum = 0.620
$y_f = (\pi/4)\ (1.176)$	$y_f = (\pi/4)\ (0.920)$	$y_f = (\pi/4)\ (0.620)$
= 0.923	= 0.722	= 0.487

8.6 SINE WAVE PRODUCT VERSUS APPROXIMATION SQUARE WAVE PRODUCT

As was stated several pages back, it is recommended that the approximation or false square wave product be used at times, though with caution. The following example, which starts with an experimentally measured square wave data, illustrates further detailed factors that should be discussed. In figure 3-13, the two lower curves are measured square wave response curves, while the upper curve for Photodiode alone is computed by taking the false square wave quotient of the other two. We shall repeat this with the full sine wave treatment, but it is interesting first to predict some of the results. Cutoff is approximately 9000 lines/inch for the original two curves, and one third of cutoff is approximately 3000 lines/inch. Above 3000 lines/inch we expect that each of the original square wave curves will run higher than the corresponding sine wave curve by the ratio 1.273.... Therefore, we should expect the false quotient curve to have the ratio 1.273.../1.273... = 1 to the true sine quotient curve. In other words, in this upper frequency range we predict that the false square wave quotient curve will actually convert to the sine wave quotient curve. The true square wave curve for the quotient will then be higher than the false one shown by another factor of 1.273....

This is shown in figure 8-6. The lower two curves are the original curves transformed to sine wave responses. The curve above these is the proper sine wave quotient, and this weaves very close to the dotted false square wave quotient carried over from the other figure. It is further noted that there are certain odd bends, common to both of these quotient curves. At first they seem to stress the close match of these curves, but there is strong evidence that they are not behaving as smoothly as actual curves should.

It is logical to complete the curve sequence by transforming the proper sine quotient curve to the true square wave curve, and this is shown as the uppermost

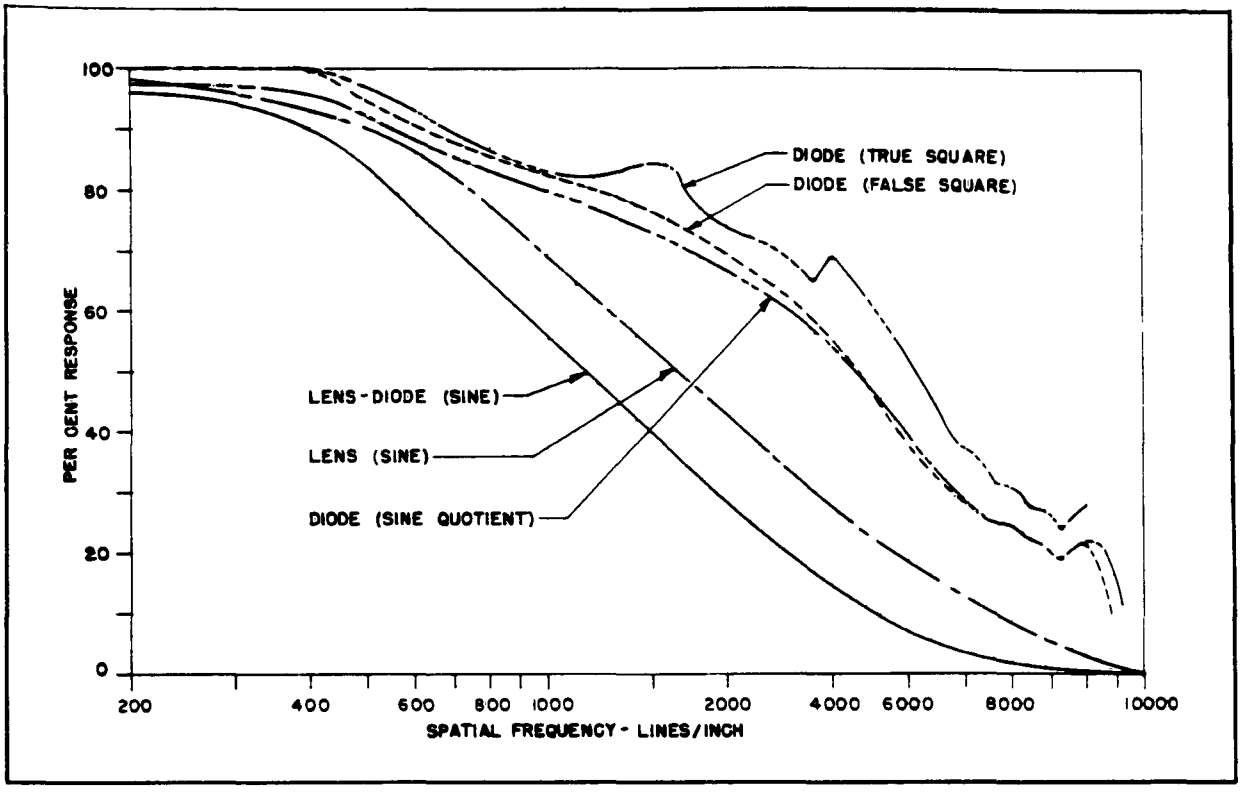

Figure 8-6. Transformed Response Curves

curve. It is seen that this true square wave curve, although maintaining the right 1.273... ratio where it should above 3000 lines/inch, oscillates most improperly at frequencies below this.

The explanation of the oscillations is that the original experimental square wave curves were improperly drawn to fairly abrupt cutoffs at frequencies above the region of direct measurement. An averaged curve drawn fairly smoothly through the oscillations would be fairly accurate. However, the oscillation defect here points out a basic defect inherent in using the idealized process of transforming all measured data to sine wave response curves. It is unreasonable to expect good measurements in the low response region at high frequency where the small A-scope signal becomes lost in the noise. Yet this high frequency response is needed for smooth transformation results.

Another experimental problem, which is not particularly illustrated by these curves, is that of deciding whether a sufficiently low frequency has been used to determine the low frequency end of the curve, to which the rest of the curve is normalized. It is likely that the discrepancy in the 400 line/inch region of figure 8-3 is due to this difficulty.

A third experimental problem contributing to error refers back to a fine detail in the mathematical definition of the square wave response. By this definition, the amplitude to be measured is that to the center of the transmitted curve of upswing (or downswing). A very exaggerated case, shown in figure 8-7, is one not likely to be encountered in actual measurements. It is assumed here that the harmonies of the original input square wave are transmitted undiminished up to a certain abrupt cutoff frequency, above which no harmonics are transmitted. Curve (a) shows the result of transmission of the fundamental and third harmonic only. Curve (b) shows transmission at a lower fundamental frequency of the fifth harmonic. In both cases the central maximum is not the highest maximum. With the curve compressed in the measurement process and with the detail of the transmitted waveform lost in noise, the measured amplitude would not correspond very accurately to the idealized central maximum which is used as the basis for the transformation equation. Although these curves are for an exaggerated case, the principle demonstrated applies pertinently to practical cases. As the input square wave frequency varies in the measurement, the shape and degree of squareness varies progressively. These details are mostly lost in the noise, and the estimate of amplitude is almost sure to be adversely affected.

These are the additional reasons referred to much earlier for favoring emphasis wherever possible on the raw direct square wave data, often with use of the approximation false square wave product instead of always introducing the time consuming transformation to sine wave response.

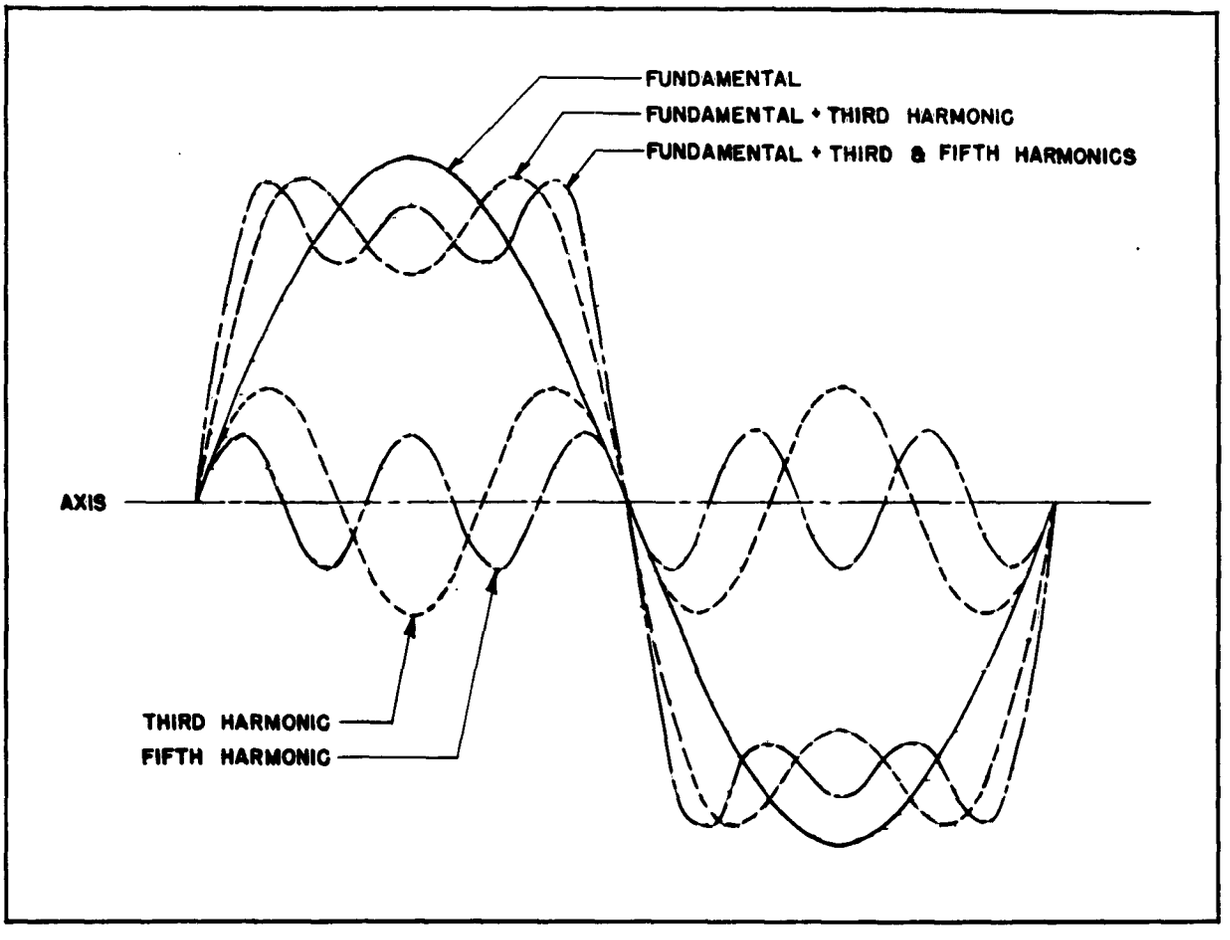

Figure 8-7. Transmitted Square Wave Patterns

9. CONCLUSIONS

Experiments have demonstrated that the Westinghouse electrostatic tape storage camera tube provides for the storage of electro-optical information at the greatest resolution density (50 line pairs per mm) and the greatest total resolution (2500 line pairs) available today. It does this with relatively high sensitivity, having a demonstrated ASA index of 12 and a clearly attainable ASA index of 50. This performance is beginning to compare favorably with that possible with photographic film yet the limit of performance has not been reached. It has the additional advantage that nothing is consumed in its use except electric power, the storage tape medium being reusable millions of times. Furthermore, the information is ready for reading immediately after exposure. A CRT display system has been demonstrated with which an enlarged hard copy on photographic film has been made of the information which had been stored electro-optically. Though these copies were made by scanning the stored picture electronically so many scan lines were used (145 lines per mm of the original optical image) that they were indistinguishable on the hard copy photograph.

Since the information is read out electronically, the standard television techniques of aperture correction and contrast enhancement may be applied in the circuits before the display or hard copy is made. Both of these techniques were demonstrated. Aperture correction provides that even areas having fine detail are reproduced in the proper contrast so that a micro-aperture densitometer will give a correct and direct reading for photometric purposes. By adjustment of the dc signal level and the signal gain, the picture contrast may be enhanced, spreading the interesting range of signal levels over all the gray levels of which the display is capable.

Since reading the signal does not, to a first approximation, erase the signal, so that in this respect it is like a photographic film recording, the user may choose to read the information off more slowly and thereby improve the resolution. Such an improvement by a factor of three has been demonstrated for a scanning speed change by a ratio of about ten. The resolutions quoted above are for a reading rate of 0.03 mm per microsecond. At slower rates as many as 75 line pairs per mm have been resolved on the final display. It has been demonstrated that this technique makes possible the recording of optical information at higher resolution than is possible by

using a comparable photographic film with a subsequent enlargement or microscopic observation.

9.1 IMAGE SECTION

The measurements on the photodiodes indicate that the resolution of the image section, while satisfactorily high in the center, falls off at the edges to quite low values. However, these measurements were made in a simple focusing coil in which no effort was made to match the electrostatic field with the magnetic field, nor was there any effort made to make the magnetic field uniform in flux density. It is certainly in order to attempt to shape the focusing coil in contour and in current density distribution to improve this situation.

9.2 STORAGE TARGET

The metal grating structure with the storage dielectric shadow evaporated on one side of each groove has proven to be the highest resolution electron charge storage target. The presence of the coplanar metal grille acts as an electrostatic shield that prevents the electric charge on a neighboring area from creating an electric field perturbation that can deflect the reading beam or its secondary electrons. This effect does occur on a simple, smooth dielectric surface and acts as the ultimate limit to the resolution at which information can be read. On the other hand grating targets can be made so fine (530 grilles per mm have been used) that no limitation is imposed upon resolution by this structure. With the present 240 grille per mm grating storage targets, no evidence of a grating structure disturbance signal has yet been detected even though stored signals of 75 line pairs per mm have been measured.

These grating storage targets have been made in both the forms of rigid squares and long pieces of thin, flexible tape. Signals have been stored and read at high resolution from both, even after the tape had been reeled up tightly for as long as 60 hours. No loss of resolution was detected by careful measurements after 40 hours. Resolution is the same both parallel and perpendicular to the grooves.

9 3 READING SECTION

Thus far during this program, the diameter of the reading electron beam has been reduced by a factor of two while the total current has been increased by a factor of 20 for a total increase in current density of 80. This is a significant step towards higher resolution and greater dynamic range. However, the importance of this part of the effort is emphasized by the experiments that indicate that this is yet the main limitation upon the resolution attainable.

10. RECOMMENDATIONS

On the basis of present performance and the probability of further improvement in resolution by a factor of more than two and in sensitivity by a factor of 40, we recommend continuation of this program.

An attempt should be made to improve the resolution of the image section by shaping the focusing coil in contour and in current density distribution.

The technology for making very long lengths of uniform grating target storage tape should be developed.

To improve resolution and dynamic range, further work should be done on the formation of high current density electron reading beams at low incident energy, on automatic reading voltage control, and on dynamic focus and alignment.

11. PUBLICATIONS

During the contract year papers were presented at three scientific meetings to report on the program:

IRE, PGED, Annual Meeting, Washington, October 1962,

AIEE, Winter General Meeting, New York City, January 1963, and

IRE, National Winter Convention on Military Electronics, Los Angeles, January 1963.

The following two written reports on this program were published:

A.S. Jensen and W.G. Reininger, "Dielectric Storage Tape for a Storage Camera Tube," Proceedings of the IRE National Winter Convention on Military Electronics, January 1963.

A.S. Jensen and W.G. Reininger, "TVIST: New Look in Photoelectric Storage Tubes," Electronics, Vol. 36, No. 25, pp. 74-76, 21 June 1963.

A brochure "Westinghouse Electrostatic Storage Tape Camera Tube" was published by Westinghouse. Copies of this were made available to the Reconnaissance Laboratory for distribution to the Air Force. This brochure was published on Westinghouse funds.

BIBLIOGRAPHY

1. Doyle, R.J., Simplified Resolution Measurements, Electronic Industries, March 1962.
2. Ryshkewitch, E., Oxide Ceramics, Academic Press, New York, 1960.
3. Nakhodnova, A.P., Izvest. Tomsk, Politekh. Inst., 91, (1956), 209-218.
4. Remy, H., "Treatise on Inorganic Chemistry," Vol. I, Elsevier Publishing Company, Amsterdam, (1956), 235.
5. American Institute of Physics Handbook, McGraw-Hill Book Company, New York, (1957), 5-115.
6. Hadley, Kramer, and Royce, JOAP, 27, 11, (November 1956), 1384-1385.
7. Hass, Ramsey, and Thun, "Optical Properties of Fluorides," JOSA, 49, 2, (February 1959), 116-120.
8. "Table of Properties," Plastic Catalog, Kaufman Glass Co., Wilmington, Delaware.
9. "Teflon FEP - Fluocarbon Film," du Pont Report, Wilmington, Delaware, (April 1959).